Experimental and Modelling Studies of Nitrogen Oxides of Interest in the Atmosphere

Deborah Jane Bird

A thesis submitted for the degree of

Doctor of Philosophy

Department of Chemistry

University of York

December 1995

BLANK IN ORIGINAL

PAGE NUMBERING AS ORIGINAL

Abstract

Different aspects of atmospheric chemistry and the sources and effects of a number of key trace gases have been examined. A study of the formation of NO and N_2O from electrical discharges through air was carried out. NO was detected by chemiluminescence and tunable diode laser spectroscopic methods, and the results confirmed that NO was formed by a thermal mechanism occurring in the heated channel after the spark.

N_2O was detected using gas chromatography with electron capture detector. Its behaviour differed from that of NO under the same experimental conditions, and it is postulated that N_2O is formed by a corona discharge both before and during the spark. It can also be destroyed at high pressures and spark energies.

The experimental results were used to estimate the global significance of the production of these species by lightning. The global production of NO is estimated to be 15.6 ± 3.4 Tg (N) yr^{-1}, corresponding to ~ 20% of the total currently identified sources. That of N_2O is predicted to be insignificant on a global scale.

Future fertiliser induced emissions of N_2O are estimated by relating fertiliser use to population. A rise from 2.25 Tg (N) yr^{-1} to 3.24 Tg (N) yr^{-1} over a 30 year period is predicted. Asia is expected to account for half of this increase, with significant future contributions from Africa and South America. Tropical regions are not predicted to contribute significantly to the increase despite a potential greater conversion rate of fertiliser to N_2O.

Finally a 1-D photochemical computer model was used to assess the effects of chemical and meteorological perturbations to the atmosphere under different conditions. A 30% increase in methane concentration over the next 30 years would lead to a reduction of global [OH] of between 2 and 10%, and an increase in $[O_3]$ of up to 4%. NO_x plays a crucial role in determining the chemistry.

Acknowledgements

Firstly I wish to thank Dr. Chris Anastasi for his advice and encouragement during the course of my studies. I am also extremely grateful to the other members of the group; Rob for his company in our 'luminous' lab, Gary for making me feel guilty about not working or training non-stop, Adam for his brilliant attitude, Mike for providing endless entertainment, and John for kindly altering highly complex computer models to order.

Thanks must also go to past and present members of our coffee group for many enjoyable events, in particular Moray for his invaluable help with the lightning work, and Sue for all things to do with wine and organic chocolate. The efforts of the technical staff were much appreciated, namely Steve, Brian, Terry, Clive, Barry and the guys in Stores. A special 'Cheers' goes to Roy, and to Steve Smith.

I am grateful to Palle Pagsberg and Alfred of the National Laboratories in Risø, Denmark for allowing us to use their TDLS equipment at such short notice, and for giving us help and advice in running the experiments.

I acknowledge the financial support of SERC/NERC and National Power plc in funding this research. On that note, thanks to all at Kites Restaurant, for employing me as slave labour but allowing me to indulge in fine food and wine at their expense.

A huge thankyou must go to my terrific friends, Sandra, Karen, Morty, Ali and Kate, who have preserved my sanity by dragging me 'reluctantly' away from my studies at regular intervals, both physically and by sending me e-mails! Thanks to Bev in this respect and also for helping out with the lightning studies. I must also thank my housemates, Rich T and the hep cats, for their relaxing influence after a hard day at the office.

Muchos gracias to Mark for plying me with heinous amounts of food and alcohol and turning all the low points into real highs. Salud chico!

Finally, I dedicate this to my family; my sister for living in highly visitable foreign locations, and my parents for their continued and much appreciated love and support through my seemingly endless student life!

Glossary

Concentrations have been given in either molecules cm^{-3} or in parts per million (ppmv), parts per billion (ppbv) or parts per trillion (pptv), where 1 ppmv = 10^3 ppbv = 10^6 pptv = 2.45×10^{13} molecules cm^{-3} at 1 atm, 298K.

Pressures are usually quoted in mbar, where 1013 mbar = atmospheric pressure = 2.45×10^{19} molecules cm^{-3} = 760 Torr, at 298 K.

Abbreviations

NO_x	$NO + NO_2$
ir	infrared light
uv	ultraviolet light
gc-ecd	gas chromatography with electron capture detector
TDLS	Tunable Diode Laser Spectroscopy
CL	ChemiLuminescent detection
CG	cloud to ground flashes
IC	intracloud flashes
VOC	Volatile Organic Compounds
NH	Northern Hemisphere
SH	Southern Hemisphere
[species]	concentrations of species
hυ	light
λ	wavelength of light

Declaration

The work contained within this thesis is entirely my own with the following exceptions:

The 1D photochemical model used in Chapter 5 was written by Fletcher (1989) and kindly donated by National Power plc. Further modifications were carried out by John Busby.

The short program for calculating future fertiliser-induced emissions of N_2O was written by Vicky Simpson.

The work for the global distribution of NO_x from lightning was carried out with the assistance of Beverley Allan.

Contents

Chapter One

Introduction

1.1 The Earth's Atmosphere

The Earth's atmosphere is a highly complex system of chemical and physical processes, involving interactions with land, oceans and biosphere. It is only over the past few decades that our understanding of this system and how human activities can affect it has improved, and much still remains undefined. However, there is strong evidence to suggest that the industrial and technological development of the human race, particularly over the past 50 years, is perturbing this system and will continue to do so in response to increasing demands of a rising population, resulting in potentially damaging long term effects.

The composition of the atmosphere changes with altitude (Finlayson-Pitts and Pitts, 1986), and comprises distinct regions of chemical, physical and meteorological behaviour, called the troposphere (0-10 km) and the stratosphere (11-50 km) as shown in Figure 1.1. The troposphere contains 90% of the mass of the atmosphere, and the majority of constituents are emitted into the first kilometre, called the boundary layer. The decreases in temperature and pressure with altitude in the troposphere promote vertical transport and thus the air in the troposphere is well mixed. The upper layers are known as the 'free' troposphere as they are relatively free from pollutants emitted from the surface and are usually removed by reactions in the boundary layer.

The troposphere consists of 99.9% nitrogen, oxygen and noble gases (mainly argon). The remaining 0.1% is made up of trace amounts of gases, including H_2O, CO_2, methane, N_2O, hydrocarbons, OH, ozone and other nitrogen oxides, all of which are either emitted naturally or as a result of human activities, or formed through chemical

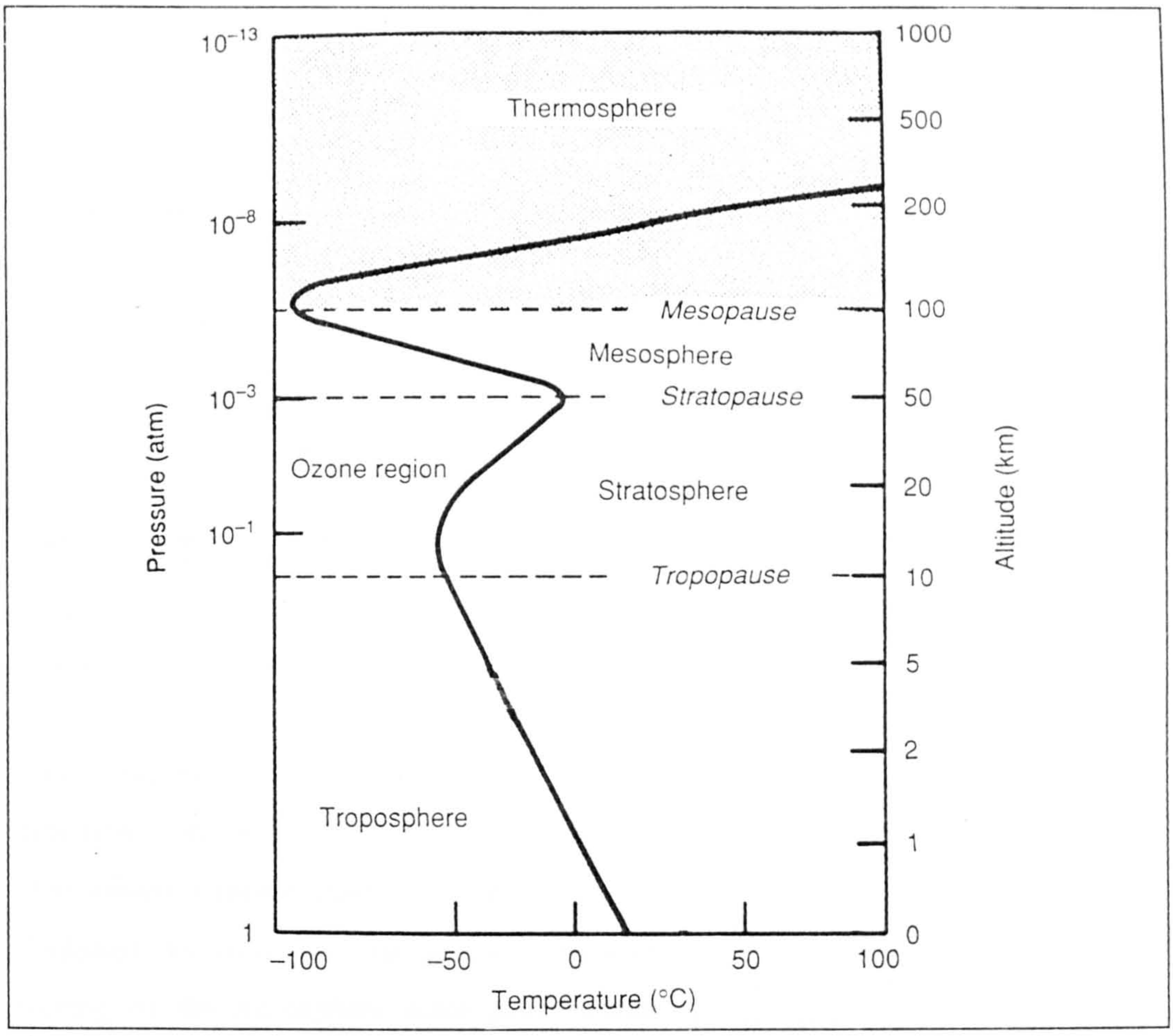

Figure 1.1 Variation of atmospheric temperature and pressure with altitude

reactions. Despite their very low concentrations, these gases play a crucial role in influencing or controlling key atmospheric processes.

Carbon dioxide is particularly important in maintaining the temperature of the troposphere (the first ten or so kilometres of the atmosphere). Solar ultra-violet (uv) radiation reaches the Earth's surface and is reflected as infrared (ir). This can be absorbed at certain wavelengths by CO_2 (and other trace gases) and reemitted, thus heating the air above the surface to an average global temperature of 288K (Wayne, 1991; Graedel and Crutzen, 1993). This phenomenon is called radiative forcing, more popularly known as the 'greenhouse effect'.

Table 1.1 Changes in atmospheric concentrations of trace gases since 1700[a]

Species	Pre-industrial concentration	1992 concentration	Rate of increase/80s	Atmospheric lifetime(years)
CO_2	280 ppmv	355 ppmv	0.4% yr^{-1}	50-200[b]
CH_4	700 ppbv	1714 ppbv	0.8% yr^{-1}	12 - 17[c]
N_2O	275 ppbv	311 ppbv	0.25% yr^{-1}	120
CFC-12	0	503 pptv	4% yr^{-1}	102

[a] data for ozone highly variable

[b] single lifetime for CO_2 cannot be given due to different rates of uptake by sinks

[c] includes indirect effect of CH_4 on its own lifetime

Increasing emissions of CO_2 from combustion processes, which have led to a rise in the atmospheric concentration (see Table 1.1), are predicted to have led to greater radiative forcing of the atmosphere since preindustrial times (1700), which may be the cause of the enhanced global average temperatures observed over the 80s. However, 40% of this increase has been estimated as arising from the increases in atmospheric concentrations of other trace gases, in particular N_2O, CH_4, ozone and the CFCs (Houghton *et al*, 1995). All these gases absorb strongly in the ir region, at wavelengths where CO_2 does not absorb (called the 'window' region), shown in Figure 1.2. Their absorption is greater on a mole by mole basis than CO_2, so that despite their relatively low concentrations their collective contribution to the radiative forcing is almost equivalent to CO_2. The effect of further increases

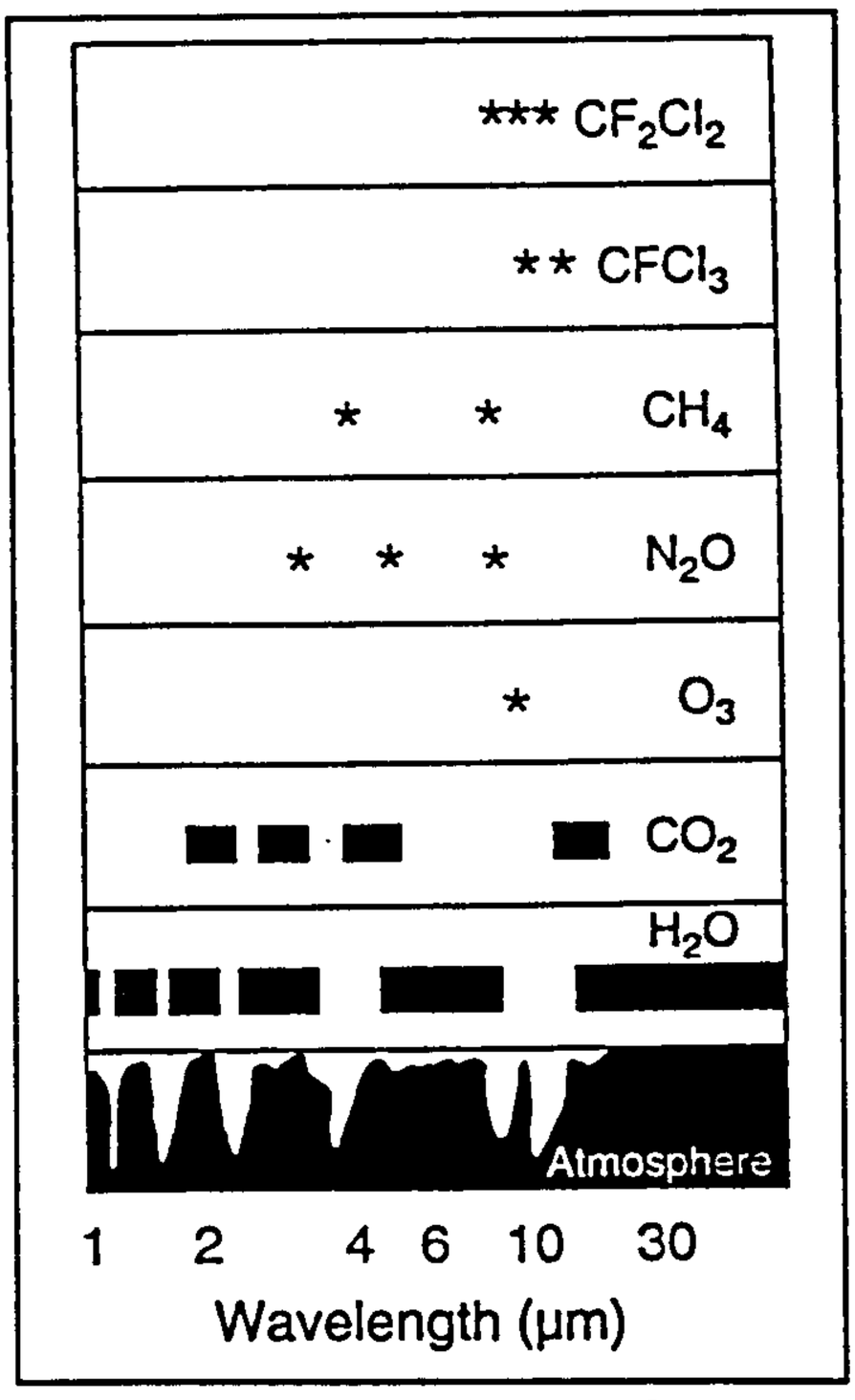

Figure 1.2 Regions of strong absorption as a function of wavelength for key greenhouse gases

in their concentrations is also anticipated to be linear, whereas that of CO_2 is not, due to its near saturation in the regions of strongest absorption.

Studies of the composition of past atmospheres, obtained from ice core data, show a strong correlation between the concentrations of CO_2 and CH_4 and the temperature, shown in Figure 1.3. This also shows the extreme variability which occurs in the atmosphere, enhancing further the difficulties present in describing the system as a whole. However, it suggests that any future increase in the concentrations of the trace gases will have a strong influence upon the climate.

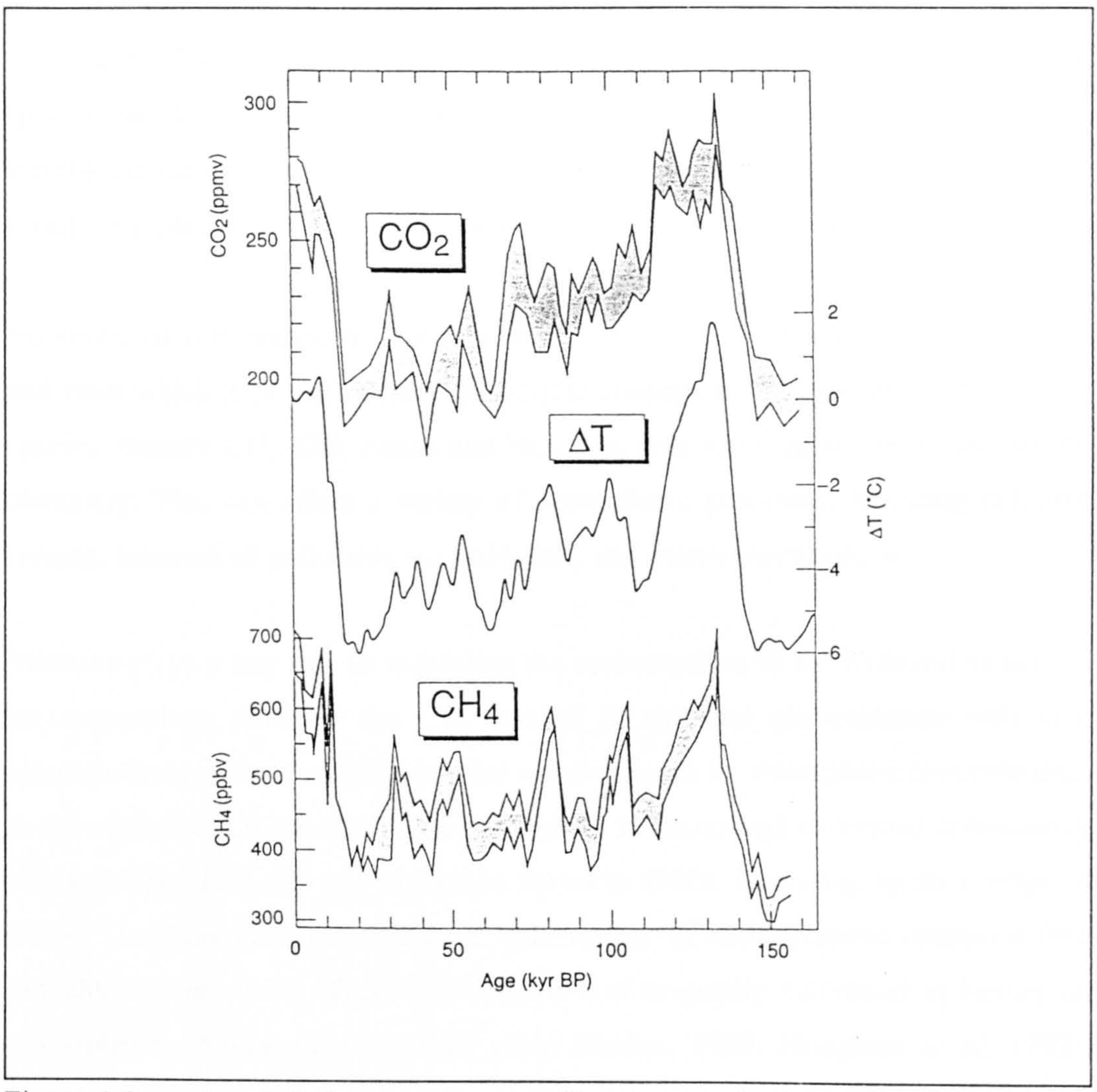

Figure 1.3 Antarctic ice core records of local atmospheric temperature, and CO_2 & CH_4 volume mixing ratios for the past 160,000 years.

Other atmospheric processes are also likely to be affected by changes in ambient levels of these species, both directly and indirectly. The chemistry of the troposphere is driven entirely by solar radiation, which can photolyse tropospheric ozone to form the important OH radical

$$O_3 + h\upsilon \rightarrow O_2 + O(^1D) \qquad (1.1)$$

$$O(^1D) + H_2O \rightarrow 2OH \qquad (1.2)$$

OH is present in highly variable and extremely low concentrations (10^6 cm^{-3}; Prinn *et al*, 1992; Thompson, 1992) in the troposphere, but reacts rapidly with many other atmospheric species, particularly hydrocarbons and reduced or partially oxidised compounds. These complex oxidation pathways lead to the removal of the relevant species but often regenerate OH (Ehhalt *et al*, 1990; Crutzen & Zimmermann, 1991), thereby maintaining constant atmospheric concentrations of many trace gases. OH is therefore regarded as the most important 'cleansing agent' in the troposphere.

However, its concentration is in turn regulated by the species with which it reacts and from which it can be formed. Significant changes in the concentrations of these species, namely CH_4, CO, ozone and NO_x, can lead to perturbations to the natural chemistry. This can affect a variety of atmospheric processes, including radiative forcing, removal of pollutants via oxidation, and stratospheric ozone.

Methane plays a key role in regulating the concentration of the hydroxyl radical in the troposphere. 90% of the CH_4 emitted is removed via oxidation with OH. Increases in emissions of CH_4 have led to increases in its atmospheric concentration, as the amount of OH present in the troposphere is not enough to remove immediately all extra CH_4. This rate was highest in the early 1980s, increasing by an average of 1% yr^{-1} and has been ascribed to a wide variety of anthropogenic emissions (see Houghton *et al*, 1995). Therefore methane was originally calculated as having an atmospheric lifetime of around 10 years (Rodhe, 1990; Houghton *et al*, 1992). Increases in its concentration can however lead to a number of feedbacks. Enhanced $[CH_4]$ reduces the concentration of OH which in turn has the effect of further

suppressing the rate of removal of CH_4, thus increasing its lifetime. This is now estimated as 14.5 ± 2.5 years (Houghton *et al*, 1995). This then increases the radiation absorption potential, and decreases the ability of OH to remove other atmospheric species.

However, the rate of increase of methane appeared to slow down towards the end of the 1980s and the beginning of the 1990s (Steele *et al*, 1992; Khalil & Rasmussen, 1993; Dlugokencky *et al*, 1992). This has been ascribed to reductions in fossil fuel exploitation and in emissions from animals and feedstocks, and adds further complexities to study of the potential feedbacks.

Whilst NO_x is itself not a greenhouse gas, its presence in the atmosphere also regulates the chemistry occurring, and thus is involved in feedback processes determining the radiative forcing. The oxidation of methane in the presence of NO_x can lead to the overall production of ozone, whereas in the absence of NO_x, ozone is destroyed. As well as being a greenhouse gas, and a precursor for OH, the presence of ozone in the troposphere can cause irritation to the respiratory tract in humans. NO_x can also lead to enhanced levels of OH. Emissions of NO_x are increasing, but its reactivity leads to a lifetime of the order of days and highly variable and source dependent concentrations, therefore NO_x is especially important on a regional scale.

Other key species include CO, and higher hydrocarbons. All are removed by reaction with OH, and their reactivity is greater than that of CH_4. Around 70% of OH is used up by reaction with CO, but the knowledge of past concentrations of CO is limited and therefore it is difficult to estimate its relative significance in terms of its effect upon atmospheric processes. Emissions, mainly from combustion sources, increased during the 1980s, but the widespread introduction of catalytic converters to vehicles and industrial processes is expected to have reversed this trend (Khalil & Rasmussen, 1994; Novelli *et al*, 1994). However, the increasing use of vehicles on a global scale is expected to lead to greater emissions of higher hydrocarbons, which may be significant in terms of regulating OH.

Changes in tropospheric concentrations of trace gases can also affect processes in the stratosphere, where conditions are very different to those in the troposphere. 90% of the ozone which occurs in the atmosphere is contained in the stratosphere and along with molecular oxygen can absorb uv radiation of wavelengths <290 nm. The exothermicity of the ensuing reactions, in addition to the absorption and re-emission of ir radiation from the troposphere by ozone, leads to heating of the stratosphere. There is an increase in temperature with altitude in the stratosphere, which means that the air in the stratosphere is not well-mixed. The absorption of this high energy uv radiation protects the Earth's surface from its damaging effects, which can lead to skin cancers and cataracts in animals, and can destroy vegetation.

Ozone is constantly formed and regenerated in the stratosphere by catalytic cycles involving molecular oxygen. The action of sunlight upon oxygen leads to the production of O atoms, which can combine with oxygen to produce ozone. This in turn can be photolysed or can combine with O atoms to reform O_2, the whole process being termed the 'Chapman cycle':

$$O_2 + h\upsilon \rightarrow 2O \ (\lambda < 242 \text{ nm}) \qquad (1.3)$$

$$O + O_2 \ (+M) \rightarrow O_3 \ (+M) \qquad (1.4)$$

$$O_3 + h\upsilon \rightarrow O(^3P) + O_2 \ (\lambda < 1140 \text{ nm}) \qquad (1.5)$$

$$O_3 + h\upsilon \rightarrow O(^1D) + O_2 \ (\lambda < 310 \text{ nm}) \qquad (1.6)$$

$$O + O_3 \rightarrow 2O_2 \qquad (1.7)$$

Species which are unreactive in the troposphere are eventually transported to the stratosphere. These can be broken down by photolysis or reaction, and can become involved in the catalytic destruction of ozone. Such species include N_2O and compounds of chlorine. Upon reaching the stratosphere N_2O is either removed by reaction with $O(^1D)$ (90%):

$$N_2O + O(^1D) \rightarrow 2NO \qquad (1.8a)$$

$$\rightarrow N_2 + O_2 \qquad (1.8b)$$

or by photolysis (10%):

$$N_2O + h\upsilon \rightarrow N_2 + O \ (< 240 \text{ nm}) \qquad (1.9)$$

The NO formed in reaction 1.4(a), and chlorine radicals also produced by photolysis of chlorine compounds, can react with ozone in the following catalytic cycles (where X = NO or Cl)

$$X + O_3 \rightarrow XO + O_2 \qquad (1.10)$$

$$O_3 + h\upsilon \rightarrow O_2 + O \qquad (1.11)$$

$$XO + O \rightarrow X + O_2 \qquad (1.12)$$

overall $2O_3 + h\upsilon \rightarrow 3O_2$

60% of stratospheric ozone is destroyed naturally by NO produced from N_2O.

Increases in the concentrations of radical precursors are therefore expected to enhance the rate of ozone depletion. The discovery of the 'ozone hole' over the Antarctic confirmed predictions by Molina & Rowland (1974) that the release of CFCs, which are inert in the troposphere but photolyse to produce Cl in the stratosphere, would lead to the reduction of the ozone concentration. Similarly, increases in N_2O concentrations are also predicted to have an effect upon the ozone layer, although the long lifetime of N_2O in the troposphere means that the effects of current emissions will not be evident for several years.

Enhanced levels of solar radiation in the troposphere may not only be directly damaging to plant and wildlife, but may also affect the photochemistry and in turn the processes mentioned above, through positive and negative feedbacks. Decreases in stratospheric ozone have been suggested as contributing to the reduction in tropospheric CO and CH_4 (Bekki *et al*, 1994). And increased photolysis of tropospheric ozone could lead to greater concentrations of OH, which in turn could react with more methane and thus reduce the potential radiative forcing. However, increases in radiative forcing by the presence of other gases in the troposphere could

lead to lower stratospheric temperatures and thus to an increase in stratospheric ozone. In addition a greater tropospheric temperature could lead to more eveporation of surface water, more atmospheric H_2O and the formation of more OH. This could also lead to a greater amount of cloud cover, which may alter the scattering of uv light from the stratosphere.

These complex feedback processes highlight the need for a complete understanding of the atmospheric processes and how they are affected by perturbations, both directly and indirectly.

1.1.1 Global Budgets

The above has demonstrated, albeit briefly, the complexities of atmospheric systems, and the difficulties which scientists face in untangling these processes. A number of trace gases have been identified as being crucial in controlling these processes, especially those whose concentrations are increasing as a result of anthropogenic emissions, namely N_2O, CH_4, O_3, and NO_x. To aid our understanding of how these gases may affect the atmosphere, both now and in the future, it is important to assess: 1) the current sources and sinks of these species, and the reasons for their increase; 2) how they affect the atmosphere; 3) potential future increases and subsequent effects. From this it is possible to develop strategies for preventing foreseeable problems.

Establishment and quantification of the sources and sinks of a gas, or its 'global budget', requires extensive study, and also requires knowledge of current and past atmospheric concentrations. For species such as the CFCs, whose only source is industrial, its production rate widely documented and whose only sink is via photolysis in the stratosphere, such inventories are reasonably straightforward.

This is not the case for the majority of other gases, whose sources may be numerous and highly variable in nature. They may also have correspondingly low, or highly variable atmospheric concentrations, which are difficult to measure. The predictions

of global source and sink strengths therefore carry a higher degree of uncertainty. Estimations of emission rates are usually carried out by experimental studies, where the process which produces the gas is examined on a small scale, by field or atmospheric measurements at a region of interest and by computer models. In all cases assumptions have to be made in the extrapolation of small scale events or simulations to events occurring over long time periods on a global scale. This adds further uncertainty to the estimations.

The present work investigates a number of these areas for some of the key species mentioned. Experimental and computer modelling studies into the current and future global significance of identified sources of NO_x and N_2O are carried out. Their regional significance is also investigated. Finally a computer model of the chemistry of the atmosphere has been used to examine the effects of short and long term chemical perturbations on both regional and global scales. This includes investigating the effect of increasing CH_4 upon OH levels in the free troposphere, the influence of NO_x and the significance of altering physical and meteorological processes.

1.2 Nitrogen Oxides

1.2.1 NO and NO_2 (NO_x)

As mentioned earlier, the presence of NO_x in the atmosphere influences the production of ozone and also the levels of OH radicals, which in turn regulate the concentration of many key species, such as CH_4, CO and halocarbons. The majority of NO_x is emitted as NO, and there are a large number of sources (see Table 1.2). Anthropogenic sources dominate, particularly fossil fuel combustion, and these sources are expected to continue rising in the near future, especially in developing countries, where regulation of emissions is not enforced.

There are large uncertainties associated with the quantification of these sources. For fossil fuel combustion an error of ± 30% is inherent, but rises to a factor of two for

other sources. In the case of lightning, probably the most important natural free tropospheric source, the uncertainty is even greater, despite several studies in this area.

NO emitted to the troposphere is converted to NO_2 by reaction with a number of species, including O_3 and peroxy radicals. The predominant removal process is by daytime reaction of NO_2 with OH to form HNO_3, or night-time reaction with O_3 to form NO_3, both of which are precipitated out. Some of the NO is recovered by photolysis of NO_2, but ultimately all NO is returned to the Earth via wet, or more rarely dry, deposition.

Table 1.2 Estimated global emissions of NO_x[1]

Sources	Magnitude (Tg N yr^{-1})	% of total
Fossil fuel combustion	24	46
Soil release (fertilised and unfertilised)	12	23
Biomass burning	8	15
Lightning	5	10
NH_3 oxidation	3	5
Aircraft	0.4	0.7
Transport from stratosphere	0.1	0.3

[1] values taken from Houghton *et al.* (1995)

The reactivity of NO means that it has a short lifetime, and thus increases in emissions will lead to more reactions and thus a moderating of the lifetimes and abundances of other atmospheric species. This also means that the distribution of NO_x is highly variable, both temporally and spatially. Studies carried out over North America showed the concentration of NO_x in the lower troposphere to vary by three orders of magnitude (Houghton *et al*, 1995). Results of several other studies indicate

that the NO_x concentration is greater in the northern hemisphere due to the greater proportion of ground emissions. The concentration at the surface is high, drops off at the boundary layer and then increases with altitude, as a result of direct inputs from lightning, the stratosphere and aircraft. At the tropopause in northern mid latitudes the concentration of NO_x reaches hundreds of ppbv. NO_x emitted from the ground has a shorter lifetime (hours) than NO_x emitted directly to the free troposphere (days) due to the number of reactions which can occur in the boundary layer.

The distribution of NO_x in the free troposphere may be due to a number of sources- transport up from the boundary layer, incursion from the stratosphere, injection from aircraft (8-12 km) or from production by lightning. Of these, lightning carries the most uncertainty. It is important to quantify accurately the contributions from these sources, in order to model the process correctly. The efficiency of ozone at absorbing radiation is greater at higher altitudes, and therefore the assessment of NO_x at these altitudes is crucial in determining ozone formation and thus the potential increased radiative forcing.

1.2.2 NO_x from Lightning

Lightning was recognised as a source of fixed nitrogen as far back as 1827 (von Liebig). However it is not until this century that studies of the lightning phenomenon, both as a physical entity and in terms of its global occurrence and distribution, have been more forthcoming, and these have allowed the mechanism of NO_x formation to be examined. This has led to estimates of the global production of NO_x from lightning to be made, although relatively little work has been carried out on the subsequent global distribution.

Lightning usually occurs in thunderclouds, which develop when warm air rises in unstable conditions. By some unknown mechanism, rising ice crystals in the cloud collide with falling hailstones, and are stripped of their electrons. In simplistic terms this leads to a net positive charge at the top of the cloud and a negative charge at the

cloud's base. This negative charge induces positive charge at a point below it on the Earth's surface, and a build up of static charge (called corona discharge) occurs until a negative spark is released from the cloud base. Positive streamers are launched up from the Earth, and when the spark meets one of them a channel forms for the visible flash, called the return stroke, producing shock waves (thunder). The flash itself is highly energetic, reaching temperatures of up to 20,000^{0}C, with virtually all this energy being converted to heat, light, motion or radiowaves. It is believed that NO_x is formed through the thermal reactions of excited nitrogen and oxygen atoms and molecules.

Storms occur with great frequency around the globe, although the distribution is not even. The warm, unstable conditions required for the formation of storms are more often found in tropical regions, and are more common over the Northern Hemisphere, especially during summer and autumn. There are relatively few storms occurring over oceanic regions. The lightning flashes described in the previous paragraph are known as cloud-ground (CG) flashes, but sparks can also occur within the clouds themselves and are known as intra-cloud (IC) flashes. The proportion of IC to CG flashes is variable, and more IC flashes occur in the tropics (Uman 1987). There have been no studies on whether the formation of NO_x is different for CG and IC flashes. Whilst CG flashes are more energetic, they occur less frequently, and the higher altitudes of IC flashes could have more impact upon the free troposphere.

Previous studies have investigated both the mechanism of NO_x formation, and also the amount which is formed, by estimating the NO_x produced by one flash and multiplying this by data for global flash frequencies. The value for NO_x per flash (P) is obtained from experimental, atmospheric or theoretical studies, and in all cases a number of assumptions have to be made, which leads to the large uncertainties mentioned in section 1.2.

1.2.2.i) Atmospheric measurements

Different types of atmospheric measurements have been made in the past. Originally the nitrogen fixation was estimated by measuring the nitrate concentration in storm precipitation. This proved to be inaccurate, as any NO_x produced by the storm could take between 12 and 20 hours to be precipitated out as HNO_3, as its formation requires the reaction of NO_x with OH.

Ground level measurements of the absorption spectrum of NO_2 near 440 nm during electrical storms were taken by Noxon (1976). However, there were a number of uncertainties associated with this method, not least the determination of the background concentration of NO_2 in the clouds, and the effect of scattering over such long distances. There was also interference from water in this region of the spectrum. Similar measurements made at the horizontal by Noxon (1978) through the air below thunder clouds yielded estimates of 10^{26} molecules NO_2 per flash, but there were no measurements of NO.

Franzblau and Popp (1983) measured the NO_x and NO_2 produced by lightning triggered with a lightning rod, using simultaneous chemiluminescence and absorption techniques. The detectors were located close to the lightning rods, and concluded that around 3×10^{27} molecules NO_x $flash^{-1}$ were formed, of which around 10% was NO_2. Drapcho *et al* (1983) measured NO_x, also with chemiluminescent analyser, continuously for 48 hours and found the concentration increased during a storm, with a high conversion of NO to NO_2. However, no estimates for the amount of NO_x formed per flash were given due to difficulties in determining the number of lightning strikes.

In other studies, aircrafts were flown near to a storm and measurements taken of the concentrations of NO in outflow regions of the storm (Levine *et al*, 1983; Davis *et al*, 1987). These were compared to the background concentrations of NO. An increase in the NO concentration was observed, but uncertainties in the dilution factors and the absolute background levels led to difficulties in predicting the NO produced on

a global scale.

1.2.2.ii) Experimental studies

Experimental studies of the formation of NO_x have been somewhat more common, although the results are not conclusive. These generally involve passing an electrical discharge of up to 1 m in length through samples of air and subsequently measuring the NO_x formed, usually by chemiluminescent techniques. This is expressed in terms of the production per joule (J) of energy input to the spark (P) and previous estimates range from 6 - 80 $\times$ 10^{16} molecules J^{-1}. From assumptions of the energy of a lightning flash the NO_x per flash can be estimated.

However, in such studies it is important to identify the differences between the experimental discharge and the lightning discharge. Often the energy per unit length of a small scale spark is less than that of lightning, and there can be energy losses associated with the experimental work which, if ignored, will affect the calculated NO_x J^{-1} value, and thus the global prediction.

1.2.2.iii) Discharge chemistry

The mechanism of NO formation in the discharge is believed to occur via the thermal process described by Zel'dovich & Raizer (1966). This occurs at temperatures above 3000K.

$$O_2 \rightleftharpoons O + O \qquad (1.13)$$

$$N_2 + O \rightleftharpoons NO + N \qquad (1.14)$$

$$N + O_2 \rightleftharpoons NO + O \qquad (1.15)$$

However, there is some disagreement about where in the discharge the NO is formed. Hill *et al* (1980) proposed that its formation occurred in the heated channel as the air cooled after the discharge. Chameides *et al* (1977) believed that the high velocity at the shock front heated up the air as it moved away from the spark channel, and that

the NO was formed there. More recent studies suggest that the velocity of the shock front is not enough to reach the temperatures required for NO formation, at least in small scale laboratory studies (Stark *et al*, 1995).

The mechanism is an equilibrium, and at very high temperatures the back reactions are significant. The equilibrium concentration of NO is reached more quickly as the gas cools, and at ~3000K the rate of cooling is fast enough that the equilibrium concentration of NO is 'frozen out', rather than being insignificant. This is explained in more detail by Stark *et al* (1995).

There is also dispute over whether NO_2 is formed from the action of the flash. Previous studies have observed no NO_2 formation (Chameides *et al*, 1977; Levine *et al*, 1981). However, other studies suggest that NO_2 is formed by the reaction of NO with ozone, which is present at ambient levels, or as a result of the flash (Harrison, 1991; Hill *et al*, 1980)

$$NO + O_3 \rightarrow NO_2 + O_2 \qquad (1.16)$$

Ozone can be formed in the corona discharge, which occurs from the build up of charge prior to the flash. There is dispute as to whether ozone is formed during the flash, with some workers suggesting that ozone production drops off when the spark passes (Peyrous and Lapeyre, 1982). There is also doubt as to whether the formation of NO_2 under experimental conditions is similar to that in the atmosphere due to the difference in diffusion processes within a reaction cell and on an atmospheric scale.

1.2.2.iv) Theoretical studies

Computer models can be used to provide validation for the mechanisms occurring in the spark, and also in the estimation of global NO_x from lightning. Hill *et al* (1980) attempted to estimate the production of NO_x from a single lightning stroke. Their simple model assumed that the NO was formed in the hot channel, therefore only reactions of atoms and molecules were incorporated, and it was assumed that the hot

air in the channel was cooled by perfect mixing with the ambient air. They concluded that the production of $NO_x$was 6×10^{25} molecules $flash^{-1}$.

Chameides *et al* (1977) used a more complex chemical scheme, including water, CO_2, and CH_4, and assumed that the energy was present in the shock wave. He estimated that 1.2×10^{26} molecules of NO $flash^{-1}$ were formed. Griffing *et al* (1977) included ionic reactions in their model, and predicted that 3.2×10^{26} molecules $flash^{-1}$ were produced. Therefore, over this small set of studies, the range of estimates is almost an order of magnitude. When further assumptions were made about flash frequencies the global production of NO_x from lightning was predicted as ranging from 4.4 - 35 Tg (N) yr^{-1}. Thus the uncertainty is enhanced.

The variation in results of the three types of study demonstrates the need for further studies which will confirm the mechanism of NO_x production, the physical parameters of a lightning flash, the frequency of lightning over the globe, and thus give more accurate predictions of the global production of NO_x from lightning.

1.2.3 The Global Budget of N_2O

The ambient concentration of N_2O is currently 310 ppbv, representing an overall increase of 15% since pre-industrial times (Houghton *et al.* 1995), and during the last decade its rate of annual increase was between 0.25% and 0.31% yr^{-1} (Weiss, 1981; Prinn *et al.*, 1990; Badr and Probert, 1992). This rise has been attributed, in part, to anthropogenic activities (Leuenberger *et al.*, 1992; Bolle *et al.*, 1986; Rasmussen and Khalil, 1986).

Determination of the global budget for N_2O is at least as uncertain as that of NO_x, primarily because the majority of emissions, both natural and anthropogenic, are from biogenic sources. This leads to high variability in emission rates, and therefore difficulties in measurement and extrapolation to obtain global values. The current estimates of sources and sinks are given in Table 1.3. From measurements of the atmospheric concentration changes, an estimate for the atmospheric increase has been

made of ~ 4 Tg (N) yr^{-1} (Houghton *et al*, 1995). However, when the current knowledge of the sinks and natural and anthropogenic sources is taken into account there is a shortfall of ~3 Tg (N) yr^{-1}. This needs to be accounted for, and could be due to either an underestimate of the sources, an unknown and important source or an over-estimation of the sinks. Therefore it is important that this area be studied in much greater depth.

Table 1.3 Estimated sources and sinks of N_2O

		Range (Tg N yr^{-1})
Atmospheric Increase		**3.1 - 4.7**
Sinks	*stratosphere*	9 - 16
	soils	?
Total sinks		**9 - 16**
Implied total sources (atm. inc. + total sinks)		**13 - 20**
Identified sources		
Natural	*oceans*	1 - 5
	tropical soils	2.7 - 5.7
	temperate soils	0.6 - 4
Total identified natural sources		**6 - 12**
Anthropogenic	*cultivated soils*	1.8 - 5.3
	biomass burning	0.2 - 1.0
	industrial sources	0.7 - 1.8
	cattle and feed lots	0.2 - 0.5
Total identified anthropogenic sources		**3.7 - 7.7**
Total identified sources		**10 - 17**

The majority of N_2O is emitted naturally as a result of microbial oxidation and reduction of nitrogen compounds in soils (nitrification and denitrification) (Bouwman, 1990; Firestone and Davidson, 1989; Arah, 1992). The release of nitrous oxide in both processes is controlled by physical parameters such as soil moisture content, soil

temperature, pH and partial oxygen pressure (Firestone and Davidson, 1989; Bouwman, 1990). Increased temperatures can lead to higher fluxes of N_2O (Blackmer *et al*, 1982; Bouwman, 1990) and studies by Prinn *et al* (1990) indicate that emissions of N_2O by latitude are greatest from 0-30^{0}N, where there is the highest proportion of tropical land area.

Natural emissions from soils are believed to have been affected by substantial changes in land management practices such as deforestation, cultivation and biomass burning (Seiler and Conrad, 1987; Cofer *et al*, 1991; Bouwman, 1990). The addition of nitrogenous fertilisers to soils can significantly enhance the N_2O flux (Cates and Keeney, 1987; Conrad *et al*, 1983; Duxbury *et al*, 1982; Firestone *et al*, 1979; Keller *et al*, 1988; Mosier *et al*, 1991; Slemr *et al*, 1984) and other anthropogenic sources, such as cars fitted with catalytic converters (Dasch, 1992; Berges *et al*, 1993), production of adipic and nitric acids (Thiemens and Trogler, 1991; Houghton, 1992) and stationary combustion sources (power stations) (Khalil and Rasmussen, 1992a; Linak *et al*, 1990; Lyon *et al*, 1989) may also produce significant quantities of N_2O. It is also possible that the disturbance of tropical ecosystems, by both natural (ie. hurricanes) and anthropogenic (deforestation, cultivation) means may lead to greater N_2O emissions that the equivalent practices in temperate regions.

Another potential source of N_2O is the atmosphere, both in terms of production by lightning, and also from reactions occurring naturally in the upper troposphere (Adema *et al*, 1990; Levine & Shaw, 1983; Khalil & Rasmussen, 1992b; Prasad, 1994). It has been suggested that this source may account for the shortfall in the N_2O budget, but a great deal more research is necessary to confirm this.

1.2.4 Fertiliser-Induced Emissions of N_2O

The most recent estimates of the magnitude of fertiliser-induced emissions suggest that on average 3.5 Tg N_2O-N, could originate from this source (Houghton *et al*., 1995). This corresponds to 60% of the currently identified anthropogenic sources, and 25% of the total identified sources This may therefore be the major anthropogenic

source, and as the use of fertiliser is expected to increase in the future it is important to understand the process in order to assess its future impact and to develop ways in which to reduce its effect.

Enhanced soil emissions as a result of the application of fertiliser are thought to occur by a number of mechanisms: direct conversion of applied inorganic nitrogen to N_2O via denitrification or nitrification, leaching of fertiliser into groundwater and fresh water ecosystems with subsequent production of N_2O (Bolle *et al.*, 1986), and N_2O dissolved in soil surface waters undergoing release from agricultural drainage water (Dowdell *et al.*, 1979). Emissions from water systems are believed to be equal to those from soils (Bouwman, 1990).

Most studies of N_2O emissions have been carried out on soils treated with commercial nitrogenous fertilisers, but limited studies show that the application of organic manure can also significantly enhance emissions (Cates and Keeney, 1987; Comfort *et al.*, 1990). However, estimates of global fertiliser-induced emissions usually exclude manure as a source despite its widespread use as a fertiliser, due to uncertainties in its global consumption rate.

Measurement of trace gas fluxes from soils are usually carried out on a small scale, using soil cover methods (Hutchinson and Mosier, 1981; Loftfield *et al,* 1992; summarised by Mosier, 1989 and 1990) but the high variability of emissions and non-uniformity of land surfaces and soil types prohibits the accurate quantification of global annual emissions based upon one set of data. Larger scale measurements, using long-path Fourier transform infrared spectrometry and tunable diode laser techniques have been developed (Mosier, 1990; Fowler and Duyzer, 1989), but these are more costly and only cover land on a square km scale. Therefore, to produce global estimates of N_2O emissions from fertilised soils it is necessary to analyse data from a wide range of studies so that averages can be calculated.

Two such methods have been adopted. Bouwman (1990) found a relationship between fertiliser use per hectare and N_2O flux, and assuming this to be a global

average, took data for the total world fertiliser consumption and the total land area under cultivation, to calculate an emission of 2.3-3.7 Tg N_2O-N yr^{-1}. Other studies have reported the average conversion of applied fertiliser nitrogen to N_2O, independent of land area, both in soil and from groundwater leaching: 1-4%, Bolle *et al.*, (1986); 0.5-1.5%, McElroy and Wofsy, (1985); ≤3%, Eichner, (1990); estimates of N_2O fluxes of between 0.2 and 3.0 Tg N_2O-N yr^{-1} were produced from these conversion factors using data for global fertiliser consumption.

Increases in N_2O are clearly related to anthropogenic activities. As populations grow, especially in the developing world where the greatest future growth is expected to occur, the demand for food means that more land will be used for this purpose. During the 1980s the use of fertiliser doubled in developing countries, whilst reaching a plateau in the developed world. This growth is expected to continue over the next few decades leading to a potential increase in emissions of N_2O (Mosier and Schimel, 1991), possibly enhanced by the fact that most developing countries are in tropical climates. Therefore it is useful to make predictions of future fertiliser consumption, to ascertain the likely future emissions of N_2O, and to assess whether these emissions can be reduced in any way.

This can be carried out by the use of computer models which relate emissions of these gases to a number of social, economic and political factors such as population growth, Gross Domestic Product (GDP), emission control strategies, land use and so on. The effects on emission rates of potential future changes in the values of these factors can then be assessed and greenhouse gas 'scenarios' developed.

1.3 Uses of Computer Modelling in Atmospheric Studies

Study of the behaviour of individual atmospheric systems, such as reactions, rates, emissions and so on can be carried out by laboratory or in some cases field measurements. However, for the purpose of studying how a group of systems interact as a whole it is necessary to use numerical computer models. By describing relevant

chemical, physical and meteorological processes in terms of a series of mathematical expressions, it is possible to stimulate the behaviour of natural atmospheric and other Earth systems, and to study the causes and effects related to the system.

Computer models are not only confined to the study of current atmospheric conditions. By simulating changes which may occur as the result of external actions, for example population changes or political action, the model can be used as a predictive tool, which is useful in policy making. This allows the generation of scenarios, which enable scientists to explore the range of possible outcomes which could occur based upon uncertainties in the extent of future changes. Such models can be simple numerical expressions, which for example relate emissions of one gas to a single factor, or can be complex, i.e. predicting future emissions of several gases and their subsequent effect upon radiative forcing.

Models can also be used to study past systems. This is useful for validating models, as past changes are better known, and can therefore be compared with results obtained from the model, to ensure that it is replicating past conditions accurately. In this way it is possible to look at the effects of past changes in the atmosphere, and to determine how these may change in the future by altering certain parameters. They are also useful for describing small systems, such as experimental conditions, industrial processes.

The complexity of models therefore varies, and depends upon the system under study and the available computational power. There is usually a trade off between the degree of spatial and temporal resolution and the complexity of chemical, physical and meteorological processes to be included. For example, if it is necessary to study a system over long time periods, the complexity of the processes and resolution over space may be higher, but if the changes in a system over short time periods is required, this restricts the spatial resolution and processes which can be included. Hence it is not currently possible to simulate all the processes occurring over the planet at every point and at regular time intervals, as the computational power is not available, and our knowledge of the necessary processes is still insufficient. It is

therefore necessary to make assumptions in modelling, and to use the most appropriate model for our needs.

1.3.1 Atmospheric Models

1.3.1.i) Box models

The simplest model which is used for describing atmospheric systems is the box model, which treats the air above the region of interest (for example a power station, an urban centre) as a stationary box and examines the processes occurring as a function of time. The box is usually set at ground level, and the appropriate species input via emissions from the ground. Their fate is then determined by reaction, photolysis, vertical entrainment, horizontal advection (wind dilution), or by ground deposition, all of which are defined by the model. The period of simulation depends upon the residence time of the air in the box, determined by the horizontal advection rate, and the length of the box, which is defined by the user.

There are two types of box model which are useful for different types of analysis. *Eulerian* models calculate the concentrations of chemical species as a function of time at fixed locations, and are much as described in the previous paragraph (i.e. Fletcher, 1989). Comparison of the results with atmospheric measurements is possible, as most measurements are made at a fixed point. The model can be represented by the diagram in Figure 1.4.

Lagrangian models simulate the path of a moving air parcel, by assuming that the box moves with air motions. This removes the need for a horizontal advection term, but requires the input of more detailed source and sink terms, which will vary as the air parcel moves. It is not so simple to compare this type of study with atmospheric measurements, as very few are made, but it is useful for the analysis of local and regional areas - ie the changes occurring in an air parcel as it moves away from a pollution source. This is shown in Figure 1.5.

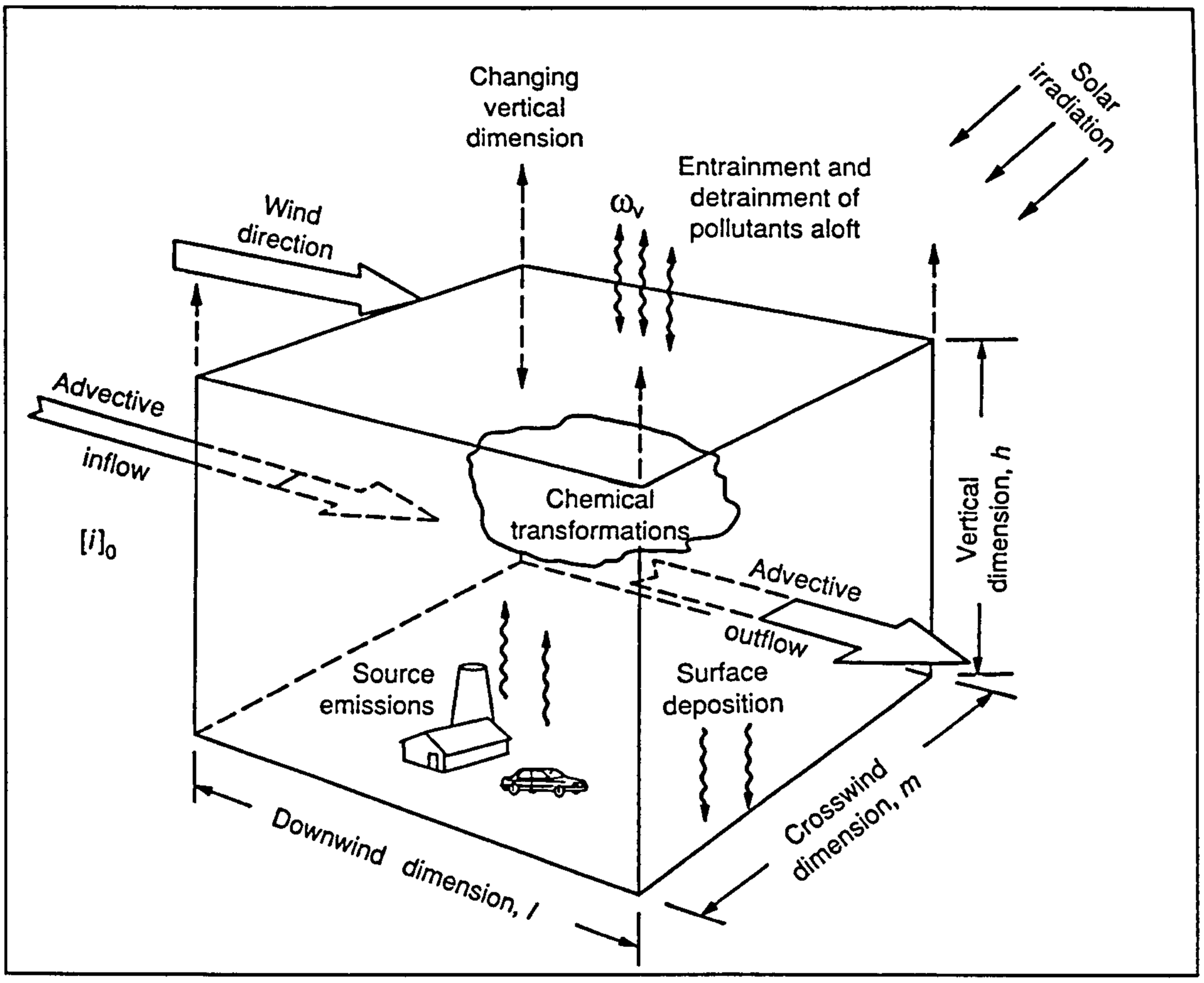

Figure 1.4 The features of a typical 0D box model of atmospheric chemistry

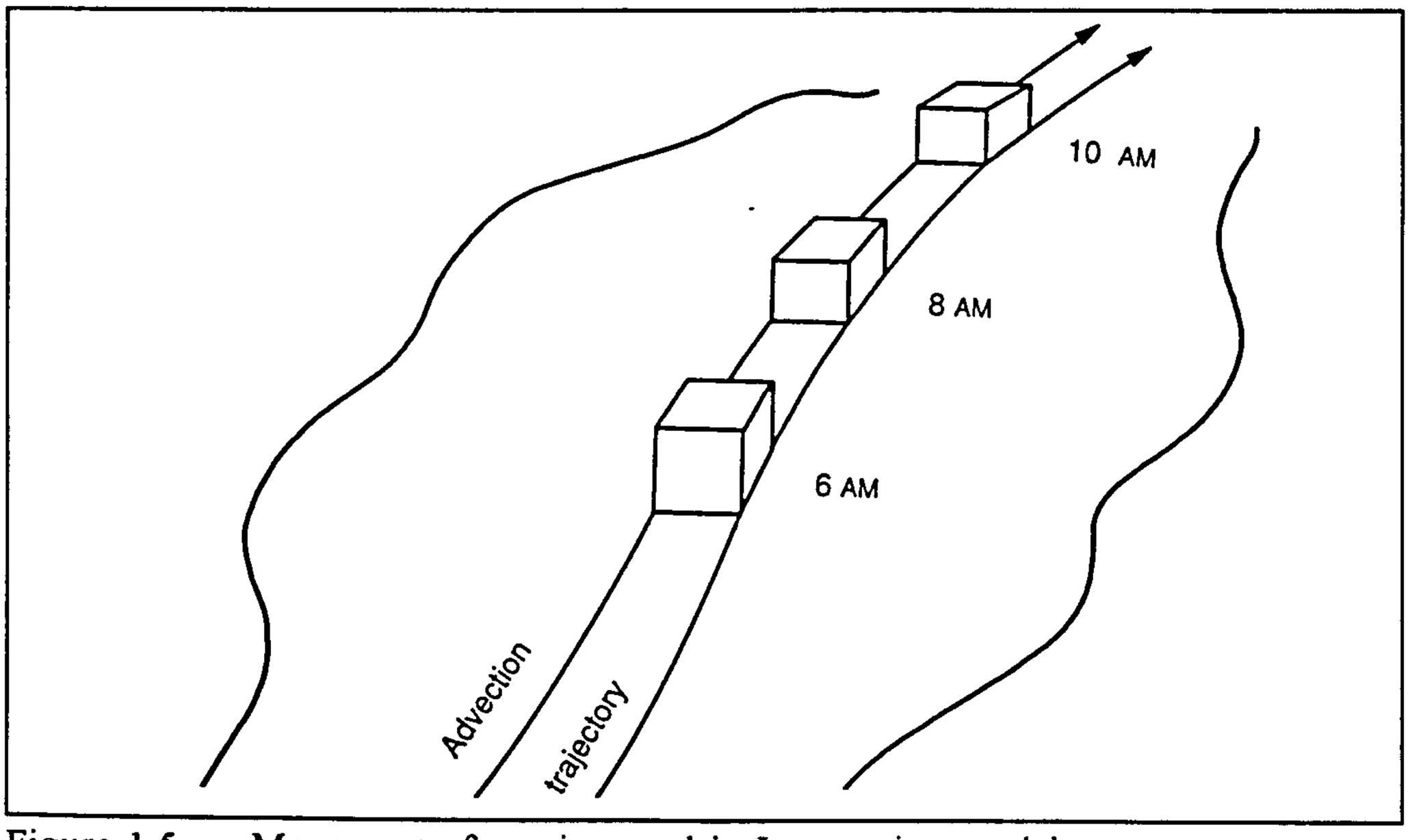

Figure 1.5 Movement of an air parcel in Lagrangian model

This type of model is obviously simplistic, and does not require detailed meteorological or emission data, needs little computational power, and has low spatial resolution. They also require the assumption of rapid mixing of species relative to their lifetimes and also that source emissions are uniform over the whole box area. This therefore produces crude results, but is ideal for a 'first look' at a particular system. However, if the system requires modelling over a longer time period it is necessary to include such effects as diurnal changes in emission rates, photolysis rates and other processes, and also may need a greater spatial resolution. This can be obtained by adding more dimensions, and including more complex processes, but at the cost of greater computer power, and perhaps of a reduction in the detailed chemistry.

1.3.1.ii) One-dimensional models

One-dimensional models allow the calculation of the concentration of chemical species concentrations as a function of both time and a spatial dimension. They are generally a series of box models placed on top of one another (i.e. Fletcher 1991) The boxes can either have equal depth or have thinner layers nearer the ground, as at these altitudes the changes occur more rapidly.

In 1D models it is necessary to set the initial conditions for each of the layers. The model then represents the conditions within each of the layers, and also the vertical transport between the layers. This is shown in Figure 1.6. The advection term is usually omitted if the conditions within the box are representative of conditions over global or very large regions. However, over small areas, it is necessary to include this term. Time dependent models follow the changes in concentration of a species over time, and are ideal for studies over short time scales. The simpler time-independent models are run for a specific set of conditions where the time is set at zero. This gives the eventual result of a permanent change in conditions, and is therefore ideal for assessing changes over long time scales.

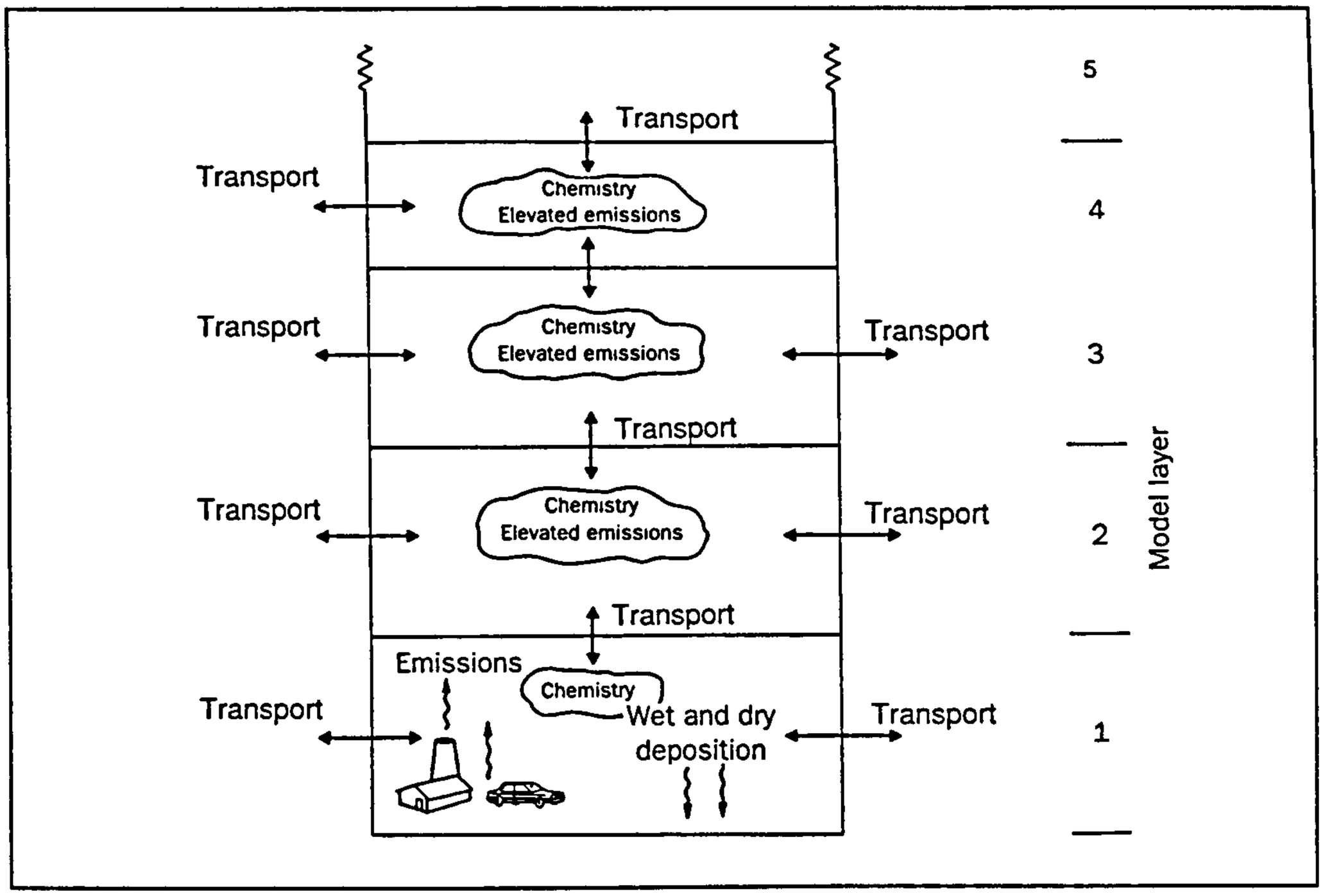

Figure 1.6 Features of 1D model of atmospheric chemistry

1.3.1.iii) Two-dimensional models

Two-dimensional models can simulate the atmosphere in terms of both height and downwind directions. They can also be used in the study of systems on a global scale, where one dimension is altitude, the other being latitude. 2D studies require the assumption that the variation in emissions over longit.ude is much less than over latitude. However, this is particularly invalid at low altitudes, where the variation in surface source emissions is large. 2D models are therefore mostly used for studies of the stratosphere.

1.3.1.iv) Three-dimensional models

The most complex, and computationally challenging models are those which replicate atmospheric conditions over three dimensions. These often have a reduced chemical complexity, due to the high power required to solve the equations for transport processes. The most common 3D models in use are general circulation models (GCMs), which simulate global weather and climate. Only with the advent of greater

computer power will GCMs be able to be coupled successfully with chemical models. For more detail on these and other models the reader is referred to Trenberth (1992) and Graedel & Crutzen (1993).

1.4 This Work

In the current work a number of experimental and modelling techniques have been employed to investigate sources and atmospheric chemistry of the nitrogen oxides, NO, NO_2 and N_2O. Laboratory studies of the mechanisms of formation of these species from electrical discharges through air have been carried out, and the results used in the estimation of their global production rates from lightning. A study of the global distribution of NO_x from this source is also undertaken.

A simple mathematical model was developed which predicts the future emissions of N_2O from one of its most important anthropogenic sources - the application of nitrogenous fertiliser to soils.

Analysis of the atmospheric chemistry in which NO_x is involved has been carried out using a 1D Eulerian 10-layer photochemical model. The effects of short and long term perturbations to this chemistry, through changing emissions of key atmospheric species and altering physical parameters within the model, has been investigated.

Chapter Two

Experimental and Mathematical Methods

2.1 Introduction

The formation of nitrous oxide and other oxides of nitrogen as a result of a discharge through air was studied using three detection methods. N_2O production was analysed using gas chromatography with electron capture detection while the formation of NO was investigated using both chemiluminescent and tunable diode laser spectroscopic techniques.

The effects of varying pressure and discharge length on the production of the oxides in air with both single and multiple discharges were investigated. Discharges through mixtures of nitrogen and NO or NO_2 were also carried out in an attempt to unravel the chemistry of oxide formation.

The experimental results were used to predict the global significance of NO_x production by lightning, and combined with an analysis of future nitrogen oxide emissions to produce global emission inventories (see Chapter 4). This was combined with more general chemical modelling of the free troposphere to investigate the impact of nitrogen oxides on the overall chemistry in Chapter 5.

2.2 Experimental Apparatus: System Development

The discharge system consisted of a vacuum line for gas manipulation, and a reaction cell into which a discharge was applied via two electrodes attached to a high voltage power supply. The system was designed for cell pressures of between 0 and 1000

mbar at room temperature.

2.2.1 Vacuum Line

The vacuum line consisted of a glass manifold to which a series of greaseless cone and ball and socket fittings were attached. To these were connected mixing and sample bulbs, pressure gauges and gas cylinders, with Teflon taps (Young's SPOR) being used throughout. The manifold was wrapped in nichrome electrical wire, which heated the glass to prevent less volatile gases from sticking to the internal walls.

The vacuum line was pumped using an oil diffusion pump (Edwards E02) backed by a two-stage rotary pump (Edwards 2S0 50B). These were connected to the line via a glass liquid nitrogen-cooled cryogenic trap, to freeze out condensable gases. The vacuum was measured using an Edwards Pirani 11 gauge (range < $1x10^{-3}$ - 1 mbar) and the pressure in other parts of the line was monitored with pressure transducers (TransInstruments; BHL-4200 head, BHL-1420 controller).

Gases were introduced into the manifold via cylinders or lecture bottles through steel or copper tubing and brass needle valves. Zero grade air and nitrogen were admitted directly into the discharge cell, but other gases were thoroughly degassed in sample bulbs using repeat freeze-thaw cycles to remove unwanted impurities. This was carried out using cold fingers attached to the bulbs and cooled with liquid nitrogen or CO_2/acetone mixtures. Gas mixtures were made by admitting the components into a 5 dm^3 mixing bulb and allowing at least 20 minutes for mixing. The mixtures were then expanded into the reaction cell.

2.2.2 Reaction Cell

The cell was a 250 cm^3 glass sphere, with 2 optically flat windows glued to each side and is shown in Figure 2.1. Two tungsten cylindrical electrodes (diameter 2 mm) were supported in the cell through greaseless ground glass sockets by teflon bungs. These bungs had double O-ring seals both externally and internally to create a good

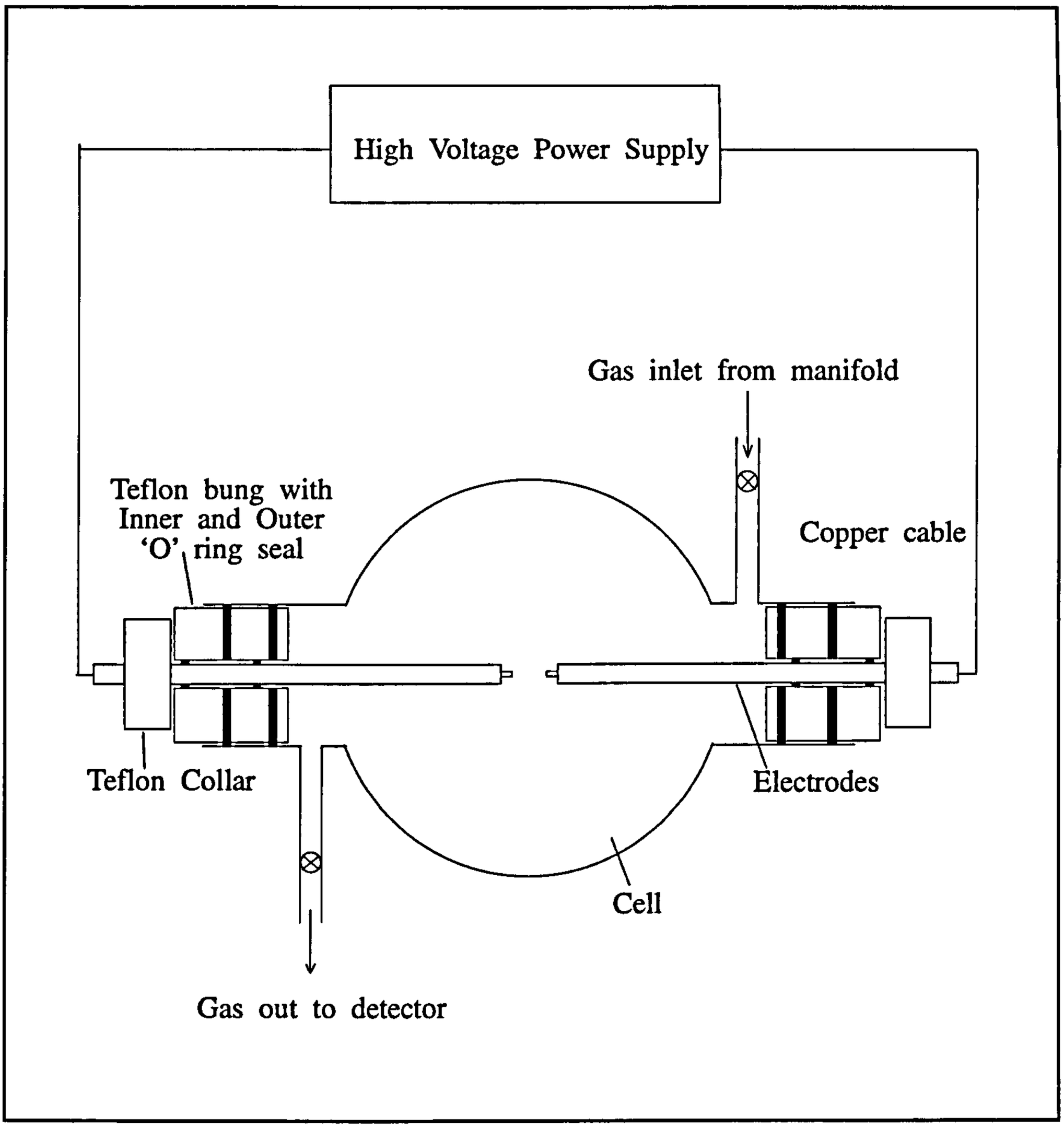

Figure 2.1 Schematic of Discharge Cell

vacuum, whilst allowing removal of them or the electrodes if necessary.

The electrodes were ground to a tip of 1 mm inside the cell and at the other end were attached to the power supply by means of insulated copper cables, of short length and large cross sectional area (40 mm^2), to minimise resistance in the circuit. Teflon collars prevented the electrodes being sucked into the cell by the vacuum, and maintained the spark gap at a constant distance.

2.2.3 Power Supply

A high voltage power supply was especially designed to produce a spark at the breakdown voltage of the gas. A 15 kV transformer was used to charge two 1 μF capacitors, which were connected to the electrodes via copper cables. The capacitors were charged until the breakdown voltage of the gas was reached, when a spark would pass across the gap. A voltmeter displayed the voltage at the time of the spark.

2.2.4 Materials

The table shows the gases used in the experiments, along with purity and supplier for each.

Gas	Purity	Supplier
Air (21% O_2, 79% N_2)	Zero Grade (99.999%)	BOC
Ar (carrier gas)	Zero Grade (99.998%)	BOC
N_2	Zero Grade (99.998%)	BOC
N_2O	99%	Matheson
NO	98.5%	Aldrich
NO_2	99.5%	Matheson
CCl_2F_2	99.5%	BDH

2.3 Detection Of N_2O - Gas Chromatography with electron capture detector

Gas chromatography (gc) fitted with an electron capture detector (ecd) was used to detect the presence of nitrous oxide in the gas mixture. This method is ideal for the separation and quantification of the components in a gas sample. The gas is passed by means of a carrier gas (in this case argon) through a long narrow column, packed

with a suitable adsorbent (Poropak Q) for the species under analysis. The difference in adsorption of each of the components leads to a different elution rate at the end of the column, which is monitored by a detector and output as a signal in the form of clearly defined peaks. Each component, under identical conditions of column temperature, carrier gas flow rate and column size and packing, will have the same elution rate, allowing qualitative determinations, and measurement of the peak height or area relative to a reference will give the amount of component in the sample.

The most suitable detector for nitrous oxide is electron capture, which is highly sensitive to electronegative species, and will detect N_2O at the low levels expected in the experiments. The principle of this method lies in the use of a beta radiation source (^{63}Ni), which emits particles that react with highly electronegative species passing through the source. The source is placed between two electrodes at a potential of 10^3 V and the carrier gas passed through the column into the detector. Argon is used as it absorbs beta rays forming secondary electrons and metastable ions. This sets up a standing current between the electrodes.

$$Ar \rightarrow Ar^+ + e$$

When an electronegative species passes through the detector, it 'captures' the electrons and reduces the standing current. This gives a signal proportional to the amount of the species, which is output via screen or chart recorder as a peak. In this case the peak area was used to determine the quantity of N_2O in a sample, as it was the least sensitive to changes in column temperature or carrier gas flow rate, which were both found to fluctuate by ±5 % on a daily basis.

2.3.1 System Optimisation

The optimum conditions for detection of N_2O in a sample of zero grade air using a gc-ecd (PYE GCD) were investigated, including methods of introducing the gas to the column and physical conditions of detector operation, such as carrier gas flow, column and detector temperature, detector current and attenuation. Zero grade air was

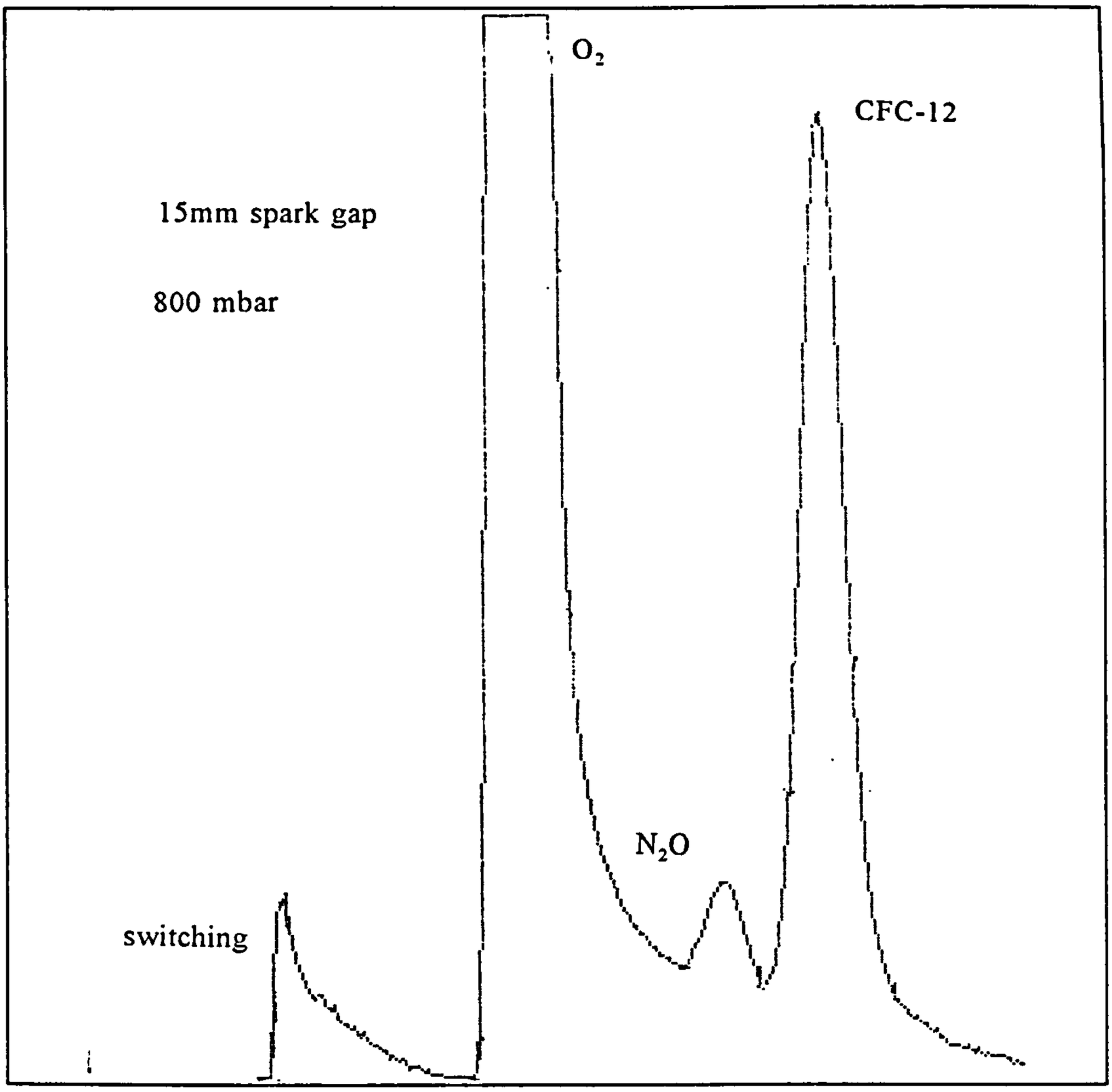

Figure 2.2 . Gc-ecd output for a sample of zero grade air

purified to remove CO_2, water and other trace species, but components such as oxygen and Freons, which are still present in the air, can be readily detected by electron capture. Therefore it was important to ensure that the nitrous oxide peak was clearly visible amongst other peaks.

2.3.1.i) Introduction of sample to the g.c.

The most effective method of introducing a gas to a column is via injection, which gives sharper peaks and minimises peak tailing. In a sample of zero air prior to discharge, three peaks were obtained and these are shown in Figure 2.2. The first relatively large peak was due to oxygen in the gas mixture, the second was identified

as N_2O and the third as a Freon, both lying on the tail of the first. Therefore the size of sample introduced was important as it had to be large enough to detect nitrous oxide, but not so large as to produce enhanced O_2 peak tailing which would obscure the N_2O.

The methods investigated for introduction of the gas to the detector were injection with syringe and flushing the gas through a sample loop. Both were carried out using a cryogenic freeze down technique and at room temperature.

In one series of experiments, withdrawing the discharged gas from the cell with a gas-tight syringe led to a number of problems. The discharge takes place in a cell of small volume and at pressures below atmospheric; therefore the pressure in the syringe was always sub-ambient. This appeared to draw in air from the laboratory which led to wide scatter in the peak areas obtained. To try and alleviate this argon was also added to top up the pressure to over atmospheric, but this served to dilute the sample and N_2O was not detected.

In a second series of experiments, a cryogenic method was employed to concentrate the N_2O and remove the interference from the oxygen peak. The air in the cell was expanded into a sample loop cooled to 77K with liquid nitrogen, passed through the loop for a constant time and then pumped to vacuum to remove nitrogen and oxygen. The remaining mixture was thawed, topped up with argon and withdrawn from the loop with the syringe. This again showed inconsistencies in the peaks, indicating that either a variable amount of N_2O was being frozen down or that the syringe method was inappropriate in this instance.

Continuing with the same cryogenic principle, the freeze-thawed mixture was instead flushed into the column with the carrier gas by means of a two-way tap. This showed that the freeze-down was not trapping a constant amount of nitrous oxide, and that some oxygen was also being trapped. Therefore a straightforward room temperature method was employed, whereby a constant amount of gas was expanded from the cell into the sample loop and flushed into the column for a set time (to avoid tailing

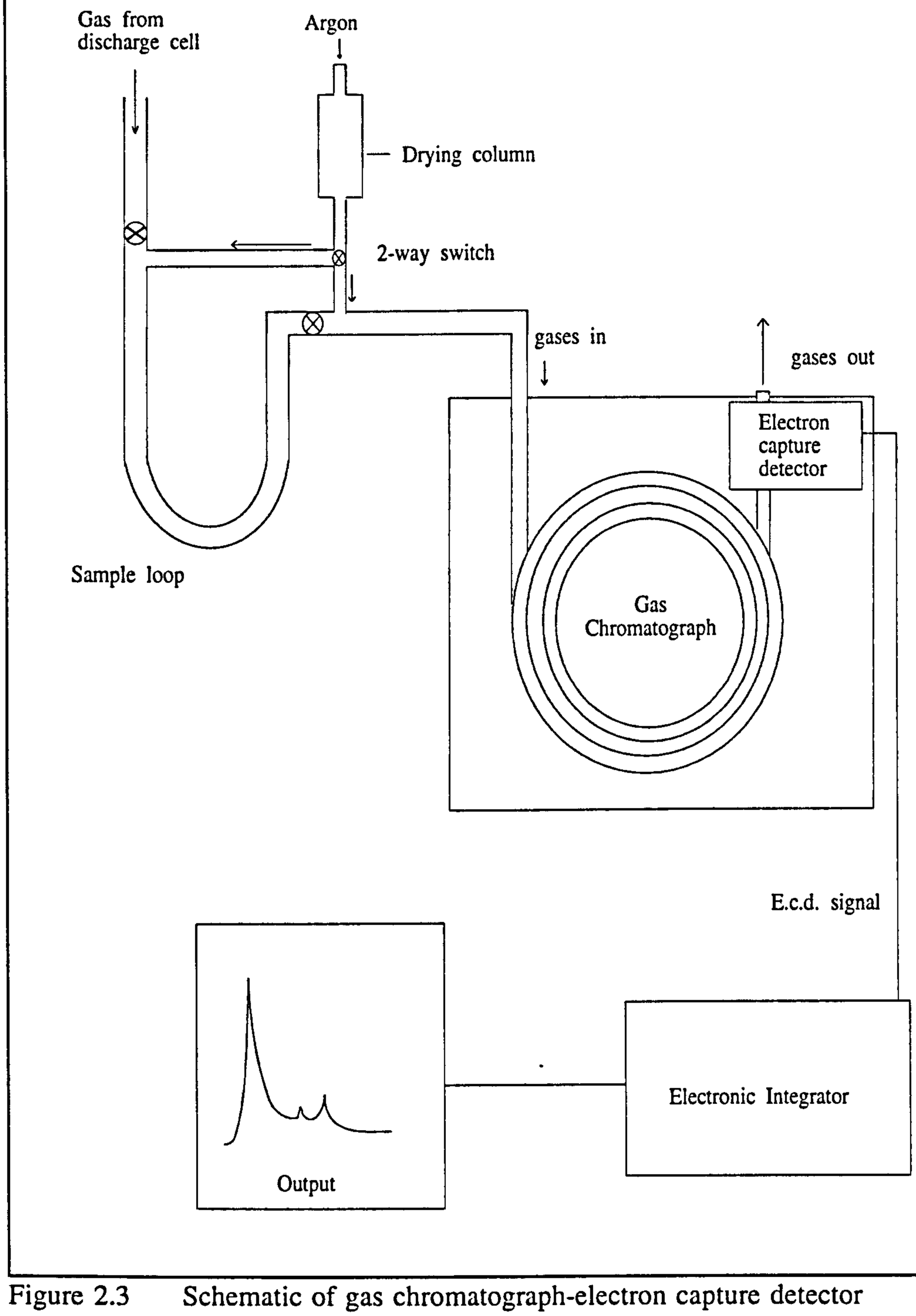

Figure 2.3 Schematic of gas chromatograph-electron capture detector

from gas trapped in sidearms of the loop). Flushing 150 mbar of gas for 30 seconds was found to give detectable and distinct peaks with minimum tailing. A schematic of the experimental set-up is given in Figure 2.3.

2.3.1.ii) Gc-ecd operating conditions

The operating conditions for the gc-ecd were varied to investigate those most suitable for the system. These were detector temperature, column length and temperature, carrier gas flow rate and standing current.

The best results were achieved using a glass column, ⅛" i.d. x 2m, packed with Poropak Q and maintained at a temperature of 43 (± 2)^{0}C. Argon was the carrier gas at a flow rate of 30 (±1) ml min^{-1} through the column, and the detector was held at 350^{0}C. The output signal from the detector was monitored by a TRIO electronic integrator, and the peak area used to quantify the amount of each component.

2.3.1.iii) Calibration

The appropriate gas mixture was admitted to both the cell and sample loop at the required pressure, the cell closed off, and 150 mbar of the blank gas mixture flushed for 30 seconds through the sample loop into the gas chromatograph. This was in order to assess the size of the corresponding N_2O peak for measurement of calibrations and experimental results. The blanks were also useful for detecting any major fluctuations in ecd output caused by changes in column temperature, carrier flow rate or ecd current.

After the blank had been recorded as a gc trace, the mixture in the cell was subjected to discharge and 150 mbar of this then flushed through the sample loop and into the gc as before. Each experiment was repeated at least 3 times to obtain a reasonable average and the breakdown voltage of each flash recorded in order to calculate the corresponding energy and hence the N_2O J^{-1} values. The effect of the action of the flash on the components of the gas can be seen in the trace in Figure 2.4: an increase in N_2O (2nd peak) is observed compared to Figure 2.2 along with a decrease in the CFC peak. This is believed to be due to the photolysis of the Freon during the flash.

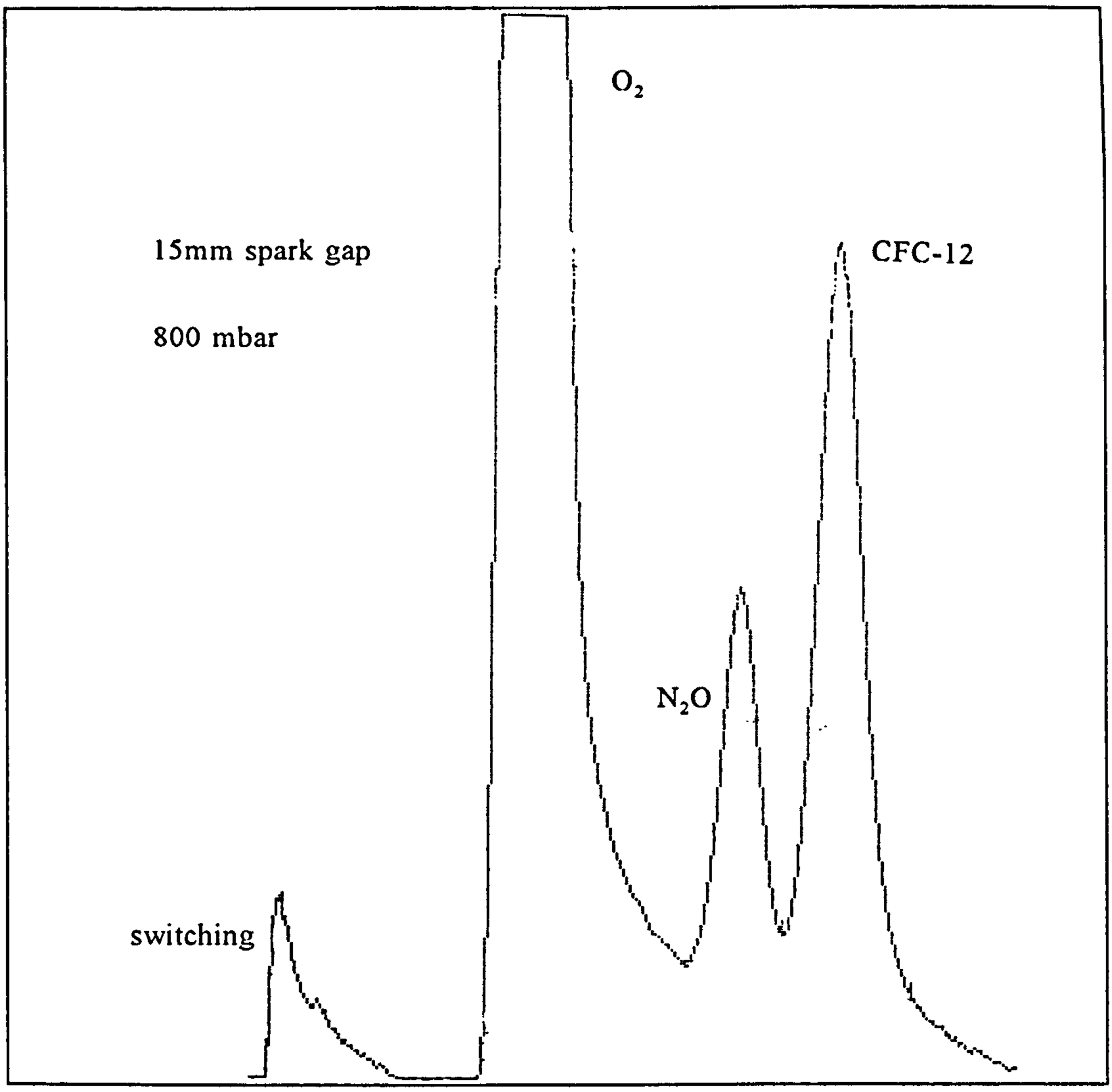

Figure 2.4 Effect of the flash upon a sample of zero air

The relatively small size of the N_2O peak in the blank (Fig 2.2) indicates the large potential errors present in the measurement of the peak size. Therefore it was important to use the most accurate measurement of peak size. Calibrations were carried out with mixtures of 0 - 1 ppm N_2O in zero air and the height and area plots compared. Both analyses gave a curved plot, the area curve fitting best to a squared polynomial equation. This is shown in Figure 2.5. Extrapolation back to the y-intercept gives the value of the background concentration of N_2O in the zero air, which is approximately 310 ppb. The area plot produces a concentration of 290 ppb, whereas the height plot gives a concentration of 190 ppb. Also, a distribution of the peak areas of the blanks (Figure 2.6) shows a normal distribution, indicating that any external factors did not influence the measurement of peak area significantly, and that

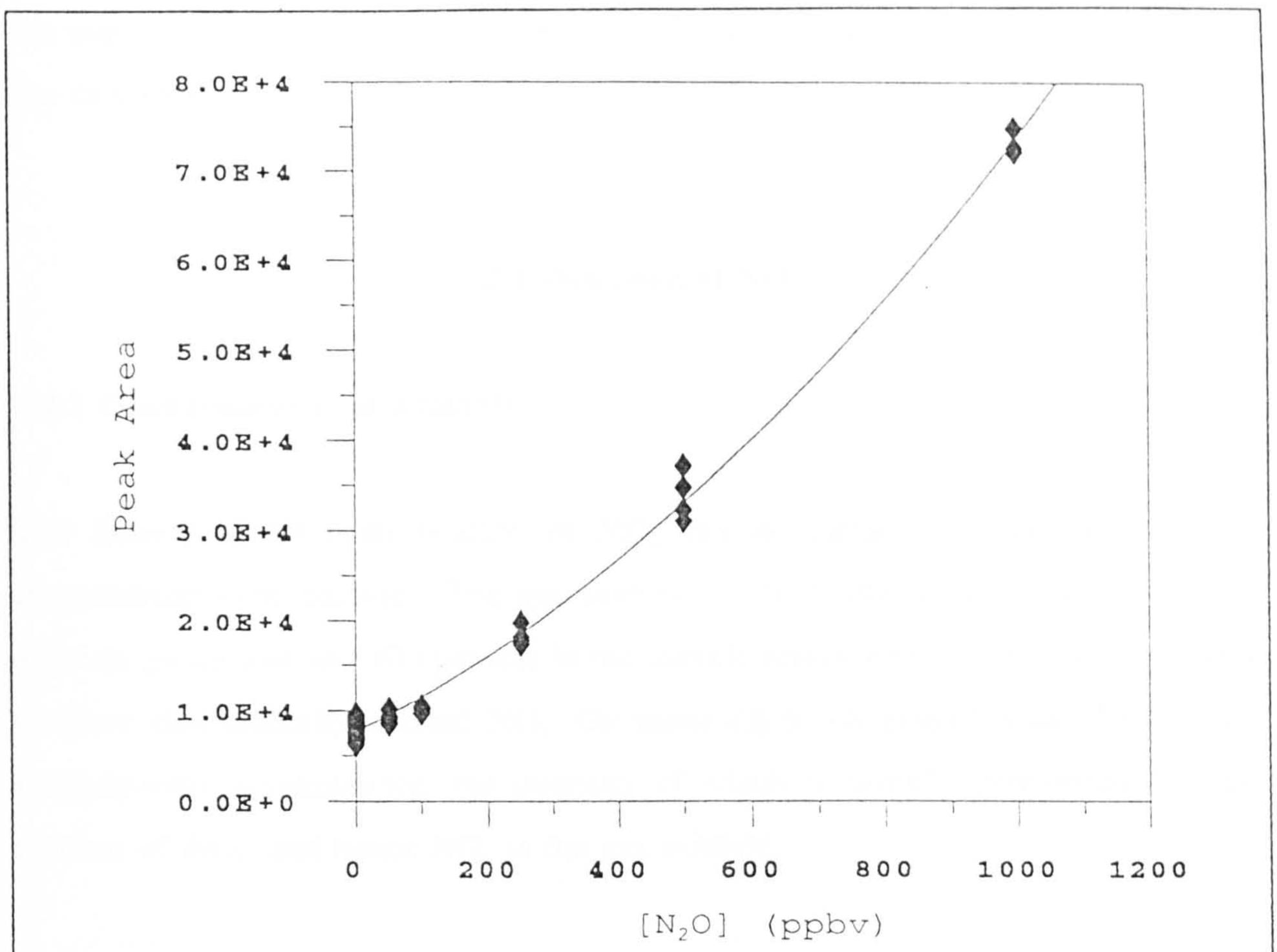

Figure 2.5 Calibration for N_2O peak area

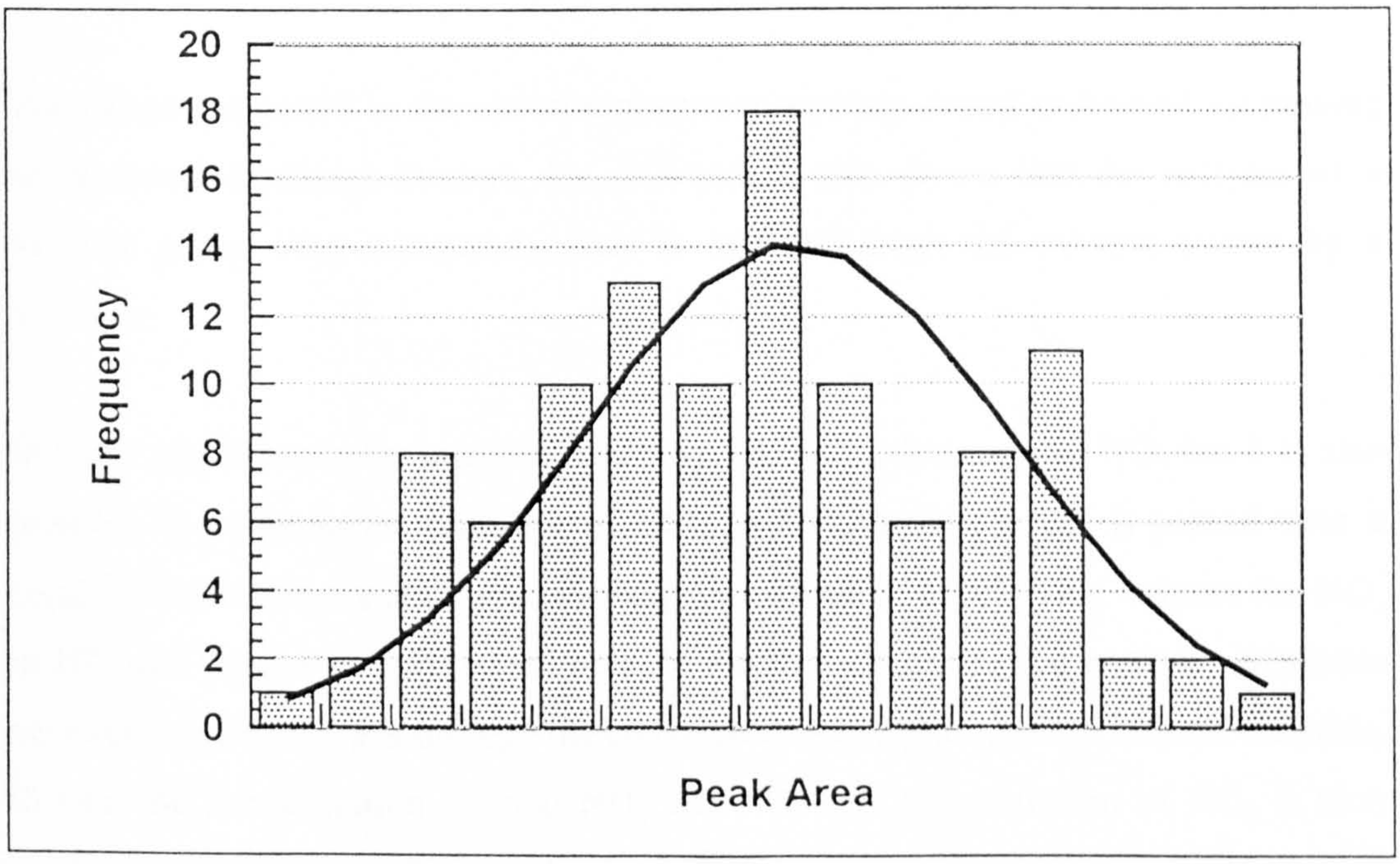

Figure 2.6 Distribution of N_2O peak area for blank samples of zero air

the use of this method was the most valid. Therefore the peak areas were used for the calculation of N_2O concentrations.

2.4 Detection of NO

2.4.1 Chemiluminescent Analysis

The detection and quantification of NO_x can be carried out by the use of a chemiluminescent analyser. The gas sample is drawn into a reaction chamber by vacuum pump and any NO present in the sample reacts with an excess of ozone to produce electronically excited NO_2. On returning to its ground state, NO_2^* emits characteristic luminescence, the intensity of which is directly proportional to the amount of NO_2, and hence NO, in the gas mixture.

The chemiluminescence is detected by a photomultiplier tube and the signal sent to a data logger/display via electronic data processing, where it is output as a peak. The amount of NO can then be measured from either peak height or area. A schematic of the chemiluminescence set-up is given in Figure 2.7.

The ozone generated in the chemiluminescent reaction vessel is formed by passing an electrical discharge through dry air which is also drawn into the analyser by a vacuum pump. Any unreacted ozone is removed from the exhaust stream by a scrubber.

In these experiments the analyser was only set up for detection of NO, but it is also possible to examine the presence of NO_2. In NO_2 mode the gas is passed over a catalytic converter containing a molybdenum screen at 625K. This reduces the NO_2 to NO and the gas is then passed into the reaction chamber. The analyser alternates between sending the gas through the converter and straight into the reaction chamber, to find the concentration of total NO_x and NO. The concentration of NO_2 is then worked out to be the difference between the two.

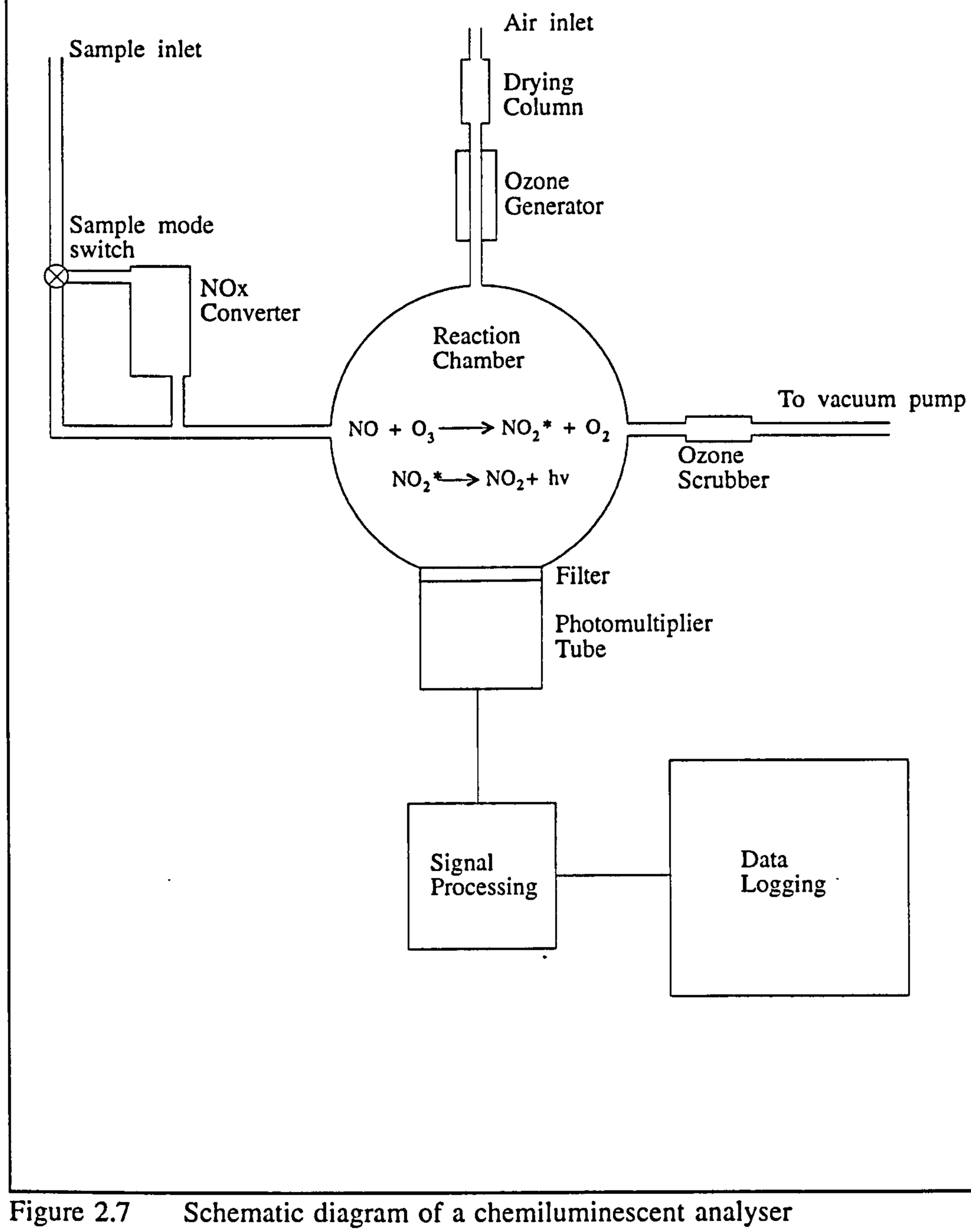

Figure 2.7 Schematic diagram of a chemiluminescent analyser

The analysis of NO in these experiments was carried out using a ThermoElectron model 14B/E (10ppm full scale). The discharge equipment was set up exactly as for the gas chromatography work. It was not possible to connect the cell directly to the

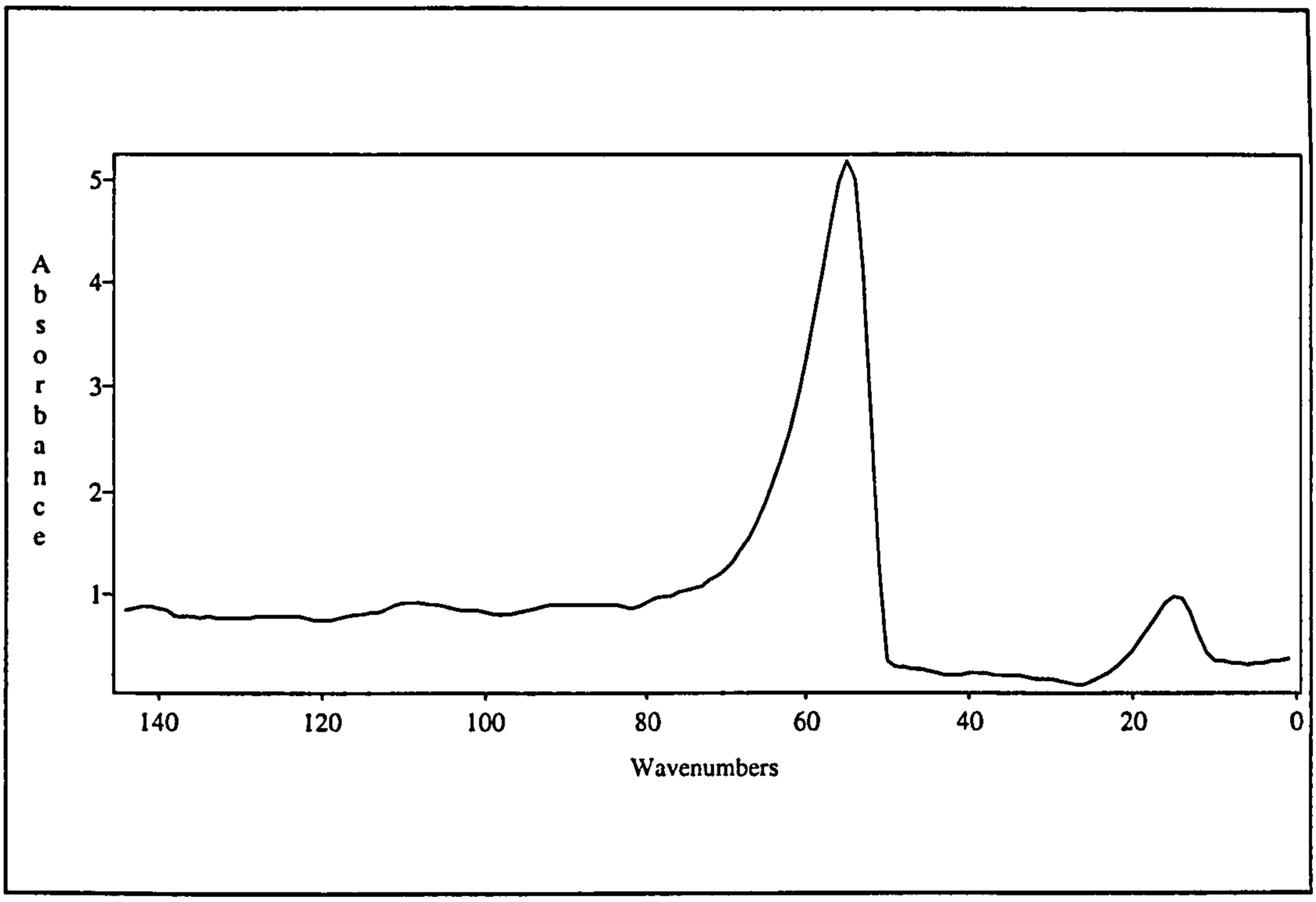

Figure 2.8 Chemiluminescent output. Right hand peak is pressure peak, left hand peak is NO

analyser, so the discharged gas samples were expanded from the reaction cell into another 250 cm^3 glass cell, and the contents transferred to a sample loop attached to the analyser inlet. A constant pressure of sample was flushed through the analyser with argon, at a flow rate of 280 ml min^{-1}. The signal was output to a Viglen PC, via a data processing unit, and analysis was carried out using a software package on the same PC.

The normal operational mode of the analyser is a continuous sample flow, with changes in the NO concentration being shown as perturbations in the output signal. In this case the experiments were performed on static samples which were transferred to the analyser via a sample loop arrangement, as indicated earlier, where the carrier flow is switched through the loop. This gives a pressure differential, which is output as a peak on the baseline signal. To avoid possible interference with the NO signal the carrier gas is therefore diverted into the closed loop until it reaches operating pressure. Once the pressure peak has been output, the loop is fully opened and the corresponding NO signal obtained (see Figure 2.8).

2.4.1.i) Calibration

In each experiment, the required pressure of zero grade air was admitted to the flash cell, a discharge passed, and the gas let into a sample loop. 170 mbar of the gas was flushed into the chemiluminescent detector using argon carrier gas at a flow rate of 280 ml min^{-1}. The corresponding NO peak was recorded and output onto the PC. It was unnecessary to record a blank for each experiment, as the concentration of NO in zero grade air is below the detection limit of the chemiluminescent analyser.

As explained in Section 2.4.1, upon flushing the sample into the detector, a pressure peak was obtained in the output signal, which interfered with the NO peak. To rectify this, the carrier gas was admitted to the closed loop containing the sample and the pressure allowed to attain that in the flow line. Once this was achieved, and the pressure peak had been displayed, the sample was flushed into the detector, and the peak obtained was then due to NO only.

The gas was flushed through the detector for up to 10 minutes, depending on the speed at which the peak returned to the baseline. For higher concentrations, the peak never quite returned to the baseline, due to NO trapped in the side arms of the glassware bleeding slowly into the detector. When the sample loop was closed off to the detector however, the baseline returned to zero.

Two scales were used for the measurements - 0.05 ppm for single flash studies, and 2 ppm for multiple flashes, where the NO formed is much higher. The NO peak heights were analysed quantitatively using a PC integration package (WINFIRST) and the concentration of NO obtained from the calibrations. These were carried out using 0 - 100 ppm NO in N_2 and the corresponding plots are given in Figures 2.9(a) and 2.9(b).

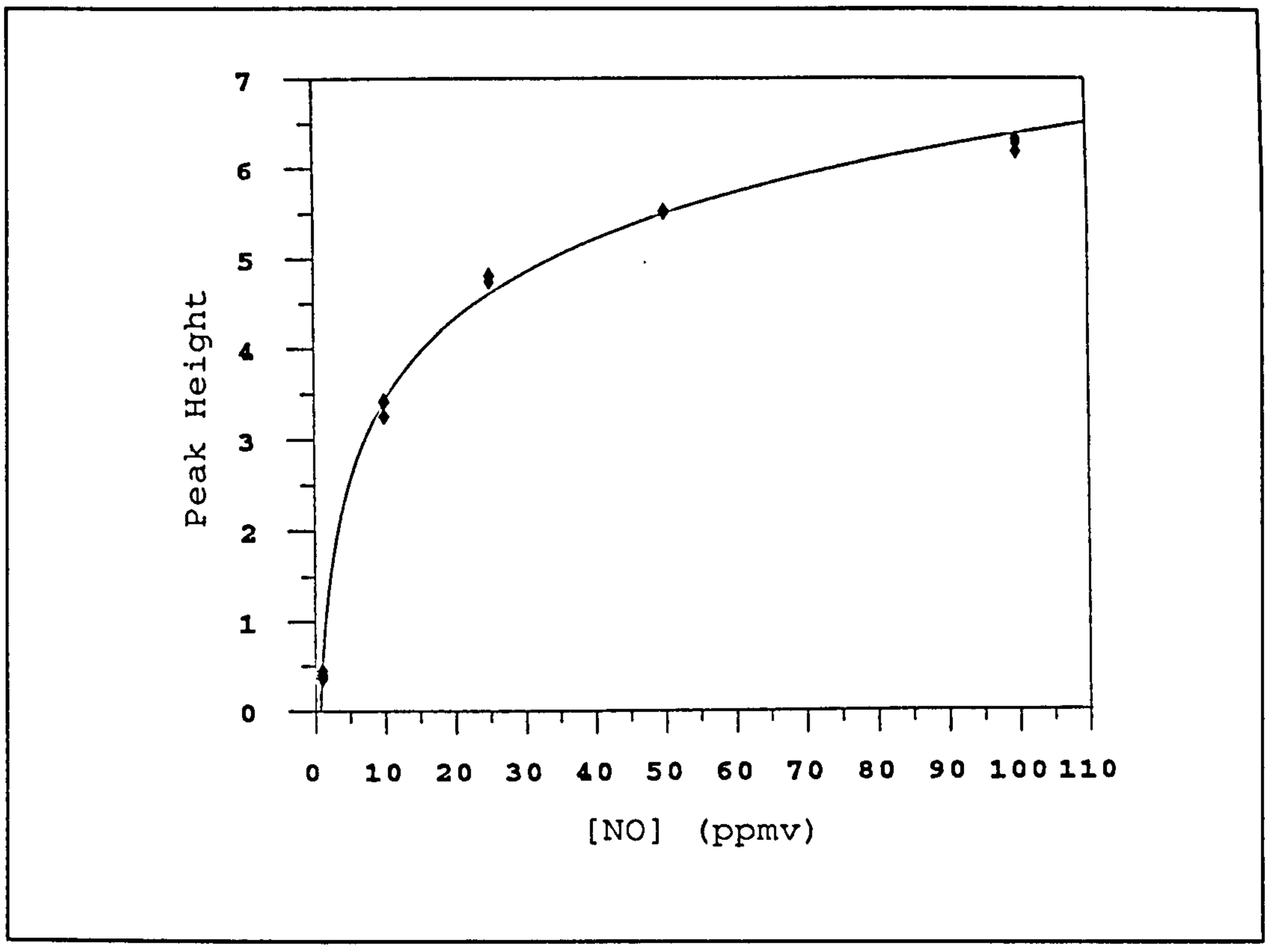

Figure 2.9(a) Calibration of NO using Chemiluminescent Detection (0.05ppm scale)

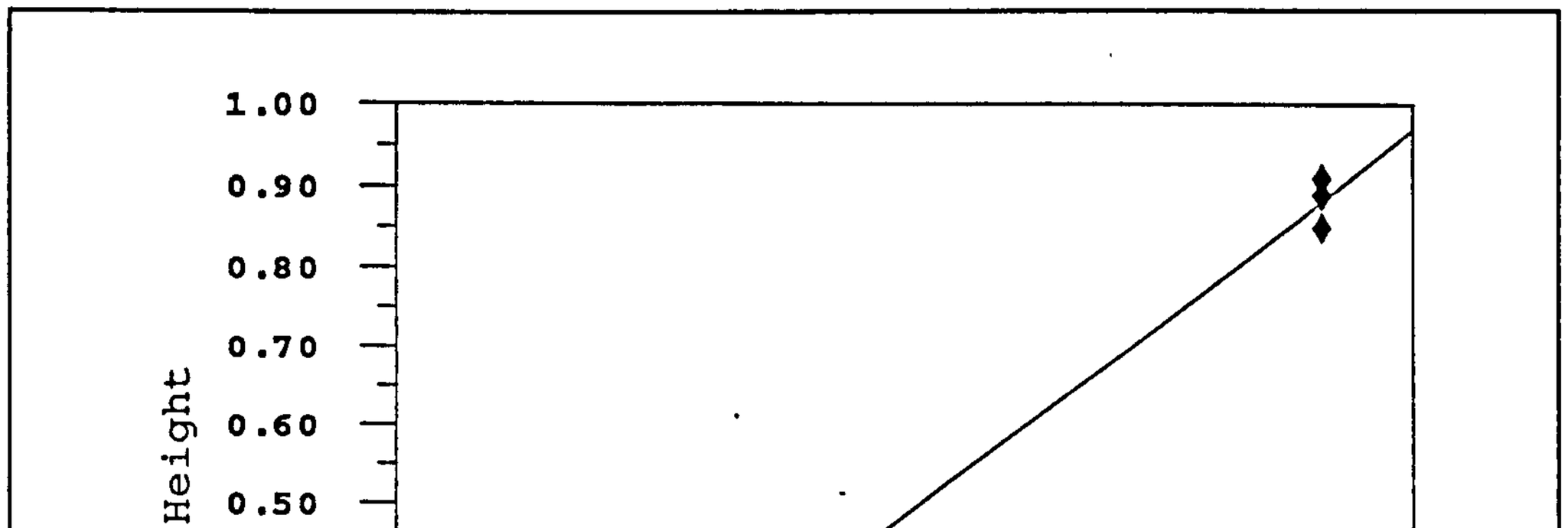

Figure 2.9(b) Calibration of NO using Chemiluminescent Detection (2ppm scale)

2.4.2 Tunable Diode Laser Spectroscopy (TDLS)

The nitrogen oxides N_2O, NO and NO_2, have strong absorption in the mid-infra-red (MIR) region of the solar spectrum (3-30μ), a region where a large number of atmospheric trace gases have absorption features. Analysis of these gases at such low concentrations requires highly sensitive infra-red spectroscopy, such as Fourier Transform, and ultimately Tunable Diode Laser Spectroscopy (TDLS). Experiments to investigate the formation of the nitrogen oxides were carried out using TDLS equipment at the National Laboratories in Risø, Denmark.

2.4.2.i) Background

TDLS employs a semiconductor diode laser, which can be tuned to a specific wavelength and can scan the spectrum over a fraction of a wavenumber. The resolution obtainable can be of the order 10^{-4} cm^{-1}, leading to detection of rovibrational lines of individual molecules. This results in high specificity and sensitivity.

TDLS can monitor a variety of spectral bands depending on the type of diode employed. In the MIR region suitable diodes are made of lead salts alloyed with Group IV - VI elements, such as S, Sn, Se and Te. Application of a current across the p-n junction causes population inversion of the electrons from the valence band to the conduction band, and electron-hole recombination is the mechanism for the stimulated emission of radiation. The frequency of radiation depends upon the temperature and the current, and this allows tuning of the diode. Each diode can scan a range of around 100 cm^{-1}.

For analysis of a component in a gaseous sample, the appropriate wavelength of absorption (usually one of the strongest) is selected by altering the temperature of the diode, which is cooled by liquid helium. By changing the current through the diode the laser emission is passed through the sample scanning a range of 1-2 cm^{-1}. The absorption by the sample (A) is detected by the change in intensity of the beam

incident on the detector (P_0) relative to a reference (P), from which an intensity ratio can be determined. This is translated into an absorbance value (A) from the equation

$$A = - \ln P/P_0 \qquad (2.1)$$

Applying the Beer-Lambert law leads to

$$P/P_0 = e^{(- \sigma(\upsilon) N L)} \qquad (2.2)$$

where L is optical path length (cm), N is concentration of species (molecule cm^{-3}) and $\sigma(\upsilon)$ is the wavenumber dependent absorption cross-section (cm^2 $molecule^{-1}$). Thus the concentration of the species under analysis can be determined.

The gaseous sample is contained within a multi-path (White) cell, which is typically 1 m in length, and which contains reflective mirrors at each end. These are used to increase the effective path length by reflecting the laser beam through the sample a number of times. Path lengths of hundreds of metres can be achieved, which is essential for signal enhancement, as the sample is often held at low pressures, and therefore in low concentrations.

Low pressures and temperatures are necessary to reduce the effects of pressure broadening, which leads to the overlap of lines and thus reduces the selectivity of the method. At >100 Torr[1] (133 mbar) collisions of molecules can increase the linewidth from a potential 10^{-4} cm^{-1} to 0.1 cm^{-1}. Most experiments are carried out in the Voigt region (13-133 mbar), as at pressures of less than 13 mbar, where the pressure broadening is minimum, the concentration of the sample is often too low to detect.

[1]At 298K, 1 atm = 1013 mbar = 760 Torr = 2.46×10^{19} molecules cm^{-3}

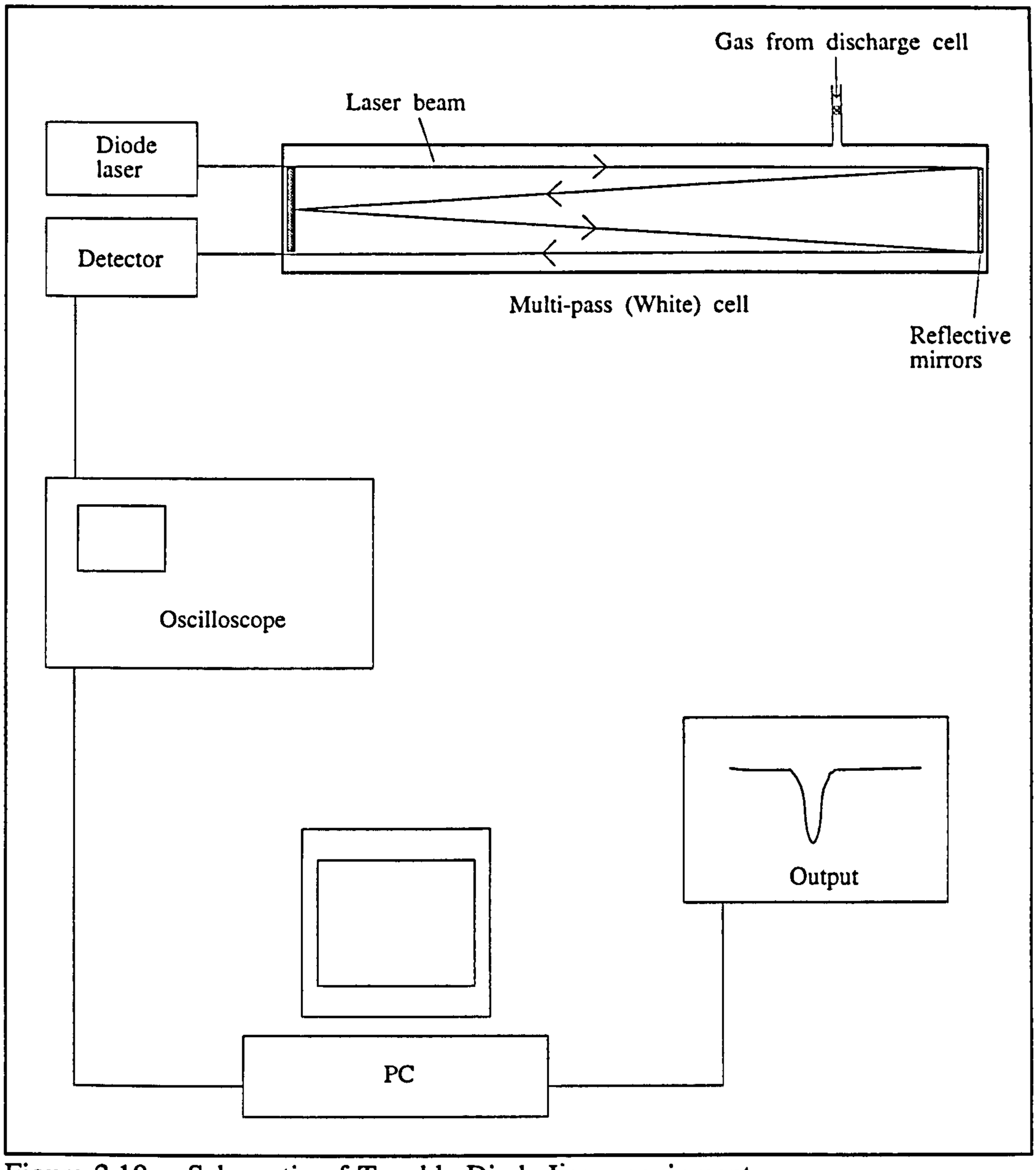

Figure 2.10 Schematic of Tunable Diode Laser equipment

2.4.2.ii) Experimental Work

In this work, the discharge apparatus described earlier in the text was connected to a stainless steel manifold via a glass-to-metal ferrule, which itself was attached to a White cell, of length 1 m and volume 15 litres. All gases were administered through stainless steel taps, and the cell was capable of producing path lengths of up to 40 m (see Figure 2.10). A fixed spark gap of 12 mm was used for all experiments, which were carried out at room temperature, and at pressures from 300 to 1000 mbar.

The air used was made up in the discharge cell from 21% O_2 and 79%N_2, both of purity 99.999%.

In this work it was necessary to work at <10 Torr (< 13.3 mbar), due to the expansion ratio from the 250 cm^3 discharge cell to the 15 l White cell. This gave very sharp absorbance peaks, but caused problems in the detection of some of the species. These are detailed in Section 3.2.

After discharge a constant pressure of gas mixture was expanded into the White cell. This was necessary to avoid changes in the absorbance due to pressure broadening. The gas was scanned over 1-2 cm^{-1} with the beam from the appropriate lead salt diode. Separate diodes were used for each of the oxides due to differences in their absorption spectra; NO at 1900 cm^{-1}, N_2O and NO_2 at 600 cm^{-1}. Each experiment was therefore repeated to allow analysis of all the oxides.

Pathlengths of between 8 and 40 m were used depending on the concentrations and line strengths of the species under analysis, and the power of the laser at the particular wavelength. A Ge-Cu detector received the output laser signal, which was modulated on a LeCroy oscilloscope. The intensity/wavenumber spectra were displayed by an IBM PC which also calculated the absorbances compared to a reference sample. References were taken at regular intervals to maintain the accuracy of the technique.

2.4.2.iii) Calibration

Mixtures of 21% O_2 and 79% N_2 were admitted to the flash cell, a discharge passed and the gas expanded into the White Cell to a pressure of 5 mbar. The corresponding absorbance was then measured. Calibrations of NO in N_2 were carried out at concentrations of 0 to 1.5 x 10^{13} molecule cm^{-3}. The relationship between concentration and absorbance over this range was shown to be linear and is displayed in Figure 2.11.

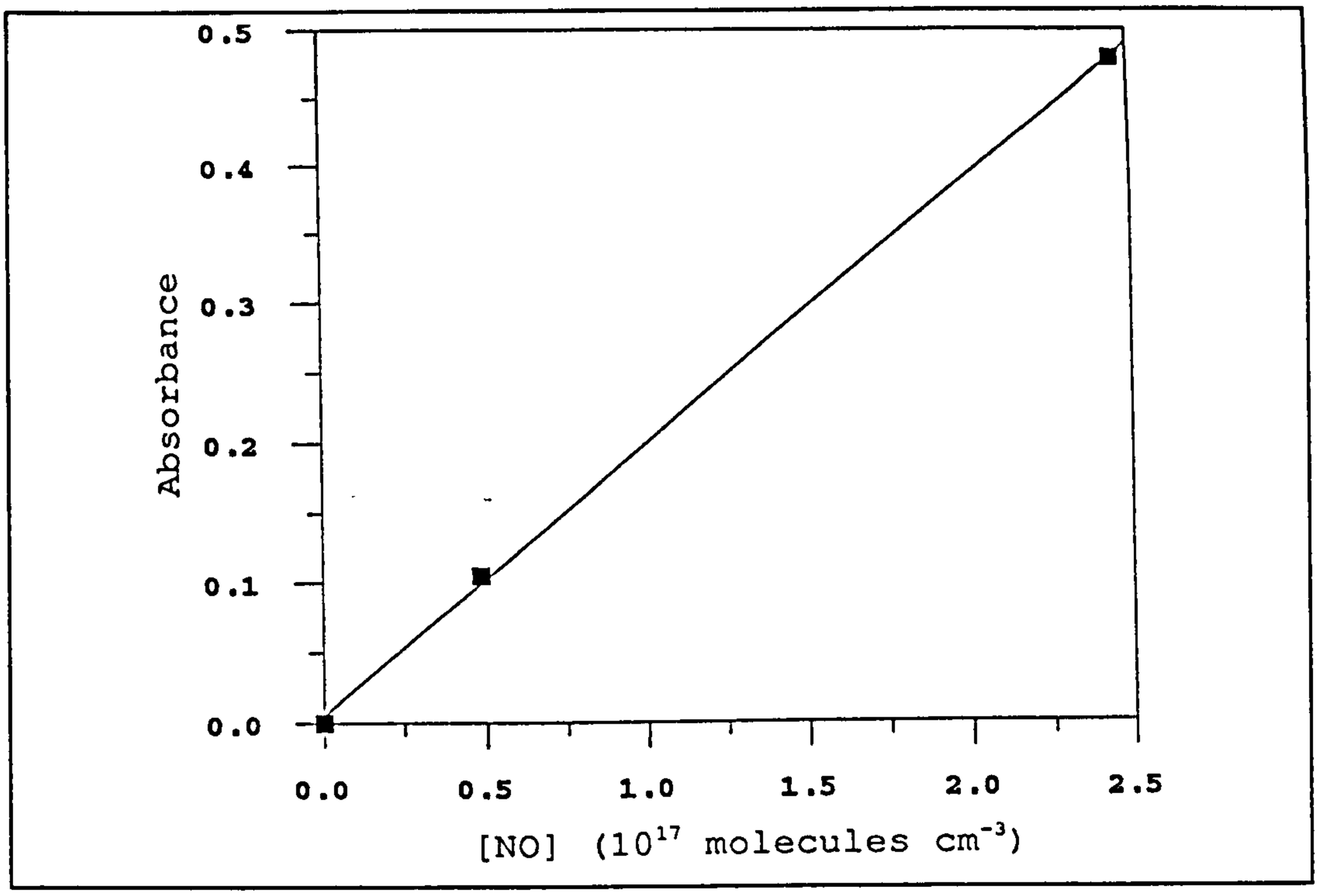

Figure 2.11 Calibration of NO using TDLS Detection

2.5 Modelling Studies

Extensive modelling of the chemistry of the atmosphere has previously been carried out using the types of models described in Chapter 1. Much of this work has involved the study of urban/polluted environments, and not that of 'clean' chemistry, such as that of the marine and free tropospheres. The free troposphere is of interest for many reasons, including the chemistry of methane and other long lived organic species, and also in the analysis of the effects on the chemistry of lightning-generated species. In this work a 1-D model [Fletcher, 1989] has been employed for this purpose and a brief overview of this model and the general principles behind mathematical modelling is provided below; for more detail see Sanderson [1994].

A chemical model requires the input of a number of variables, most importantly a set of chemical reactions, the corresponding rate constants, and the initial concentrations of the individual species included in these reactions (see Figures 1.4 and 1.6). From this, the concentrations of the species change with time, as a result of the reactions

and the conditions under which the model is set (ie pollutant levels, meteorology, etc). To calculate this, the model translates the reaction scheme (and other processes, such as transport) into a set of coupled ordinary differential equations (ODEs), where the number of ODEs is equal to the number of individual species in the scheme. Solving the ODEs by integration over small time steps produces the concentrations of the species at a required times.

The concentrations of species change at different rates with time, and this is a problem, as the presence of species with fast changes in concentration require very short time steps for integrations, but this requires intensive computational time, and is often unnecessary during periods of slow concentration changes. If there are large differences in the rate coefficients, the model is described as stiff, and this corresponds to that used in this work.

To overcome this, the model uses a predictor-corrector method to solve the ODEs. The value of each of the steps is predicted by extrapolation of the results of previous steps and compared to the value obtained when it is used in an integration of the ODEs. The difference between the predictor value and the corrector value then determines whether the step size needs to be changed, which produces small integration steps during periods of fast change, and larger steps over more constant concentrations.

The 1-D model also uses this method for calculating the concentrations as a function of altitude, and to represent the transport of species vertically layer by layer. The photolysis rate constants are calculated as a function of altitude and solar zenith angle, thus allowing the model to be set in any latitude or season, and the temperature and pressure vary with altitude based upon the latitudinally dependent lapse rate.

Chapter Three

Experimental Results and Preliminary Discussion

3.1 Introduction

Lightning is believed to be a significant source of NO_x in the atmosphere and has been the subject of a large number of experimental and theoretical studies (Tuck, 1976; Chameides *et al*, 1977; Hill *et al*, 1980; Levine *et al*, 1981; Goldenbaum & Dickerson, 1993), as well as atmospheric measurements (Noxon, 1976; Drapcho *et al*, 1983; Franzblau & Popp, 1989). However, as explained in Chapter 1, the magnitude of this source and the mechanism of NO_x formation remain highly uncertain. Experimental studies are generally used to make global estimates of NO_x production, by multiplying the measured amount of NO_x formed per unit energy input and the estimated total global energy dissipation from lightning. The uncertainties in these parameters are demonstrated by the values obtained in previous studies, which vary by over two orders of magnitude (1.8 Tg(N) yr^{-1} - 220 Tg(N) yr^{-1}; see table 4.1, in Chapter 4). This is largely due to the variation in the assumed length of atmospheric discharges (10^3 - 10^4 m) and their energy dissipation per unit length 10^4 -10^5 J m^{-1} (Dawson, 1979). These can also differ from the values obtained in experimental studies, which adds to the uncertainties.

Harrison (1991) carried out laboratory experiments using electrical discharges of lengths between 4 and 20 mm through air, to determine the NO_x formation under a variety of different conditions, including alteration of the pressures, discharge lengths and composition of the air, as well as studying physical parameters such as the spectroscopy of discharges and shock front velocities. In a study by Stark *et al* (1995), in which these results were used, it was suggested that NO_x was formed by the Zel'dovich mechanism in the heated spark channel, as proposed by Hill (1980), and not at the shock front, which had been previously postulated (Chameides, 1979;

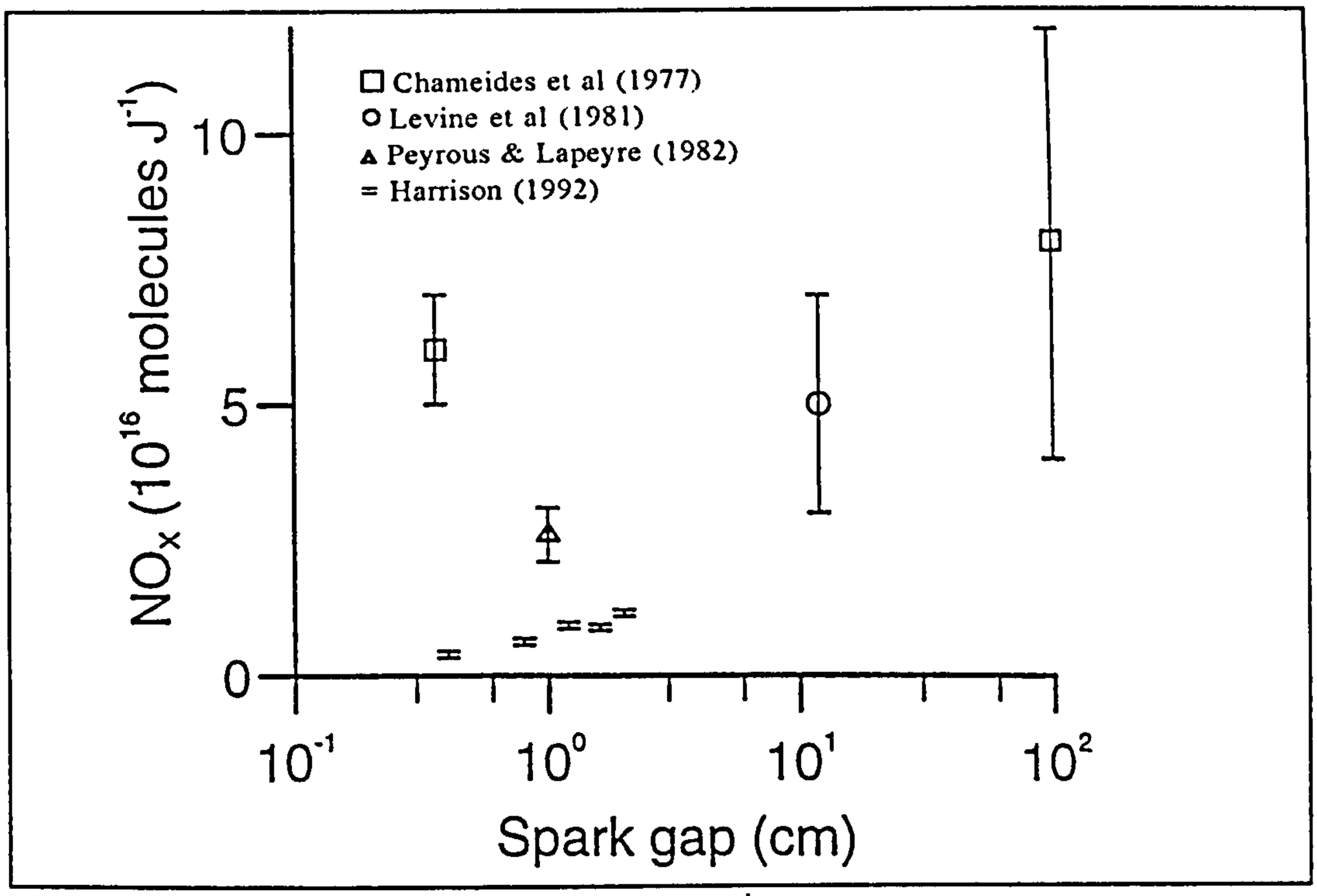

Figure 3.1 Variation of experimental NO J^{-1} with spark gap

Tuck 1976; Goldenbaum & Dickerson, 1993). This study also estimated that a very large proportion (up to 95%) of the calculated total input energy to the discharge, upon which the original NO_x J^{-1} values were based, was lost as heat in the electrodes in Harrison's experiments, thus producing an underestimate of the NO_x J^{-1} which was likely to occur under loss-free atmospheric conditions. Studies carried out at longer spark gaps (up to 1m), where the energy losses were assumed to be minimised, suggested NO_x J^{-1} values of the order 10^{16} - 10^{17} molecules J^{-1}, and this is shown in Figure 3.1. Accounting for these losses in Harrison's work led to an estimate of the NO_x global production rate of $(9 \pm 2) \times 10^{16}$ molecules NO_x J^{-1} (Stark *et al*, 1995), which was in agreement with the value suggested by Borucki & Chameides (1984).

The formation of activated atoms and molecules of nitrogen and oxygen as a result of an energetic lightning discharge through the atmosphere might also be expected to produce other oxides of nitrogen, namely N_2O. As explained in Chapter 1, the global budget of N_2O is by no means certain, and identification and quantification of its sources has so far proved inconclusive. Studies into N_2O formation by lightning are more limited than those for NO_x, but airborne measurements by Levine *et al*

(1983) and experimental studies (Levine *et al*, 1979; Donohoe *et al*, 1977) indicate that electrical discharges can lead to enhanced levels of N_2O. However, work into the mechanism of N_2O formation, and its potential global significance remains uncertain.

A few researchers have studied the formation of N_2O from the types of species found in electrical discharges. As early as 1952, Bates *et al* (in Prasad, 1981) suggested that N_2O could be formed from the reaction of unexcited ozone with nitrogen

$$N_2 + O_3 \rightarrow N_2O + O_2 \qquad (3.1)$$

However, a rate constant for the reaction of 5×10^{-28} cm^3 s^{-1} at 298 K was subsequently determined (Prasad, 1981) which is too slow for this reaction to be of significance. The reaction was not studied under the high temperature conditions occurring in the flash. The proposal that this reaction is more likely to occur with excited ozone was instead put forward by Prasad (1981 and 1994), where excited ozone (O_3^*) is formed with a 62% chance in the three body combination reaction

$$O + O_2 + M \rightarrow O_3^* + M \qquad (3.2)$$

$$O_3^* + N_2 \rightarrow N_2O + O_2 \qquad (3.3)$$

$$\rightarrow N_2 + O_3 \qquad (3.4)$$

Griffing (1977) used a theoretical model to estimate the amount of N_2O produced by lightning, proposing that the major route of formation was via the reaction of nitrogen with an oxygen ion to form N_2O^+ with subsequent capture of an electron from O_2

$$O^+ + N_2 + M \rightarrow N_2O^+ + M \qquad (3.5)$$

$$N_2O^+ + O_2 \rightarrow N_2O + O_2^+ \qquad (3.6)$$

This study stated that no reaction of an oxygen atom with nitrogen would be efficient enough to occur. However this is challenged by a number of studies which suggest that a variety of possible reactions of both ground state and vibrationally excited N_2

with oxygen species, such as O_2, $O(^1D)$ and $O(^3P)$, could be potential routes for N_2O formation. DeMore and Raper (1962) proposed that ground state nitrogen could react with singlet oxygen to produce nitrous oxide:

$$N_2 + O(^1D) + M \rightarrow N_2O + M \qquad (3.7)$$

Greater interest, however has been shown in the reactions of metastable and vibrationally excited N_2 ($N_2(A^{3+}{}_g)$ and $N_2(^1\Sigma)$ respectively), both of which are readily formed in discharges by the bombardment of N_2 with low energy secondary electrons. The free radiation lifetime of $N_2(A^{3+}{}_g)$ has been found to be of the order 2s, but its quenching by O_2 can occur as rapidly as 10^{-10} s (Hill *et al*, 1984). This can also lead to a reaction forming N_2O, which has been studied by Zipf, and Zipf and Prasad (both 1980), who found that the quantum yield of N_2O was 0.6 ± 30% compared to the quenching. Other studies have given lower efficiencies of N_2O formation under different conditions (Hill *et al*, 1984)

$$N_2(A^{3+}{}_g) + O_2 \rightarrow N_2O + O(^3P) \qquad (3.8)$$

$$\rightarrow N_2 + O_2 \qquad (3.9)$$

Quenching of $N_2(^1\Sigma)$ by O atoms has also been studied (Donohoe *et al*, 1977), with $O(^3P)$ being the most likely to react due to the low efficiency of the $O(^1D) + N_2$ reaction

$$N_2(^1\Sigma) + O(^3P) + M \rightarrow N_2O + M \qquad (3.10)$$

In addition, N_2O may be formed from secondary reactions of NO_x formed by the discharge (Hill *et al*, 1984; Harteck & Dondes, 1956)

$$NO + N \rightarrow N_2O \qquad (3.11)$$

$$N + NO_2 + M \rightarrow N_2O + O + M \qquad (3.12)$$

Other reactions of excited molecules have been suggested as potential sources of N_2O

in the troposphere (Prasad, 1994). However, neither these nor those described above has been confirmed and there is thus much potential for further investigation in this area.

The work in this chapter is mainly concerned with the study of N_2O formation from electrical discharges, using a similar experimental set-up to Harrison (1991), as described in Chapter 2. By observing N_2O production under the same conditions as those used previously it was anticipated that a value for the atmospheric N_2O J^{-1} could be determined and used in global studies to assess whether lightning was a significant source of N_2O. These results, coupled with results of varying the composition of the air through which the discharge was passed, could also be used in the analysis of the mechanism of formation of N_2O, and a comparison with NO_x made.

Initially it was necessary to repeat the work of Harrison (1991), in order to ensure that no major differences between the experimental apparatus were present. NO formation was analysed using chemiluminescence detection, as before, and also with tunable diode laser spectroscopy (TDLS), to check the reproducibility of the work with different detection methods. The study was carried out over the same pressure and spark gap range and, in addition, the effects of the application of more than one flash were also investigated. It was not possible to analyse the formation of NO_2 due to a fault with the chemiluminescent analyser. However if the results of the NO study corresponded to those of Harrison it could be assumed that NO_2 formation would be the same in this case.

The same experiments were then repeated, with N_2O analysed using gas chromatography with electron capture detection. Comparison of the results for NO and N_2O would then indicate whether the physical and chemical mechanisms of formation were similar and thus whether the same assumptions for the determination of the quantity of N_2O formed from atmospheric discharges could be used.

3.2 Formation of NO

Harrison (1991) investigated the effect of increasing the pressure of the air through which the discharge was passed and also of increasing the spark gap. Both lead to greater breakdown energies, but also to greater NO_x J^{-1}. It was suggested by Stark *et al* (1995) that the increase in NO_x J^{-1} at higher pressures was due to a higher proportion of the energy remaining in the gas between the electrodes as the gas cooled to the NO freeze out temperature, thus leading to greater NO_x formation. This loss of heat to electrodes will not be experienced by atmospheric discharges, and is discussed in more detail later.

In this work, for each of the detection methods, a single flash was passed through the air in the discharge cell at pressures of between 100 and 1000 mbar and at spark gaps of between 4 and 15 mm. The NO was measured and the NO J^{-1} value calculated from the expression

$$E = \tfrac{1}{2} C V^2 \qquad (3.13)$$

where E is the total energy available on the capacitors at the time of breakdown, C is the total capacitance (2 μF) and V is the voltage at the point of breakdown measured on the voltmeter. This assumes that all the energy is available for the formation of NO, which as discussed previously may not be the case. However the results obtained can be directly compared with those of Harrison (1991).

The effect of multiple flashes was also examined. The suggested mechanism of NO formation would be expected to give a constant amount of NO with each successive flash until the concentration of NO in the vessel is equal to the freezeout concentration. Further discharges would not then increase the yield of NO. However, in the case of N_2O this may not be true, and the application of multiple flashes allowed a comparison between the methods of formation of the two species. Each set of experiments was repeated at least three times and the average value taken for the purposes of comparison.

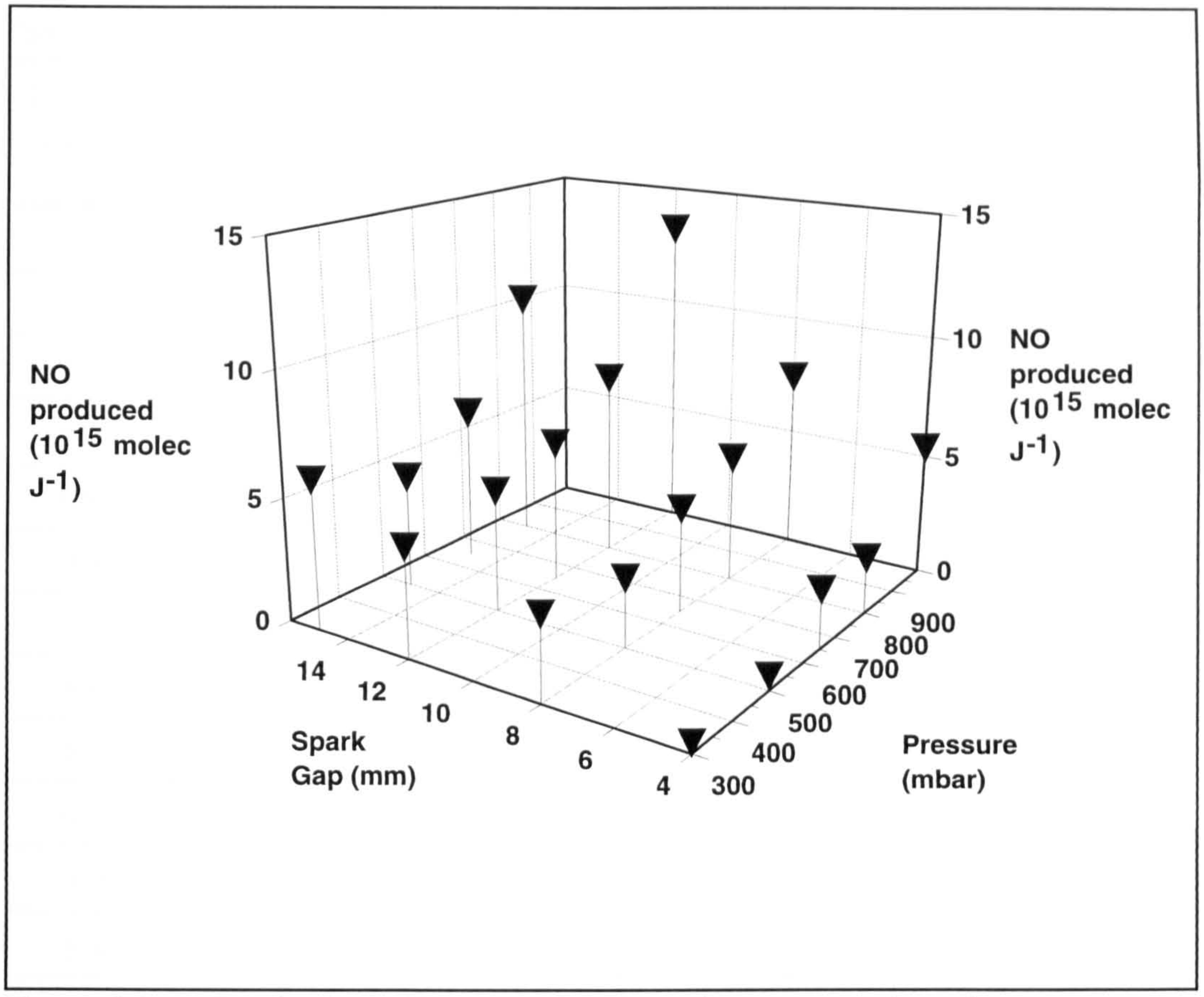

Figure 3.2 Production of NO as a function of pressure and spark gap

3.2.1 Chemiluminescent (CL) Detection

3.2.1.i) Spark gap and pressure studies

The results of increasing the pressure and spark gap are summarised in the 3-D plot in Figure 3.2, and in Table 3.1. The figure shows that the NO J^{-1} values rise at a steady rate with both spark gap and pressure. At 300 mbar there is an increase of 1500% between 4 mm and 15 mm, but at the higher pressure of 800 mbar this is not so extreme, NO J^{-1} rising by 850% over the spark gap range. Therefore at higher pressures the increase in NO J^{-1} with spark gap appears to be less pronounced, although still significant. This is also shown in the cross-sectional plot in Figure 3.3.

Table 3.1 NO J^{-1} as a function of spark gap and pressure

Pressure (mbar)	Spark Gap (mm)	B/down voltage (kV)[1]	Ave NO/J[2]	% std error[3]	% increase[4] (cf 4mm)	%increase[5] (cf 300mb)
300	4	4.5	0.387	8	-	-
500	4	5	0.558	11	-	44
650	4	5.5	2.43	17	-	530
800	4	5.5	2.31	28	-	500
1000	4	6	5.38	0	-	1300
300	8	5.5	3.39	1	780	-
500	8	6.5	2.82	5	400	0
650	8	7.5	4.27	11	76	26
800	8	8	5.23	11	85	54
1000	8	9	7.43	4	38	120
300	12	5.5	4.39	3	1000	-
500	12	7.5	4.95	8	790	13
650	12	8	5.81	11	140	32
800	12	9 .5	7.61	8	230	73
1000	12	10.5	13.2	5	150	200
300	15	6	6.00	12	1500	-
500	15	8	4.60	20	720	0
650	15	9.5	6.33	12	160	6
800	15	10.5	10.5	12	350	74

[1] - spark energy calculated from $E = CV^2$ (see 3.2.2.i)); C = 2 μF, V = breakdown voltage (kV)
[2] - 10^{15} molecules J^{-1} calculated from total NO/spark energy - average of 3 experiments
[3] - standard error of the mean expressed as a percantage to allow comparison between results of different magnitudes
[4] - % difference compared with 4 mm value at the same pressure
[5] - % difference compared to 300 mbar value at same spark gap

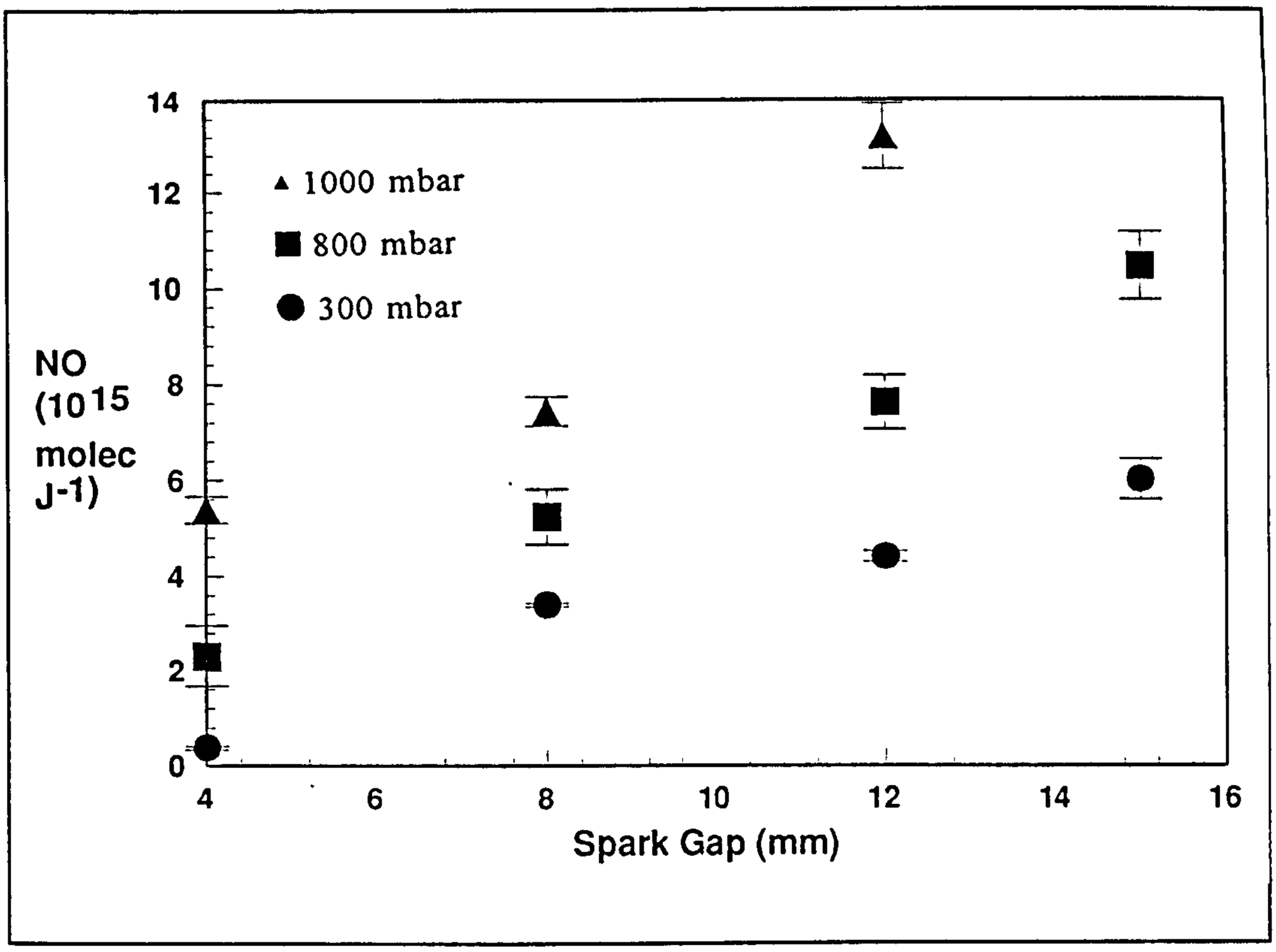

Figure 3.3 Production of NO as a function of spark gap at different pressures, showing standard errors (average of 3 experiments).

At 4 mm the rise in NO J^{-1} with pressure is greatest (500%), decreasing to 74% at the longer spark gaps. The experiments carried out at 1000 mbar give slightly higher NO J^{-1} values than would be expected from the lower pressure measurements, and the rise in these values with increasing spark gap appears to be more rapid than at lower pressures. This may be due to the lower comparative energy losses at these higher pressures, where more of the energy is retained by the gas after the spark, thus producing a greater amount of NO J^{-1}. However, as it was not possible to measure the NO at 1000 mbar and 15 mm, this trend may not be so sharp.

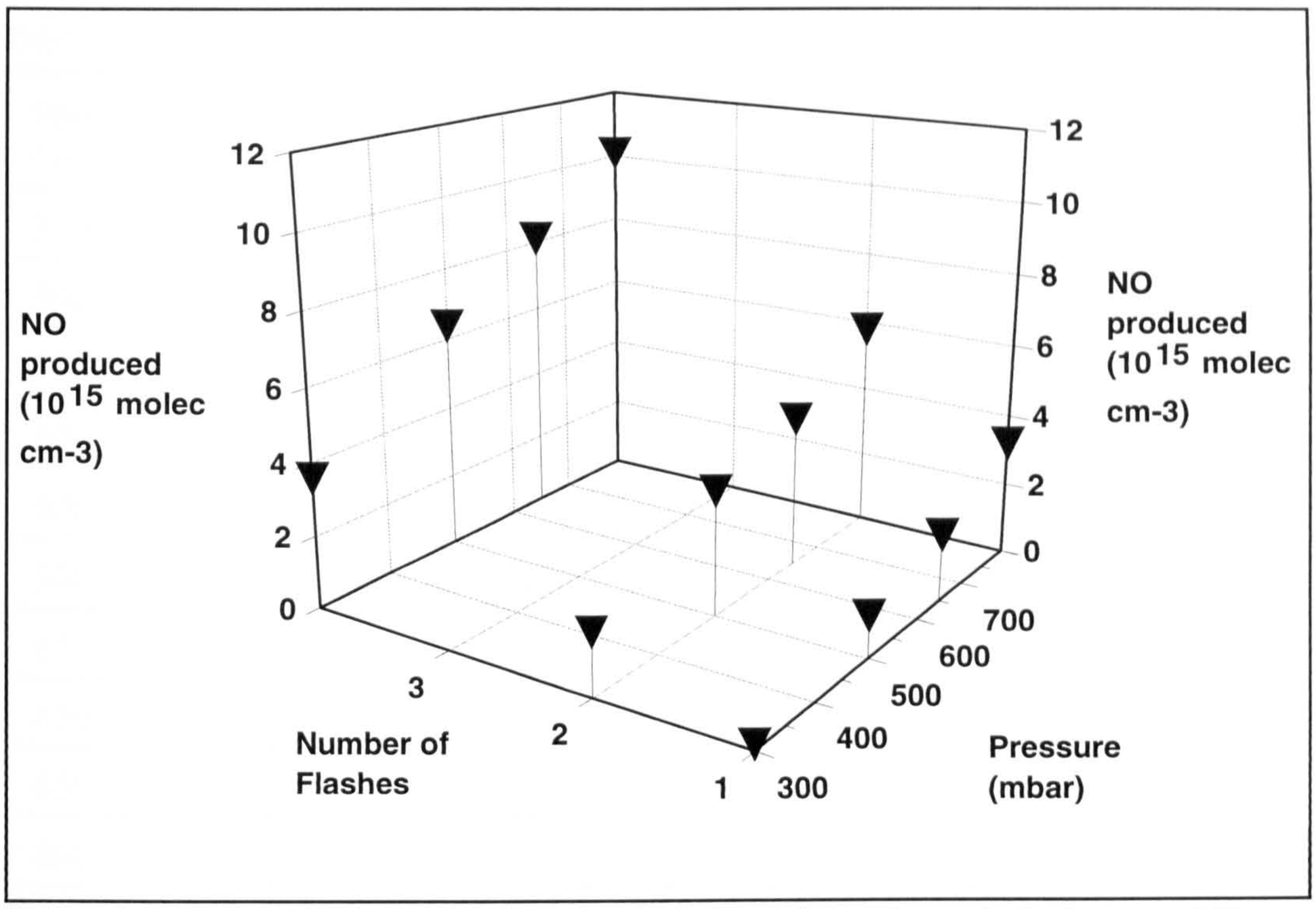

Figure 3.4 Production of NO as a function of number of flashes at different pressures Experiments carried out at 15 mm spark gap..

3.2.1.ii) Multiple flashes

The effect of passing 1, 2 and 4 flashes through the air in the cell at 15 mm spark gap and pressures of between 300 and 800 mbar is shown in terms of the total NO formed in Figure 3.4. The errors and values are given in Table 3.2. At each pressure an approximately linear increase in the amount of NO formed with each flash is observed. The total NO formed is greater at higher pressures, although the overall increase in NO from 1 - 4 flashes is slightly lower than those at lower pressures. The amount of NO formed by each successive flash at a single pressure is approximately constant. The slight differences are a result of the observed variations in the breakdown voltages and thus energies of each flash. The errors in the measured values are in fact quite small but cannot incorporate losses of energy, which are unknown, and could be quite variable.

Table 3.2 Production of NO as a function of multiple flashes at 15mm spark gap

Pressure (mbar)	No. of flashes	Average total NO[1]	% std error[2]	% increase[3] (cf 1 flash)
300	1	0.71	6	-
300	2	1.71	6	140
300	4	3.57	1	400
500	1	1.17	9	-
500	2	3.43	4	190
500	4	6.37	1	450
650	1	1.86	13	-
650	2	4.20	3	130
650	4	8.11	1	340
800	1	3.20	12	-
800	2	5.78	4	80
800	4	10.1	1	210

[1] - 10^{15} molecules cm^{-3} NO produced after x flashes

[2] - standard errors given in terms of percentages, and correspond to the total NO after x flashes

[3] - % increase compared to NO formed by one flash at the same pressure

The constant production of NO is to be expected, as its mechanism of formation is via a simple chemical reaction requiring thermal activation. The whole process occurs before the next flash passes, and as it is unaffected by any possible pre-discharge processes will produce a constant amount of NO under the same conditions of pressure spark gap and energy. NO is also not destroyed as a result of the flash under these conditions.

3.2.2 Tunable Diode Laser Spectroscopic Detection

As indicated earlier (Chapter 2), the TDLS experiments were conducted at the National Laboratories in Risø, Denmark. Due to the limited time available for experiments, it was only possible to carry out a set of experiments over a range of pressures at 12 mm spark gap. The results of these experiments for NO are given in Figure 3.5 and Table 3.3, along with those of Harrison (1991) for an 8 mm spark

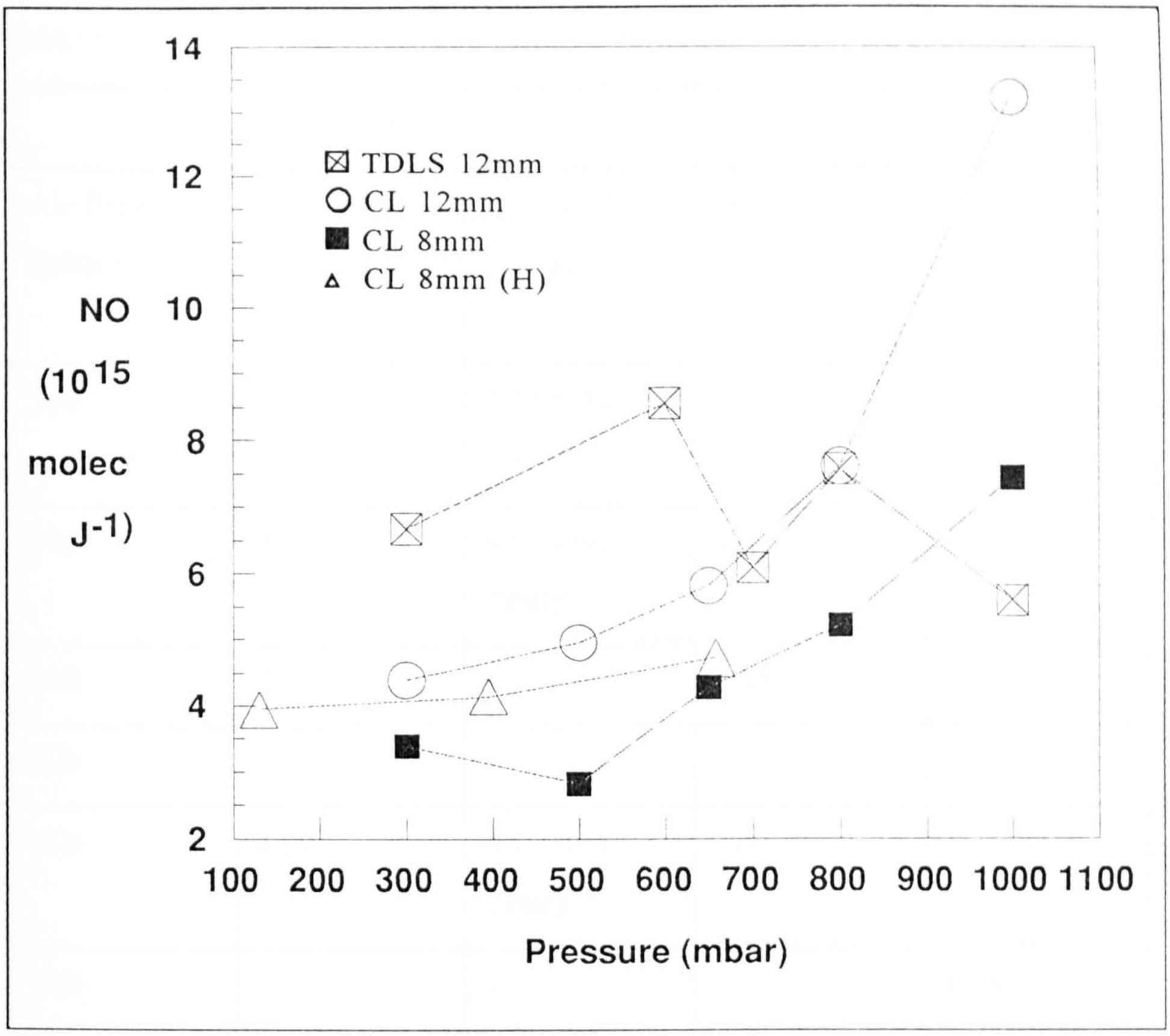

Figure 3.5 Comparison of TDLS and Chemiluminescence: Production of NO as a function of pressure. (H) corresponds to work of Harrison (1991)

gap, and this work (8 and 12 mm), the latter using chemiluminescent detection. This allows a comparison between the different types of detection.

The figure shows that the results of the 8 mm chemiluminescent work carried out in this study and those of Harrison (1991) are in good agreement. This implies that there are no major differences between the experiments. However, the results of the TDLS work, although of similar order to the chemiluminescent data, show a different trend over the pressure range, with values of NO J^{-1} being slightly higher at lower pressures, and decreasing until the difference between the values at 1000 mbar is quite significant.

Table 3.3 Comparison of TDLS and chemiluminescent detection for NO

NO Produced (10^{15} molecules J^{-1})				
Air Pressure (mbar)	This work (CL 8 mm)	Harrison (CL 8mm)	This work (CL 12 mm)	This work (TDLS 12 mm)
200	-	3.94 (132 mbar)	-	-
300	3.39	4.13 (395 mbar)	4.39	6.67
500	2.82	-	4.95	-
600	-	-		8.55
650	4.27	4.71 (658 mbar)	5.81	-
700	-	-	-	6.08
800	5.23	-	7.61	7.57
1000	7.43	-	13.2	5.60

The major reason for this is the large difference between the breakdown voltages at 1000 mbar, which was 11.5 kV for the CL studies at 12 mm spark gap, and 14.5 kV for the TDLS experiments. As the energy (J) is calculated from the square of the breakdown voltage (see Section 3.2.2.i)), a difference of 3 kV is significant. This difference is not present at lower pressures, where comparison of the breakdown voltages shows good agreement. The reason for this difference is unknown, as it was not possible to repeat any of the TDLS work, although it may be due to electrode effects.

Due to time constraints the experiments carried out using the TDLS detection could only be carried out once. Therefore the errors are assumed to be higher than for the

CL work. However, the agreement between the results of the different studies confirms that this is not the major source of error. The difference in breakdown voltage at 1000 mbar appears to be the most important component of the discrepancies between the studies.

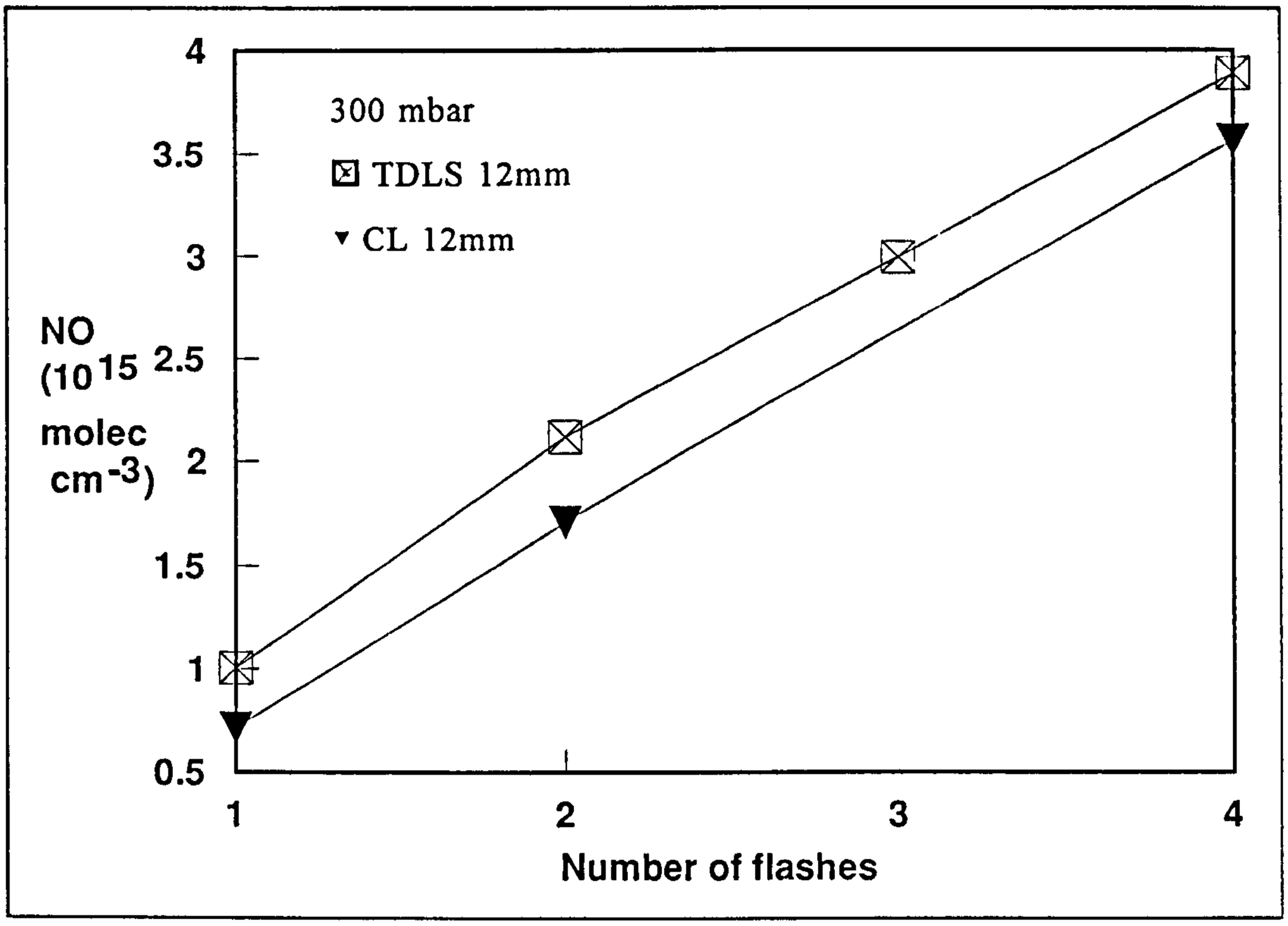

Figure 3.6 Comparison of TDLS and Chemiluminescence: Production of NO as a function of multiple flashes.Experiments carried out at 300 mbar, 12 mm spark gap.

Comparison of the multiple flash work at 300 mbar also shows good agreement, as presented in Figure 3.6. The TDLS results are slightly higher than those of the chemiluminescent studies, but also include results from 3 flashes, and both demonstrate that a constant amount of NO is produced with each flash.

Studies into the formation of NO_2 and N_2O were also carried out. However, it was not possible to obtain a long enough path length to detect these species with the diodes available. With the use of either diodes in regions of stroger absorption, or

with longer path lengths it would be possible to study the formation of all three species with the same detector, which is highly desirable.

3.2.3 Summary

The results of the experiments into the formation of NO from electrical discharges can be summarised as follows:

- The NO J^{-1} increases at a steady rate with spark gap and pressure, the increase being most regular over spark gap than over pressure. At 1000 mbar the values are comparatively higher than those at the lower pressures.
- The application of multiple flashes leads to a constant increase of NO, which would be expected if it is formed via the thermal Zel'dovich mechanism.
- Comparison of the results with those of Harrison using the same equipment show good agreement, and therefore allow the use of the assumptions of Stark *et al* (1995) in the estimation of global production of NO, and of N_2O if the mechanism of formation is thermal.
- If the atmospheric NO J^{-1} value is assumed to be $(9 \pm 2) \times 10^{16}$ molecules J^{-1}, the proportion of total calculated energy which is used in the experimental formation of NO is approximately 5 - 10% (based upon the average experimental NO J^{-1} value obtained over the pressure and spark gap ranges obtained in this study).

3.3 Formation of Nitrous Oxide (N_2O)

The investigation of N_2O formation was carried out using gas chromatography and electron capture detection (ecd) with the apparatus described in Section 2.3. As for NO, the production of N_2O from an electrical discharge through air at pressures between 300 and 1000 mbar and at spark gaps ranging from 4 to 15 mm was examined, as well as the effect of multiple flashes. In addition to this, experiments were carried out where the composition of the air was varied, by changing the N_2:O_2 ratio, and through addition of NO and NO_2 to the air before discharge. This was intended to extend the conditions under which N_2O was formed and thus help in the

elucidation of the chemical mechanism of N_2O formation.

3.3.1 Spark Gap and Pressure Studies

Passing an electrical discharge through air led to the enhancement of the N_2O peak area on the ecd output, as demonstrated in Figure 2.4. The effects of varying the pressure and the spark gap upon this enhancement are shown in Figure 3.7, and the actual increments and errors displayed in Table 3.4. The table shows that the amount of N_2O formed is a factor of 10^3 less than NO, which suggests that it is harder to form, requiring either more energy, or a greater abundance of precursor species.

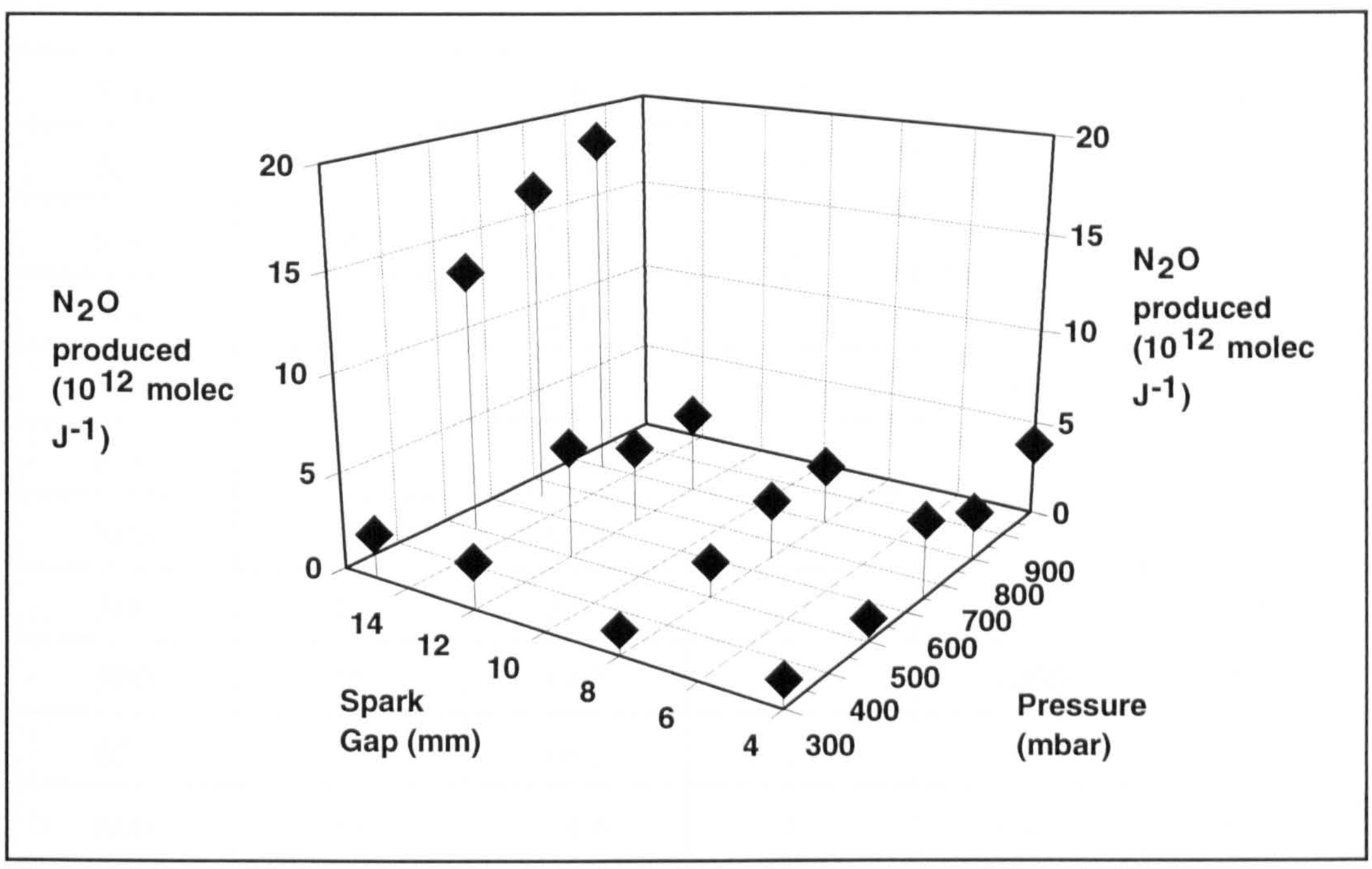

Figure 3.7 N_2O production as a function of Pressure and Spark Gap

Like NO, N_2O is formed in greater amounts as the spark gap and pressure increase. At 4mm spark gap there is an increase of a factor of 2-3 as the pressure increases from 300-800 mbar, from 1.34 to 2.49 $\times$ 10^{12} molecule J^{-1}, but at 15mm a greater increase is observed over this pressure range, N_2O increasing from 2.57 $\times$ 10^{12} to

18.64 × 10^{12} molecules J^{-1}. This is predominantly due to the fivefold increase between 300 and 500 mbar at 15 mm which begins to plateau as the pressure is increased beyond this.

Table 3.4 Production of N_2O as a function of spark gap and pressure

Air Pressure (mbar)	Spark Gap (mm)	Average N_2O/J^1	% std error	%increase (cf 4mm)[2]	%increase (cf 300mb)[3]
300	4	1.34	45	-	-
500	4	1.16	43	-	0
650	4	3.99	9	-	200
800	4	2.49	41	-	86
300	8	1.25	21	0	0
500	8	1.82	28	57	46
650	8	3.06	9	0	145
800	8	3.12	2	25	150
300	12	2.44	25	82	0
500	12	5.78	10	398	137
650	12	4.06	14	2	66
800	12	4.28	10	72	75
300	15	2.57	16	92	0
500	15	13.7	15	1096	433
650	15	16.9	12	326	556
800	15	18.6	17	649	626

[1] - 10^{12} molecules J^{-1} calculated from $E = ½ CV^2$ (see 3.2.2.i)) - average of 3 experiments. Breakdown voltages equal to those in NO experiments, see Table 3.1.

[2] - % difference compared with 4 mm value at the same pressure

[3] - % difference compared to 300 mbar value at same spark gap

As the spark gap is lengthened a steady increase in N_2O J^{-1} is apparent at all pressures, excepting the very high values for 15mm at >300 mbar, which exhibit a sharp rise in N_2O. Therefore it would appear that the production of N_2O shows anomalies at higher spark gaps and pressures. This suggests at an early stage that

there may be some major differences between the mechanisms of formation of NO and N_2O.

3.3.2 Multiple Flashes

Passing more than one flash through the gas in the cell may give an idea of the chemistry occurring in the formation of N_2O and also an idea of the physical processes involved. A linear increase in N_2O production would show that the species involved in the formation of N_2O originate from the pre-discharge air mixture and not from any products of the initial flash and that the products of the flash do not have any effect on the chemistry during subsequent flashes. Any other trends would suggest that the products inhibit or accelerate N_2O formation or that N_2O formation is not via a simple mechanism, unlike NO. To investigate this, a series of experiments was carried out at a 15 mm spark gap, at pressures between 300 and 800 mbar, for 1, 2 and 4 discharges. The results are given in the 3-D plot of Figure 3.8, and errors and increments displayed in Table 3.5.

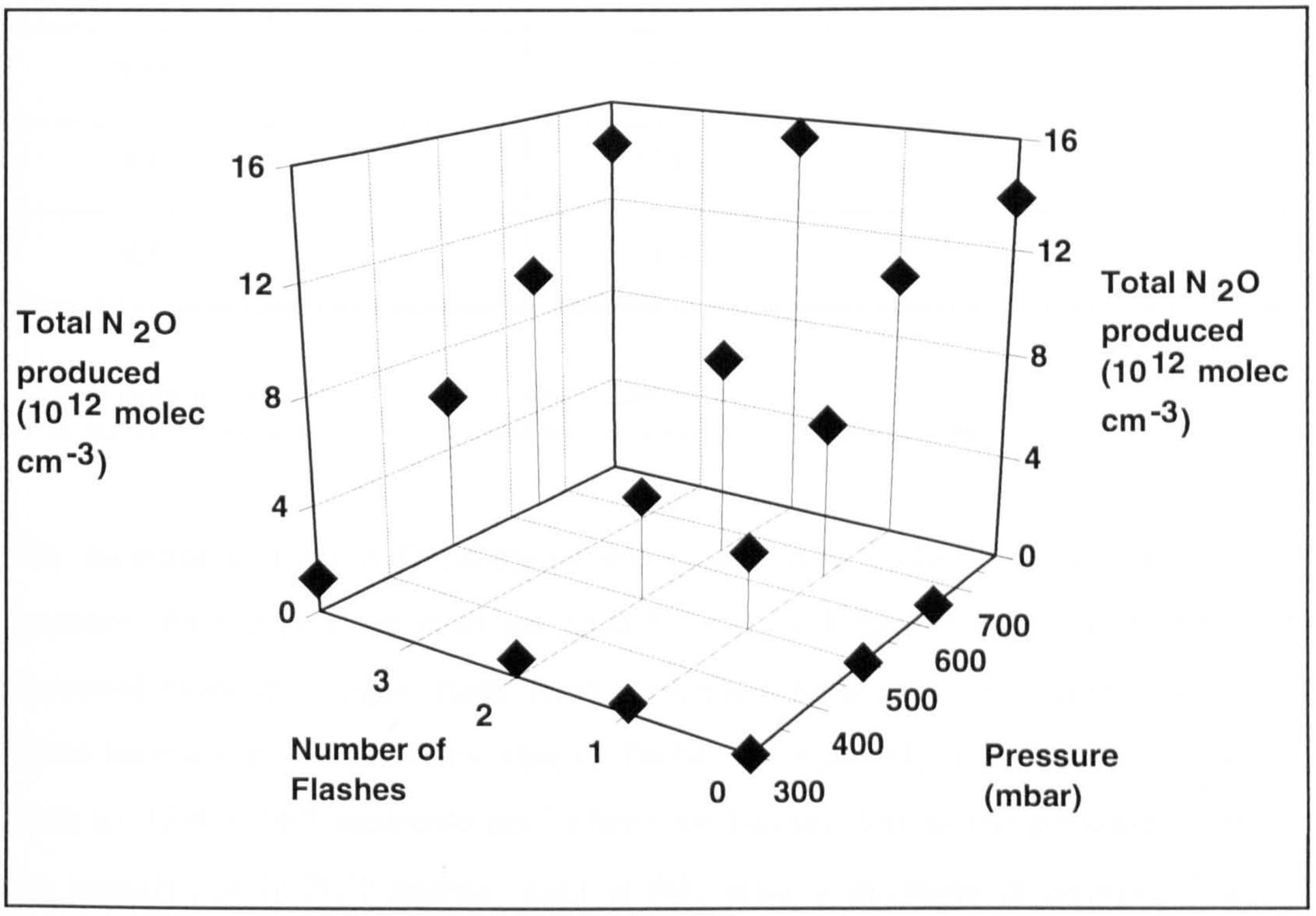

Figure 3.8 Total N_2O produced as a function of pressure and multiple flashes at 15 mm spark gap. At zero flash, $N_2O = 0$, except at 800 mbar.

Table 3.5 N_2O production as a function of multiple flashes at 15 mm spark gap

Air Pressure (mbar)	No. of flashes (x)	Average total N_2O[1]	% std error	% increase[2] (cf 1flash)
300	1	3.53	15	-
300	2	6.47	7	83
300	4	12.4	10	250
500	1	28.6	19	-
500	2	39.6	10	38
500	4	60.9	9	113
650	1	59.4	14	-
650	2	76.7	22	29
650	4	97.4	17	64
800	1	104	14	-
800	2	154	8	48
800	4	143	13	38

[1] - 10^{12} molecules cm^{-3} N_2O produced after x flashes
[2] - % increase compared to N_2O formed by one flash at the same pressure

The increase in total N_2O produced with successive flashes is different for each pressure. As the pressure rises the total N_2O at each flash frequency increases, as expected from the single flash work described before. At 300 mbar an almost linear increase in N_2O with number of flashes is observed, from 3.53×10^{12} at one flash to 12.4×10^{12} molecule cm^{-3} after four flashes, but as the pressure increases the overall rise in N_2O lessens, until at 800 mbar a decrease of between 2 and 4 flashes is apparent, giving an overall rise of 38%. Therefore it would appear that a

constant amount of N_2O is not formed with each flash, except at low pressures, and that it is somehow being inhibited or even destroyed by the action of subsequent flashes.

Another set of experiments was conducted over the same pressure range in which the electrodes were charged to just before the point of breakdown and the energy 'dumped' into the capacitors rather than across the spark gap. At 800 mbar only, it was observed that N_2O was produced at a concentration greater than that obtained after one flash (13.0×10^{12} molecules cm^{-3} compared with 10.4×10^{12} molecules cm^{-3} -see Figure 3.8). Although this value lies within the standard error for one flash, the peak areas obtained were consistently higher than those for one flash. This suggests that at the higher pressures the formation of N_2O may be initiated by a pre-discharge mechanism, followed by partial destruction of this N_2O by the flash itself.

3.3.3 Composition Studies

The composition of the gas through which the discharge was passed was altered to investigate the chemistry involved in N_2O formation. The effect of O_2 was of particular interest, due to its possible reactions with nitrogen species to form N_2O (explained earlier in Section 3.1). To investigate this, the proportion of O_2 in nitrogen was varied from 0 to 21% and the corresponding N_2O measured. As before, 3 experiments were carried out for each mixture at a spark gap of 15 mm and a pressure of 300 mbar.

A typical gc-ecd trace for nitrogen is shown in Figure 3.9, and shows that in the absence of ambient levels of oxygen there is a trough in the normal O_2 position (compare with Figure 2.2). This is a result of switching the taps to introduce the carrier gas through the sample and then back to normal, and is usually disguised by the large O_2 peak. However, the N_2O and CFC peaks remain, as even 99.99% N_2 contained trace levels of these gases.

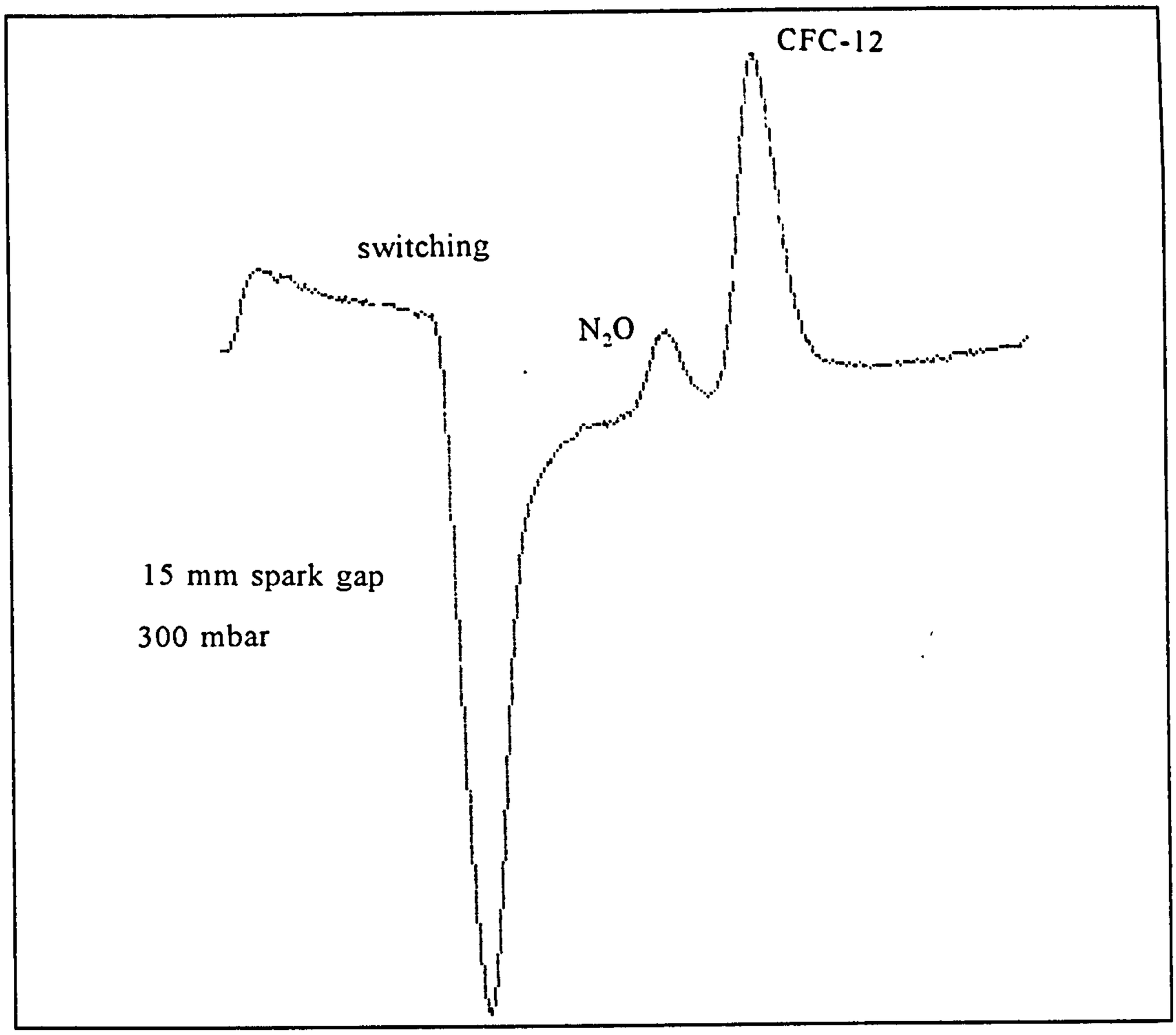

Figure 3.9 Gc-ecd trace for pure nitrogen

When a spark discharge was passed through the pure nitrogen, the effect upon the trace gas peaks was the same as for air, N_2O increasing in peak area, and CFC reducing in size. The fact that N_2O is formed suggests that an oxygen containing precursor is present in the nitrogen. This is highly likely, as the levels of oxygen required to produce such a small amount of N_2O are of the order ppbv, which would be easily found either in the gas itself or as a result of the presence of a trace amount of ambient air in the cell.

It is therefore interesting to note the effect of adding oxygen to the nitrogen in terms of the N_2O formation. Figure 3.10 shows that as the concentration of oxygen increases towards ambient levels, the peak area of N_2O actually decreases. Its initial concentration is the same in all mixtures, but adding oxygen reduces the amount of additional N_2O which is formed as a result of the flash. In absolute terms, the

concentration of N_2O formed increases fourfold as the $[O_2]$ is reduced to zero, from 1.1×10^{12} molecules cm^{-3} at ambient $[O_2]$ to 4.0×10^{12} molecules cm^{-3} at ppbv levels of O_2. This therefore suggests that the presence of O_2 in significant quantities actually inhibits the N_2O formation in some way.

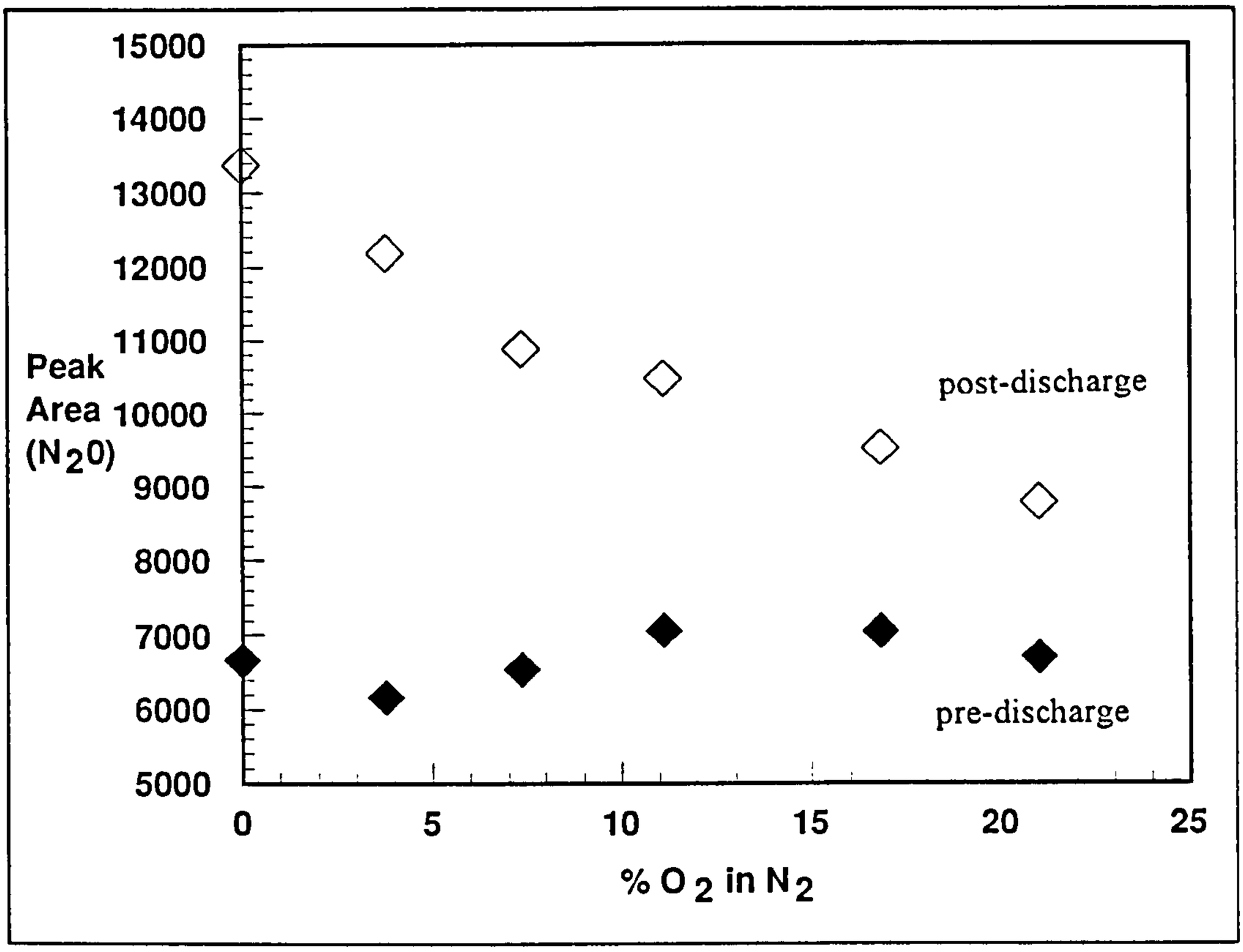

Figure 3.10 Peak Area of N_2O as a function of $\%O_2$ in air. Experiments carried out at 15 mm spark gap, 300 mbar.

Similarly the effect of O_2 on the CFC peak is also examined and displayed in Figure 3.11. The amount of CFC increases with O_2 (due to a slightly higher concentration of CFC in zero grade air compared to nitrogen), but the amount destroyed (indicated by the difference between pre- and post-discharge values) decreases with addition of oxygen. This indicates that the presence of oxygen also inhibits the destruction of CFC.

The addition of NO and NO_2 to mixtures of nitrogen and air was also examined, in order to assess their potential as N_2O precursors. However, there were problems with integration of the gc-ecd traces, and this work was inconclusive.

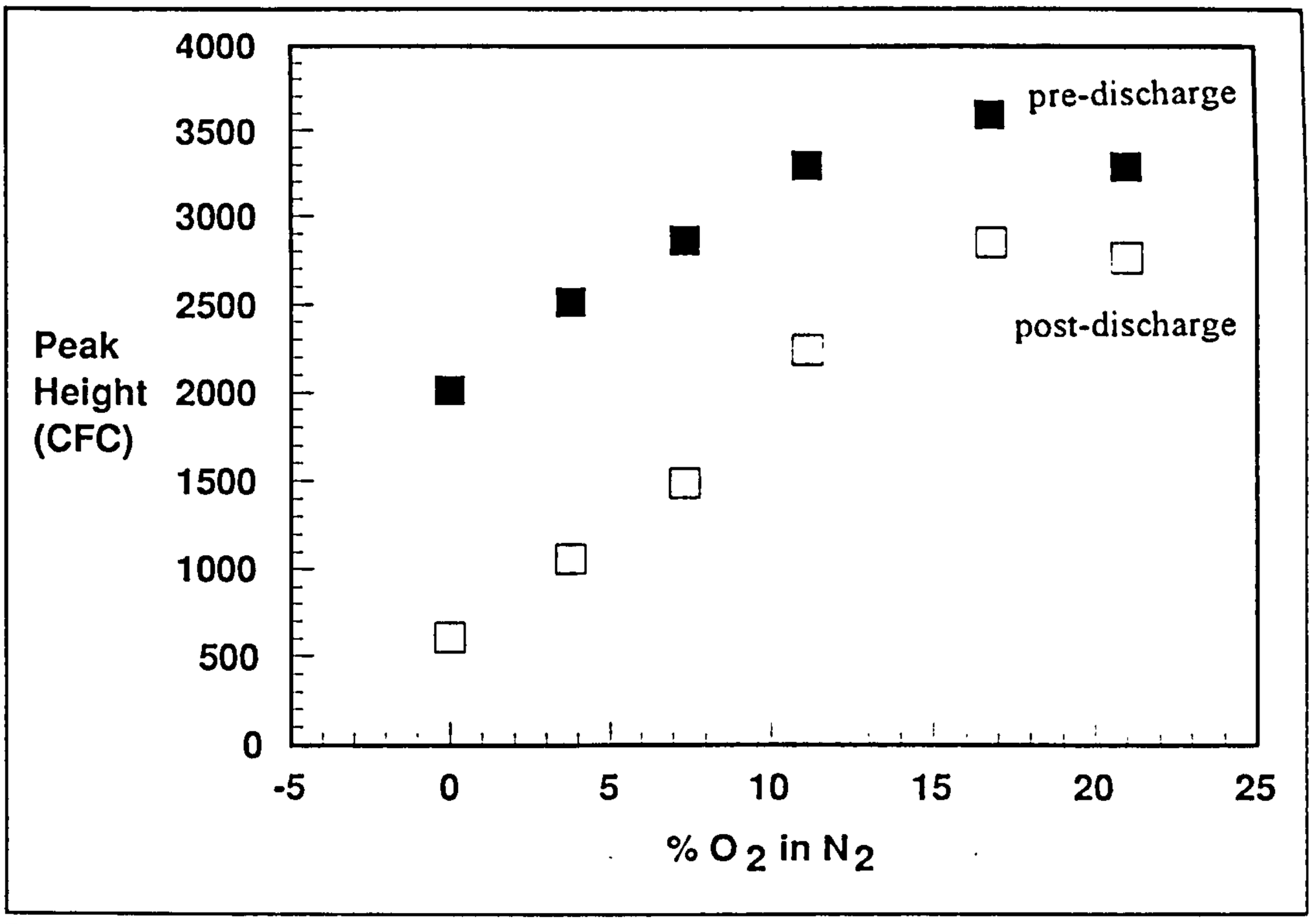

Figure 3.11 Peak Height of CFC-12 as a function of $\%O_2$ in air. Experiments carried out at 15 mm spark gap, 300 mbar.

3.3.4 Discussion

The results of the experimental work carried out to detect the formation of N_2O from electrical discharges through air can be summarised as follows:

- The background concentration of N_2O is enhanced by the application of a spark discharge through air by between 0 and 700 ppb within a 250 cm^3 cell.
- The extent of this enhancement depends upon the pressure of the air in the cell and the length of the spark gap - increasing each causes an increase in the breakdown energy required for the air, and thus it can be assumed that a larger breakdown energy leads to a greater formation of N_2O. However, this effect is not linear.
- The amount of N_2O increases with the number of flashes. This rate appears to be constant at low pressure (300 mbar), but to decline as the pressure increases, until at 800 mbar N_2O may even be destroyed after 4 flashes.

- At 800 mbar there is evidence that N_2O may be formed prior to the spark discharge, and a fraction of this destroyed by the action of the spark.
- At 300 mbar, reducing the concentration of the O_2 in the air to zero leads to a greater formation of N_2O, despite a corresponding reduction in breakdown energy.

It can therefore be assumed that N_2O is formed under the experimental conditions employed here by a mechanism involving different physical and chemical processes than that which forms NO.

3.3.4.i) Reaction mechanisms

From the experimental evidence above and observations of other studies it is proposed that the formation of N_2O from electrical discharges occurs via the reaction

$$N_2 (^1\Sigma) + O(^3P) + M \rightarrow N_2O + M \qquad (3.10)$$

This was suggested by Donohoe *et al* (1977), in a experimental study of N_2O formation from discharges. In this work it was postulated that N_2O was formed as a result of the corona discharge, which occurs as a result of the build up of charge on the electrodes prior to the spark discharge. The release of high energy electrons from the surface of the electrodes leads to the formation of vibrationally excited $N_2(^1\Sigma)$. This process is highly efficient in a discharge (Schulz, 1966).

The production of $O(^3P)$ and $O(^1D)$ will occur via photolysis of oxygen as a result of the light output of the flash. The reaction of $N_2(^1\Sigma)$ with $O(^1D)$ was found to be inefficient (Donohoe *et al*, 1977), but as $O(^3P)$ will be formed more readily, there is plenty of opportunity for reaction with $N_2(^1\Sigma)$. However, there will also be competition for $O(^3P)$ by other O atoms, but mainly from O_2, which will be present in equivalent or greater quantity than vibrationally excited $N_2(^1\Sigma)$, and which also reacts readily with $O(^3P)$. This may explain why the removal of O_2 leads to a greater formation of N_2O. As there is sufficient O_2 present for $O(^3P)$ to form, but a much reduced amount of O_2 to react with them, the reaction with $N_2(^1\Sigma)$ will become more

important, and thus the amount of N_2O formed will be enhanced.

This does not explain why N_2O is formed prior to discharge at higher pressures, nor why the formation of N_2O is not constant with each flash. There must therefore be a process which can form N_2O without the action of the flash, and also a process which either inhibits production of or actually destroys N_2O, both of which appear only to occur at greater pressures, and therefore higher breakdown energies.

It is proposed that the pre-discharge formation of N_2O occurs through the same reaction as above, with the $O(^3P)$ also being formed as a result of the corona. This was observed by Harrison (1991), who was investigating the formation of NO_2 in a discharge by the reaction of NO and O_3. He found that by charging the capacitors up to breakdown at a lower rate (and thus for longer than normal - 60 s compared to 15 s) and then analysing the NO_x formed from the spark, the majority of NO_x was formed as NO_2, instead of around 10% at the higher charge rate. This inferred that ozone was being formed by the corona discharge, and therefore that $O(^3P)$ was also formed, as ozone is produced by the reaction

$$O_2 + O(^3P) + M \rightarrow O_3 + M \qquad (3.14)$$

Therefore if $O(^3P)$ is present, it is possible that reaction with $N_2(^1\Sigma)$ will occur. This would appear only to occur at the higher breakdown energies of these experiments, where the energy of the corona discharge will be sufficient to produce $O(^3P)$.

The destruction of N_2O observed as a result of the flash at 800 mbar is likely to be due to either the direct photolysis of N_2O, or more probably due to its reaction with $O(^1D)$, which is also favourable. At the higher spark energies, the intensity of the spark is increased, which will lead to enhanced production of $O(^1D)$ via the photolysis of O_2. The photolysis of N_2O also produces $O(^1D)$, which can then further react with any available N_2O. Therefore at high energies it would appear that the production of N_2O is determined by the rate of pre-discharge and post-discharge formation and the rate of destruction via direct and indirect photolytic processes. In

the case of the 800 mbar experiments, the destruction is much more significant.

3.3.4.ii) Comparison with other studies

Studies of N_2O production from electrical discharges through air have been made using both experimental and theoretical methods. There are wide discrepancies in the mechanisms and N_2O production rates which have been proposed.

Experimental studies by Levine *et al* (1979) found that the concentration of N_2O in ambient air increased from 310 ppbv to 600 ppbv after a discharge of 17.5 kJ. This was assumed to be the result of thermal reactions in the shock front, as proposed by Chameides *et al* (1977) for NO, and was calculated to occur at a rate of 4.3×10^{12} molecules J^{-1}. The results of the present work are in disagreement with this study, as the behaviour of N_2O is different to that of NO. In addition, it has been found in modelling studies of the thermal chemistry (Stark, 1995) that the levels of N_2O found in these experiments are not predicted to be formed via a thermal mechanism if N_2O is assumed to freeze out at 2200K, as stated by Levine *et al*, (1979).

As mentioned in the previous section, experimental studies by Donohoe *et al* (1977) proposed that N_2O was produced by a corona discharge occurring prior to the flash at a rate of 9.85×10^{-4} moles (Ampere second)$^{-1}$. This is equivalent to 4×10^{16} molecules J^{-1} of corona energy although it is dependent upon the duration of the corona. Hill *et al* (1984) suggested that N_2O could also be produced by corona discharges occurring during the flash, and from modelling studies of the hot air chemistry around the heated channel proposed that between 3×10^{15} and 6×10^{16} molecules J^{-1} (corona) of N_2O were formed in the corona associated with the spark alone.

In this work it is postulated that N_2O is produced by a combination of the two types of corona discharge, and not by a thermal mechanism. It is also proposed that N_2O can actually be destroyed by photolysis which occurs as a result of the light output of the flash. As the energy associated with these processes is unknown for the

experiments it is difficult to express the N_2O production in terms of unit energy, and thus also to compare the results of this work directly with those of other studies. It is therefore also difficult to estimate a global production rate for N_2O, as the differences between the experimental spark and atmospheric lightning in terms of these processes is currently uncertain. The global production rates of both NO and N_2O are discussed in greater detail in the following chapter.

Chapter Four

Global Inventories of Sources of Nitrogen Oxides

4.1 Introduction

As discussed in Chapter One, increasing concentrations of key atmospheric trace gases as a result of human activities has led to the need for more detailed studies of these gases. It is necessary to know as much as possible about the complete atmospheric cycle of each of the species, from its sources, to its behaviour in, and effect upon, the environments in which it exists (i.e. its ability to absorb radiation, its reactions and so on) and ultimately to its loss route(s). These processes are inherently linked to the amount of the species which is available and the length of time it resides in the atmosphere. Once the values of such parameters are known they can be used to predict the potential environmental effects of likely perturbations to the values, such as increases in emission rates, and to estimate the most effective methods of preventing major atmospheric change.

Over recent years the development of global inventories of annual trace gas sources, emission rates, concentrations, and sinks has been widespread. However, a great deal of uncertainty still surrounds the quantification of many of these parameters, mainly due both to the complexities involved with deducing global values from predominantly regional measurements and to a lack of sufficiently sensitive measurement facilities. Until these problems can be rectified the uncertainties in global estimates will remain, in some cases varying by orders of magnitude .

There are a number of ways in which estimates can be made, using one or a combination of the following: field measurements, laboratory investigation and theoretical/computer studies. Measurement of concentrations of species in ambient air at the site of interest (i.e. in a city, over a remote region, over an area of biomass

burning) can be either carried out *in situ*, or from taking air samples for analysis elsewhere. Laboratory analysis can involve the measurement of collected air samples from field studies, or simulation of the source on a laboratory scale, such as the use of smog chambers to represent urban pollution. In both cases the results obtained are only representative of emissions of species from a particular source and over a specific region. The extrapolation of the data to global events therefore requires a large degree of averaging, as it is impossible to measure concentrations and emissions of species at all relevant points on the globe simultaneously (although the recent use of remote sensing has brought researchers a step closer to this).

The use of computer models for both small scale simulation of the atmosphere near to a source and for the calculation of global values using field or laboratory measurements as inputs is extensive (see Houghton *et al*, 1995; Graedel and Crutzen, 1993, and references therein). They can also be used to evaluate the global distribution of species, as it is well known that the concentration of trace gases is not evenly distributed in the atmosphere, but depends upon factors such as source location, and the lifetime of the molecule. However, in all cases the degree of error is high, and thus research into improving the accuracy of producing global inventories is continuous.

The work in this chapter covers three aspects of the inventory work described above. Firstly, laboratory scale measurements of the production of NO_x from electrical discharges (from Chapter 3) have been used along with assumptions of lightning behaviour, to estimate its annual global production from lightning. This value has then been used in conjunction with satellite measurements of regional lightning frequency to investigate the global distribution of NO_x from lightning. In addition, an investigation into the potential global significance of N_2O production from lightning has been carried out .

In a separate study, future emissions of N_2O from the addition of fertiliser to soils have been predicted. As explained in Chapter 1, the use of nitrogenous fertilisers on soils can enhance the production of N_2O and is believed to be its most important

anthropogenic source. As it is linked to food production and thus population, this source is expected to continue increasing, and therefore studies of the long term effects are important. The work was carried out using a simple computer model which relates the use of fertiliser to population and calculates the corresponding future N_2O emissions by using United Nations data for population growth between 1990 and 2025.

4.2 NO_x from Lightning

In general, estimates of global NO_x production from lightning discharges (G) have been made from the product of experimentally determined values of NO_x per flash and the estimated total number of flashes occurring around the globe during one year. This has been represented by Liaw *et al.*, (1990) as

$$G = C\ P\ F \qquad (4.1)$$

where C is a conversion factor for NO_x expressed in molecules s^{-1} to NO_x in Tg (N) yr^{-1}, F is the number of flashes s^{-1} globally, and P is the number of molecules of NO_x produced by one flash.

Values of P have been obtained by two of the methods described above. One of these is by direct field measurements, where the ambient concentrations of NO_x have been analysed directly after a flash or series of flashes. This has been carried out near to ground level using chemiluminescent and/or absorption spectroscopic detection of the species produced during a thunderstorm (Noxon, 1976 and 1978; Drapcho *et al*, 1983; Franzblau and Popp, 1989), and also by the analysis of air collected during flights through thunderstorms (Levine *et al*, 1983; Davis *et al*, 1987). An alternative approach is to determine the amount of NO_x formed per joule by small scale laboratory discharges (Chameides *et al*, 1977; Donohoe *et al*, 1977; Levine *et al*, 1981, and 1984; Peyrous and Lapeyre, 1982) which can then be multiplied by the average energy of a lightning flash to give the total amount of NO_x formed by one

flash. The energy of a lightning flash has been estimated as a result of laboratory investigations, or via theoretical calculation.

Table 4.1 Previous Estimates of Global NO_x Production

Study	NO_x J^{-1} $/10^{16}$ molec.	Energy $flash^{-1}$ $/10^9$ J	Channel length /km	NO_x f^{-1} $/10^{25}$ molec.	Flash freq. $/s^{-1}$ [a]	Tg (N) per year[a]
Tuck (1976)	(1.8) t	(0.625)	6.25	1.1	500	(4.2)
Griffing (1977)	10.0 t	(3.2)	10	(32)	100	(23.5)
Chameides *et al.* (1977)	6.0 l	(2.0)	5	(12)	400	35.0
Hill *et al.* (1980)	(80.0) t	(0.075)	5	6.0	100	(4.4)
Dawson (1980)	6.0 l	(0.15)	10	(0.9)	500	3.3
Levine *et al.* (1981)	5.0 l	(0.1)	10	(0.5)	500	1.8
Drapcho *et al.* (1983)	-	-	30	40 f	100	29.3
Borucki *et al.* (1984)	9.0 t	0.4	(5)	(3.6)	100	2.6
Franzblau *et al.* (1989)	(60.0)	5.0	7	300 f	100	220.0
Liaw *et al.* (1990)	-	5.0	7	Lab Theor Field	200[b] 200 200	19 ± 10 72 ± 96 152 ± 60

( ) - calculated numbers, not stated in original paper

[a] - global values; [b] - strokes s^{-1}

l - laboratory, t- theoretical, f - field measurements

The results of previous laboratory (l), field (f) and theoretical (t) studies are given in Table 4.1. In each case the conditions under which each study was performed

or the values assumed for the physical parameters (such as flash energy, or channel length) vary greatly and this leads to a wide range of estimated G values, from 1.8 - 220 Tg (N) yr^{-1}. In an attempt to remove these discrepancies, Liaw *et al.* (1990) applied the identical parameters (flash energy 5.0 x 10^9 J; channel length 7 km; and global flash frequency 200 s^{-1}) to the values of P used in each of the studies and grouped the resulting values of G according to the type of study (f, t or l). The values given demonstrate the range of uncertainty that still remains, and also show the differences between each type of study.

In each of the studies mentioned, it has been assumed that all flashes are the same. This is not the case, as there are two major types of lightning flash; those that occur between a cloud and the ground, and those that discharge solely within the cloud itself. These are called cloud-to-ground (CG) and intra-cloud (IC) respectively, and both occur within thunderstorms, the proportion of each depending upon the physical conditions within the thunderclouds (Price & Rind, 1993; MacKerras & Darveniza, 1994).

A typical CG flash is between 3 and 7 km long (Uman, 1987; Franzblau and Popp, 1989), and has an energy of 10^9-10^{10} J (Uman, 1987). IC flashes are believed to occur most frequently at altitudes of between 5 and 14 km (Holmes *et al.*, 1980), with centres of lightning activity observed at 6-8 km and above 11 km (Mazur *et al.*, 1984). They are thought to be a third as energetic as CG flashes (Franzblau and Popp, 1989), are of a shorter length, but occur with greater frequency. The globally-averaged IC to CG ratio in a typical thunderstorm has been estimated by satellite data as 4:1 by Prentice and MacKerras (1977) and more recently as 2.3:1 by MacKerras and Darveniza (1994). The ratio has been found to vary with latitude, with a greater number of IC flashes normally occurring in tropical regions, where the conditions required for thundercloud formation are at higher altitudes.

This study has investigated the relative importance of each typé of flash in the calculation of global NO production from lightning. Using the value of $(9 \pm 2) \times 10^{16}$ molecules NO J^{-1} obtained in the work of Stark *et al.*, (1995) along with a flash

energy of 5×10^9 J, P is calculated from equation (4.2).

$$P = M\,[(N_{IC} \times E_{IC}) + (N_{CG} \times E_{CG})] \qquad (4.2)$$

where M is the number of NO molecules produced J^{-1}, E_{IC} and E_{CG} are the energies of IC and CG flashes, where $E_{IC} = 1/3\ E_{CG}$, and N_{IC} and N_{CG} represent the proportion of IC and CG flashes ($N_{IC} + N_{CG} = 1$).

The value of P thus obtained is then multiplied by the global flash frequency, which in this study has been taken as 100 s^{-1} (Borucki & Chameides, 1984), and converted into a tonnage of NO produced per annum from lightning. The effect upon this estimate of altering the IC:CG ratio was examined and is discussed along with each of the individual parameters in the next section.

4.2.1 Results and Discussion

The global emission rate of NO from lightning using a NO J^{-1} value of $(9 \pm 2) \times 10^{16}$ molecules, a flash energy of 5×10^9 J, a global flash frequency of 100 s^{-1} and an IC:CG ratio of 4:1 has been calculated as 2.1×10^{26} molecules s^{-1}. This can be converted into a total global production from lightning of 15.4 ± 3.4 Tg (N) yr^{-1}, which lies at the lower end of the range of values (19 ± 10 Tg (N) yr^{-1}) presented by Liaw *et al.* (1990) for the laboratory studies.

The similarity between these studies is perhaps fortuitous, due to the different approaches taken in the interpretation of flash frequencies and energies. Liaw *et al* (1990) used a flash frequency of 100 s^{-1}, but then assumed that each flash consisted of an average of two strokes, each of which produced NO_x, thus equivalent to a flash frequency of 200 s^{-1}. The veracity of this assumption is disputed by other studies, which have made suggestions such that there are more than two strokes to each flash or that the first stroke is the most important one, and this is clearly an area which requires further investigation.

Liaw *et al* also assumed that each flash had an average energy of 5×10^9 J, whereas this study, although using this value for the CG flashes, has taken into account the differences between IC and CG discharges. Thus it would be expected that the results of this study would be lower, as at an IC:CG ratio of 4:1, there will be substantially less energy, coupled with half the number of flashes. The fact that it is not half of the mid-range value must be a result of the differences between the NO J^{-1} value used here and those of the other studies.

However, it is important to point out that the values of Liaw *et al* are in terms of NO_x whereas this work has so far only considered the production of NO. Studies by Harrison (1991) indicated that there was a significant formation of NO_2 (up to 30% of NO_x in some cases) from passing an electrical discharge through air. This was ascribed to the reaction of ozone with NO, as mentioned in Chapter 1. Therefore, if an average value of 10% NO_x is taken to be NO_2, this increases the overall estimated global NO_x production from lightning to 16.9 ± 3.8 Tg (N) yr^{-1} in this study.

If NO_2 formation from lightning is non-trivial, it provides a direct tropospheric input, which may have a significant effect on the chemistry of regions where lightning occurs frequently, such as the tropics. NO_2 is important in terms of the production of ozone and OH in the troposphere, the latter being the major route for removal of many pollutants. Hence an understanding of the factors which affect its concentration is essential in terms of studying the chemistry of the atmosphere. This is covered in more detail in Chapter 5.

The IC:CG ratio of 4:1 was taken from work by Prentice and MacKerras (1977), and represents an average global value. However, more recent work has produced an estimate of 2.3:1 or lower (MacKerras and Darveniza, 1994), and this will obviously have a significant effect upon the NO_x prediction. Figure 4.1 shows how the estimated NO changes when the IC:CG ratio is altered. Two extremes of 1:1 and 9:1 were included, to demonstrate the relationship, and as expected the NO values drop as the proportion of lower energy IC flashes rises. This is important both on a global and a regional scale. In tropical areas, the proportion of IC flashes has been predicted

as greater than in temperate areas due to the meteorology, which may result in a lower production of NO_x. However, the frequency of flashes is much higher in tropical regions, thus counteracting this effect, although the extent of this will vary. The subject of regional lightning/NO_x distribution is discussed in more detail in Section 4.4.

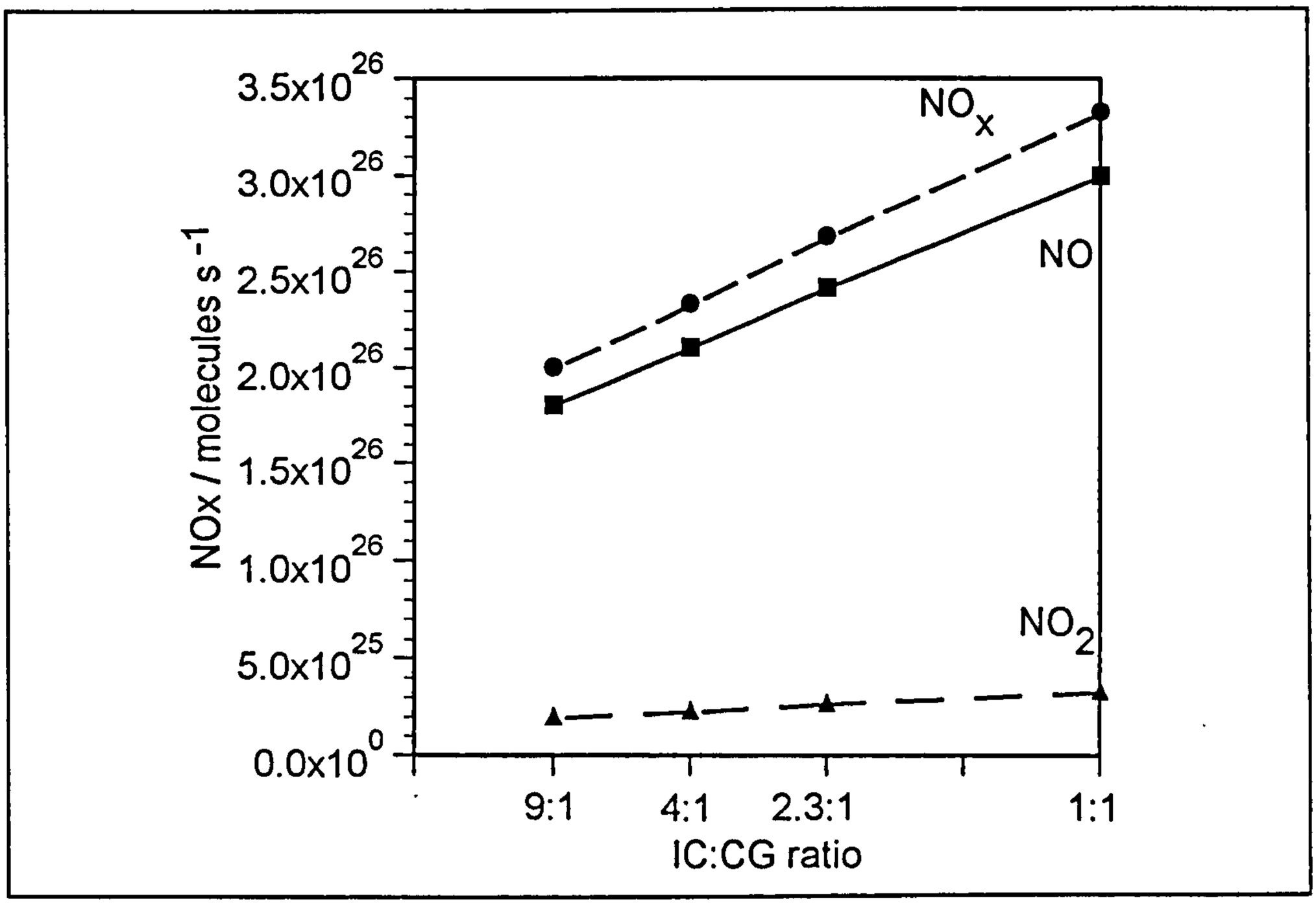

Figure 4.1 The effect of altering the IC:CG ratio upon the global NO_x production rate as calculated in the model.

The attempt at removing discrepancies between the different types of study (laboratory, field and theoretical) made by Liaw *et al* (1990) proved to be unsuccessful, demonstrating that even when similar values of physical parameters are used, the values taken for the production rate of NO_x have a major effect upon the extrapolated global predictions. Therefore it is crucial to ensure that the values of all contributing factors are as accurate as possible, as errors on the small scale will be magnified when making global estimates, as demonstrated by the considerable range over which Liaw's estimates span.

The laboratory studies, as outlined in Chapters 2 and 3, are based upon small scale

electrical discharges, which are several orders of magnitude shorter than the average lightning flash. Although the energies associated with smaller length discharges are also smaller, the production of NO_x does not scale down in a linear fashion (as discussed in Chapter 3). This is due to the losses which occur within a closed experimental system, which do not take place in the atmosphere. Therefore, whilst laboratory work is important in allowing the study of phenomena which are not easily accessible in their natural form, it is essential that the differences between the simulated and actual event are recognised and accounted for in order to reduce errors when scaling up.

Field studies of lightning are concerned with the measurement of concentrations of gases after a storm, and the number of flashes/flash energies within that storm. Combining these gives an estimate of the production of NO_x. However, there are a different set of problems associated with such work, not least the determination of the background concentrations of species, and the associated dilution factors which occur during the turbulent conditions. For example, in a sample of air taken from the middle of a storm, how much of the species has been formed by lightning strikes around that point, and how much has been transported from previous strikes? And once this has been estimated, there is then the question of whether the storm was representative of the majority of storms globally, or whether it was particular to that region. With such complex uncertainties, it is not surprising that large differences exist between the laboratory and field studies. However, field work is essential in our understanding of the lightning phenomenon; not least in the monitoring of flash frequency and global distribution and the possible validation of models.

In the case of theoretical studies, the models which have been developed to represent the physical and chemical aspects of lightning/electrical discharges are currently inadequate, as shown by the large range of estimates in Table 4.1. However, if further experimental work is carried out into investigating these areas, combined with refinement of these models, it will provide a useful tool in the general study of this field and may lead to more accurate global predictions of the role of lightning in the chemistry of the atmosphere.

It is not just the estimation of lightning NO_x which is surrounded with uncertainty. The total global NO_x production from all sources is also ambivalent, mainly because its atmospheric concentration is so variable and therefore difficult to measure, as are the natural sources (see Table 1.1). Previous studies have predicted total sources of up to 400 Tg (N) yr^{-1} (Chameides, 1977), of which lightning has been reported as contributing between 10% (Levine *et al.*, 1984) and 50% (Franzblau and Popp, 1989). However, more recent studies suggest that this is more likely to be about 52 Tg (N) yr^{-1} (Houghton *et al.*, 1995), with lightning making up 10% of this total. The uncertainty in these estimates is large, with that of lightning being over 100%, and highlighting the need for more extensive study in this area. Interestingly, if the estimates of the field studies (150 Tg (N) yr^{-1}) are applied to the figures in Table 1.1, the total global NO_x sources would be 200 Tg (N) yr^{-1}, with lightning contributing 75%. This would seem unlikely, even with the uncertainty surrounding current knowledge. However, if our estimate of 16.9 Tg (N) yr^{-1} is included, the contribution from lightning would amount to ~20%, which is perhaps a more reasonable estimate.

4.2.2 Conclusions

In summary, the results of laboratory measurements of NO_x formation from electrical discharges have been used to estimate the global production of NO_x from lightning. A value of 16.9 Tg (N) yr^{-1} has been obtained, assuming that 10% is formed as NO_2. When compared to work by Liaw *et al* (1990), who summarised the results of a variety of field, laboratory and theoretical studies in this area, this showed that the uncertainties in the estimates of each type of study is high, and highlighted the need for further research in this area, in order to produce a more accurate global budget for NO_x. To address this will require:

- better understanding of the lightning mechanism, its physical characteristics (energy, length, frequency, number of strokes) and its occurrence and distribution over the globe.
- knowledge of the chemical effects of lightning and how they are affected by the different physical parameters, in terms of the formation of other species and their subsequent effect upon the chemistry of a region.

This will only be obtained by the combination of more realistic field, laboratory and theoretical studies, which are crucial to developing our understanding of the atmosphere.

4.3 N_2O from Lightning

As explained in Chapter 3, the formation of N_2O from electrical discharges in air does not appear to occur via a thermal mechanism, as is the case for NO. It is proposed in this study that N_2O is formed from corona discharge both prior to and during the flash, and possibly destroyed by the action of photolysis from the flash. If the energy of the corona discharge could be determined, a value of N_2O J^{-1} could be assumed, and the global production of N_2O could be approximated in a similar way as for NO, whilst bearing in mind the differences between the experimental discharges and atmospheric lightning flashes.

It was not possible to determine the value of the corona energy in the present work, but it has been attempted in previous studies, and was used to estimate the global production of N_2O. Hill *et al* (1984) calculated that the formation of N_2O occurred at a rate of 1.1×10^{21} molecules $stroke^{-1}$. Assuming that the average corona energy available in one lightning stroke was 1.5×10^4 J m^{-1}, and that 300 strokes per second occurred over the globe (based upon 100 flashes s^{-1}, and 3 strokes per flash) a global production rate of 2.24×10^3 tonnes N_2O yr^{-1} was calculated.

If the production of N_2O from point corona discharges was also accounted for (Donohoe *et al*, 1977), this value was estimated at between 2.3 - 3.0×10^3 tonnes N_2O yr^{-1} (or 1.5 - 1.9×10^{-3} Tg (N) yr^{-1}). At present, from current knowledge of the atmospheric concentration, sources and sinks of N_2O, the total identified sources of N_2O have been estimated to produce 14 - 17 Tg (N) yr^{-1}, with a potential 2-3 Tg (N) so far unidentified. Comparison of the lightning estimates with the total suggest that under the assumptions made, lightning is not a significant source of N_2O. In order for lightning to be important (~0.5 Tg (N)), either the energy dissipated from corona

discharges or the production rate of N_2O J^{-1} would have to be a factor of 250 higher, which would appear to be a rather large discrepancy.

However, the degree of uncertainty associated with the experimental studies, and the need to know with accuracy how atmospheric systems work demand that further work be carried out in this area, especially in conjunction with studies of NO production. Photolysis has not been considered in the large scale estimates, and this is a topic where little research has been carried out. Its effect upon N_2O and other species in the vicinity of a flash may be important. Also, despite the fact that N_2O is well-mixed in the troposphere and that lightning is probably a negligible source of the gas, the fact that $[N_2O]$ has been shown to be enhanced in regions of lightning discharges may have consequences for transport rates to the stratosphere. These are, therefore, areas which require further work.

4.4 Global Distribution of NO_x

As explained in Chapter One, lightning is the result of a build up of charge in the atmosphere, most often in thunderclouds. These are formed when warm moist air rises, encountering decreased temperatures and producing unstable conditions, where water droplets are colliding with ice crystals (Uman, 1986), and by some mechanism stripping them of electrons to produce highly charged regions within the cloud. Lightning is therefore more common over tropical regions, where the atmospheric conditions are favourable (MacKerras and Darveniza, 1994; Price and Rind, 1993; Krehbiel *et al.*, 1983) and also during the summertime in temperate regions. It is also more likely to occur over land areas, as cloud-ground (CG) flashes require a point at which to discharge. This point is usually the highest point in close proximity, as less energy is required to discharge, which explains why trees, tall buildings and mountainous areas are the most prone to strikes, whereas lightning over oceans is much rarer (Uman, 1986).

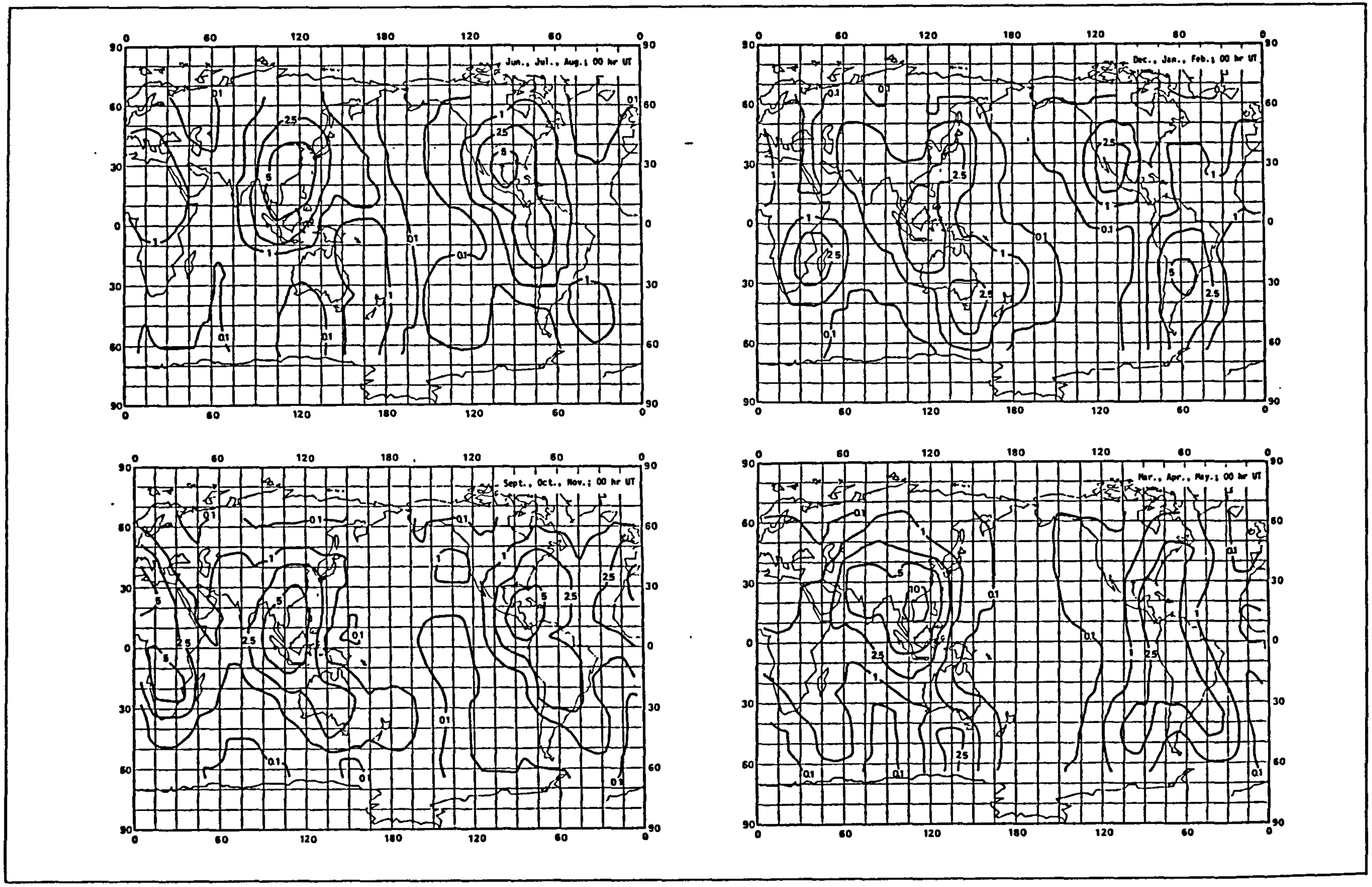

Figure 4.2 Global flash frequencies for each season (from Kotaki and Katoh, 1983)

This means that the latitudinal distribution of lightning over the earth is not even, and consequently neither is the associated production of species such as NO_x. This has implications for both the regional and global atmospheric chemistry of NO_x. If the global distribution of lightning and thus the formation of NO_x can be examined, the results can be used as inputs to chemical modelling schemes, for analysis of the effects of lightning on the chemistry at different altitudes and latitudes.

Kotaki and Katoh (1983) carried out satellite measurements of the global occurrence of lightning. They produced plots of seasonal distribution of lightning for March - May (MAM), June - August (JJA), September -November (SON) and December - February (DJF) (given in Figure 4.2) where the regional lightning density is represented by contour lines. The average global flash frequencies were calculated as 54, 55, 80 and 64 s^{-1} for the respective seasons which results in a global annual average of 64 flashes per second. This is lower than that of 100 s^{-1} used in the previous sections. The contour maps have been used to investigate the occurrence of lightning on a regional basis and, using data obtained from the last section, estimates for relative NO_x production in terms of latitude and continent have been determined. It is important to note that the study is more concerned with relative rather than absolute values, as the latter have been shown in the previous section to depend greatly upon the NO_x $flash^{-1}$ and flash frequency values employed in the calculation.

4.4.1 Results

4.4.1.i) Global flash frequencies

Initially the plots were divided into latitude bands representing tropical and temperate north and south, 0-30N and S, and 30-70N and S. All areas on the map were bound by two contour lines, and hence two frequency values, each representing an upper and lower limit. Flash frequencies were calculated in terms of both upper and lower values, and once all maps had been analysed, the average seasonal flash frequency range was calculated and compared to the values of Kotaki and Katoh. These values are shown in Table 4.2 and the original values were found to be around 85% of the

upper value. Therefore for the purpose of further analysis, the 85% values were used to calculate the NO_x production. This was obtained by multiplying the previously determined NO_x per flash value (see Section 4.2) of 2.33×10^{26} molecules (corresponding to a global IC:CG ratio of 4:1) to obtain the total amount of NO_x produced in each area.

Table 4.2 Comparison between flash frequencies of Kotaki and Katoh and this work

Season	Flash s^{-1} [a]	% [a]	Range[b]	%[b]
JJA	55	22	22-65	21
SON	80	32	35-89	31
DJF	54	21	22-64	21
MAM	64	25	31-80	27

[a] - Kotaki and Katoh (1983)

[b] - This work

The total NO_x produced by lightning was estimated to be between 4.74 (lower limit) and 12.64 (upper limit) Tg (N) yr^{-1}, of which the 85% value, and thus that of Kotaki and Katoh, is estimated at 10.74 Tg (N) yr^{-1}. This value is slightly lower than that obtained by using the previous model, 16.9 Tg (N) yr^{-1}, and is a direct result of the use of two different flash frequencies. However it is important to bear in mind that the flash frequency is only an average value and is not constant on an annual, seasonal, temporal or latitudinal basis. The investigation carried out here is intended to give an indication of the relative contribution of different regions of the globe to the production of NO_x, and is not concerned as much with the absolute values, which are not constant.

Table 4.2 shows that the greatest proportion of flashes occurs during the NH autumn (SON;31%), followed by the spring (MAM;27%) with the summer and winter lightning events being the least active. As explained before, lightning is more likely

to occur when the temperature at ground level is warmer. Therefore it might be expected that it would be at its highest during summer. However, on a global basis, during the summer of one hemisphere it is the winter of the other, and so the enhanced activity of the summer is obviously cancelled out by the simultaneous reduced activity in the opposite hemisphere. Therefore it would appear that when temperatures are more even the lightning activity is more widespread. This is investigated in more detail by treating the NH and SH and the tropics and temperate regions separately, and estimating the lightning activity of each on a seasonal basis.

4.4.1.ii) Latitudinal analysis

The results are tabulated in Table 4.3 and show that the contribution of the tropics to global lightning activity is greatest during all seasons of the year, with up to 62% of total lightning flashes occurring between 30S and 30N during SON. At the IC:CG ratio used in this study, this is to be expected, as the flash densities of lightning in the tropics is shown to be much higher on the contour maps. The Northern Hemisphere accounts for ~60% of lightning activity in all seasons except winter (DJF), when the Southern Hemisphere accounts for 54%, it being SH summer. The greater land mass of the NH results in the higher percentage for the majority of the year, as explained earlier. As a consequence of these factors, the northern tropics have the highest proportion of lightning, again except during NH winter.

Table 4.3 Relative NO_x Production by Latitude and Season

Season	30-70S	0-30S	0-30N	30-70N	Tropics	NH
JJA	17%	19%	35%	29%	54%	64%
SON	15%	27%	35%	23%	62%	58%
DJF	25%	29%	24%	22%	53%	46%
MAM	21%	21%	34%	25%	55%	59%
Overall					56%	57%

A study was carried out to investigate the flash density of each region, as the areas of the latitude bands were different. Table 4.4 confirms the previous work, as it was found that the tropical NH has the highest flash density in all seasons except for NH winter, when the tropical SH is greatest (shown in Table 4.4) and suggests that the potential production of NO_x is greatest at all times over the tropics, especially between 0 and 30N.

Table 4.4 NO_x produced per square km by Latitude and Season

Season	30-70S[1]	0-30S[1]	0-30N[1]	30-70N[1]
JJA	1.86	2.95	5.34	3.30
SON	2.28	4.37	7.33	3.62
DJF	2.81	4.37	3.61	2.47
MAM	2.82	3.79	6.05	3.35

[1] all units in molecules NO_x s^{-1} km^{-2}

4.4.1.iii) Continental analysis

In a second analysis, the plots were divided approximately into the land masses of Europe, USA and Asia. The areas used are shown in Figure 4.2. An identical approach to that given above was used to determine the total number of flashes for each area in each season and the NO_x value calculated.

Bearing in mind that the area of Asia is nearly three times that of Europe and USA, it was calculated that 25% of global lightning activity occurs over Asia, with ~5% over the USA and ~2% over Europe (see Table 4.5). Approximately 4% of lightning in the NH occurs over Europe, whereas this is around 8% over the USA. If the area is taken into account it is found that the lightning density is also greater in Asia, suggesting that this is an important region for production of NO_x.

Table 4.5 Relative contribution of continents to NO_x Production

Season	Europe		USA		Asia
	% world	% NH	% world	% NH	% world
JJA	2	3	7	11	24
SON	3	6	4	6	18
DJF	2	4	4	9	16
MAM	1	2	4	7	29
Overall	2	4	5	8	25

4.4.1.iv) Variation of IC:CG ratio

The analysis so far has assumed an IC:CG ratio independent of latitude. The results of other studies have shown that this ratio can vary, with more IC flashes occurring in tropical regions (Uman, 1986). This is a result of the meteorology occurring over tropical regions. In Section 4.2 it was suggested that the production of NO_x was dependent upon this ratio, with less NO being produced at higher ratios. Therefore at the tropics although there are proportionally more flashes the number of IC flashes is greater, and hence the amount of NO produced relative to temperate regions will depend upon the product of these two values. To investigate this aspect, ratio data from MacKerras and Darveniza (1994) was applied to the corresponding NO_x flash^{-1} values obtained from Figure 4.2. Their results showed that the ratio varied from 2.3:1 between 0 and 20 to 1.3:1 between 40 and 60. Modification of these values to incorporate the latitude bands used in this work led to ratios of 2.3:1 for 0-30 and 1.6:1 for 30-70 with corresponding NO_x production values of 2.65 and 2.95×10^{26} molecules flash^{-1} respectively. As before, the flash frequencies for each of the regions were multiplied by the NO_x data to obtain the relative NO_x production.

Once again, the relative values have been taken, as a result of the use of a different

ratio than in the base case. The results are given in Table 4.6 and show that there is a slight decrease in the tropical contribution to NO_x production during each of the seasons when the difference between the IC:CG ratio of the tropics and temperate areas is approximately a factor of two. However, the decrease is not large enough to reduce the proportion of NO_x production from the tropics significantly. This would only be the case if the difference between the IC:CG ratios for temperate and tropical zones were to be much greater than 2, and as this difference is not a constant, it would seem unnecessary to apply this principle to the calculation of regional NO_x production of lightning.

Table 4.6 Effect of varying IC:CG ratio with latitude

Season	Tropics (P)	Tropics (N)
JJA	54%	51%
SON	62%	59%
DJF	53%	49%
MAM	55%	51%

P = original results;

N = results of changing IC:CG ratio

4.4.2 Conclusions

In conclusion it would appear from the analysis of the global distribution of lightning, that over 50 % of lightning activity occurs between 30S and 30N during all seasons of the year, with the NH tropics having the greatest lightning densities, except during the NH winter. The NH accounts for around 60% of the lightning activity, except during the winter, with the US contributing 8% and Europe contributing 4% of this. This would therefore appear to support the atmospheric observations that [NO_x] is higher in the NH than in the SH, which is ascribed to the greater land emissions (Houghton *et al*, 1995), but could also be due to more lightning activity. Asia is the most important region for lightning, accounting for 25%

of the global lightning activity. This therefore has implications for the formation of NO_x on a global basis.

The analysis of IC and CG flashes suggests that unless there are significantly greater proportions of IC flashes in the tropics compared to temperate regions, the lower energy of these flashes does not reduce the importance of these regions as a tropospheric source of NO_x.

It would be interesting to measure the $[NO_x]$ above regions of high ground emissions, and compare this with concentrations in regions where there was high lightning activity but low ground emissions. This will be the only way to determine more absolutely the effect of lightning upon the local chemistry. In Chapter 5, this is considered in terms of a chemical model.

4.5 Future N_2O Emissions from Fertilised Soils

As explained in Chapter 1, the global budget of N_2O is also highly unbalanced, with total estimated sources exceeding sinks by around 4 Tg (N) yr^{-1} to account for the atmospheric increase. The relative contributions of each of the sources identified to date is uncertain, and it is possible that there are sources which are as yet unidentified. As with NO_x, many of the sources are biogenic, and thus difficult to measure and quantify on a global scale. However, unlike NO_x, the contribution of lightning to the formation of N_2O is estimated in Section 4.2 to be negligible.

It is thought that the reason for the atmospheric increase, although anthropogenic in origin, is not industrial but a result of human disturbance of natural ecosystems, such as deforestation, biomass burning, and cultivation of soil. The addition of nitrogenous (N) fertilisers to soils has been known for two decades to enhance directly the natural emission of N_2O through the acceleration of the nitrification and denitrification processes described in Chapter 1. Equally, N_2O is emitted indirectly through leaching of fertiliser into groundwater and freshwater systems (Bolle *et al.*, 1986) and from

the release of N_2O dissolved in soil surface waters and agricultural drainage waters (Dowdell *et al.*, 1979). It is also believed that the emission of N_2O from the addition of N-fertiliser to tropical soils is enhanced compared to temperate areas (Keller & Reiners, 1994).

The most recent estimates of the magnitude of global fertiliser-induced N_2O emissions suggest that up to 3.5 Tg (N) yr^{-1} of the atmospheric increase could originate from this source (Houghton *et al.*, 1995). As global populations grow and the demand for food rises, especially in developing countries, the need for cultivation of land for food production will grow. This is borne out by the doubling in fertiliser use in the developing world over the past decade, whilst the demand of the developed world has reached a plateau. Therefore N_2O emissions and hence the atmospheric concentration are anticipated to continue rising, and at a potentially greater rate than previously experienced if tropical emissions are more substantial. This has worrying consequences for both the climate and the depletion of stratospheric ozone and merits further investigation.

Predictions of future atmospheric trace gas concentrations are often made using mathematical models by relating emissions to a number of social, economic and political factors, such as population growth, emission control strategies, land use and so on. By changing the values of these factors within the models, the effects upon the emission rates and thus concentrations can be assessed, and 'scenarios' developed. A disadvantage of this multi-variable approach is that uncertainties in the future values of the various parameters are propagated through to the final emission predictions, and hence the greater the number of variables the greater the potential error.

In this study, a model has been developed which relates emissions of N_2O from fertilised soils to a single variable, population, which may be predicted over a 35 year period with a reasonable degree of certainty. This work follows earlier studies on the predictions of future CO_2 and CH_4 concentrations in the atmosphere using the same approach (Anastasi *et al.*, 1990, 1992 and 1993).

4.5.1 Model Development

Full details of the general approach used in this study are explained by Anastasi *et al.*, (1990, 1992 and 1993) and need not be described in detail here. Briefly, in this case, a relationship is established between population and N-fertiliser use, and by studying population predictions until 2025 the future levels of N-fertiliser consumption can be calculated. This is then converted into an N_2O emission rate by means of a conversion factor, calculated by Eichner (1990) based upon analysis of a wide range of N_2O/fertiliser studies.

In previous work, the estimation of global fertiliser-induced N_2O emissions has been carried out in one of two main ways, both based upon the results of field studies as described in Chapter 1. Bouwman (1990) found a relationship between fertiliser use per hectare and N_2O flux, and assuming this to be a global average, took data for the total world fertiliser consumption and the total land area under cultivation, to calculate an emission of 2.3 - 3.7 Tg (N) yr^{-1}. Other studies have reported the average conversion of applied fertiliser nitrogen to N_2O, independent of land area, both in the soil and from groundwater leaching: 1 - 4%, Bolle *et al.*, (1986); 0.5 - 1.5%, McElroy and Wofsy, (1985); ≤ 3%, Eichner, (1990). Estimates of N_2O fluxes of between 0.2 and 3.0 Tg (N) yr^{-1} (for 1990) were produced from these conversion factors using data for global fertiliser consumption.

The conversion factor of Eichner (1990) was used here as it represented the most comprehensive analysis of field studies available at the time of the investigation (1992).

4.5.1.i) Classification of countries

The analysis is based on the division of countries into groups with similar fertiliser use per capita. The most recent statistics available for N-fertiliser use are for mid-year 1989 to mid-year 1990 (FAO, 1990); data is given for 140 countries, corresponding to a total world consumption of 79.1 Tg fertiliser-N over this period.

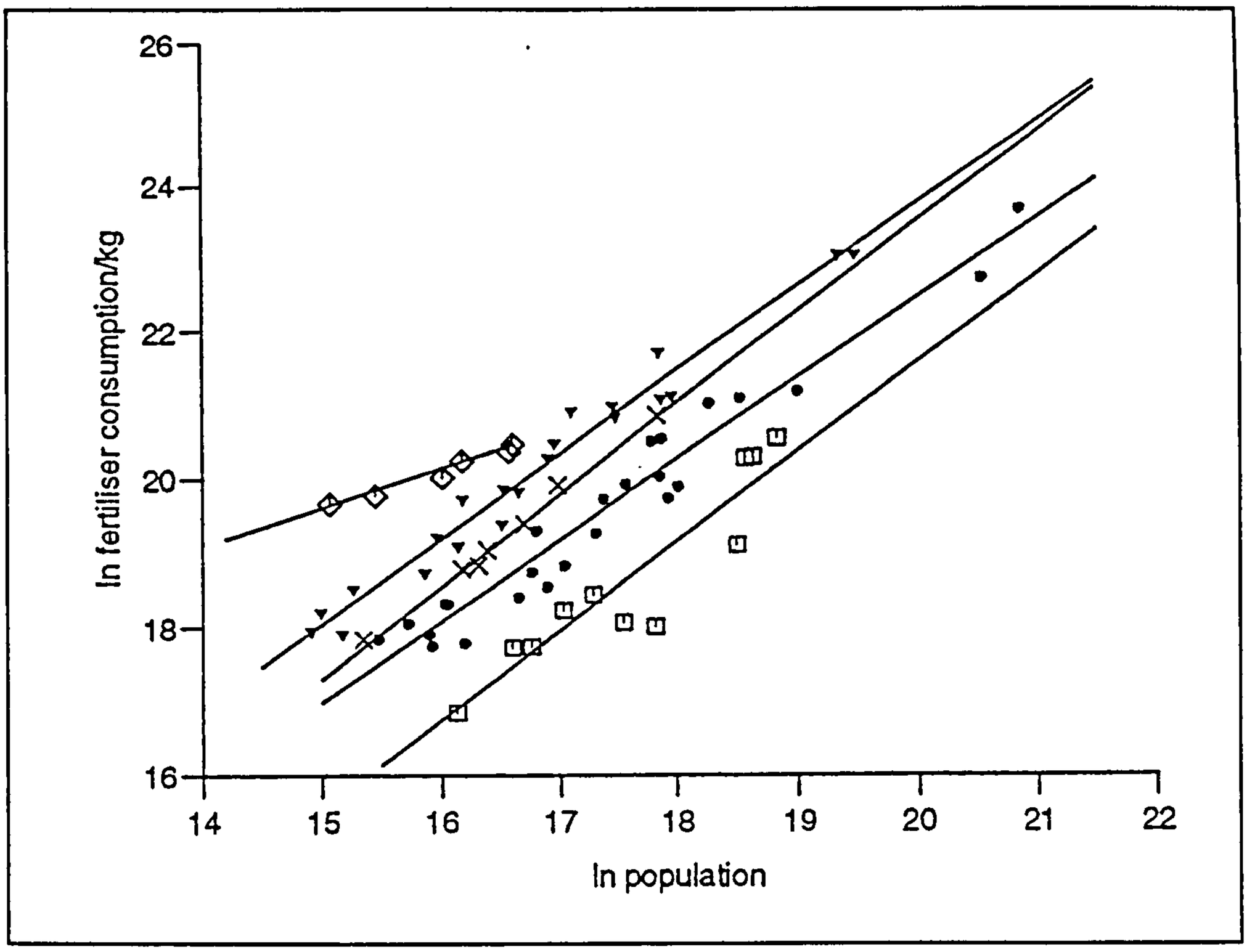

Figure 4.3 Fertiliser consumption as a function of population for the 71 'A' countries in this study. Class 1 (◊), 2 (▾), 3 (×), 4 (•), and 5 (□).

71 of the countries (referred to as `A' countries) used >99% of this total and were considered the most important for the purposes of this study. The remaining 69, (referred to as `B' countries throughout this work) have very small land areas, and so although their use of fertiliser may increase over the next 25 years, collectively their use is relatively insignificant, and hence they are treated separately in a variational analysis

Using United Nations (1992) population data for 1990 a plot of fertiliser use as a function of population was made for the 71 countries, and this is shown in Figure 4.3. These were then grouped into 5 classes according to national *per capita* use of fertiliser, so that countries with different populations but similar agricultural activity were in the same class (see Table 4.7). A series of regression analyses were performed to assess the optimum number of classes for the study based upon how close the predicted values of fertiliser use for 1990 were to the FAO data. These classes were chosen to maximise the goodness of fit for the data points of each

country. A single class regression analysis resulted in 1990 fertiliser predictions 80% of the FAO total, while increasing the number of classes improved the accuracy of the predictions compared to the data. The optimum was found to be 5, which predicted the fertiliser use to within 95% of the FAO data; no significant difference was observed from a greater number of classes.

4.5.1.ii) Population predictions

National population forecasts for 5-yearly intervals from 1990-2025 were used in the model (United Nations, 1989). Initially, medium variant population forecasts for each country were chosen as the most representative allowing for changes in birth and death rates and inter-regional migration. By assuming the relationship found between fertiliser use and population for each class in 1990 remains linear, and that fertiliser use *per capita* is constant over the next 35 years (see section 2.4), population forecasts are used in the model to calculate the total fertiliser consumption for each class up to 2025.

4.5.1.iii) N_2O emissions

Emissions of N_2O have been calculated from predicted fertiliser use based upon the conversion factors reported by Eichner, (1990), who suggests that if 100 Tg fertiliser nitrogen were consumed in the year 2000, 2-3% of the nitrogen would be converted to nitrous oxide. As discussed previously the high degree of variability in emission rates, and the limited measurements carried out in some areas of the world, prevent subsequent accurate quantification of global N_2O fluxes; therefore, the use of an average conversion is the best approach possible at this time. The conversion factor used here is chosen as the most accurate assessment of data from a large number of field studies, but is limited in that it is based upon temperate regions. This is discussed in Section 3. A 3% conversion value is used in the model as a base case for the purposes of a variational analysis; this value is chosen as a worst case estimate, to account for possible increases in fertiliser use *per capita* and the potentially higher emissions from tropical soils.

Table 4.7 Classification of 'A' countries

Class 1	Class 2	Class 3	Class 4	Class 5
		lnF/lnP[a]		
>1.22	1.18-1.22	1.16-1.18	1.10-1.16	<1.10
Bulgaria	Canada	Chile	Egypt	Algeria
Czechoslovakia	Costa Rica	Israel	Morocco	Nigeria
Denmark	Cuba	Malaysia	S. Africa	Argentina
Finland	Nicaragua	Syr. Ar. Rep	Tunisia	Brazil
former GDR	USA	Turkey	Zambia	Afghanistan
Hungary	Dem. Rep. Kor	Portugal	Zimbabwe	Bangladesh
Ireland	Saudi Arabia	Yugoslavia	El Salvador	Iran
	Albania		Guatemala	Japan
	Austria		Mexico	Myanmar
	Belg-Lux		Colombia	Nepal
	France		Ecuador	Greece
	former FRG		Peru	
	Netherlands		Venezuela	
	Norway		China	
	Poland		India	
	Romania		Indonesia	
	Spain		Iraq	
	Sweden		Rep. of Korea	
	UK		Pakistan	
	Australia		Philippines	
	USSR[b]		Sri Lanka	
			Thailand	
			Vietnam	
			Italy	
			Switzerland	

[a] - F is fertiliser consumption/kg; P is population

[b] - data only available for former USSR as a whole

4.5.1.iv) Model validation

In previous work validation of the model has been achieved to some degree by applying the model to historical data, and predicting forward to the present to compare predicted values with actual data (see Anastasi *et al.*, 1992). Examination of fertiliser and population statistics from 1970, for which there is data for 67 of the 71 (`A') countries, shows that this approach cannot be used here due to non-linearity in the increase of fertiliser consumption over this period. In the case of North America and Europe, fertiliser use and population have risen at similar rates. However, the growth rate of fertiliser use in Asia exceeded that of population until 1985, so that Asia now consumes ~50% of total world fertiliser compared to 23% in 1970. A linear relationship cannot therefore be assumed for the world as predictions from 1970 would vastly underestimate the current fertiliser consumption.

Instead, an analysis was performed to calculate the changes in fertiliser use *per capita* since 1970 and assess whether it was reasonable to assume a constant *per capita* consumption of fertiliser post-1990. Most developed countries exhibited little change in *per capita* values - and in some cases had shown constant values - since 1980. Countries in South America and Africa had increased *per capita* values slightly, but overall contributed a small amount to total fertiliser use. The *per capita* values for Asia (especially China) had increased quite significantly until 1985 but began to reach a plateau towards 1990. Therefore, the general trend was towards constant *per capita* values by 1985, and the assumption of constant national *per capita* fertiliser use was considered fair for the purposes of this study.

To illustrate this, the average *per capita* values from 1970-1990 were plotted for each class and are shown in Figure 4.4. Although the absolute *per capita* values upon which the 1990 classifications are based will not be valid in 1970 due to their being lower, examination showed that countries tended to remain in the same *per capita* bands over a five yearly period. Any sudden increase or decrease generally occurred on a yearly basis and was cancelled out in the next one or two years. Classes 2,3 and 4, which contain the majority of countries, demonstrate constant *per capita* values

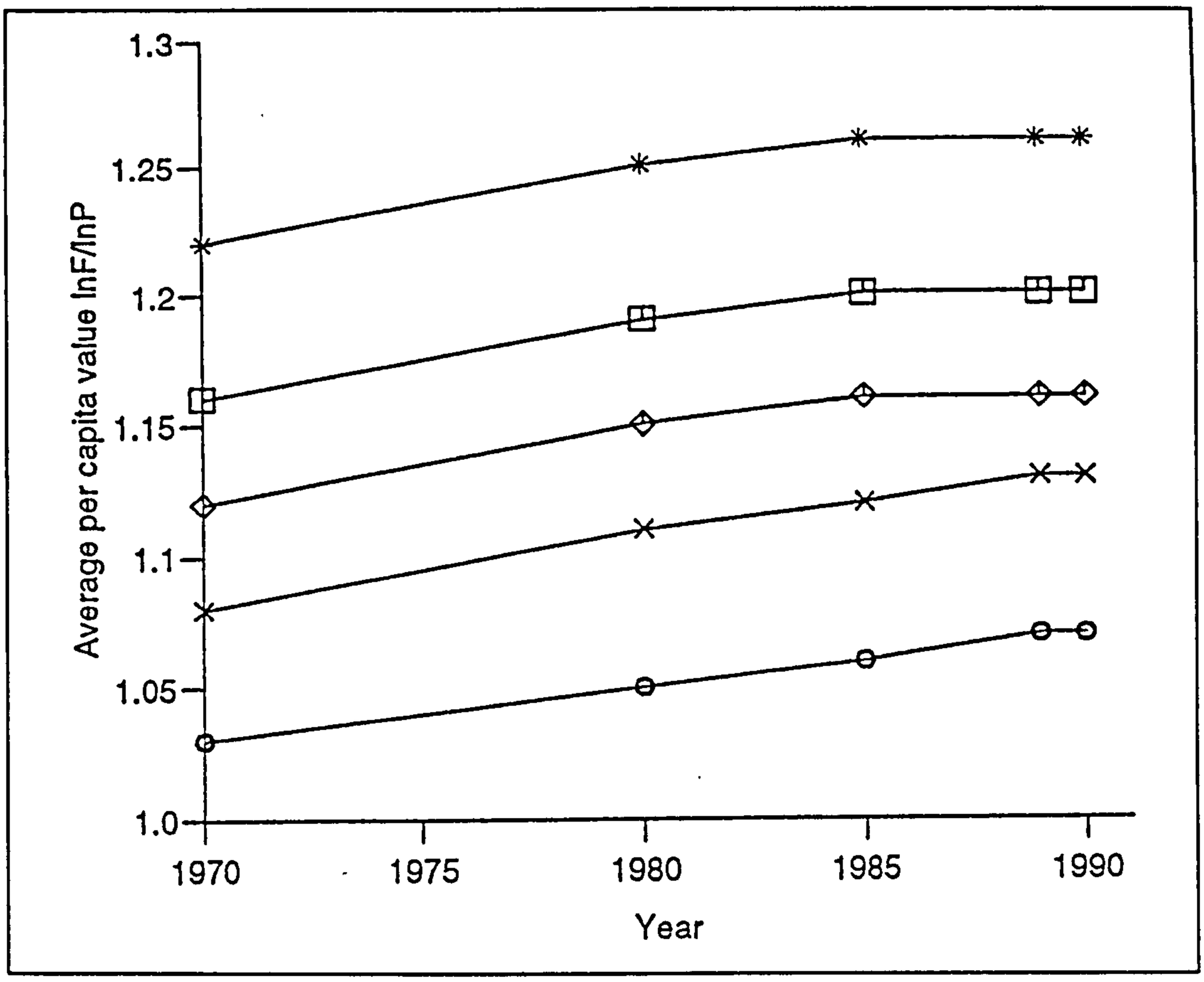

Figure 4.4 Average *per capita* consumption of fertiliser-N for each class from 1970 - 1990. Class 1 (*), class 2 (□), class 3 (◊), class 4 (×), and class 5 (○).

from 1985, suggesting that the basic assumption is acceptable, at least over the time scale considered in this study. In the case of classes 1 and 5, large fluctuations in *per capita* values between 1989 and 1990 for Finland (class 1) and Greece and Iran (class 5) had a marked effect on the average *per capita* values for their respective classes, a consequence of the small number of countries in each of these classes. These points were removed from the plot, resulting in lines similar to those of the other classes. The effect of such fluctuations is negligible in terms of the model as each of these countries contributes a total of less than 1% to the total fertiliser consumed.

4.5.2 Results and Discussion

The model predicts that fertiliser-induced emissions of N_2O will rise from 2.25 Tg N_2O-N in 1990 to 3.24 Tg N_2O-N in 2025, an average increase of 1.3% yr^{-1},

significantly higher than the current rate of increase for total N_2O. The model is based upon three basic assumptions: firstly that the population is predicted to rise to approximately 8 billion by 2025, secondly that the national fertiliser use *per capita* of 1990 will remain constant over the following 35 years, and thirdly that 3% of fertiliser nitrogen is converted to nitrous oxide. These assumptions have been examined in a variational analysis which also includes an investigation of the effects of including the `B' countries in the model and an analysis of emissions by region.

Very few other studies have made predictions over the period covered in this work, but those that have employ slightly different methods than those used in this study. A comparison between the studies is given in Table 4.8. Both the IPCC Working Group (Houghton *et al.*, 1992) and Eichner (1990) apply a conversion factor to future fertiliser forecasts, where the latter is related to past trends and potential economic and political factors, as well as the future demands of population. Both the predicted N_2O emissions and fertiliser consumption derived in the present work are slightly lower than the other reported values, and therefore confirm that population is a dominant factor.

Table 4.8 Comparison of future predicted N_2O emissions

Reference	**Predicted N_2O Emissions ($Tg\ N_2O\text{-}N\ yr^{-1}$)**			**Predicted Fertiliser Use ($Tg\ N\ yr^{-1}$)**	
	1990	**2000**	**2025**	**1997**	**2000**
Eichner (1991)		2-3			100
World Bank (1987)				93.5	
IPCC IS92a scenario *Houghton et al* (1992)	2.20	2.70	3.80		
This study	2.25	2.58	3.24	84	86

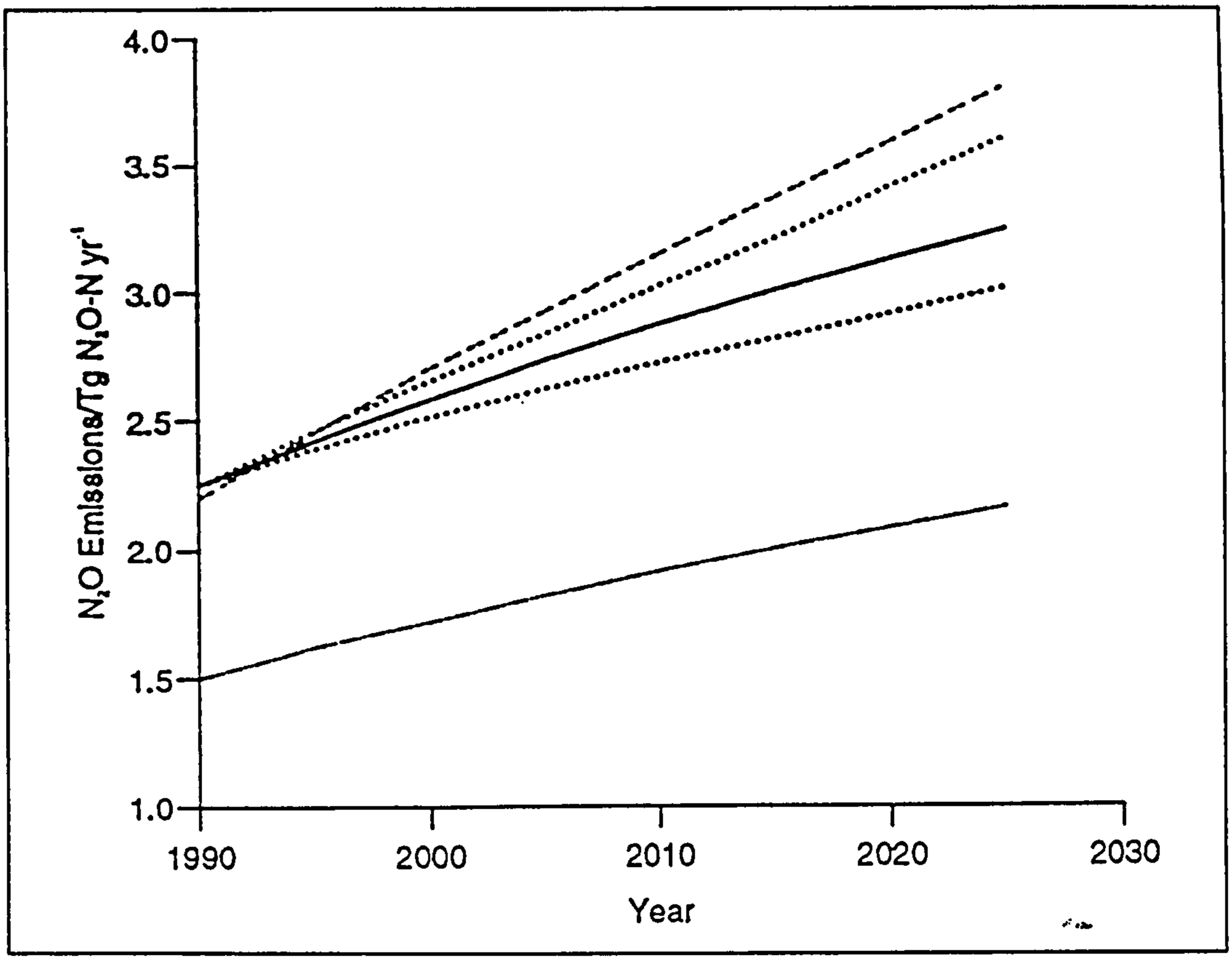

Figure 4.5 Results of a variational analysis relative to the base case (—) for high and low population forecasts (...), 2% conversion (——) and IPCC predictions (– – – –).

4.5.2.i) Variational analysis

To examine the effect of population on the final emission predictions, UN low and high variant population forecasts were incorporated into the model. The resulting changes in predicted N_2O emissions relative to the base case are shown in Figure 4.5, indicating an increase of +11% and a decrease of -8% respectively. The figure also shows the predicted emissions made using a 2% conversion factor, for medium population forecasts, resulting in a 33% decrease relative to the base case, as expected.

The assumption that each country will maintain a constant *per capita* consumption of fertiliser implies that the rate of food consumption *per capita* will remain constant. Developed regions of the world have a much higher food consumption *per capita* than developing areas, and it is expected that these regions will follow the growth of

developed nations although how fast and to what extent is not certain. This does not necessarily mean that *per capita* values will rise, since efficiency of fertiliser use tends to increase as more knowledge is gained about application methods. However, the sensitivity of this model to changes in *per capita* values was investigated by assessing the effect on predicted emissions of moving countries between classes. Increasing the fertiliser use *per capita* of any country which used less than 1 Tg fertiliser nitrogen per year led to no change in predicted emissions, and only nations using greater than this amount were considered. The developed countries which came into this category were United States, Canada, United Kingdom, France, the former Federal Republic of Germany and Spain, all of which are in class 2. It was considered unlikely that the consumption characteristics of any of these countries would change significantly; the study therefore focused only on developing regions. The countries considered were China (class 4), India (4), Pakistan (4), Turkey (3) and Mexico (4). China and India were moved separately from class 4 to both classes 3 and 2, Turkey was moved from class 3 to 2 and Mexico, Indonesia and Pakistan were moved together from class 4 to 2.

As expected due to their large fertiliser consumption and populations, increases in 2025 emissions of between 41% and 52% were observed by moving China and India separately to both classes 2 and 3. In both cases, this was equivalent to an increase in fertiliser consumption of a factor of 3 or more. Conversely, moving Turkey only increased emissions by 1%, and moving Mexico, Indonesia and Pakistan collectively gave increases of between 18 and 20%, implying that the effect of these countries individually is minimal. The model is sensitive to changes in *per capita* values of countries with very large populations and also *per capita* consumption. This is significant only if these countries are likely to increase their *per capita* use of fertiliser over the next 35 years. In the case of the United States this is unlikely, as discussed earlier. However, this may be possible for countries such as India and China and therefore the emissions estimates calculated by this model could represent a minimum, or best case scenario, with emissions potentially rising to 5 Tg N_2O-N if both China and India increase their use of fertiliser by a factor of 3.

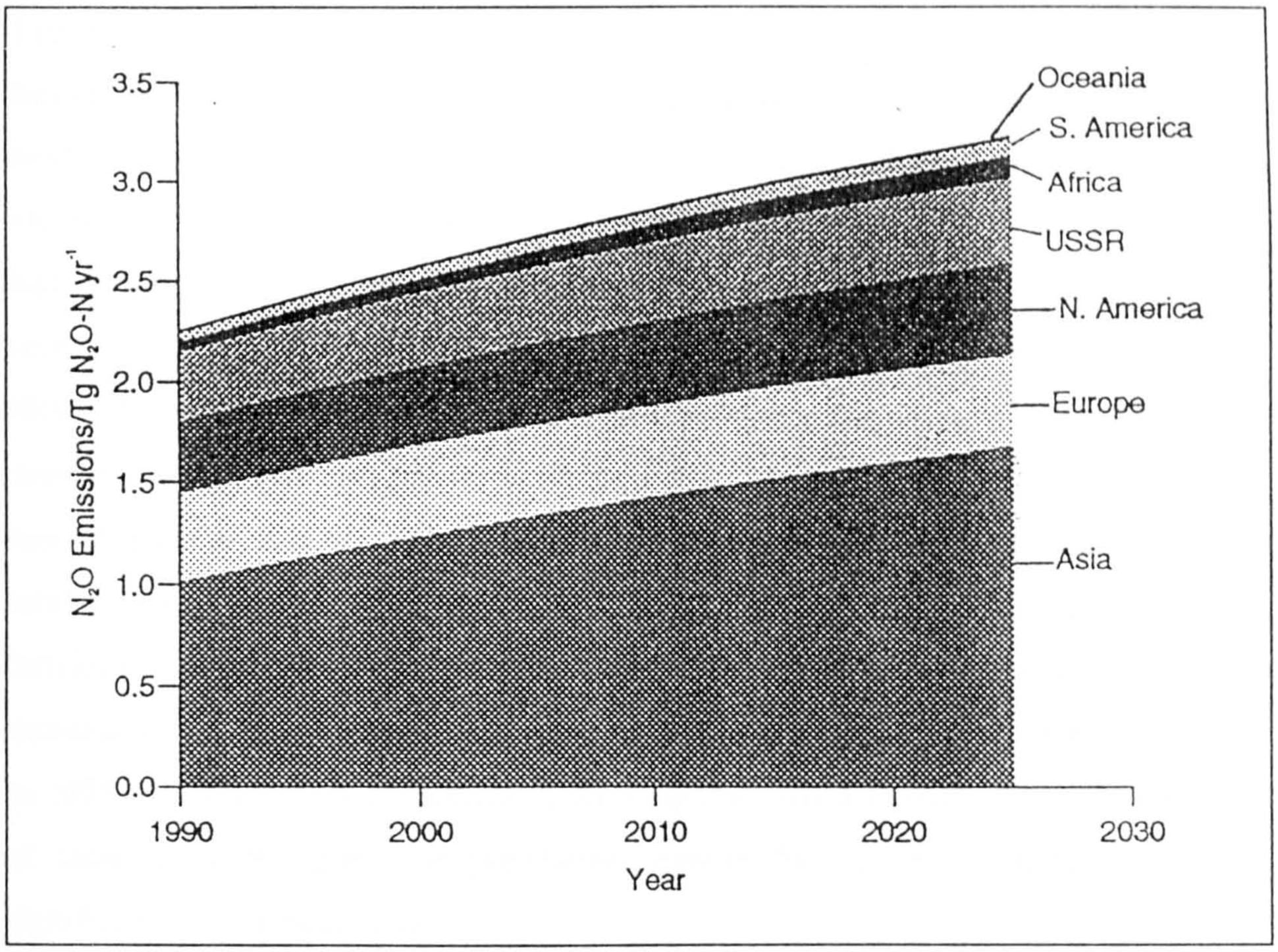

Figure 4.6 Predicted N_2O emissions shown in terms of regional contributions from 1990 - 2025[1]

An analysis was carried out to examine the proportion of total fertiliser consumed by the seven regions Europe, North America, South America, Asia, Africa, Oceania (in which only Australia has significant fertiliser use) and the former USSR (at present, statistics are only available for the former Soviet Union as a whole, but future work will allow separate analysis of each of the former member states). The predicted changes over a 35 year period to 2025 are given in Figure 4.6. This shows that the most important region is Asia due to the substantial consumption of China and India, contributing 45% of the total in 1990, rising to 52% in 2025[1]. Africa and South America exhibit small increases in relative contribution whilst the developed world shows decreases. Further work is necessary in Asia to evaluate whether emission rates from this area, a large proportion of which lies in tropical latitudes, differ by a significant extent to those in temperate regions.

---

[1] Changes of percentage contribution for 1990-2025 as follows: Asia 44.8%-51.9%; Europe 15.35-13.2%; N. America 15.7%-14.2%; former USSR 19.4%-14%; Africa 2.1%-2.6%; S. America 2.2%-3.5%; Oceania 0.6%-0.6%

The analysis has, so far, only considered the emissions of N_2O from 'A' countries. Emissions from `B' countries are insignificant if constant *per capita* values over the next 35 years are assumed. Many of these countries are small and have shown little increase in fertiliser consumption over the past 20 years. Exceptions include Ethiopia, Kenya and Sudan but these are unlikely to have much effect overall and it therefore seems fair to assume constant *per capita* values for the purposes of this study. However, the World Bank estimates that developing countries will have shown a dramatic rise in fertiliser consumption in the decade up to mid-1997, similar to that seen already in Asia. Therefore, an analysis was performed to assess the impact on total emissions (`A' and `B' countries) of a large rise in the rate of increase of fertiliser use for all `B' countries. To investigate this the average annual rate of increase was altered by factors of 10 and 50. This led to increases in total emissions in 2025 of 7% and 31% respectively, showing that only a growth rate in fertiliser use of more than 50 times the population growth for all `B' countries would be significant on a global scale.

The globally averaged conversion factor suggested by Eichner (1990), used in the present study and others, has a number of limitations, not least that the data set employed is taken predominantly from temperate areas, and most of the studies are taken over short time periods and are therefore not truly representative of annual emission patterns, or indeed global emission conditions. However, in view of the limited number of studies which have been carried out over long time periods and in tropical areas, this work is the most reasonable summary of the current knowledge of emissions from fertilised soils.

Nevertheless it is important to assess the impact of different conversion factors. There is the possibility that application of fertiliser to warmer soils leads to a greater enhancement of emissions compared to temperate zones. An attempt to demonstrate the significance of tropical areas has been made by assuming that 5% of fertiliser nitrogen is converted to N_2O-N in these regions and examining the effects on predicted emissions. China is excluded from this analysis on the basis that the vast majority of its land area lies in temperate latitudes, and it has been assumed that

India, Mexico, Brazil, Saudi Arabia and Bangladesh have half their land area in tropical regions. From the model analysis of tropical `A' countries, it can be seen that in 1990, `A' countries in tropical zones consumed 11% of total global fertiliser, rising to 21% in 2025. If a 5% conversion factor is applied to these countries, total emissions increase by 7% in 1990 and by 14% in 2025. Therefore emissions from tropical regions would appear not to be as important as those from temperate zones.

The predictions made in this work are based upon the effects of application to soils of commercially produced nitrogenous fertilisers only. The effect of treating soils with manure, a common practice in all parts of the world, is not considered due to a lack of detailed knowledge about the induced release of N_2O and of the global consumption. However, this may be an important source of nitrous oxide and is an area that requires further examination as it could alter emission estimates significantly. Other commercial fertilisers, such as phosphates and potash, have also been excluded as application of these to soils would not directly increase the inorganic nitrogen pool. However, a study by Keller *et al.* (1988) found that addition of phosphate to tropical forest soil led to a slight increase in N_2O emissions, possibly as a result of phosphate stimulating the mineralisation of nitrogen by soil microflora; emissions were 15 times less than those from soils treated with nitrate and, on a global scale, this source is insignificant compared with nitrogenous fertilisers.

4.5.3 Conclusions

Global emissions of N_2O from soils treated with nitrogenous fertilisers have been predicted to rise from 2.25 Tg N_2O-N in 1990 to 3.24 Tg N_2O-N in 2025, an average annual increase of 1.3% yr^{-1}. These values are slightly lower than those of other studies, implying that population may well be a dominant but not the only factor influencing future emissions of N_2O from fertilised soils.

Over half of future fertiliser-induced emissions of N_2O are predicted to originate from Asia, mainly due to the large consumption of fertiliser in China and India, and the substantial increase in population expected over the next 35 years in this region.

increase in population and development will also lead to an increase in relative emissions from South America and Africa.

The emissions predictions are only significantly affected by changes in *per capita* values of countries with high population and fertiliser consumption, namely India and China. Here it is estimated that increasing the rate of growth of fertiliser consumption by a factor of three times more than the growth of population over the same time scale, will lead to an increase in total predicted emissions of 50%.

Tropical regions are not predicted to be significant sources of future N_2O emissions, even if fertiliser conversion factors are assumed to be greater than those of temperate areas. Adopting a conversion factor of 5% for tropical regions only increases predicted emissions by up to 14 % by the year 2025.

Changing the value of the conversion factor has a significant effect on the values of the predicted emissions. However, this factor becomes less important in the context of other studies, as the conversion factors employed by these studies are similar. The conversion factor chosen represents the best available assessment of field studies, and accounts for indirect emissions from drainage waters as well as direct emissions.

However it is important to note that, unlike NO_x, the site of ground emission of N_2O is actually irrelevant as its lifetime in the troposphere is long enough for it to be well mixed. It is therefore the total global emission of N_2O which is significant and the increasing use of fertiliser implies that this source will continue to contribute a major part of these emissions. Control of emissions will be difficult but not impossible, if agricultural practices could be developed which utilise knowledge of the response of emissions to certain factors, such as type, form and amount of fertiliser treatment, the use of nitrification inhibitors and so forth. Studies have shown that careful fertiliser management can lead to higher crop yields but also lower N_2O emissions, which is encouraging for the future.

Chapter Five

Chemical Modelling of the Free Troposphere

5.1 Introduction

The use of computer models to study the chemistry and composition of the atmosphere is now extensive and, as outlined in Chapter 1, various types of models have been developed to simulate a number of atmospheric conditions. The models range from chemically complex 0-D box models to 3-D models in which the inclusion of transport processes limits the complexity of the chemistry due to the pressures on computational power. These models are intended to mimic the behaviour of atmospheric systems, and to predict the effects of perturbations to these systems, both chemical and physical.

Many studies have been concerned with localised polluted environments, such as urban centres, and the regions downwind from industrial plumes. Pollutants from these sources are released into the first kilometre of the troposphere which is called the boundary layer (see Figure 1.1). The turbulent conditions in this layer lead to stronger horizontal and vertical mixing than in layers above and this is enhanced by temperature inversions which effectively entrain the air below them thus preventing vertical mixing between layers. Thus many of the reactive species produced at ground level are removed either by reaction or by deposition at the ground or sea surface before they can reach the upper layers. Therefore the more reactive and short-lived a species, the less likelihood there is of this species being transported into the upper troposphere, leading to a much 'cleaner' atmosphere as the altitude increases. The composition of the atmosphere without the presence of pollutants is described as the 'background' chemistry of the atmosphere, primarily involving oxidation reactions of naturally occurring species such as methane, CO, NO_x and hydrocarbons.

The chemistry of the 'free' troposphere, as it is called, is driven by the solar-activated photolysis of ozone, which leads to the production of the highly reactive OH radical.

$$O_3 + h\upsilon \rightarrow O_2 + O(^1D)\ (\lambda \leq 310\ nm) \qquad (5.1)$$

$$O(^1D) + H_2O \rightarrow 2\ OH \qquad (5.2)$$

Despite the low atmospheric concentration of OH (estimated at 10^6 molecules cm^{-3} averaged globally over 24 hours; Prinn *et al*, 1992) it is the most important 'cleansing agent' of the troposphere. Many of the naturally occurring trace gases which are present in the free troposphere exist in reduced or partially oxidised forms, and are therefore susceptible to oxidation by reaction with OH (exceptions to this include N_2O and CFCs, which are ultimately destroyed in the stratosphere). This leads to the initiation of complex reaction sequences, in which OH and ozone are regenerated, allowing the process to continue without removing OH. Hence OH, and indirectly ozone, can be regarded as the most important removal mechanisms for those species, both natural and anthropogenic, which reach the free troposphere.

However, observations of decreasing OH and increasing ozone concentrations in the free troposphere over the past few decades (Thompson and Cicerone, 1986; Khalil and Rasmussen, 1985; Levine *et al*, 1985) have led to concern about the future capacity of the troposphere to remove pollutants. The changes in concentrations observed have been ascribed to perturbations to the composition of the free troposphere which have been occurring over the last few decades as a result of human activity. These include increases in ground emissions of trace gases such as methane and other hydrocarbons, CO, and nitrogen oxides, increases of direct high-altitude NO_x inputs from aircraft, and changes in the solar radiation flux to the troposphere caused by the destruction of the ozone layer. Anthropogenic emissions of these gases are expected to rise over the next few decades and it is therefore important to establish the background chemistry of the clean troposphere in order that studies of the significance of these increases, especially in terms of the ability of the troposphere to remove the extra burden, can be examined.

This study makes use of a 10-layer, 1-D computer model of the troposphere to investigate such phenomena, by the analysis of short-term and long-term perturbations to both chemical and physical parameters. Firstly, the effects of long-term increases in methane and NO_x concentrations upon the oxidising capacity of the troposphere under different chemical and latitudinal background conditions have been examined. The model has also been used to look at the effect of short term direct inputs of NO_x at all altitudes through a representation of the lightning phenomenon. Lastly, the significance of changing a number of input parameters within the model, such as vertical transfer rates, wind dilution rates, stratospheric incursion, and photolysis rates, was explored. In all cases the changes in concentrations of key species compared to a base case were analysed.

5.2. The Model

As indicated above, the free troposphere was simulated using a 10 layer 1-D model which incorporates a comprehensive chemical scheme representing that of the free troposphere. Each layer is of depth 1 km. The original model was developed to study the marine troposphere (Fletcher, 1989), and consisted of 73 species (plus one inert tracer) and 181 reactions. This was modified to remove the reactions of sulphur and iodine compounds, which were found to be insignificant in modelling a non-marine environment, as expected. The modified scheme contains 55 species (plus tracer) and 140 reactions and is listed alongside the references for the appropriate reaction rate constants in Appendix A. The tracer enables parameters such as vertical transfer rates to be examined without the effect of chemistry.

The model starts with initial inputs of a number of physical and chemical parameters, and, by the use of ordinary differential equations (ODEs, explained in Chapter 2), calculates the concentrations of each of the species as a function of time and altitude. These concentrations are governed by rates of emission at ground level, stratospheric incursion of species such as O_3, chemical reaction, photolysis, vertical transport, deposition, and wind dilution, as well as initial background concentrations.

5.2.1 Input Parameters

5.2.1.i) Chemistry

The chemistry of the model can be divided into inorganic and organic chemistry, although the interrelationships between them are complex. The inorganic H/N/O chemistry is described by reactions 1-37 in Appendix A, and the major reactions shown in Figure 5.1.

The role of NO_x is crucial in the determination of the fate of OH and O_3 in the catalytic oxidation cycles involving hydrocarbons, and its free tropospheric chemistry is similar to that of polluted environments, but occurring at lower concentrations. This chemistry is well-established, and includes the major sinks of NO_x, HNO_x, N_2O_5 and NO_3, as well as HO_2NO_2.

In the free troposphere only the concentrations of primary hydrocarbons containing less than three C atoms are significant as more reactive hydrocarbons are present in smaller concentrations and are removed by reaction in the boundary layer. Therefore only alkanes and alkenes up to C_3 and C_2H_2 have been included and these are given in reactions 38-110 (Appendix A). The major reaction of all hydrocarbons in the free troposphere is the oxidation with OH (or in the case of ethene with OH and O_3), forming peroxy radicals. The fate of these radicals depends upon the concentration of NO_x, which, if low, leads to peroxy-peroxy interactions becoming more important. The products of these and their kinetic data are not fully established, and hence those which are known have been used to represent all cases.

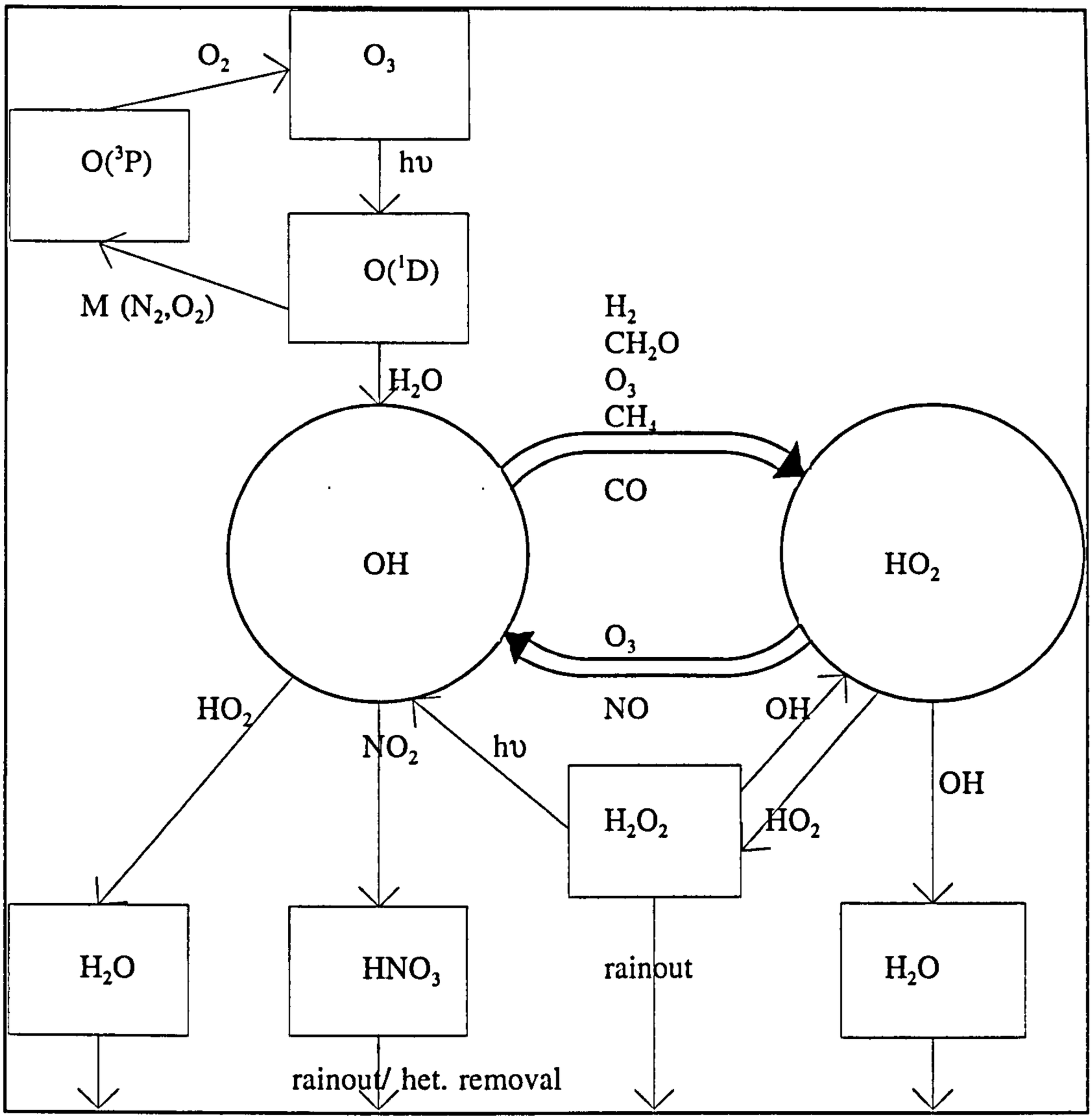

Figure 5.1 HO_x cycle with major reactions and sinks

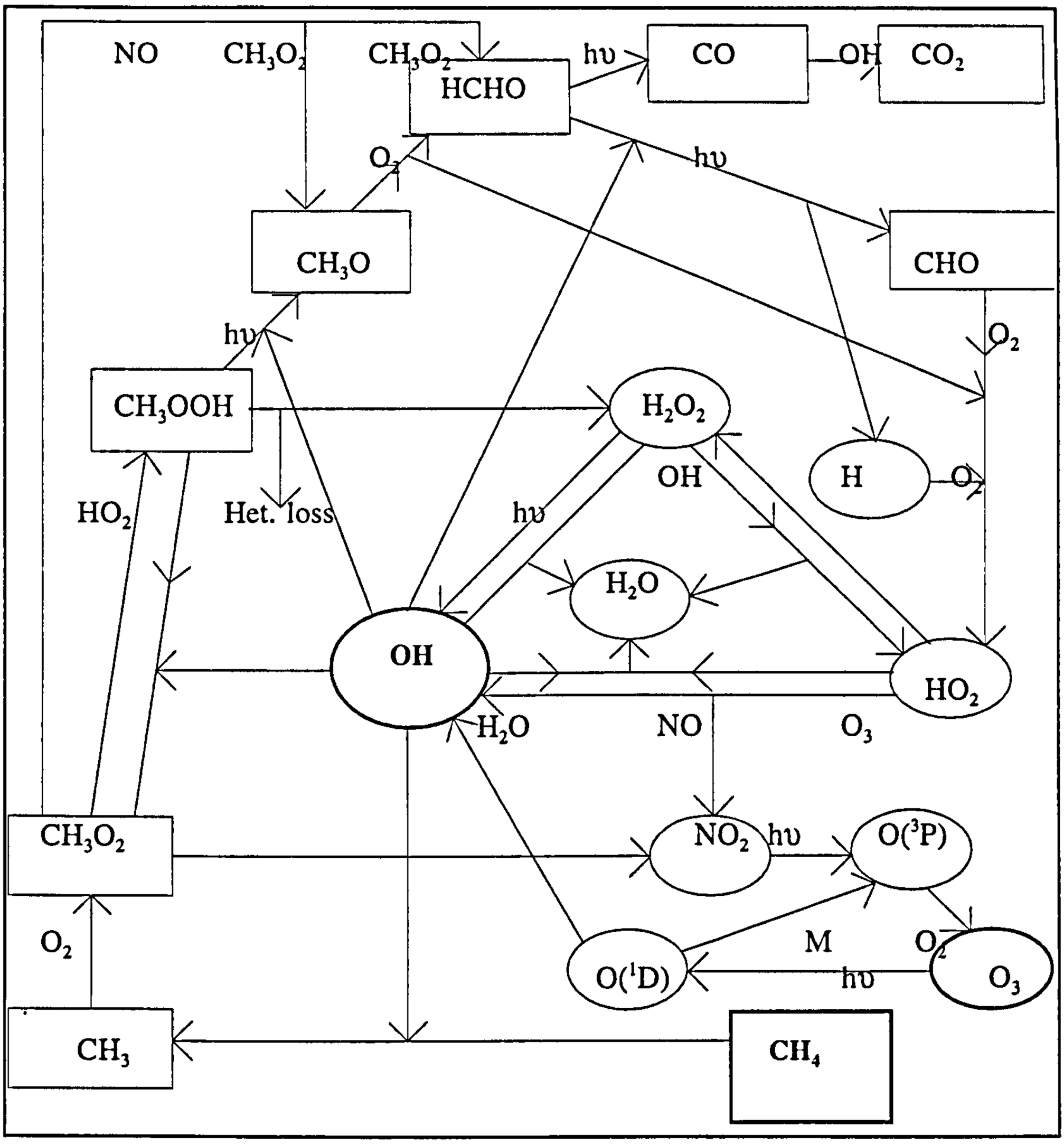

Figure 5.2 Methane Oxidation Scheme

Reactions of CO are also important in determining the OH and ozone concentrations, and these reactions are included in the hydrocarbon scheme, as the oxidation of alkanes leads to the production of CO. The major atmospheric processes involved can be represented in the form of diagrams, and Figures 5.2 and 5.3 show the oxidation of RH (where R is an alkyl group), and of CO, indicating the relevance of other species in the cycle.

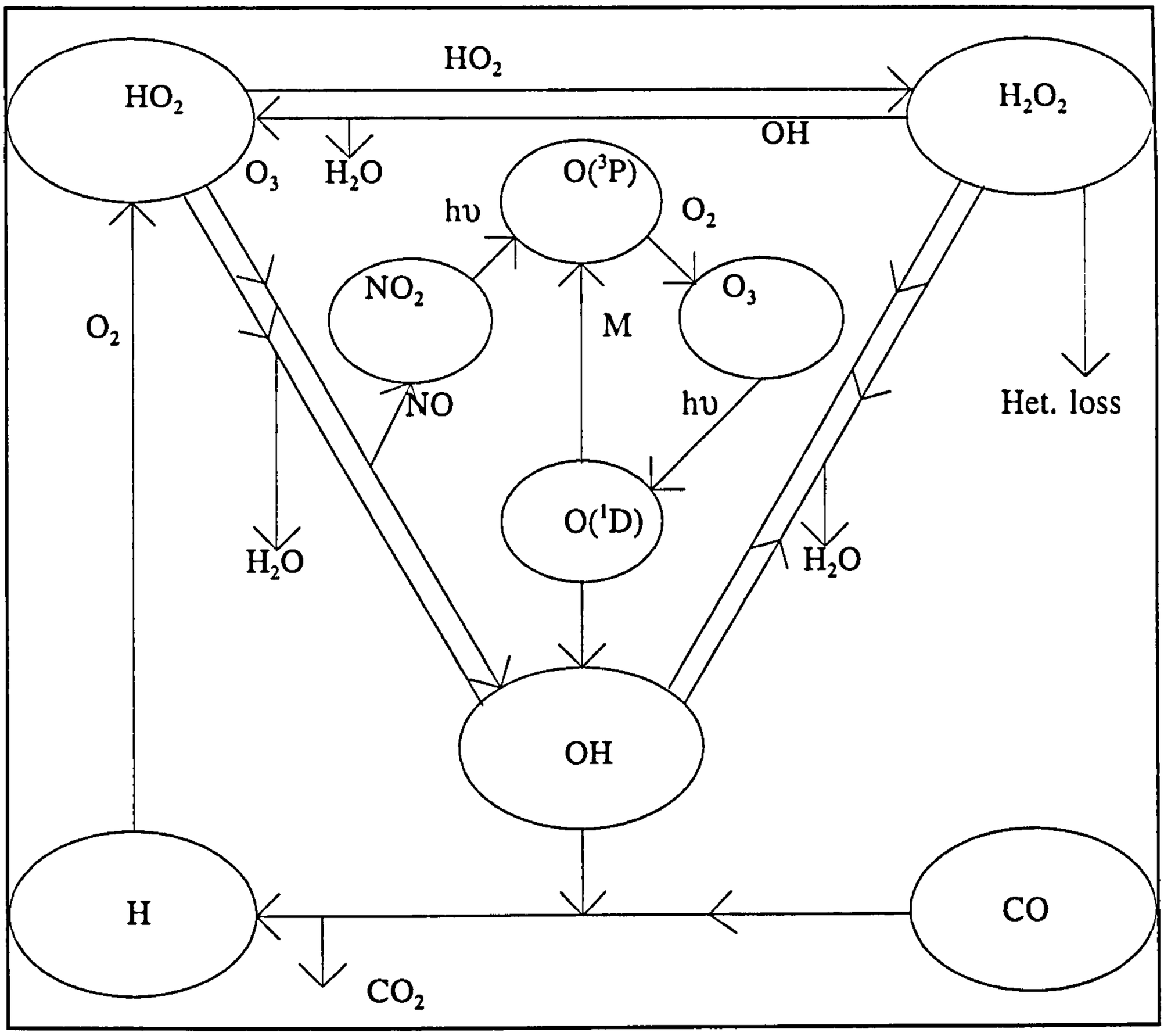

Figure 5.3 CO Oxidation Scheme

Reactions of CH_3Cl, emitted from industrial production of solvents, and other halogen compounds, are also included in the scheme (reactions 111-140). Cl reacts readily with VOCs, although this process is not so significant in the free troposphere where the Cl concentration is low. Other reactions of Cl are included, although overall the chemistry is relatively unimportant in the context of this study.

5.2.1.ii) Photolysis rate coefficients

Photolysis rates vary with the time of day, the season and the latitude as the Earth moves in relation to the Sun. The model incorporates specification of all these parameters, and the rate coefficients can be calculated using the equation (5.3),

$$k_{h\upsilon} = \alpha\, e^{-\beta \sec\theta} \qquad (5.3)$$

where θ is the solar zenith angle, and α and β are functions of altitude. Formulae for the α and β terms are given in (5.4) and (5.5), where h is altitude,

$$\alpha = a_0\{a_1 - 1/(a_2h^2 + a_3h + 1/(a_1 - 1))\} \quad (5.4)$$

$$\beta = b_0 - b_1h^{b2} \quad (5.5)$$

The constants a_0, a_1, a_2, a_3, b_0 and b_1 and b_2 are derived from fitting the above expressions to photolytic data of Demerjian *et al* (1980) for the photoactive species O_3, H_2O_2, CH_3CHO, NO_2, HNO_3, HNO_2 and HCHO. For those species whose rate coefficients are not well-characterised, rate coefficients proportional to other species have been assumed. Therefore N_2O is related to O_3, organic peroxides to H_2O_2, -CHO groups to CH_3CHO, and others are assumed proportional to NO_2. The model also assumes cloudless conditions and therefore maximum insolation appropriate to location and time. This assumption is tested later in the study.

5.2.1.iii) Temperature and molecular density

The temperature decreases with altitude in the troposphere (called the lapse rate), with greater rates of decrease at lower latitudes. This profile is incorporated in the model. The molecular density has been calculated to change with height by the expression (5.6),

$$\rho = 2.55 \times 10^{19} (T/T_0)^{4.26} \quad (5.6)$$

where ρ is the molecular density (molecules cm^{-3}) at height h (the molecular density at ground level is taken as 2.55 x 10^{19} molecules cm^{-3}), and T and T_0 (K) are the absolute temperatures at h and sea level respectively. All values appropriate to mid-layer height are used in the model.

5.2.1.iv) Transport coefficients

The vertical transport of species between layers has been represented by the standard parameterisation of eddy diffusion (see Thompson and Cicerone, 1982), where the vertical diffusion coefficient is constant and defines the rate of change of concentration of each species due to transport by the differential equations (5.7), (5.8) and (5.9),

$$dc_{i1}/dt = E_i - D_i c_{i1}/h + K_z(c_{i2}\rho_1/\rho_2 - c_{i1})/(h_1 h_2) \quad (5.7)$$

$$dc_{in}/dt = K_z(c_{im}\rho_n/\rho_m - c_{in})/(h_n h_m) - K_z(c_{in} - c_{ik}\rho_n/\rho_k)/(h_n h_k) \quad (5.8)$$

$$dc_{i10}/dt = S_i - K_z(c_{i10} - c_{i9}\rho_{10}/\rho_9)/(h_9 h_{10}) \quad (5.9)$$

where c_{ij} is the concentration of species i in layer j, n = 2 - 9, m = n + 1 and k = n - 1. E is the emission rate of each species (molecules cm^{-3} s^{-1}) into layer 1 (where layer 1 is the lowest layer), D_i is the deposition velocity (m s^{-1}) to the ground, S_i is the stratospheric incursion rate (molecules cm^{-3} s^{-1}) into layer 10, and K_z is the eddy diffusion coefficient (m^2 s^{-1}). ρ is the molecular density (molecules cm^{-3}) in layer j, h_j the depth of layer j (1000 m in each case) and t is the time (s).

Diffusion was ignored for radicals, whose lifetime was considered too short for any significant diffusion to occur. The value of K_z was taken to be 10 m^2 s^{-1} (Thompson and Cicerone, 1982). There is no transport from the troposphere to the stratosphere, as this would require an estimate of the concentrations of relevant species in the lower stratosphere, about which there is much uncertainty.

5.2.1.v) Wind dilution

The transport of species horizontally can be incorporated by using a wind dilution factor in the model. In 1-D box models it is assumed that the wind travels in one direction only, bringing species into and removing them from the box. In the present

model the desired wind speed is input to the model, and a first order rate coefficient for removal of the species (k_w) is calculated by dividing by the box length. The removal rate $k_w[X]_t$ of the species, X, at time, t, depends upon the concentration of the species at that time. Similarly the input rate of species is determined by the same rate coefficient and the initial concentration of each species, $k_w[X]_0$.

The representation of wind dilution in the present model is a simplification of what really occurs and therefore the results obtained when including wind dilution in the model have to be treated with care. In this model, the initial concentrations of radicals are zero, as they are generated by reactions of other species. Therefore when wind dilution is included the concentrations of radicals are artificially low, as they are not being input by the wind but are being removed. Similarly without wind dilution, the concentrations of more stable species generally reach steady state values which are lower than the initial concentrations after a couple of days' simulation. This is due to the initialisation of the chemistry and the formation of radicals. If wind dilution is included, the species are input at a rate based upon these high initial concentrations, which maintains average concentrations higher than those otherwise obtained.

To address this problem it is necessary to work out the diurnally-averaged steady state concentrations of all species (including radicals) and then input them to the model. However, this is beyond the limitations of the current model. For the purposes of this work wind dilution is omitted, but is analysed in more detail in a later section.

5.2.1.vi) Input and loss of species to and from the model

Initial concentrations of species in layers 1 and 2-10 respectively are required along with ground emission rates, stratospheric incursion rates and deposition velocities. The latter two are the same as those of Fletcher (1991), with stratospheric incursion rates given in Table 5.1. The concentrations and emission rates used in the original model were retained initially to check the outputs of the reduced model against the original version, but for the purpose of the subsequent simulations the concentrations

and/or emission rates of NO_x, O_3, and CO were changed depending upon the region of study. The background concentration of CH_4 was given the updated value of 1714 ppbv (Houghton *et al*, 1995) rather than 1610 ppbv, and that of N_2O 310 ppbv (also Houghton *et al*, 1995) instead of 288 ppbv. The concentrations of all radicals were initially set to zero, therefore it was necessary to run the model for a few days in order to initialise and equilibrate the chemistry.

Table 5.1 Stratospheric incursion rates

Species	Rate (molecule cm^{-3} s^{-1})	Reference
NO	4×10^2	Thompson and Cicerone (1986)
NO_2	8×10^2	Thompson and Cicerone (1986)
O_3	8×10^5	Fishman and Crutzen (1977)
HNO_3	1.3×10^3	Thompson and Cicerone (1986)

5.3 Model Simulations

5.3.1 Initial Runs and Chemically Coherent Regions

Initially two sets of simulations were performed, firstly to confirm that the results of the revised model agreed with those of Fletcher (1991) and secondly to check that photolysis rates were altered by changing the start date of the run.

5.3.1.i) Comparison with original model

Using the input parameters of the original model (excepting the methane and N_2O concentrations described earlier) with the revised chemical scheme, the model was run at latitude 60^0N, starting on June 21st (Day 172 - midsummer's day), for 11 days at the low and high NO_x scenarios used by Fletcher (zero and 1×10^6 molecules cm^{-3} s^{-1} ground emission rates). Comparison with Fletcher's work showed that the removal of the sulphur and iodine compounds had no significant effect on the output. Concentration/time profiles of NO, NO_2, O_3 and OH are given in Figures 5.4(a) - (d)

(for comparison with later work, those for a tropical scenario are shown-the only differences occur in the peak values).

5.3.1.ii) Altering model start date

In the second case the start date was set to October 31st (day 303), and January 31st (day 31), representing northern hemisphere (NH) autumn and winter respectively. All other conditions were kept the same in order that the effect of photolysis rates could be investigated. Again, analysis of NO, NO_2, OH and ozone was carried out and compared with the results of the modified model for start date June 21st. The OH summertime simulation gave a peak concentration 100% higher than the rest of the year, to be expected from the enhanced insolation. The autumn and summer profiles followed the same shape, but that of the winter profile gave 'thinner' peaks, i.e. they lasted for a smaller time due to the reduced insolation.

In the case of NO_2 the values of the peak concentrations were the same in all seasons, but in autumn and winter the time over which these peaks occurred was longer than in the summer. This is because the reduced insolation leads to a slower photolysis, and thus removal, of NO_2 during the day. The profiles for NO changed very little with season. There was a slight decrease in the width of the peaks in the autumn and winter, but the overall peak concentrations remained the same. This is consistent with the behaviour of NO_2, which would be expected as the two are so closely linked.

5.3.1.iii) Regional input conditions

The model was then used to carry out an investigation into the interrelationship between the major atmospheric species, and especially the effect upon the concentrations of the tropospheric oxidants OH and O_3. As the model automatically alters the photolysis rates with latitude and season, it was possible to take a latitudinal approach and examine global regions where the chemical inputs and backgrounds are similar.

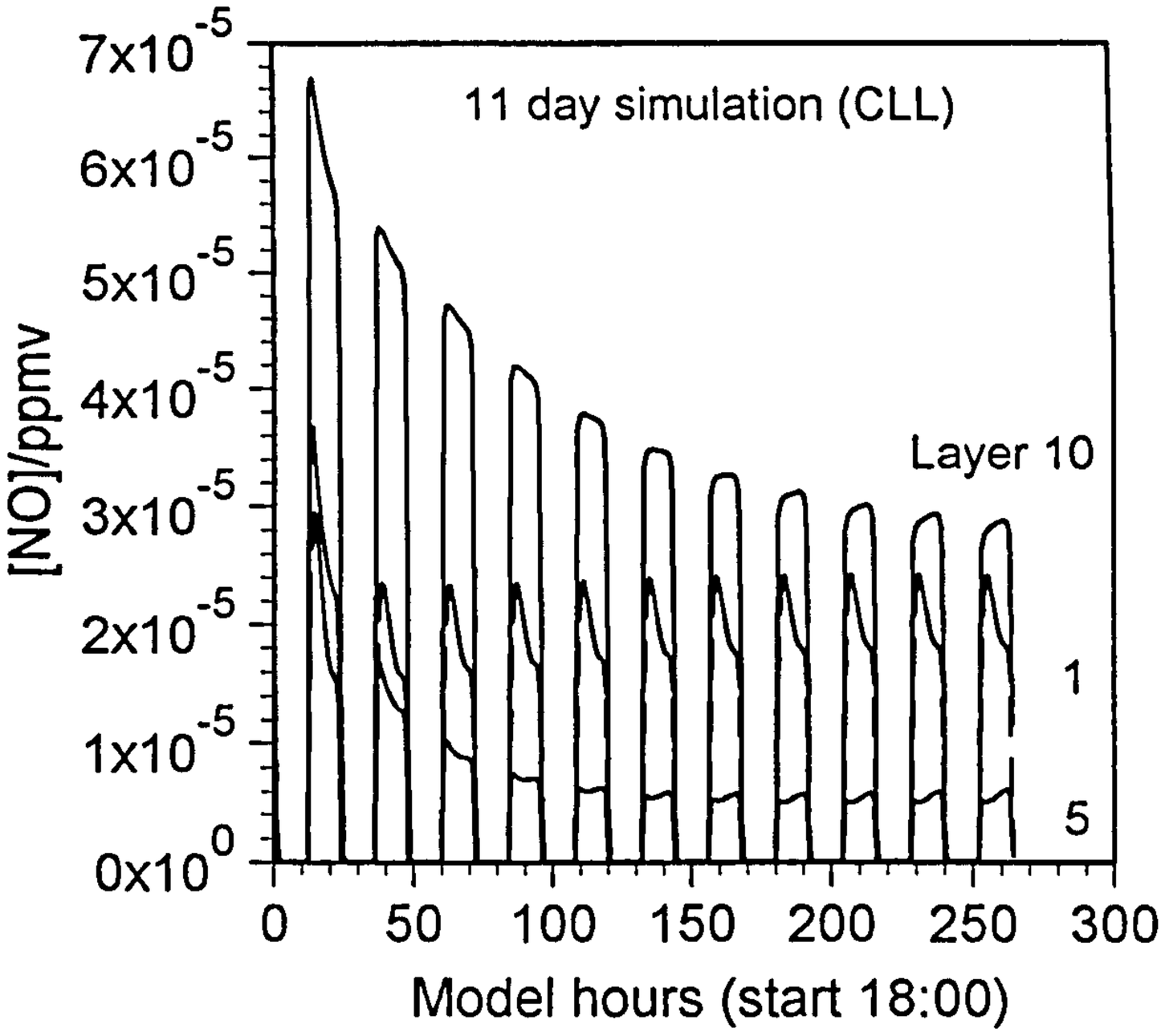

Figure 5.4a) Concentration/time profile for NO under CLL conditions, run for 11 days starting June 21st at latitude 20^{0}N, for layers 1, 5 and 10.

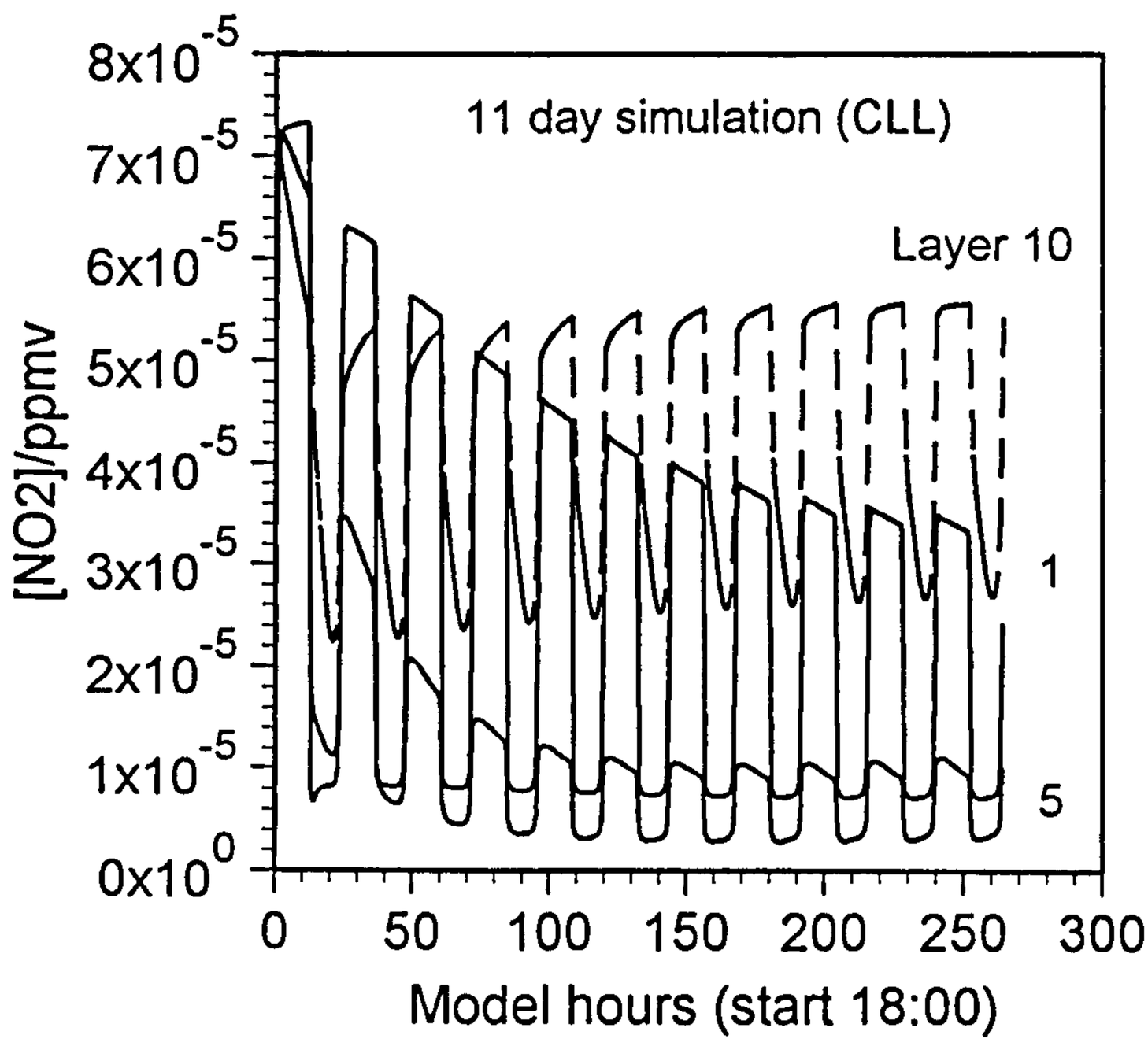

Figure 5.4b) Concentration/time profile for NO_2; CLL conditions, 11 day simulation, starting June 21st at latitude 20^{0}N layers 1, 5 and 10 shown.

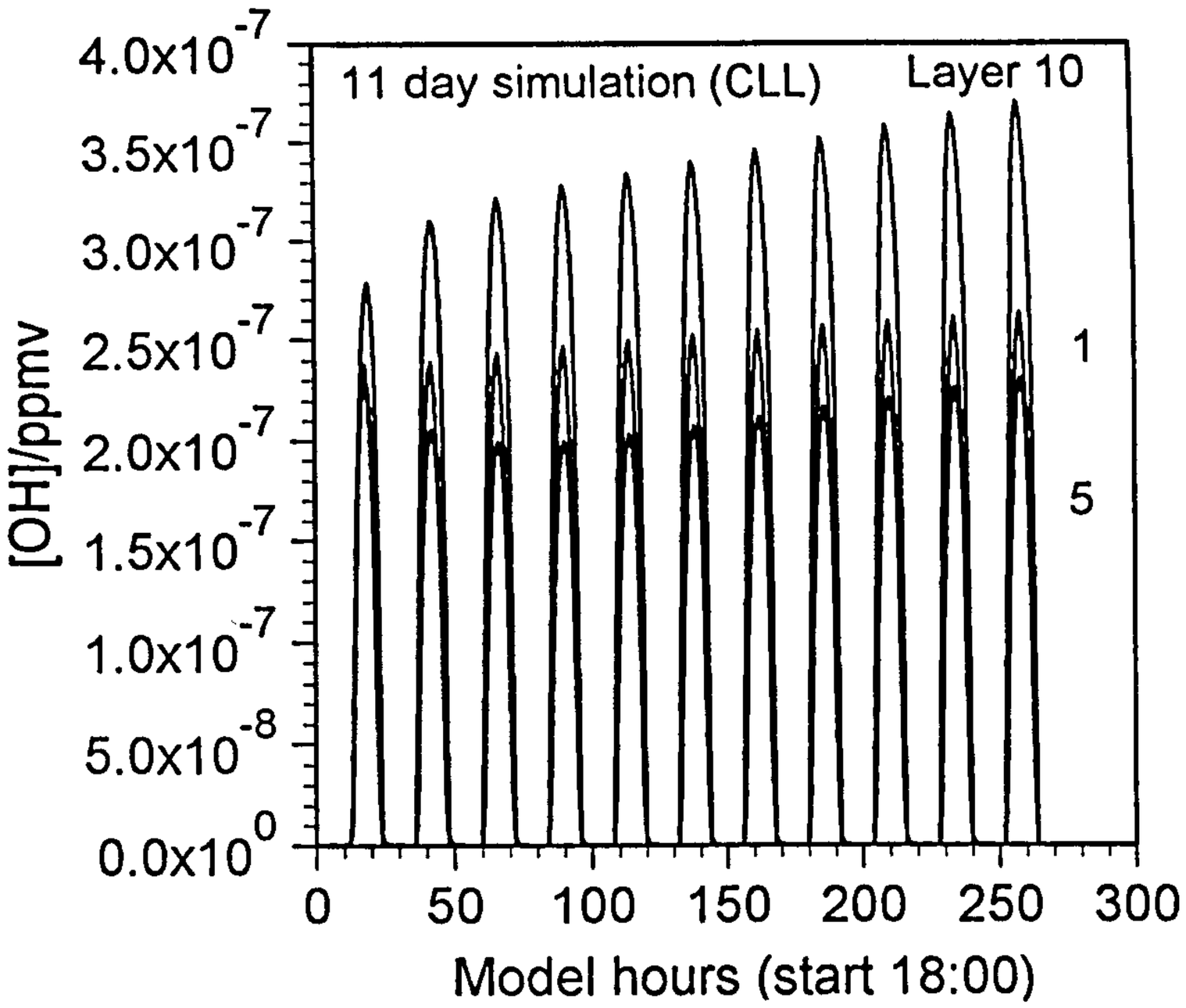

Figure 5.4c) Concentration/time profile for OH; CLL conditions, 11 day simulation starting June 21st at 20^{0}N, for layers 1, 5, and 10

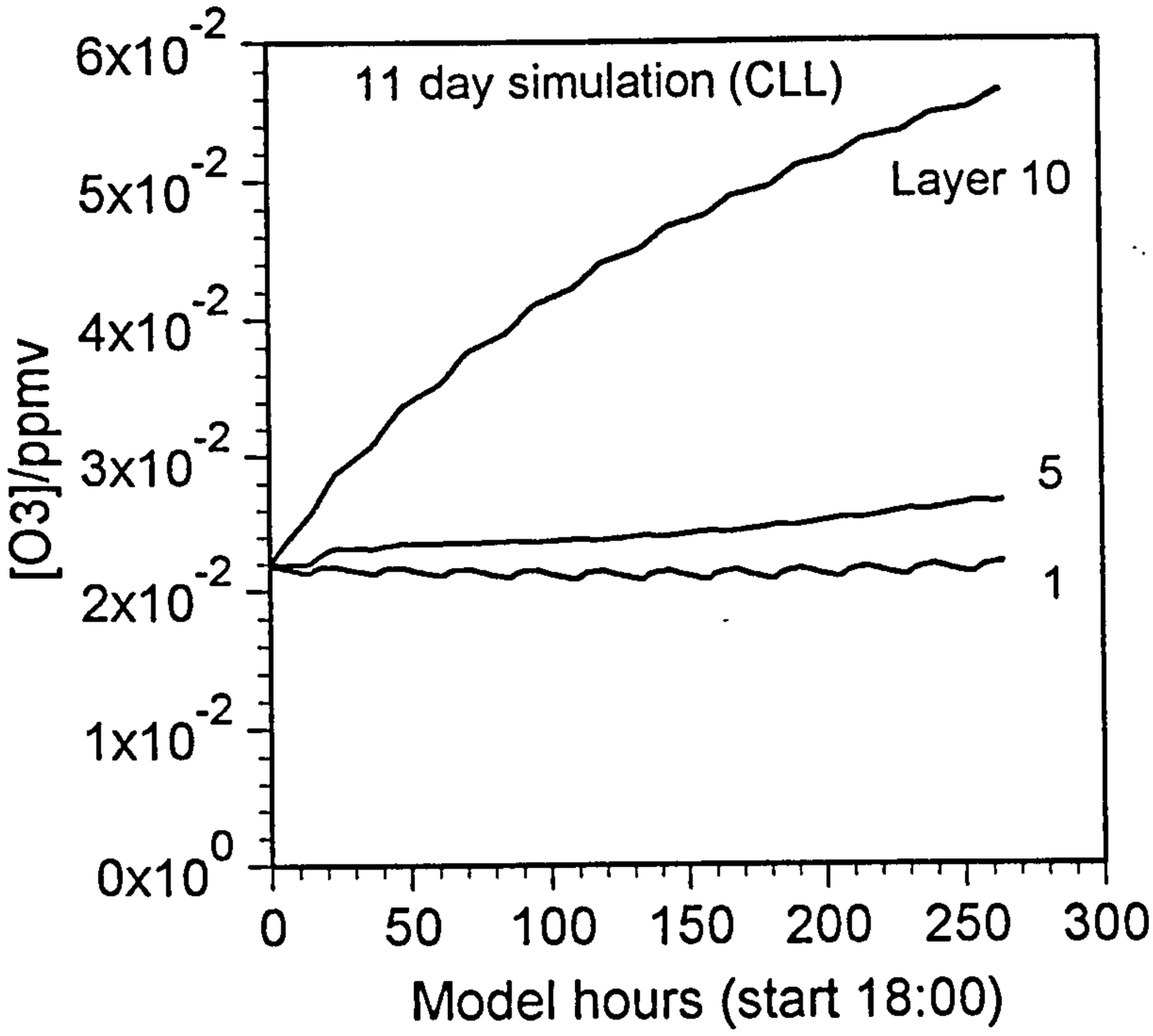

Figure 5.4d) Concentration/time profile for O_3; CLL conditions, 11 day simulation starting June 21st at latitude 20^{0}N, for layers 1, 5, and 10.

A study by Thompson *et al.* (1990), investigated the perturbations on tropospheric oxidants caused by changes in background concentrations of species such as methane and CO. This study also used a 1-D box model, and defined eight chemically coherent regions in terms of the background concentrations of ozone and both the ground emissions and concentrations of NO_x and CO. These were based upon the geographical distributions of NO_x described by Hameed and Dignon (1988). The regions are shown in Figure 5.5.

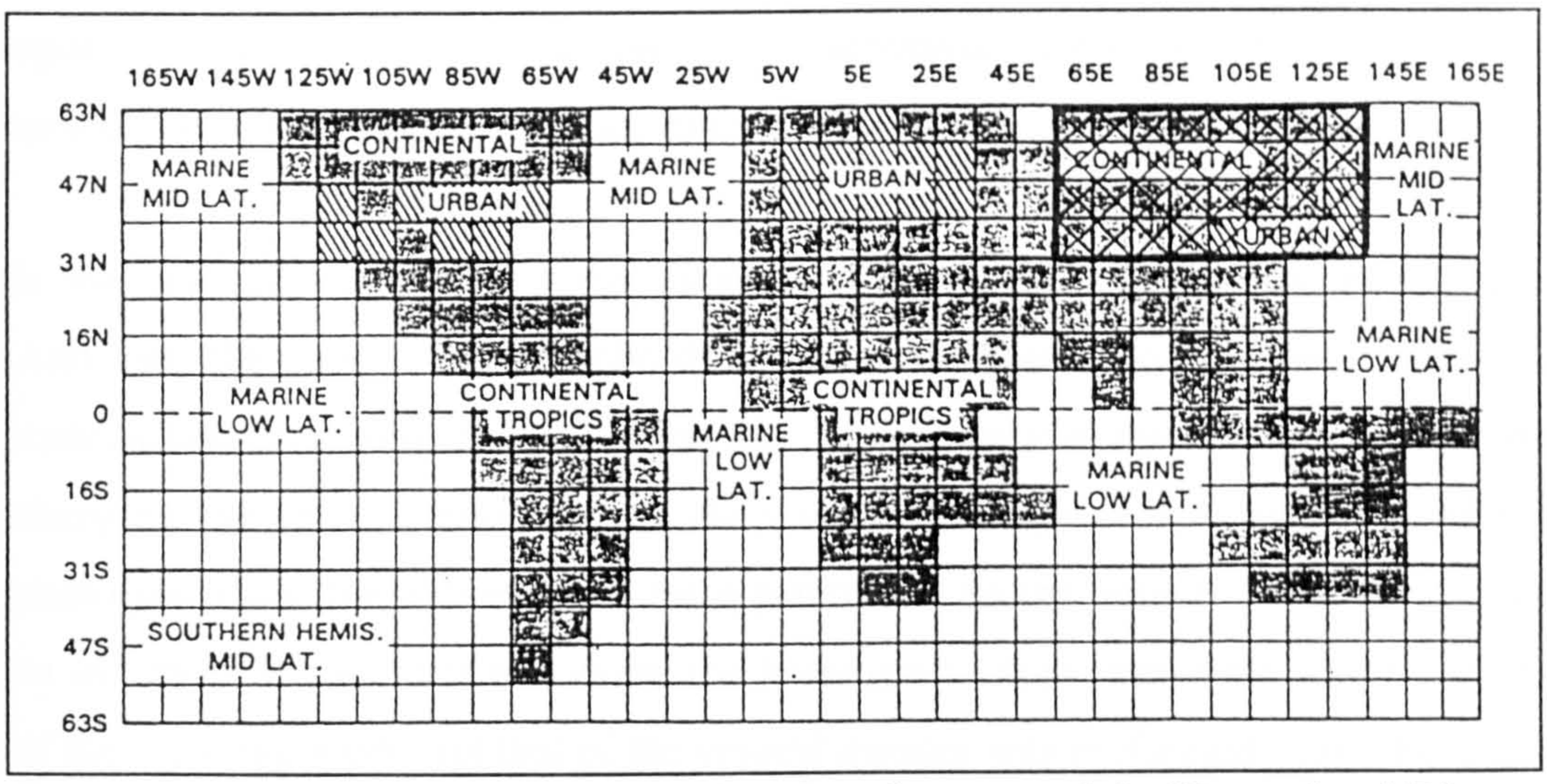

Figure 5.5 Chemically coherent regions based upon work by Hameed and Dignon (1988). Distinction between regions is summarised in the text (Section 5.3.1.iii))

For the purposes of this work, four of these regions were used, in order that a comparison between the studies could be made and to investigate the differences between the chemistry in different chemically coherent regions. These regions were the marine mid-latitude (MML) for comparison with the Fletcher work, the continental mid-latitude (CML) which represented non-urban environments, continental low-latitudes (CLL) representing tropical areas, where biomass burning is a significant source of NO_x and CO, and urban mid-latitudes (UML). Whilst the model is not designed to simulate the complex chemistry occurring in the urban boundary layer, it is interesting to observe the effects in the free troposphere of higher concentrations of pollutants such as NO_x, CO and ozone. All scenarios were set in the northern hemisphere, over a simulation time of 11 days to allow ample

initialisation and stabilisation of the chemistry. The effects of increasing NO_x emissions and CH_4 and CO background levels upon OH and O_3 were analysed for each of the regions.

The CLL scenario was then used to investigate the effect of inputting NO_x directly at all layers rather than solely from the ground or the stratosphere. This was intended to represent the NO_x formed from lightning during a storm event over the tropics (where lightning occurs with the greatest frequency). A base case was developed, upon which variational analyses were performed and the effects upon the concentrations of different species examined.

It was also possible to alter the values of a number of model input parameters. Although the model is primarily designed to represent the complex chemistry, meteorological factors play a major role in determining this chemistry, and by changing the vertical transfer rates, the wind dilution (horizontal transfer) and the photolysis rates, the influences of these parameters on the outputs of the model can be surveyed. In the latter two cases, the investigation was carried out in the context of the lightning work, but that of the vertical transfer was performed using the tracer species to examine the rates of transfer between the layers. The importance of stratospheric incursion of NO_x and O_3 upon the chemistry was also investigated.

5.3.2 Perturbations to Tropospheric Oxidants

A study was made of the effect upon OH of increasing the NO_x emission rates. This initially leads to the production of more OH from the reaction of HO_2 with NO (see Figure 5.1), but increasing the NO_x beyond a certain point will provide enough NO_2 for reaction with OH to occur, removing both active species. By applying these NO_x increases to each of the scenarios, the presence of different concentrations of other species can also be assessed.

The consequences of increasing methane background concentrations were also investigated. Over the 1980s, methane levels rose by an average of 1% per year.

There was an exception to this during the early 90s, when a significant drop in methane growth was observed (Steele *et al*, 1992; Khalil & Rasmussen, 1993; Dlugokencky *et al*, 1994), but more recently levels have begun to rise once more. This suggests that the slowing down may have been a short term effect, in keeping with the highly variable nature of atmospheric methane (see Figure 1.3) and the potential for future methane increases may still be high.

The longer term rise has been suggested as the reason behind a slight drop in global OH as discussed in Chapter 1 (Khalil and Rasmussen, 1985; Levine *et al.*, 1985), although this is a matter of some discussion. It is also possible that the observed increase in tropospheric ozone is due to an increase in its production from the oxidation of methane in the presence of high concentrations of NO_x. An estimated increase of 50% in ozone over Europe since the 1960s has been observed, although the rate of increase may have fallen over the past decade, and increases of around 15% have occurred over North America (Houghton *et al*, 1995). However, both [OH] and $[O_3]$ vary significantly over space and time, and therefore it is important to assess both local and global effects in studies of trends and effects.

In the present work, the methane concentrations input to the model were increased by an equivalent of 1% yr^{-1} for five year periods between 1995 and 2025 for each of the scenarios. To compare this with the work of Thompson *et al.* (1990), who carried out a similar study between 1985 and 2035, the emission rate of CO was also increased by 0.5% yr^{-1} (equivalent to Global Scenario 1 in their work). Both studies use 1-D models, the main differences being that Thompson *et al.* used a 15 km altitude range, a 1995 methane concentration of 1.815 ppmv (based upon extrapolation from the 1985 level) and the chemical scheme is limited to 25 species.

The same type of study was also performed for each of the scenarios using growth rates of 2% yr^{-1} equivalent, increasing methane whilst maintaining constant CO concentration, and increasing methane with enhanced NO_x backgrounds. This was to examine the relative effects of each of these species in determining the OH and ozone concentrations. The concentrations used are given in Table 5.2.

Table 5.2 Methane inputs for predictions of future OH and O_3

Year	$[CH_4]$ - 1% yr^{-1} increase	$[CH_4]$ - 2% yr^{-1} increase
1995	1.77 ppmv[a]	1.77 ppmv
2000	1.86	1.95
2005	1.95	2.15
2010	2.03	2.37
2015	2.13	2.62
2020	2.24	2.89
2025	2.36	3.19

[a] - corresponds to a 6% greater NH concentration if the global average is taken as 1.714 ppmv (Houghton *et al*, 1995).

The concentration/time profiles of the intermediates involved in the CH_4 oxidation sequence were also analysed, to see whether the reaction routes were affected by altering the methane concentration. These included CH_3O_2, CH_3OOH and HCHO, the reactions of which contribute to determining the amount of OH which is regenerated at the end of each oxidation (see Figure 5.2).

5.3.3 Simulation of NO_x Input from Lightning

The model has previously been used by Fletcher (1989,1991) to study the effects of alterations to the input values, such as changing ground emissions and background concentrations of species. In the case of lightning events, as discussed in previous chapters, the effect of a lightning strike is to perturb the chemistry around the channel at all altitudes over a very short time period, through the formation of reactive species such as nitrogen oxides. Thus inputs of NO_x, rather than occurring solely from the ground or stratosphere, are made at all altitudes through which the lightning passes. As discussed in Chapter 1, lightning is the most important free tropospheric source of NO_x, and it is therefore important to look at the impact on the

chemistry of enhanced NO_x concentrations as a result of a lightning strike.

To investigate the effects of such direct inputs on the overall chemistry of a region, a modification was made to the model, such that a storm event occurring over a specified area for a specified time could be represented in terms of the NO_x input from the lightning event. In addition to the usual inputs, as outlined earlier, the model requires the input of the timing of the lightning event and the total NO_x produced by the event. The model then simulates the production of NO_x from lightning as an emission into each layer based upon these inputs.

5.3.3.i) Base case

A base case scenario was developed to test the model, upon which a series of variational analyses was carried out. It was assumed that a storm event of 8 hours duration occurred over an area of 100 x 100 km^2 (based upon measurements made in Florida, see Uman, 1987) at latitude 20^0N during NH spring time (starting day 105; April 15th). This was based upon the results of Kotaki and Katoh (1983 - see previous chapter) whose analysis of the global distribution of lightning indicates that a large proportion of storm activity occurs over the tropical NH during the spring months. A flash density of 10^{-4} flashes $(100\ km^2)^{-1}\ s^{-1}$ was assumed, also from the work of Kotaki and Katoh, which, along with the value of 2.33×10^{26} molecules NO_x per flash estimated in the previous chapter, was used to calculate the total amount of NO_x produced over this region for 8 hours. This is input to the model as a tonnage, which is then converted to an emission rate equivalent (molecules $cm^{-3}\ s^{-1}$) for each layer. An even distribution of NO_x formation with altitude was assumed.

As the base case is set to occur over tropical regions, the background and emission data for the CLL scenario were employed. This allowed comparison of lightning studies with non-lightning work (referred to herein as the 'blank' run) carried out in earlier sections. The simulation is run for 11 days, starting at 18:00, with the lightning event occurring between the 166th and 174th hours (16:00 - 00:00 on Day 7). This was to allow the chemistry to initialise before input of NO_x.

5.3.4 Variational Analysis

The model is not required to simulate exactly the events occurring during a storm, as this would involve highly complex physical and chemical processes which are beyond the scope of a simple 1-D photochemical model. Therefore in modelling the effect of perturbations to the chemistry as a result of a lightning event, a number of assumptions had to be made in the base case. To analyse their significance, a series of variational and sensitivity analyses were performed whereby chemical, temporal and physical inputs to the base case were altered. These included varying the timing, magnitude and altitude distribution of the NO_x inputs, and altering the wind dilution and photolysis rates.

5.3.4.i) Wind dilution

Thus far wind dilution has not been included in the model. The limitations of the treatment of wind dilution in this model were explained in Section 5.2.1.v). As the perturbation of NO_x was expected to be small compared to the background it was anticipated that including wind dilution initially would disguise the effect. However, wind is a fundamental part of a storm, and therefore it was considered necessary to incorporate it into the model. Equivalent wind speeds of 2, 4 and 8 ms^{-1} were included and the effects upon the concentration/time profiles assessed.

5.3.4.ii) Photolysis rates

Another fundamental aspect of a storm is the cloud cover and therefore reduction in photolysis rates. The model has previously assumed cloudless conditions, but this is obviously unrealistic in terms of a lightning event, and therefore a further modification was made to the model whereby the photolysis rates could be altered. This modification allowed the rates to be varied at any specified time and in any layer, the only limitation being that all rates had to be changed by the same amount. It was assumed that the presence of cloud cover would completely remove photolysis below the cloud during the storm. However, this is not strictly true, as the presence

of cloud cover has a complex effect upon the solar radiation. It can lead to scattering of the radiation and can even enhance the radiation, as well as reducing it. However, the processes are too uncertain and complex to incorporate in this model, therefore the assumption that cloud cover reduced the amount of radiation and therefore photolysis below it was necessary.

Four simulations were carried out for the analysis. Firstly, the photolysis rates were set to zero for the duration of the whole simulation, to observe the effects on the concentration profiles of the species under investigation, and to see whether NO_x input was significant. Secondly, the rates were set to zero for an hour either side of, and during the storm, between 165 and 175 hours. Finally, two runs were carried out in which the lightning event was compressed into the bottom eight and five layers respectively with photolysis rates above the storm remaining as in the base case, and those below set to zero during the storm. The total NO_x input was the same as in the base case, and its distribution spread evenly between the layers, to see whether increasing the amount of NO_x emitted in a particular layer would lead to a proportionate enhancement of the concentration.

5.3.5 Changing Model Input Parameters

The concentrations and thus the chemistry of species at different altitudes and times are also dependent upon two parameters thus far unexplored, namely the rate of vertical transfer of molecules and the rate of stratospheric incursion of the key tropospheric gases NO_x and O_3. The significance of these parameters was therefore investigated by altering the input values.

5.3.5.i) Altering the rate of vertical transfer

Varying the rate of transfer between layers was explored in three ways. Firstly, the value of the eddy diffusion coefficient ($K_z = 10\ m^2\ s^{-1}$ in equations (5.5) - (5.7)) was both doubled and halved. As this constant is one of the factors which determines the actual rate of transfer, the effect should be dependent upon the altitude. Secondly, the

actual transfer coefficients were increased and decreased by a factor of two, through a modification to the model itself. In each case, the concentration/time profiles for NO, NO_2 and OH were examined, alongside that of the inert tracer species. The tracer was taken to have a ground emission rate of 1×10^6 molecules cm^{-3} s^{-1}, with no other emission or deposition rates, and is not involved in the chemistry, thus allowing analysis of the rate at which species are transferred between layers without any other effects playing a role.

5.3.4.ii) Altering the stratospheric incursion rates

Stratospheric incursion is an important tropospheric source of NO_x and O_3. However, the rate of incursion of each is highly variable, and therefore the use of an average value has been tested. The rates of stratospheric incursion of NO_x and O_3 were set respectively to zero, and the effects upon the concentration/time profiles of NO, NO_2, OH, O_3, HNO_2, HNO_3, NO_3, and N_2O_5 at all altitudes examined.

5.4 Results of Perturbations to Tropospheric Oxidants

5.4.1 Increasing NO_x emissions

The ground emission rate of NO_x was increased for three of the regions; the original Fletcher marine input, an urban environment (UML), and NH tropical regions (CLL). The subsequent effects on the OH concentrations were examined (the actual use of regions is superfluous, as it is the relationship between NO_x and OH under different background conditions which is being investigated and the regions provided a convenient method for such an analysis). The data for the emissions was taken from Derwent *et al* (1990)[1], and represented a range of emission densities experienced over

[1]The values of NO_x emissions are given in Derwent in terms of tonnes NO_2 km^{-2} yr^{-1}. The range of values used here corresponds to emissions from the cleanest remote areas, to averages of emissions over large regions (ie Northern Europe), to emissions on a local scale (ie major cities). All inputs have been converted to molecules NO or NO_2 cm^{-3} s^{-1} assuming that NO_2 is emitted as 10% NO_x.

different regions of Europe. The input values are given in Table 5.3. The concentration/time profiles of OH in layers 1, 2, and 5 were examined for each of the scenarios under increasing NO_x emissions, and the value of the peak concentration after 11 days plotted against NO_x.

Table 5.3 Input values for each scenario

Species	Fletcher	CLL	CML	UML	MML
NO_x analysis	✓	✓		✓	
CH_4 analysis		✓	✓	✓	✓
Latitude/^{0}N	60	20	50	50	50
$[CH_4]$/ppmv[1]	1.714	1.766	1.766	1.766	1.766
[CO]/ppbv	120	100	134	360	110
CO emission[2]	0	1.6×10^6	2.2×10^6	7.0×10^6	9.9×10^5
$[NO_x]$/ppbv	1.0×10^{-2}	7.2×10^{-2}	2.0×10^{-1}	1.4	2.0×10^{-2}
NO_x emission[3]	0	3.5×10^4	9.3×10^4	6.6×10^5	3.4×10^3
$[O_3]$/ppbv	50	22	42	59	24

[1] - 1.714 ppmv corresponds to global average concentration, 1.766 ppmv represents the NH concentration assuming 6% greater CH_4 in NH than SH; [x] =concentration of species x

[2] - molecule cm^{-3} s^{-1} from the ground, converted from Thompson's data (molecule cm^{-2} s^{-1}) by assuming immediate mixing into first 1 km layer;

[3] - molecule cm^{-3} s^{-1}, used in the CH_4 analysis only.

Values ranged from 0 - 25 tonnes (NO_2 as NO_x) km^{-2} yr^{-1} in NO_x analysis (taken from Derwent *et al.*, 1990)

The resulting profiles are given for comparison in Figures 5.6a) - c). Analysis of Figure 5.6a) for layer 1 shows that in each scenario increasing the NO_x emission rate leads to an initial increase in [OH] followed by a decline. The rate of increase and the maximum values differ for each of the scenarios, with OH rising most rapidly and reaching a higher peak value in the tropical scenario. The UML curve reaches a peak at the greatest NO_x emission rate of the three scenarios, with the value of the peak concentration being lower than that of the tropics by approximately 15%. For layers 2 and 5 (Figures 5.6 b) and c)) the same relationship is present, but a peak value for [OH] is only reached in layer 2 for the CLL region. The OH concentrations are lower in these layers, as expected from the profile in Figure 5.4c).

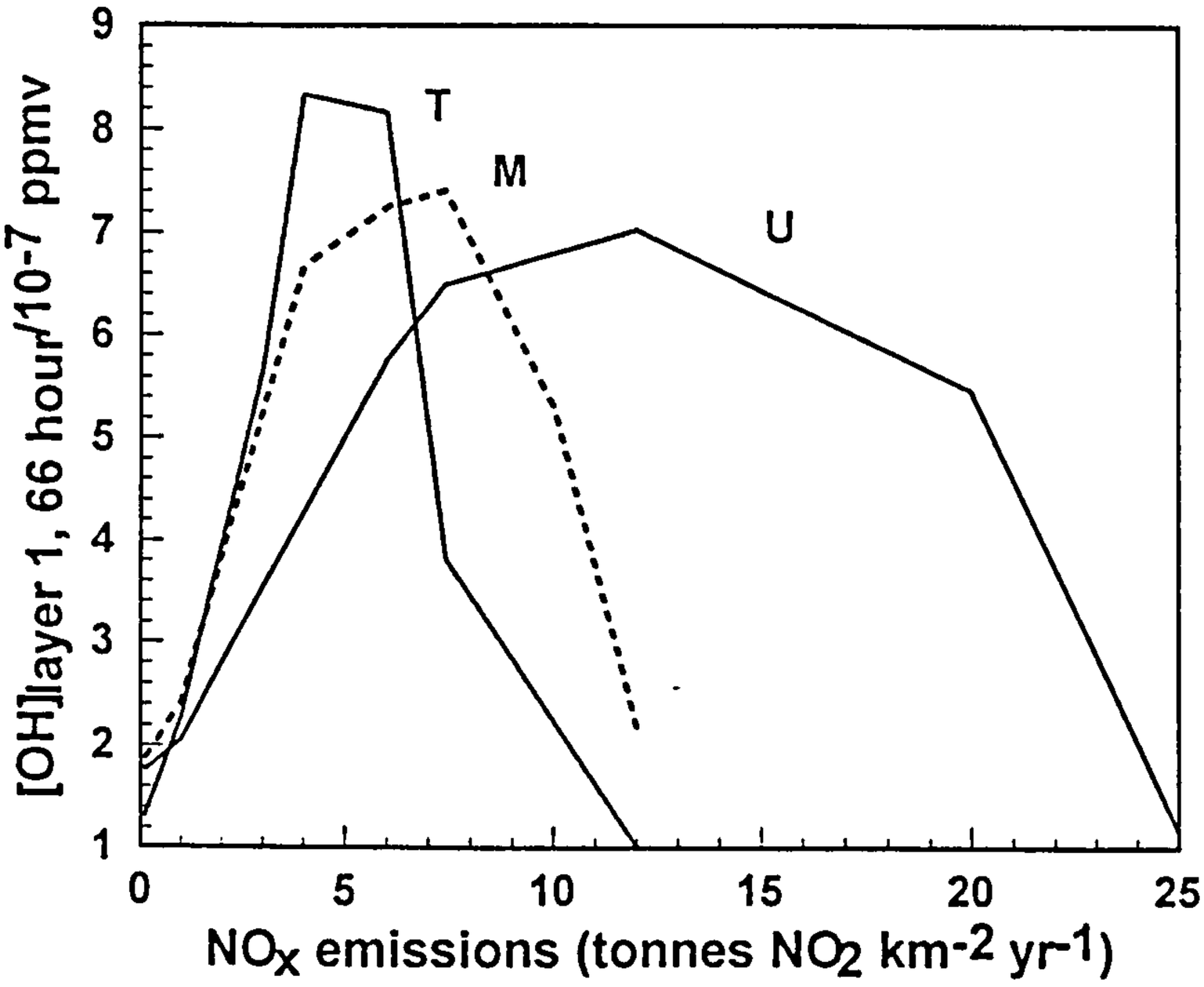

Figure 5.6a) The effect upon the OH concentration in layer 1 of increasing ground emissions rates of NO_x for different chemically coherent regions. T = tropical CLL; M = marine MML; U = urban UML.

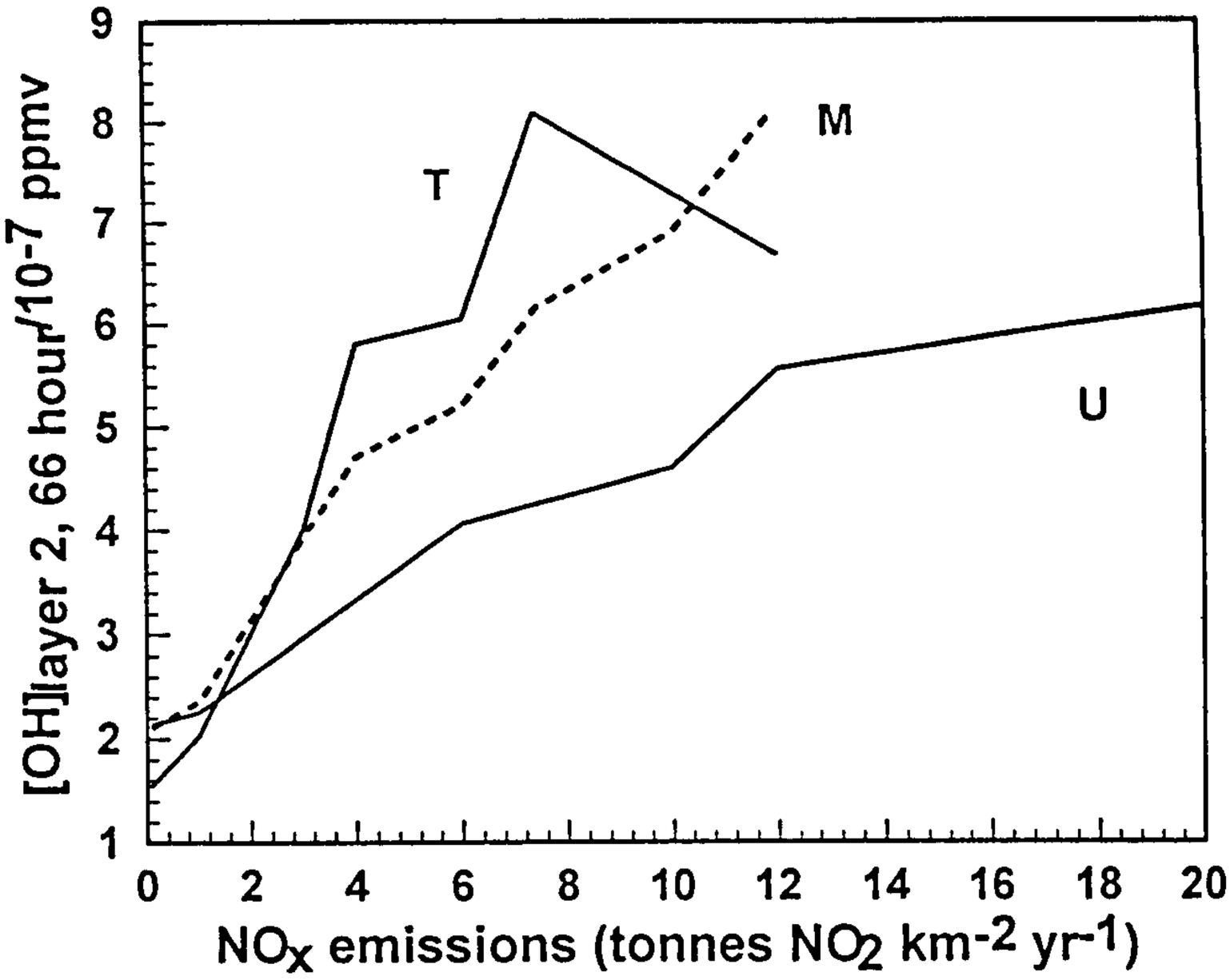

Figure 5.6b) The effect upon the OH concentration in layer 2 of increasing ground emission rates of NO_x for different chemically coherent regions. T = tropical CLL; M = marine MML; U = urban UML.

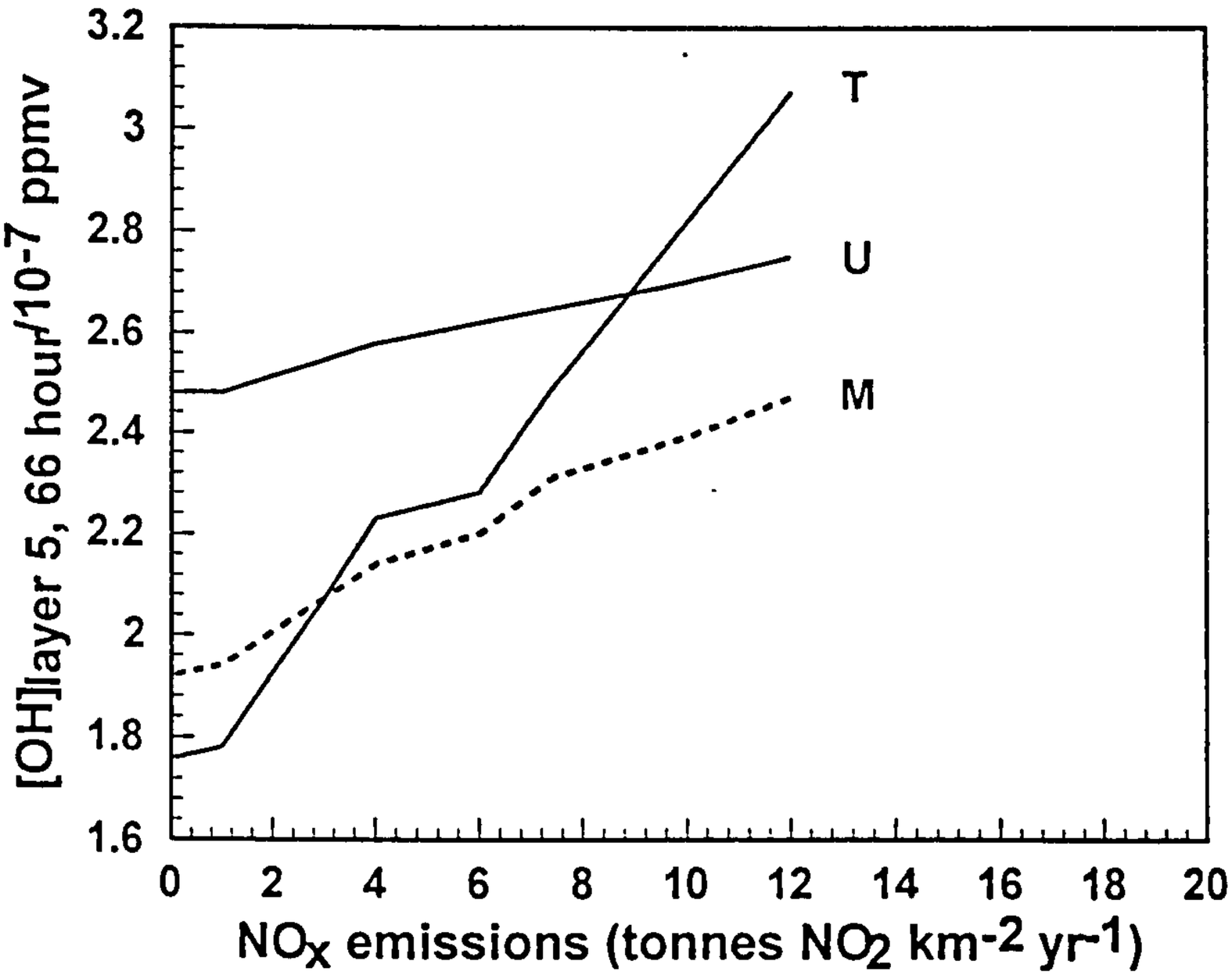

Figure 5.6c) The effect on the OH concentration in layer 5 of increasing ground emission rates of NO_x for different chemically coherent regions. T, M and U as above.

The concentration of OH would be expected to rise with the initial increase in NO_x, all other parameters remaining constant. OH is formed from the photolysis of ozone and the subsequent reaction of $O(^1D)$ with H_2O (see reactions (5.1) and (5.2)).

Although NO_x is not required for OH formation, its concentration plays an important role in determining how much OH is regenerated as a result of the catalytic oxidation chains initiated by reaction of OH with methane and CO. At high NO concentrations the conversion of NO to NO_2 by peroxy radicals leads to the regeneration of the OH consumed (reactions numbered as in Appendix A).

$$OH + CO \rightarrow CO_2 + H \qquad (38a)^2$$

$$H + O_2 + M \rightarrow HO_2 + M \qquad (38b)$$

and

$$OH + CH_4 \rightarrow CH_3 + H_2O \qquad (39a)$$

$$CH_3 + O_2 + M \rightarrow CH_3O_2 + M \qquad (39b)$$

$$CH_3O_2 + NO \rightarrow CH_3O + NO_2 \qquad (40a)$$

$$CH_3O + O_2 \rightarrow HCHO + HO_2 \qquad (40b)$$

(where M is a third body N_2 or O_2)

then

$$HO_2 + NO \rightarrow NO_2 + OH \qquad (21)$$

HO_2 is very strongly linked to OH as interchange occurs very rapidly between the two in the atmosphere (they are often combined and referred to as HO_x), and therefore any production of HO_2 will also lead to OH production via reaction with NO. In reaction 40(b), HCHO is the first intermediate of methane oxidation with a lifetime longer than a few seconds. It therefore reaches appreciable concentrations and can be removed by three different mechanisms in a NO_x rich environment.

$$HCHO + h\upsilon \rightarrow H_2 + CO \qquad (57)$$

---

[2] reaction of CO and CH_4 with OH and then with O_2 assumed in model to be one step. In reality, OH reaction is rate determining, and reaction with O_2 is rapid.

$$\rightarrow HCO + H \qquad (58a)^3$$

$$OH + HCHO \rightarrow HCO + H_2O \qquad (59a)$$

$$HCO + O_2 \rightarrow HO_2 + CO \qquad (58b), (59b)$$

The HCO formed by two of these mechanisms can then react with oxygen to produce HO_2, thus overall leading to the return of 25% more HO_x than is consumed in the form of OH. However, the converse is true in a NO_x poor situation as the HCHO formation is limited, leading to reduced formation of HO_2 and thus OH.

OH is also involved in termination reactions, which can depend upon the concentration of NO_x.

$$OH + HO_2 \rightarrow H_2O + O_2 \qquad (17)$$

$$HO_2 + HO_2 + M \rightarrow H_2O_2 + O_2 + M \qquad (14)$$

$$OH + NO_2 + M \rightarrow HNO_3 + M \qquad (20)$$

Reactions 17 and 14 are the principal radical loss reactions in clean air, whereas reaction 20 is the major loss route in polluted air. Under low NO_x conditions, the latter reaction is insignificant, and OH and HO_2 radicals are lost through the first two. This coupled with the low rate of recycling of OH leads to low concentrations of OH when NO_x is low.

As the concentration of NO_x rises, conversion of NO to NO_2 via peroxy radicals becomes more significant, and the concentration of OH rises. This can be shown by reference to the diagram in Figure 5.1. The termination of OH is not significant as the increase in NO_2 is not large enough to compensate for the relatively low reaction rate. However, [NO] eventually reaches a level where conversion to NO_2 via HO_2 is so rapid that the concentration of HO_2 falls, and that of OH and NO_2 is large enough for reaction between them to occur. The latter then becomes the dominant reaction route for OH, and [OH] begins to fall as ever greater concentrations of NO_2 occur.

---

[3] reaction 58 and 59 combined with $HCO + O_2$ reaction in model

The differences in the rates of increase of OH with NO_x for each of the scenarios can be explained in terms of the variations in the physical and chemical background conditions. The most important factor in determining the OH production rate is the insolation, and as the solar flux at 20^0N (the CLL region) is much higher than for the other two, this will increase the rate of photolysis of ozone, and will lead to a greater concentration of OH. As the concentration of NO_x increases, the photolysis of NO_2 will be enhanced, which will lead to a greater production of ozone and thus OH from the reactions

$$NO_2 + h\upsilon \rightarrow NO + O(^3P) \ (\leq 400 \text{ nm}) \qquad (3a)$$

$$O(^3P) + O_2 + M \rightarrow O_3 + M \qquad (3b)$$

$$O_3 + h\upsilon \rightarrow O_2 + O(^1D) \qquad (12)$$

$$O(^1D) + H_2O \rightarrow 2OH \qquad (35)$$

This therefore leads to a rapid rise in [OH] as emissions of NO_x increase. Similarly, levels of NO_2 and OH which are high enough for their reaction to become significant are also reached more quickly, and [OH] drops as rapidly as it rises.

In the case of the marine and urban regions, the insolation is lower due to their position at higher latitudes (60^0 and 50^0N compared to 20^0N for CLL). This leads to a lower generation of OH compared to the tropical region, despite the higher concentrations of O_3 present in these scenarios. However, the differences between the OH profiles of these two regions is a result of the differences in the background conditions.

The marine region has a lower methane concentration, a slightly higher [CO] and a much higher concentration of O_3. OH is converted to HO_2 by the CH_4 and CO (and possibly by the extra O_3, although this reaction is slow in comparison to the former two). At low NO_x levels, HO_2 can only be converted to OH via reaction with O_3 (also slow) or via H_2O_2, which is relatively insignificant at low insolation (see Figure 5.1). Therefore HO_2 can react with OH or self-react, and is removed from the scheme. It therefore requires a greater amount of NO compared to the tropical

scenario before the conversion of HO_2 is fast enough to increase [OH].

In the case of the urban region, the levels of CH_4, CO and O_3 are high. Thus OH is readily converted to HO_2, more so than in the marine scenario. Therefore even more NO_x is required in order for OH to be produced.

In the layers above the boundary layer, there is an increase in [OH] with rising NO_x emissions for the same reasons described above. However, the amount of NO_x which reaches these layers from its release at ground level is much less than for layer 1, due to the reactions occurring there, and this decreases with altitude. Therefore greater emissions of NO_x are required to produce an equivalent increase in [OH] in these mid-layers. In the top layers the concentration of OH is unaffected by the NO_x emissions. However, the fact that there is a rise in [OH] in these mid-layers indicates that in regions of high NO_x emissions even the mid-tropospheric oxidising potential may be affected, although it is unlikely to produce a reduction in OH levels.

Therefore the OH profile is a useful indicator of the relationship that exists between the trace gases discussed here and NO_x in the lower troposphere. Applying different background conditions shows how this relationship is affected by both chemical and physical factors. A similar study by Ehhalt *et al* (1990) showed the same effects, and both studies indicate that although the concentration of OH is affected by the levels of NO_x, the actual change in [OH] is relatively small compared to the degree of increase of [NO_x]. It would appear that only in regions of excessively high NO_x emissions would the ability of the atmosphere to chemically remove trace gases be affected, and this would correspond to areas directly around power station stacks and over small areas in urban centres.

The application of high emission rates to the marine environment is unrealistic as such emission rates would never occur over the ocean. Also, as mentioned in earlier sections, the chemistry of the model is not specifically designed to simulate urban centres. However, the inclusion of both scenarios demonstrates the close relationship between the chemistry of the trace gases in the troposphere, and shows the

importance of NO_x in determining the fate of the major oxidation cycles. It is a matter of some interest whether the emission rates of NO_x included here are likely to occur in the future. Development of new technology will produce cleaner and more efficient cars, and reduce emission from power stations and will be in use in developed countries over the next decade. However, the question remains as to whether less developed countries will be in a position to use this technology as it becomes available, or whether old technology will dominate. In the latter case, there is still a cause for concern about the effects of high concentrations of NO_x on the levels of oxidants in the atmosphere, especially in the regions of highest emissions, and this is an area which requires further study.

An investigation into the effects of high NO_x emissions on the upper altitudes would also be worthwhile.

5.4.2 The effects of future increases in CH_4 on [OH] and [O_3]

5.4.2.i) Comparison with the work of Thompson et al

Increasing the concentrations of CH_4 and CO by 1% yr^{-1} and 0.5% yr^{-1} respectively over a thirty year period has led to a predicted suppression of OH of ~8% and an enhancement of O_3 of ~2% in four chemically coherent regions. Figure 5.7 shows the increase in O_3 and decrease in OH for layers 1, 5 and 10 in the CLL region. The results for all regions are also given in Table 5.4, where they are compared to similar work carried out by Thompson *et al.*, (1990) for the same increases and regions. This shows that there is reasonable agreement between the two studies, except in the case of the urban scenario, where Thompson *et al.*, predict a lower OH loss and a greater O_3 gain.

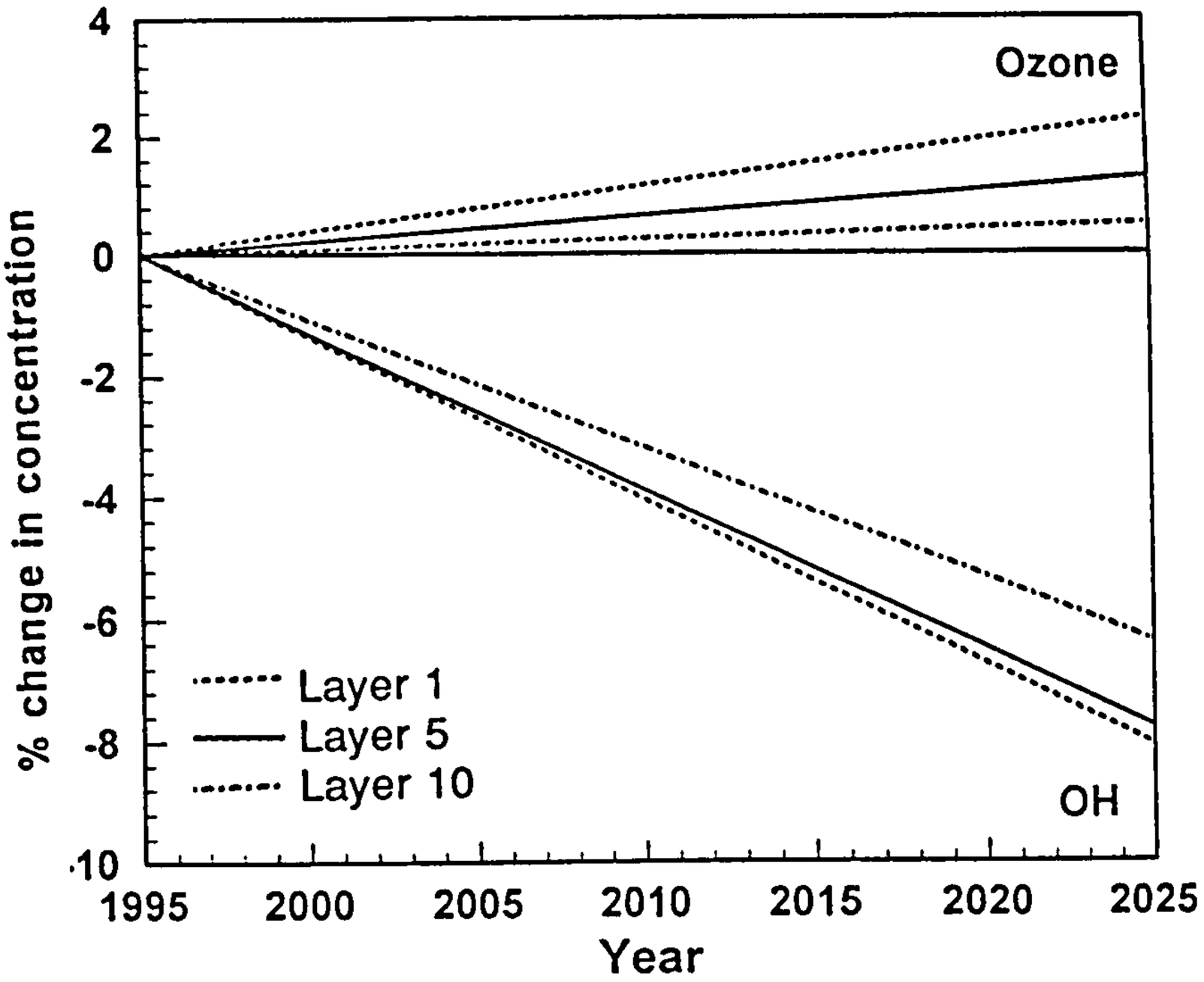

Figure 5.7 Predicted change in concentrations of OH and ozone in layers 1, 5 and 10 as a result of an equivalent increase of 1% yr^{-1} CH_4 and 0.5% yr^{-1} CO for 1995 - 2025. CLL conditions, 11th day concentration plotted.

Table 5.4 Comparison of tropospheric oxidant prediction studies

Scenario	Δ[OH] 1995 - 2025		Δ[O_3] 1995 - 2025	
	This work[a]	Thompson *et al*[b]	This work	Thompson *et al*
UML	- (6 - 9)%	- 3%	+ (2 - 4)%	+ 10%
CML	- (6 - 9)%	- 8%	+ (1 - 3)%	+ 5.5%
CLL	- (6 - 8)%	- 8%	+ (0 - 3)%	+ 5.5%
MML	- (9 - 10)%	-10%	+(0 - 1)%	+ 4%

[a] - shows the range of % increments over all layers taking the peak concentration value after 11 days

[b] - % increment over 30 years integrated over 15 km altitude

As discussed in Section 5.4.1, increasing the concentrations of methane and CO would be expected to lead to decreases in [OH] at constant [NO_x]. The concentration of NO_x in all scenarios is high enough to be referred to as NO_x rich[4], and under these conditions the oxidation of CH_4 and CO will lead to no overall destruction of OH or HO_2, and to net production of ozone.

$$OH + CO \rightarrow H + CO_2$$
$$H + O_2 + M \rightarrow HO_2 + M$$
$$HO_2 + NO \rightarrow OH + NO_2$$
$$NO_2 + h\upsilon \rightarrow NO + O(^3P) \ (< 400 \text{ nm})$$
$$O(^3P) + O_2 + M \rightarrow O_3 + M$$
net $$CO + 2O_2 \rightarrow O_3 + CO_2 \quad \text{(ozone production)}$$

$$OH + CH_4 \rightarrow CH_3 + H_2O$$
$$CH_3 + O_2 + M \rightarrow CH_3O_2 + M$$
$$CH_3O_2 + NO \rightarrow NO_2 + CH_3O$$
$$CH_3O + O_2 \rightarrow HCHO + HO_2$$
$$HO_2 + NO \rightarrow OH + NO_2$$
$$NO_2 + h\upsilon \rightarrow NO + O(^3P) \quad (\times 2)$$
$$O(^3P) + O_2 + M \rightarrow O_3 + M \ (\times 2)$$
net $$CH_4 + 4O_2 \rightarrow HCHO + H_2O + 2O_3 \text{ (ozone production)}$$

Therefore increases in the concentrations of CH_4 and CO will lead to an overall reduction in [OH] caused by the increased reactions, and to an overall increase in [O_3] and this is observed in the results of the study. The scenarios differ slightly in the ranges of % changes in OH and ozone, this work predicting a greater decrease in OH in the marine scenario, but a greater increase in ozone in the urban case. For OH, the difference is negligible due to its low concentration, but in the case of ozone, which has a background concentration of the order 10^{-2} ppmv, the differences may be more significant.

---

[4] A NO_x rich environment is defined as one where [NO]/[O_3] $>2 \times 10^{-4}$ (Crutzen & Zimmerman, 1991). All scenarios can be thus described, calculated from the data in Table 5.3.

The work of Thompson *et al.*, (1990) also predicts a greater increase in $[O_3]$ in the urban scenario, as well as a smaller decrease in [OH] and suggested that this was a result of the enhanced NO_x levels in the urban scenario. As the NO_x levels in the urban scenario are significantly higher than in the other scenarios, the net production of O_3 during the oxidation processes may be higher and this will lead to a greater production of OH via ozone photolysis (reactions 5.1 and 5.2). This will therefore counteract the decrease in OH caused by increasing CH_4 and CO but will lead to a lower overall decrease in [OH] for the urban region compared to the other regions.

The differences between the predicted results of this work and that of Thompson *et al.* (1990) are likely to be a result of differences between the parameters included in the models. As those of Thompson *et al* are not known specifically, it is not possible to compare the results in depth, but as the results are reasonably in agreement this is sufficient at present.

5.4.2.ii) Variational analysis

To investigate the significance of other species in determining the oxidising capacity of the troposphere, a series of simulations were run in which the background conditions and rate of increase of methane were altered. These were carried out on the CLL region as it represents medium emissions of all species, and the concentration/time profiles of intermediate and by-product species CH_3O_2, HCHO and CH_3OOH were also examined. This was in order to assess whether the reactions in the oxidation sequence assumed the same relative importance in each of the variations. Variational analyses were carried out whereby the methane concentration was; (1) increased by 1% yr^{-1} without any other increases, (2) increased by 2% yr^{-1} and (3) increased as in (1) but with greater NO_x backgrounds.

Table 5.5 gives the changes over 30 years in OH and ozone occurring for each of the simulations. These are also shown in Figures 5.8(a) - (c). Increasing methane alone by 1% yr^{-1} with no change in [CO] leads to a smaller decrease in [OH] in the upper layers compared to the original run, but no change in the lower layers or in ozone

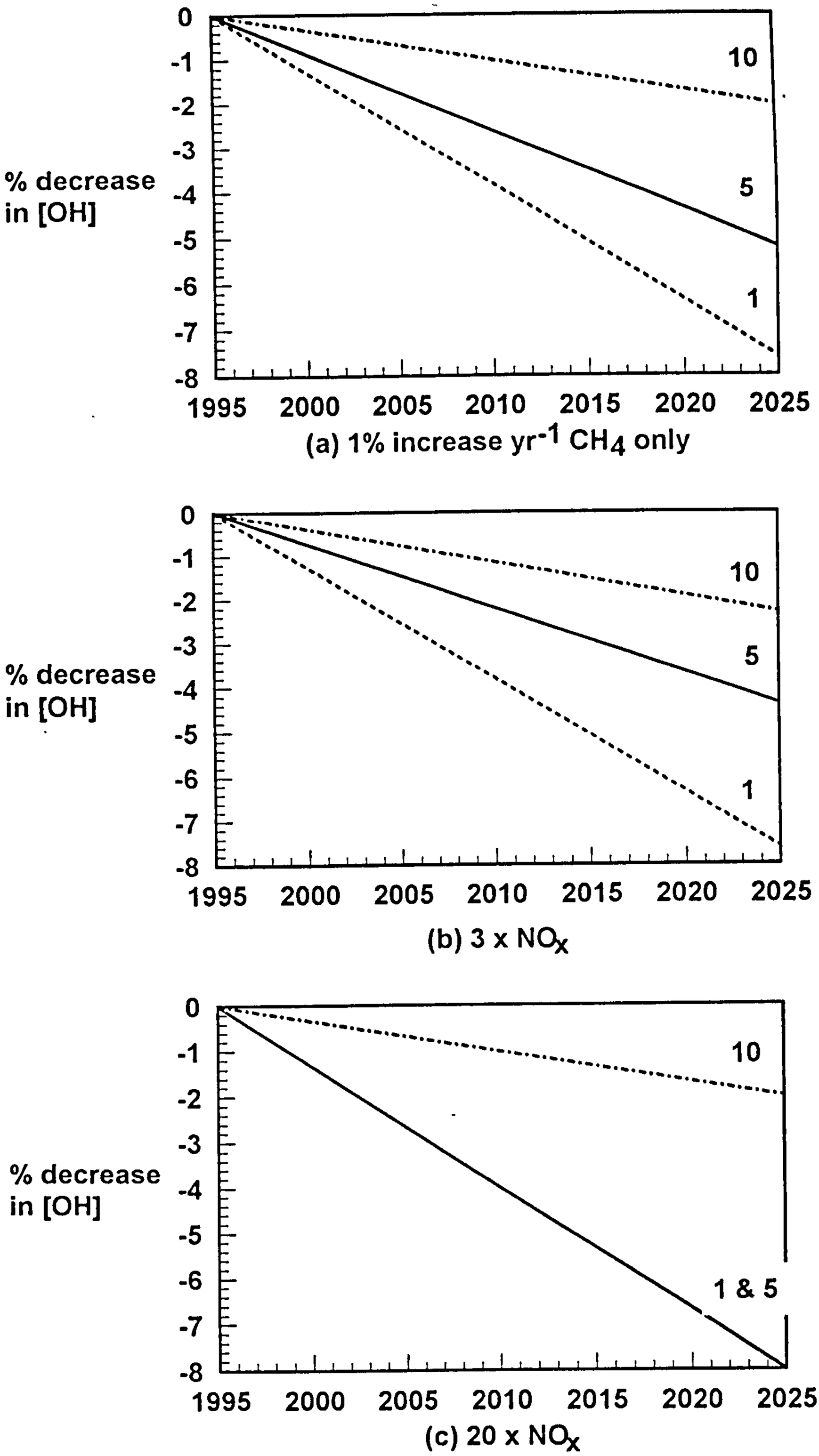

Figures 5.8 a) - c) Effect upon [OH] in layers 1, 5 and 10 of increasing the concentration of CH_4 under different chemical backgrounds for the CLL scenario.

at any altitude. Increasing [NO_x] and [CH_4] leads to a rise in the absolute background levels of both OH and ozone, increases the ozone enhancement over the thirty year period, but does not affect the [OH]. Increasing the methane by 2% yr^{-1} causes a doubling in the OH and ozone changes relative to the methane-only simulation (1).

Table 5.5 Comparison of perturbations to tropospheric oxidants for different variational analyses

Variational analysis	Δ[OH] (1995-2025)	Δ[O_3] (1995-2025)
Original CLL[a]	- (6 - 8)%	+ (1 - 3)%
CLL (+1% yr^{-1} CH_4 only)	- (2 - 8)%	+ (1 - 3)%
CLL (+2% yr^{-1} CH_4)	- (5 - 16)%	+ (2 - 8)%
CLL (3× NO_x input)	- (2 - 8)%	+ (1 - 4)%
CLL (20× NO_x input)	- (2 - 8)%	+ (4 - 6)%

[a] - corresponds to increases of 1% yr^{-1} CH_4 and 0.5% yr^{-1} CO

Increasing the concentration of CO by 15% over the thirty year period affected the concentration of OH only in the upper layers. Increasing methane whilst maintaining constant [CO] led to a smaller decrease in [OH] at higher altitudes. This can be explained with reference to the input values of the model. The initial background concentration of CO is the same in all layers, but the ground emissions are large enough to cause this concentration to increase in the lower layers over the course of the simulation. Therefore any increases in initial background concentration (such as those imposed upon the original simulation) will have relatively little effect upon the lower layers. However, in the upper layers ground emissions of CO do not perturb the background concentration, and therefore any change in the input value will have a significant effect upon [CO] in these layers. Thus when the concentration of CO is increased, [OH] will decrease in the upper layers to a greater extent than when

[CO] remains constant. Therefore increasing [CO] would appear to be insignificant compared to CH_4, if ground emissions of CO are already appreciable.

Increasing the NO_x would be expected to raise the levels of OH and ozone, as explained in the previous section, and this is observed. However, the overall decrease in [OH] due to the methane is not affected by NO_x, as the conditions in the CLL scenario are NO_x-rich and therefore increases in [NO_x] would not be expected to alter the overall OH recycling. However, ozone is affected, the increase due to methane being higher as the NO_x increases. This is ascribed to extra O_3 being produced from the NO_x-induced pathways, as explained previously in 5.4.2.i).

Doubling the rate of CH_4 increase leads to approximate doubling of the effects on OH and ozone. Although the increase in ozone and decrease in OH resulting from a 1% yr^{-1} increase in methane appear quite small, on a global scale this amounts to a significant change in the total amounts available in the troposphere and thus in the oxidising potential. The consequences of this are very complex and not clear-cut. On the one hand, decreases in OH may reduce the ability of the troposphere to remove trace gases, which could lead to increased atmospheric residence times and in the case of greenhouse gases such as methane, to enhanced global warming. On the other hand, increases in ozone could lead to greater OH production, thus counteracting the effect of OH decreases, but could also lead to increased global warming (as ozone is itself a greenhouse gas) and enhanced damage to animal and plant life caused by greater deposition to the ground.

A doubling of the rate of increase of methane would therefore be an even greater cause for concern if the effect upon OH and O_3 is linear. Such an increase may appear to be a gross over-estimation of the future increases in methane, especially in light of the decrease in the growth rate observed in the late 1980s (Houghton *et al*, 1995). However, there is much potential for emission rates to be elevated, especially with the switch in energy use from coal and oil to natural gas, which is predicted to occur over the next decade. Natural gas is a cleaner burning fuel, releasing less CO_2 and other pollutants per Joule of energy, thus making it

theoretically less deleterious to the environment. However, the transportation of natural gas from the source to the point of use via pipelines may lead to conceivably high methane leakages, especially in regions where technology is old (Tie & Mroc, 1993). Therefore whilst a 2% yr^{-1} increase may appear to be an outside estimate it is not implausible especially over a short time scale (5-10 years).

5.4.2.iii) Other species

The concentration/time profiles of intermediates and by-products of methane oxidation were examined for all of the above simulations. These were CH_3O_2, which is formed rapidly from the reaction of the methyl radical with oxygen (reaction 39), CH_3OOH, which is one product of the reaction between CH_3O_2 and HO_2 (41), and HCHO, which is fundamental in determining the net amount of OH that is formed or lost.

Table 5.6 Effect of increasing methane and other species on concentrations of intermediates.

Simulation	$\Delta[CH_3O_2]$	$\Delta[CH_3OOH]$	Δ[HCHO]
	ave 10^{-6} ppmv	ave 10^{-4} ppmv	ave 10^{-4} ppmv
+1% yr^{-1} CH_4 only	+ (20 - 26)%[a]	+ (29 - 39)%	+ (25 - 27)%
3× NO_x input	+ (17 - 26%)	+ (30 - 34)%	+ (26 - 27)%
20× NO_x input	+ (22 - 31)%	+ (39 - 47)%	+ (26 - 30)%
+2% yr^{-1} CH_4	+ (50 - 52)%		+ (57 - 65)%

[a] - range of percentage changes in concentrations over all layers after 30 years.

Table 5.6 shows the percentage changes in the concentrations of each of the species as a result of running each of the simulations. This shows that increasing methane by 30% leads to approximately the same increase in each of the intermediate species,

as expected. As a greater amount of NO_x is input, each of the species is affected differently. The CH_3O_2 experiences a small rise in background concentration (by up to 10% for the higher NO_x), and very little change in the overall increase due to methane. The absolute background concentration of CH_3OOH *falls* by up to 40% at the highest NO_x levels compared to the base case, but there is an overall increase in concentration at all altitudes as a result of greater methane. HCHO experiences a comparatively huge increase in background concentration of up to 80% at the highest NO_x levels, but the overall increase due to methane is approximately the same at all NO_x levels.

The diagram of CH_4 oxidation (Figure 5.2) gives a simple picture of the reactions which occur and the relationship between them. The overall concentration of CH_3O_2 would be expected to rise at the same rate as methane, as it is an eventual and rapidly formed product of methane's reaction with OH. The fact that the concentrations of the other two species rise at the same rate over the thirty year period indicates that the reaction pathways of CH_3O_2 are affected equally by an increase in its concentration.

Increasing the NO_x concentration leads to an increase in the initial concentrations of CH_3O_2 and HCHO, but a decrease in that of CH_3OOH. By looking at the reaction scheme, an increase in [NO], leading to enhanced concentrations of OH (as discussed earlier), will allow more methane to be oxidised, thus causing an increase in $[CH_3O_2]$. The fact that [HCHO] increases and $[CH_3OOH]$ decreases suggests that more of CH_3O_2 is able to react with the NO to eventually form HCHO, and less is involved in reaction with HO_2 to form CH_3OOH. With reference to Table 5.6, the percentage changes in the concentrations of each of the species over the thirty years are therefore slightly misleading, as they imply that the concentration of CH_3OOH rises at a significantly greater rate. This is a direct consequence of the fact that $[CH_3OOH]$ is halved as a result of a twentyfold increase in NO_x emissions, which will lead to any changes caused by *methane* increases to be relatively greater than in the original simulation.

The effect of increasing methane by 2% yr^{-1} is to approximately double the increases of the intermediate concentrations over the 30 years. This implies that the relationship between the intermediates and methane is straightforward.

5.4.3 Comparison of model with atmospheric observations

Although the primary intention of this work is to look at the relative effects of perturbations to the tropospheric chemistry, in any model it is important that the actual predicted concentrations of the species are in reasonable agreement with either experimental or atmospheric measurements. Therefore the results obtained from this work have been compared with atmospheric observations of concentrations of NO_x, OH and ozone.

As mentioned in Chapter 1, the concentration of NO_x can vary widely from pptv to ppbv levels. Therefore it depends very much upon the location. In this study NO_x levels of almost 10^{-4} ppmv (or 10^2 pptv) have been predicted. These values obviously depend very much upon the ground emission rates, stratospheric incursion rates and background concentrations chosen initially, but are of the same order as those measured. The concentrations also follow a 'C' shape with altitude, being large at the bottom, decreasing in layer 2, and then gradually increasing up to layer 10, which is in agreement with observations (Houghton *et al*, 1995).

The levels of OH measured by Prinn *et al* (1992) varied with location and time, but produced a globally and diurnally averaged value of 10^6 molecules cm^{-3}. The concentrations obtained in the present work rise up to peak values of nearly 10^{-6} ppmv for the CLL scenario, which is equivalent to 10^6 - 10^7 molecules cm^{-3}. Therefore the model is in good agreement with Prinn *et al* (1992).

In the case of ozone, the concentrations predicted in the model are dependent upon the initial concentrations, and also the stratospheric incursion rates. In the atmosphere, ozone is also highly variable, and ranges from pptv to hundreds of ppbv. Therefore the values of around 20 - 100 ppbv used in this model are reasonably

representative of atmospheric conditions.

5.4.3 Summary

The investigation into the relationship between atmospheric species and the effects of perturbations to their concentrations upon those of the oxidants OH and O_3 can be summarised as follows:

- Insolation is the key factor in determining the background concentration of OH. However [OH] is increased initially by increasing NO_x concentrations, but at high enough levels can actually react with NO_2, thus reducing [OH]. The concentration of NO_x required depends upon the presence of other species, namely CH_4, CO, and, to a lesser extent, O_3. Therefore the effect upon OH is highly localised. Increased emissions of NO_x also lead to increases in [OH] in the middle troposphere, although to a lesser extent than those in the lowest layer.

- Increasing [CH_4] by 30% leads to a predicted decrease in [OH] of up to 10%, and an increase in atmospheric [O_3] of up to 4%. This is also dependent upon the concentration of other species. CO appears to have little effect upon [OH]. Higher concentrations of NO_x raise the initial concentrations of OH and ozone, lead to a greater overall increase in ozone as methane increases, but has no effect upon the decrease in OH. Doubling the increase in CH_4 also doubles the predicted changes in OH and O_3.

- The relative role of each of the reactive intermediates involved in the oxidation of CH_4 by OH changes slightly when NO_x is increased, but not by a significant amount.

- The concentrations of species predicted by the model are in good agreement with atmospheric measurements.

5.5 Lightning Studies

5.5.1 Base Case

Initially the concentration/time profiles of NO and NO_2 with the NO_x 'lightning' inputs were examined for each of the layers and compared to those obtained under tropical (CLL) conditions without the 'lightning' (referred to as blank runs throughout the text). As shown earlier (Figures 5.4a) and b)), the profile of NO exhibits strong diurnal behaviour, peaking during daylight hours (06:00 - 18:00) partly due to the photolysis of NO_2. The diurnally-averaged concentration of NO is initially large and then decreases to a constant over the 11-day simulation, the decrease being greatest in the upper layers. The profile of NO_2 peaks during night-time, due to the lack of photolysis, and also decreases to a constant over the simulation, with layer 1 having the largest concentration as a result of the lower photolysis rates which are present at lower altitudes. For NO, the concentration is greatest in the upper layers due to the lower levels of peroxy radicals in these layers, with which NO reacts readily.

The lightning simulations show increases in the concentrations of NO and NO_2 as a result of the NO_x input. In the case of NO, the input of NO_x occurs as the concentration of NO is declining into night-time minimum (see Figure 5.9) and leads to an enhancement of the minimum concentration of around 5% in the lower layers and up to a factor of 10^5 in the upper layers (this is not visible in the figure). The input ends halfway through the night-time minimum, but at the start of Day 8 an enhancement of the NO concentration is observed in all layers, especially at the higher altitudes where increases of up to 25% are present. No further augmentation occurs beyond Day 8 in the lower layers, but is seen to a lessening degree to the end of the simulation in the top layers, as the concentrations decline to the blank levels.

For NO_2, the input occurs during the night-time peak (see Figure 5.10), and causes an enhancement of between 1% (layer 1) and 2% (mid-upper layers). This enhancement continues in the higher altitudes throughout the simulation, decreasing gradually over time. Therefore, the input of NO_x directly to the middle layers appears

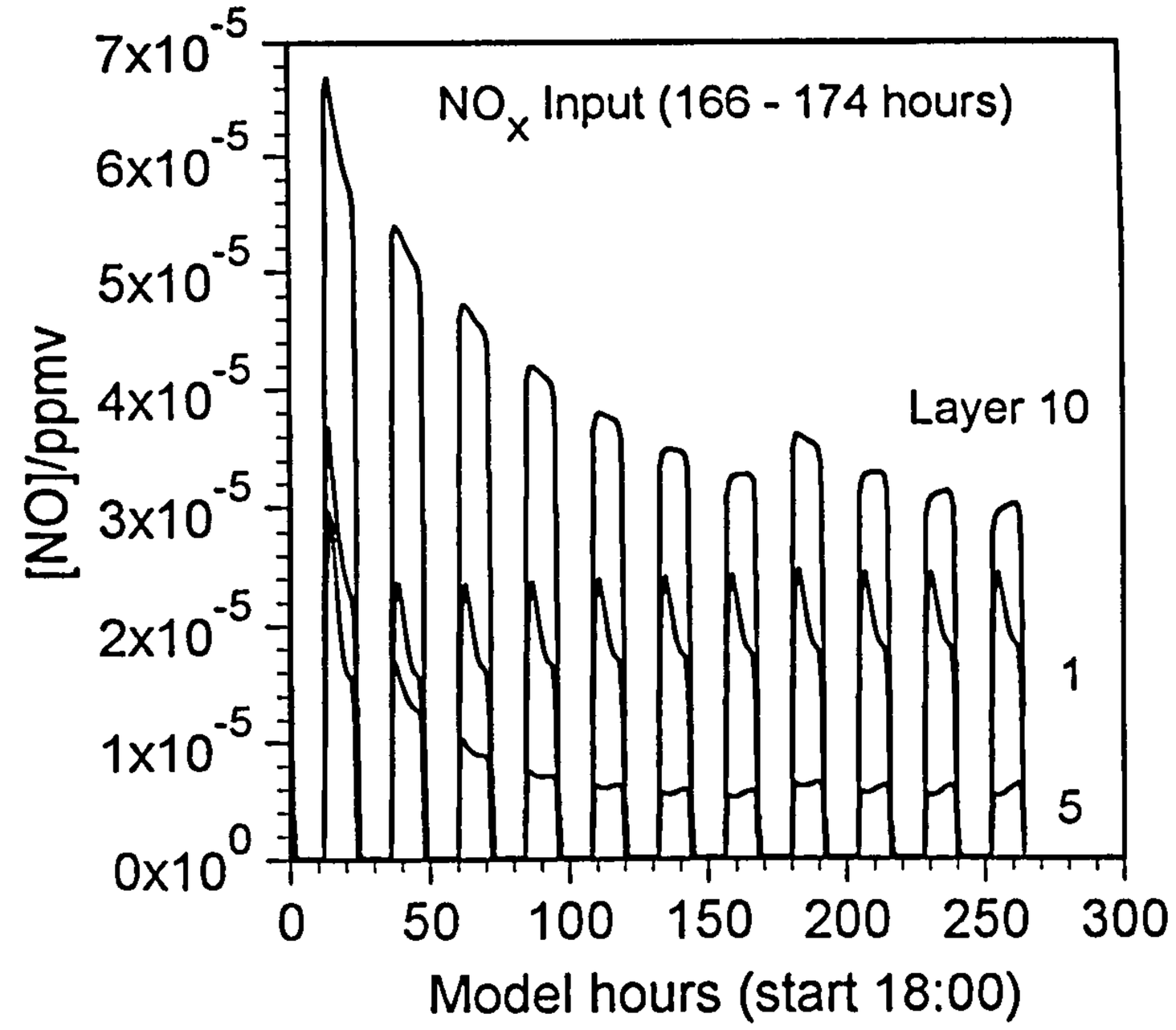

Figure 5.9 Effect of 'lightning' input of NO_x upon the concentration/time profile of NO. CLL conditions, 11 day simulation.

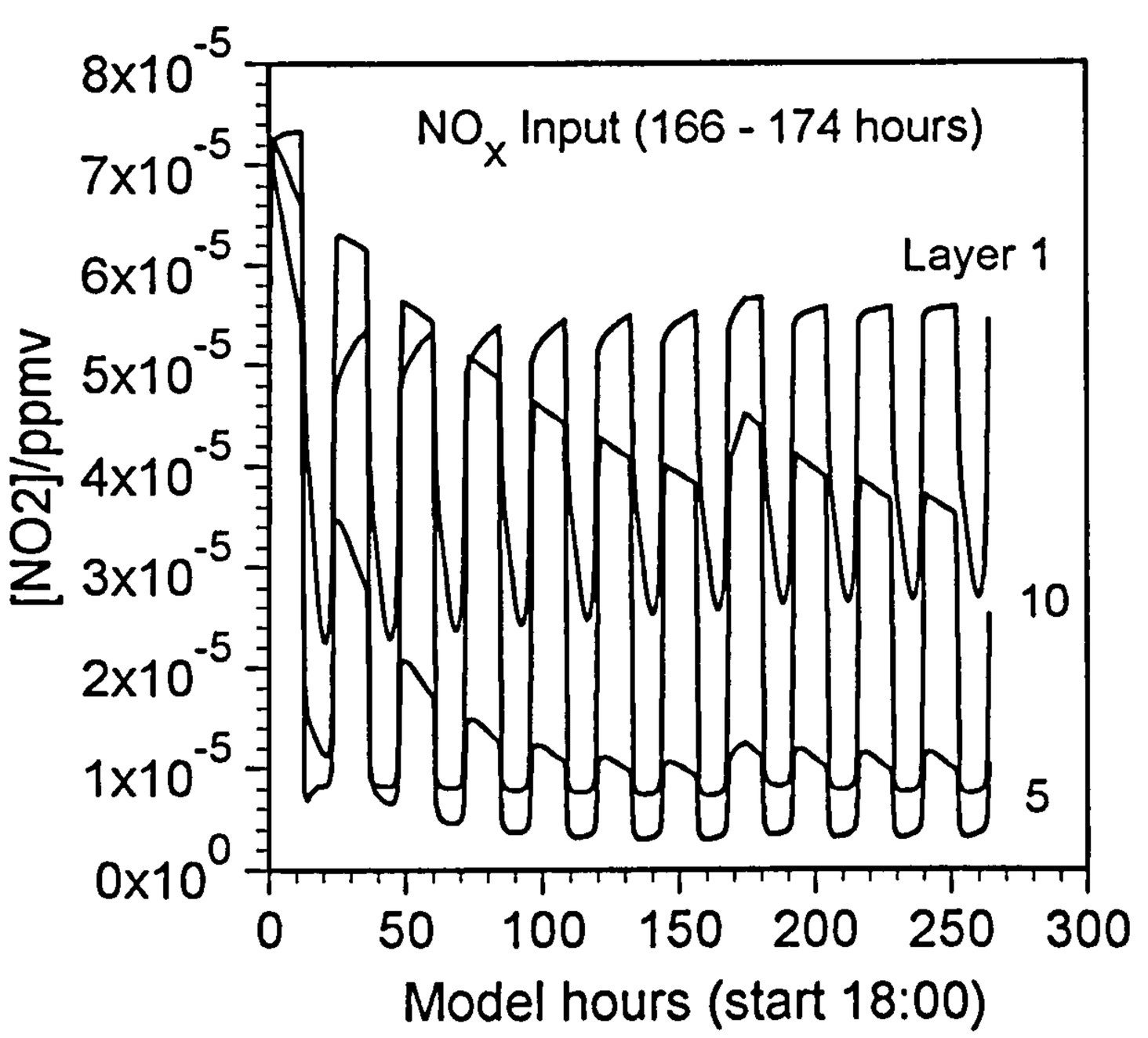

Figure 5.10 Effect of 'lightning' input of NO_x upon the concentration/time profile of NO_2. CLL conditions, 11 day simulation.

to have a significant effect upon the concentration. In the lowest layers, the ground emission of NO_x would seem to produce a high enough concentration that inputs at these levels do not greatly affect the background.

It is important to note at this point that a constant input rate of NO_x for all layers will obviously lead to greater concentrations in the upper layers, due to the lower pressures. However, this is quite important in terms of the chemistry, as inputs at higher layers will obviously be more significant.

If 'lightning' inputs of NO_x perturb the background concentrations of NO and NO_2 for a number of days, then it would be expected that other species involved in the complex sequence of NO_x-related reactions would also be affected by these inputs, such as OH, HNO_2, HNO_3, NO_3, N_2O_5 and possibly ozone. The concentration/time profiles of each of the species (see Figures 5.11a) - e)) were also output and it was found that all apart from O_3 increased to some extent as a result of the NO_x inputs.

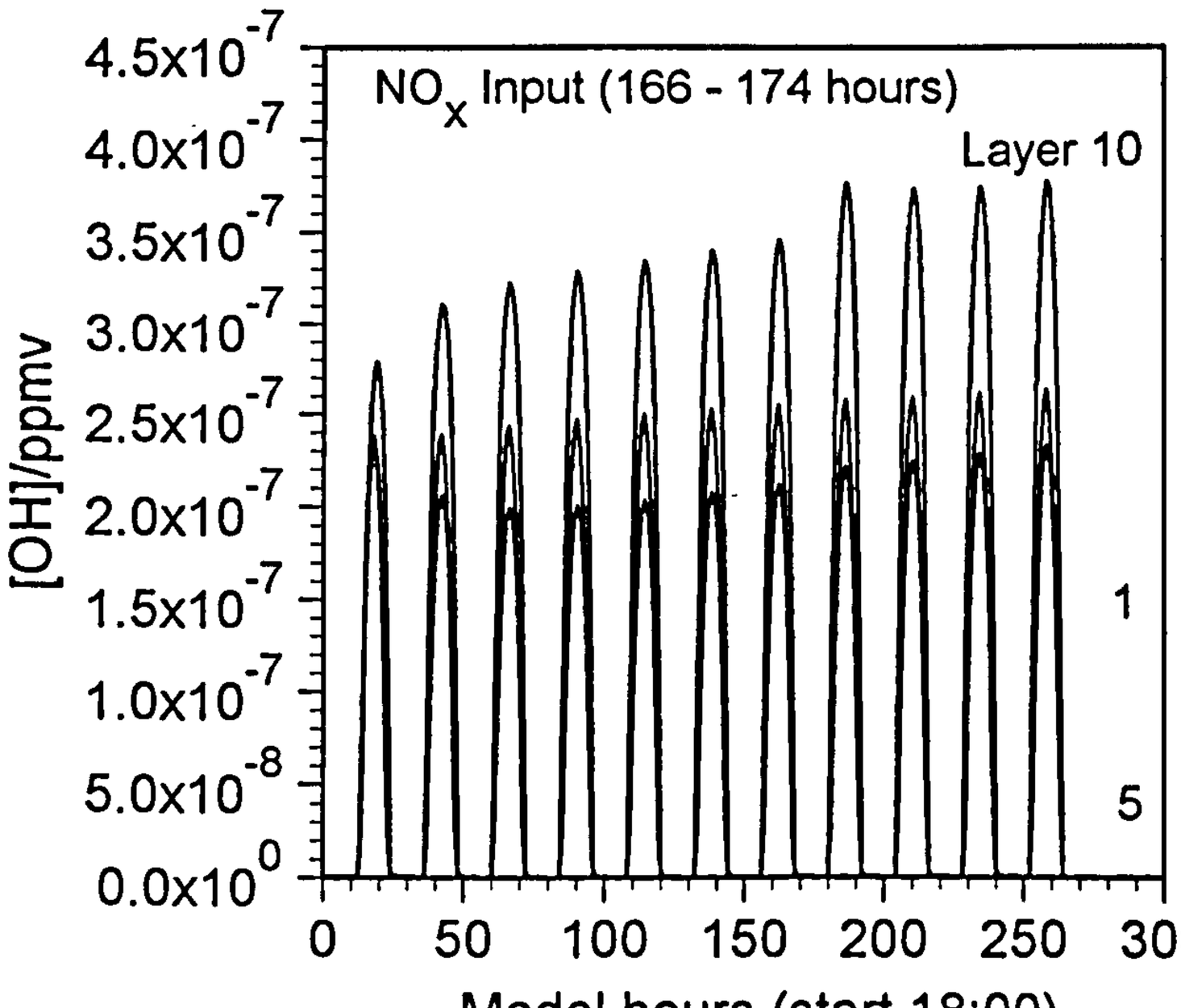

Figure 5.11 a) Effect of 'lightning' input upon concentration/time profile of OH. CLL conditions, 11 day simulation.

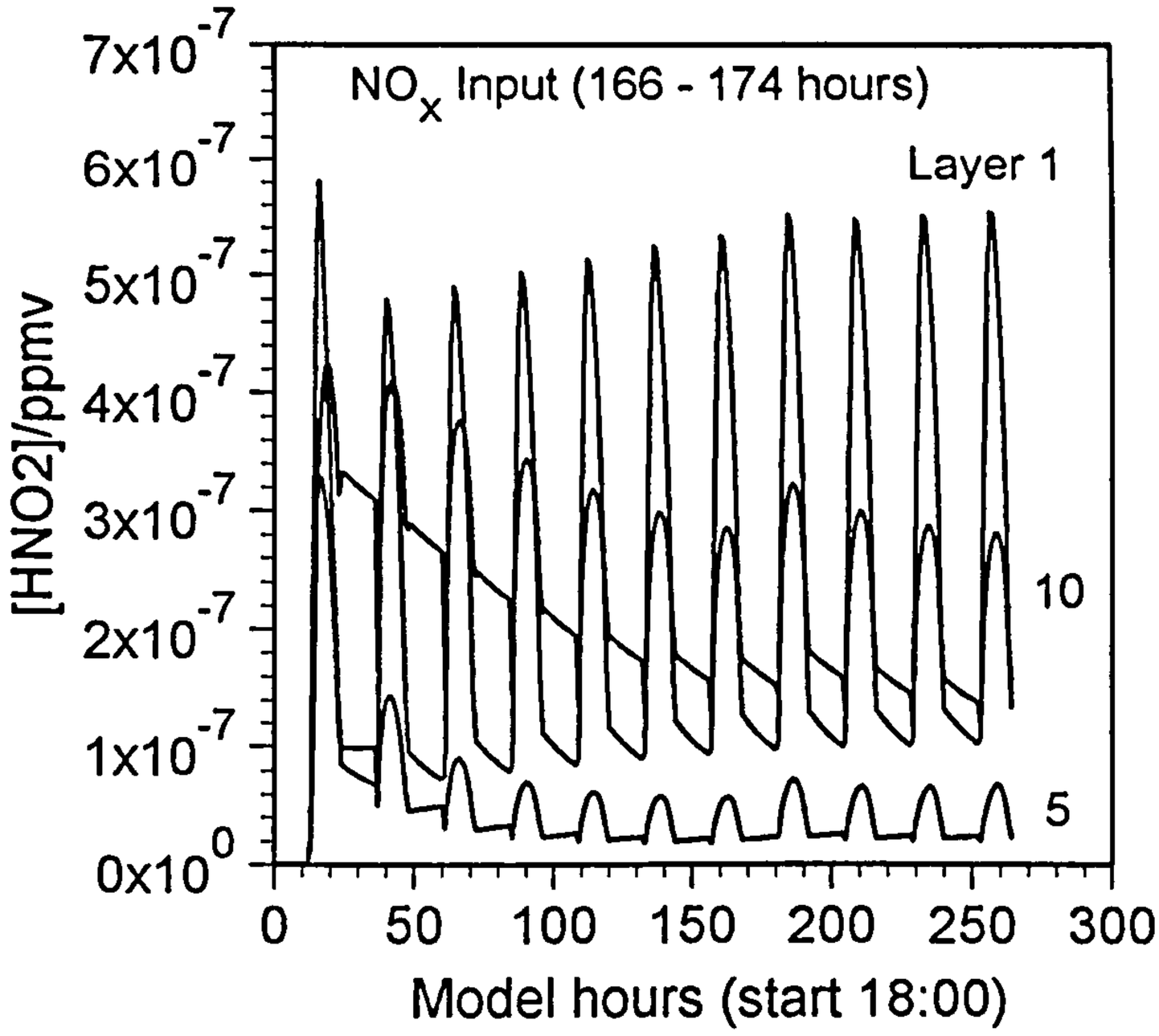

Fig 5.11 b)

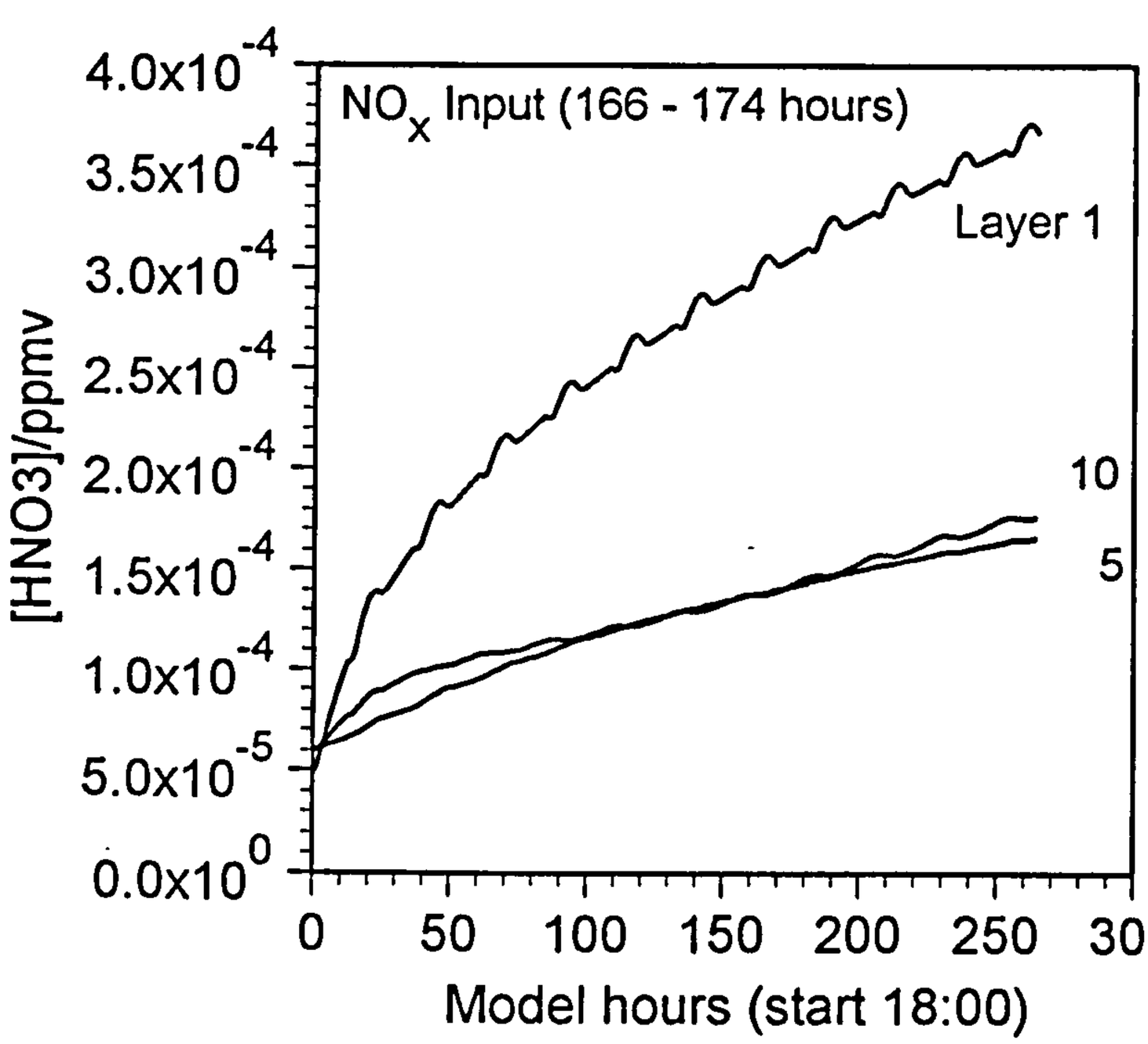

Fig 5.11 c)

Figures 5.11b) and c) Effect of 'lightning' input of NO_x upon concentration /time profiles of b) HNO_2 and c) HNO_3

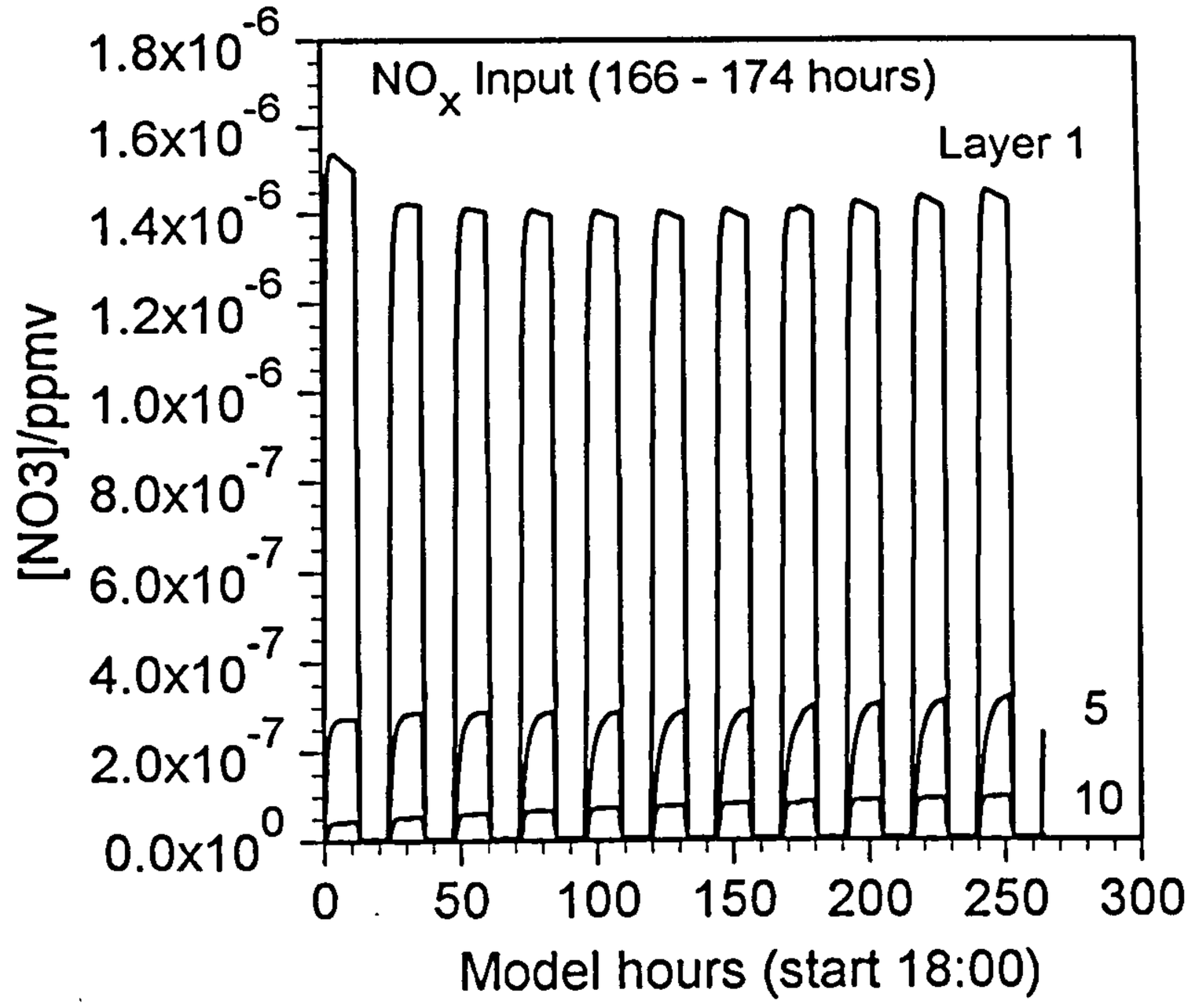

Figure 5.11 d)

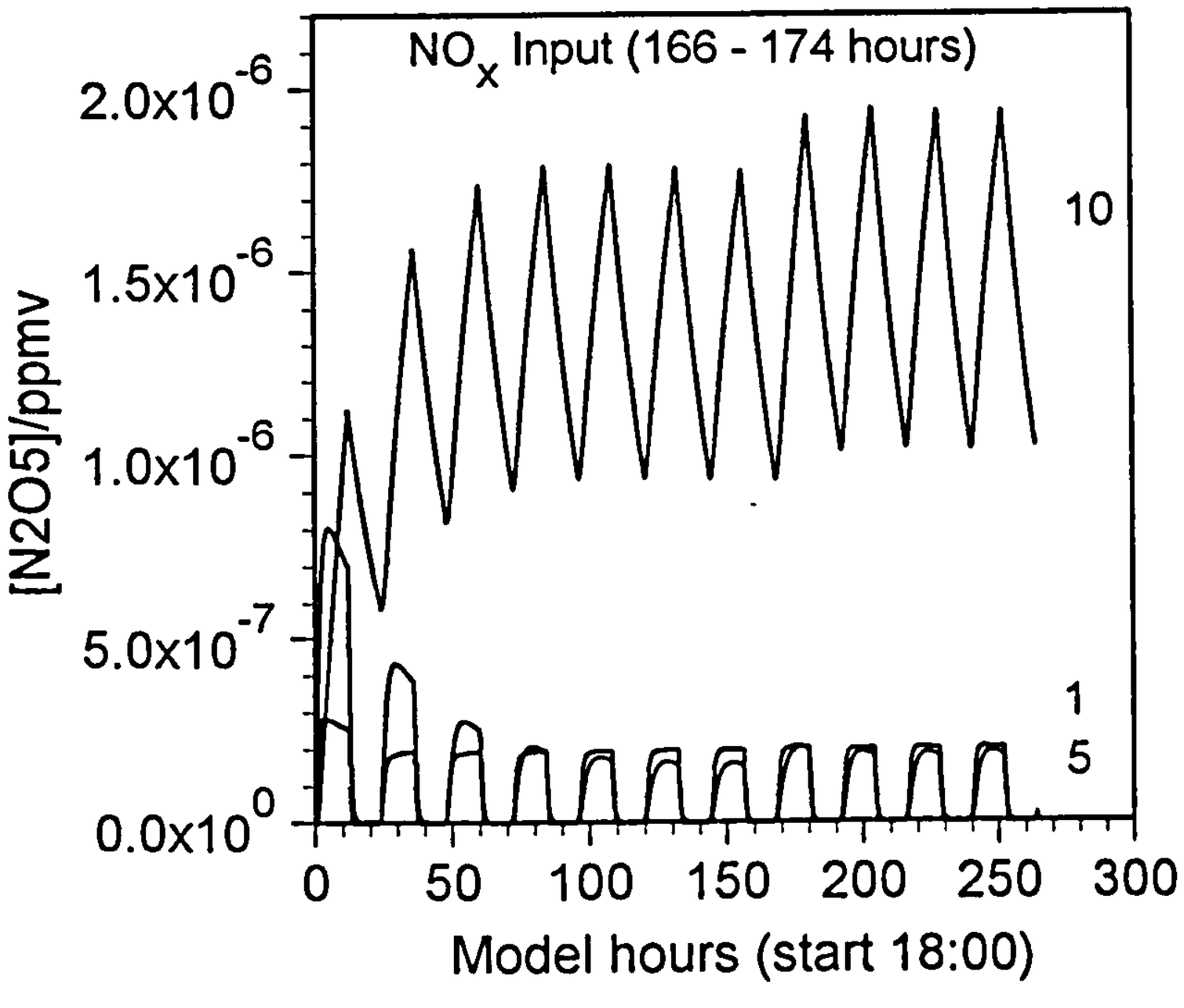

Figure 5.11 e)

Figures 5.11 d) and e) Effect of 'lightning' input of NO_x upon concentration/time profiles of d) NO_3 and e) N_2O_5

All the species exhibit some degree of diurnal behaviour, with OH, HNO_2 and HNO_3 reaching peak values during the day, and NO_3 and N_2O_5 peaking at night-time. The latter is a result of the photolysis of NO_3 during the day, and the fact that N_2O_5 is formed from the reaction of NO_2 and NO_3, both of which are only present in sufficient concentrations for reaction to occur during night-time. The extent of the increases ranges from 2% for HNO_3, which has a higher background concentration than the others and is therefore less susceptible to small perturbations, to 10% for OH and NO_3 and up to 20% for N_2O_5. In the middle layers, an even higher increase is noticeable as a result of the lower concentrations in these layers.

Ozone is less likely to be affected by the input of NO_x as its concentration is a factor of 10^5 higher than the equivalent increases in concentration occurring in NO_x as a result of the inputs.

The base case indicates that an input of NO_x to all layers has a significant and relatively long-lived perturbation on the chemistry, especially in the upper layers, leading to changes in the concentrations of not only NO_x, but also of species involved in reactions with NO_x. The lower layers are relatively unaffected, due to both the higher levels of ground emissions compared to the stratospheric incursion rates and to the pressure dependency of concentration with altitude. If the ground emissions were lower, a greater perturbation as a result of NO_x input may be seen at the lowest layers.

5.5.2 Variational Analysis of the Base Case

5.5.2.i) Changing chemical input and timing of the 'storm' event

The effects of changing the chemical inputs and backgrounds on the NO_x enhancement were considered. Firstly the timing of the input was altered. In the base case, the lightning is set to occur from the late afternoon through to midnight on Day 7, as this is the time of day when the air at ground level has been heated enough to cause instability in the cooler air above. However, in tropical weather systems, where

the temperatures are high for long periods of time, instability is quite common and can lead to thunderstorms which recur over an area. Therefore the NO_x input was set to occur during Day 7 (10:00 to 18:00) and during the late night/morning on Day 8 (00:00 to 08:00). This was to assess whether alterations to the timing would lead to changes in the degree of enhancement of the background concentrations, or whether, as in the previous section, the overall effect depended only upon the total NO_x emissions.

The concentration/time plots in Figures 5.12(a) and (b) show that in the case of NO, although there is some difference in the degree of enhancement during input, this difference is insignificant by the end of the simulation, although the values are all higher than those of the 'blank'. This is also true for NO_2. Therefore, although the concentrations at the time of input are different, the levels are the same after a few days, suggesting that the timing of input is unimportant compared to the total input value of NO_x

This was examined in more detail by both doubling and halving the total NO_x input under the same conditions as the base case. The effect of doubling the NO_x input was to increase the NO concentration during the 'lightning' event by up to a factor of two in the mid layers, by up to 50% in the upper layers, but by only 10% at the lowest altitudes. After the input the concentrations gradually returned to approximately 2% above base case levels by the end of the simulation, except in the lower layers, where the values converged quicker. The effect on NO_2 was much smaller, leading to increases of a maximum of 30% in the mid-layers, and 10% in the upper layers. However, the concentrations also remained slightly higher than the base case at the end of the run. OH concentrations were enhanced, but to a lesser extent (between 2 and 10%, depending upon altitude, but following the same pattern as NO and NO_2) and they returned to base case values after about 2 days.

Halving the NO_x input led to a greater reduction in the case of NO than the amount of enhancement caused by doubling the input. Approximately the same degree of reduction as enhancement was observed for the other species. However, at the end of the simulation, all values were around 4% lower than those of the base case.

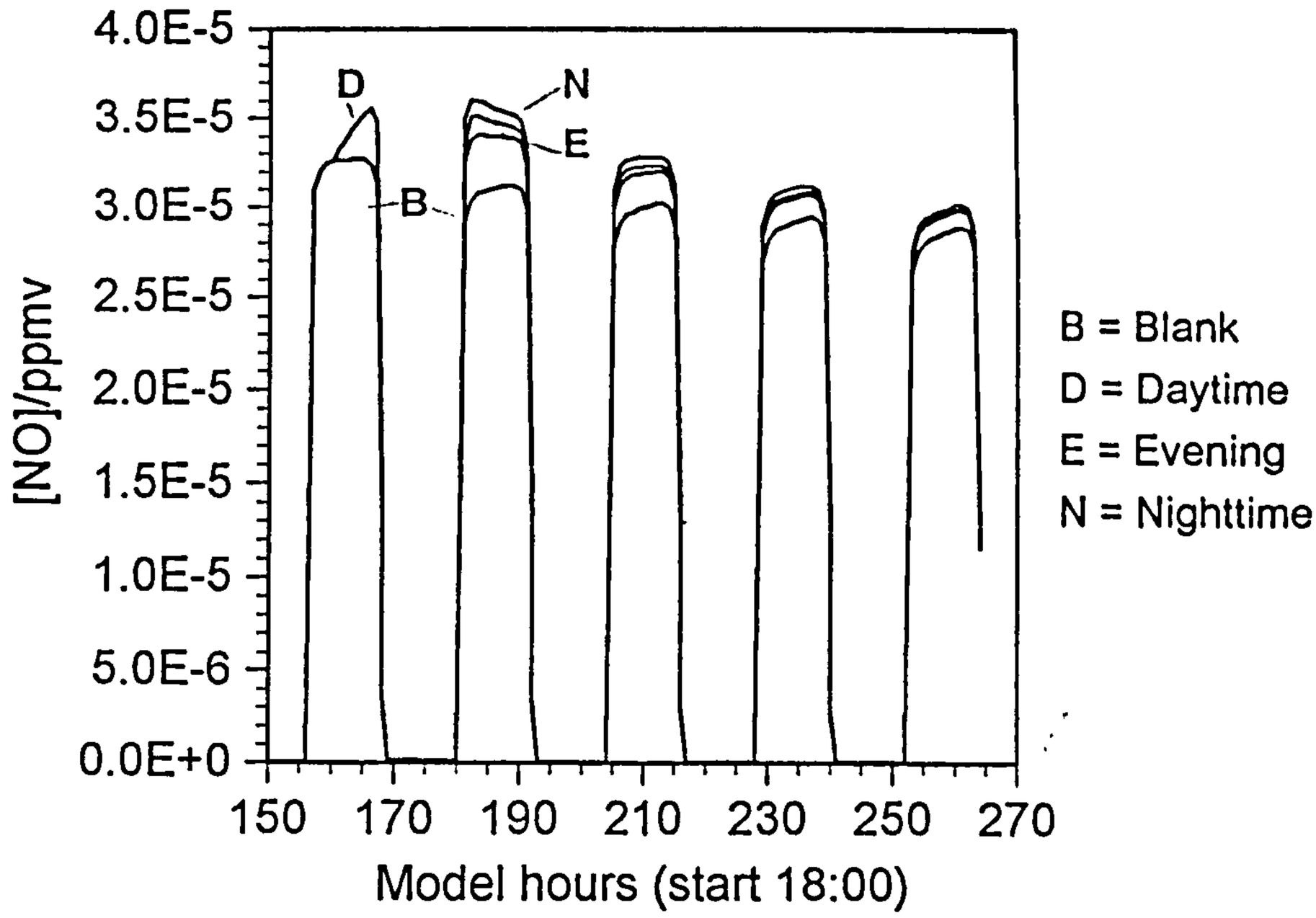

a)

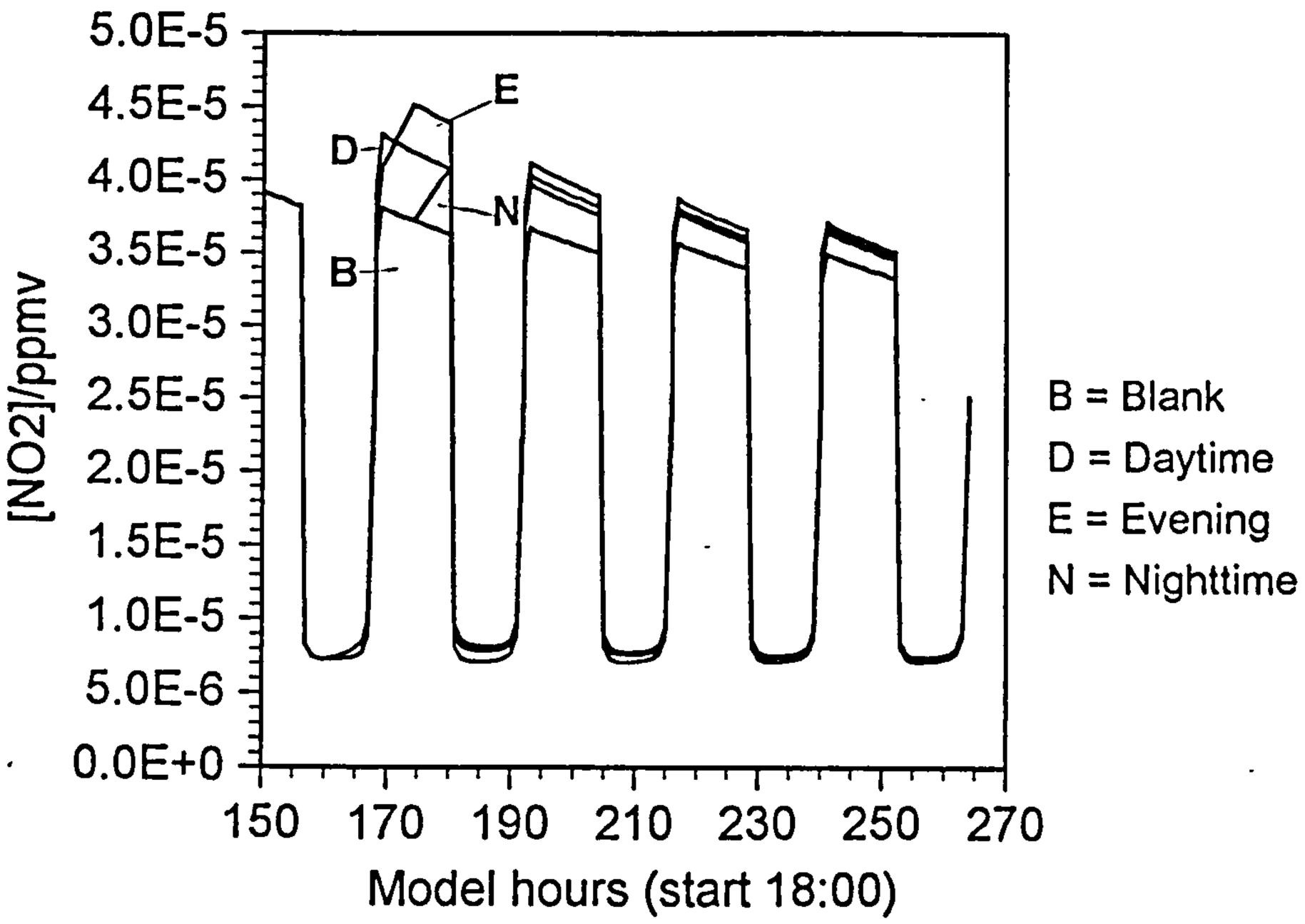

b)

Figures 5.12 a) and b) The effect of altering the timing of the 8 hour 'storm' input of NO_x. Blank = no NO_x input; Daytime = 160 - 168 hours; Evening = 166 - 174 hours; Nighttime = 172 - 180 hours.

Therefore, the effect of doubling and halving the NO_x input from 'lightning' is to enhance and reduce the concentrations of all species respectively, not by 100% in the case of NO and NO_2, but by a maximum of 50% (for NO), and in most cases by much less. The concentrations remain enhanced only by a few percent relative to the base case, suggesting that whilst a change in the total NO_x input alters the concentrations immediately after the input, the long term effects are small. Increasing the input will lead to a greater amount of NO_x background, but this enhancement reduces quicker the more that is input.

5.5.2.ii) Changing horizontal wind dilution rates

The addition of wind dilution to the simulation led to changes in the relative concentrations of NO and NO_2 with respect to both time and altitude. Figure 5.13(a) and (b) show that as the wind dilution increases, the average concentration of NO in all layers increases when compared to Figure 5.4(a), most especially in the middle and upper layers such that the concentration of NO increases with altitude, rather than decreasing from the lower to the middle layers and then increasing towards the highest altitudes. This was also observed for NO_2, O_3, and the other species in the study (see Figure 5.13(c)), and in each case the concentrations remained constant over the course of the simulations. The values of the minimum concentrations also increased such that the differences between the maxima and minima decreased in proportion to the degree of wind dilution.

The effect of NO_x input was suppressed significantly, especially at the higher wind speeds. It is difficult to compare these values directly with those of the base case due to the augmentation of the background concentrations, but the increases as a result of NO_x inputs are around a half to a third as large as those observed in the base case.

The fact that the addition of wind dilution led to enhanced concentrations of species is a result of the way in which the wind dilution is calculated in the model which is dependent upon the initial concentrations of the species as explained in Section 5.2.1.v) and needs to be addressed in future studies.

a)

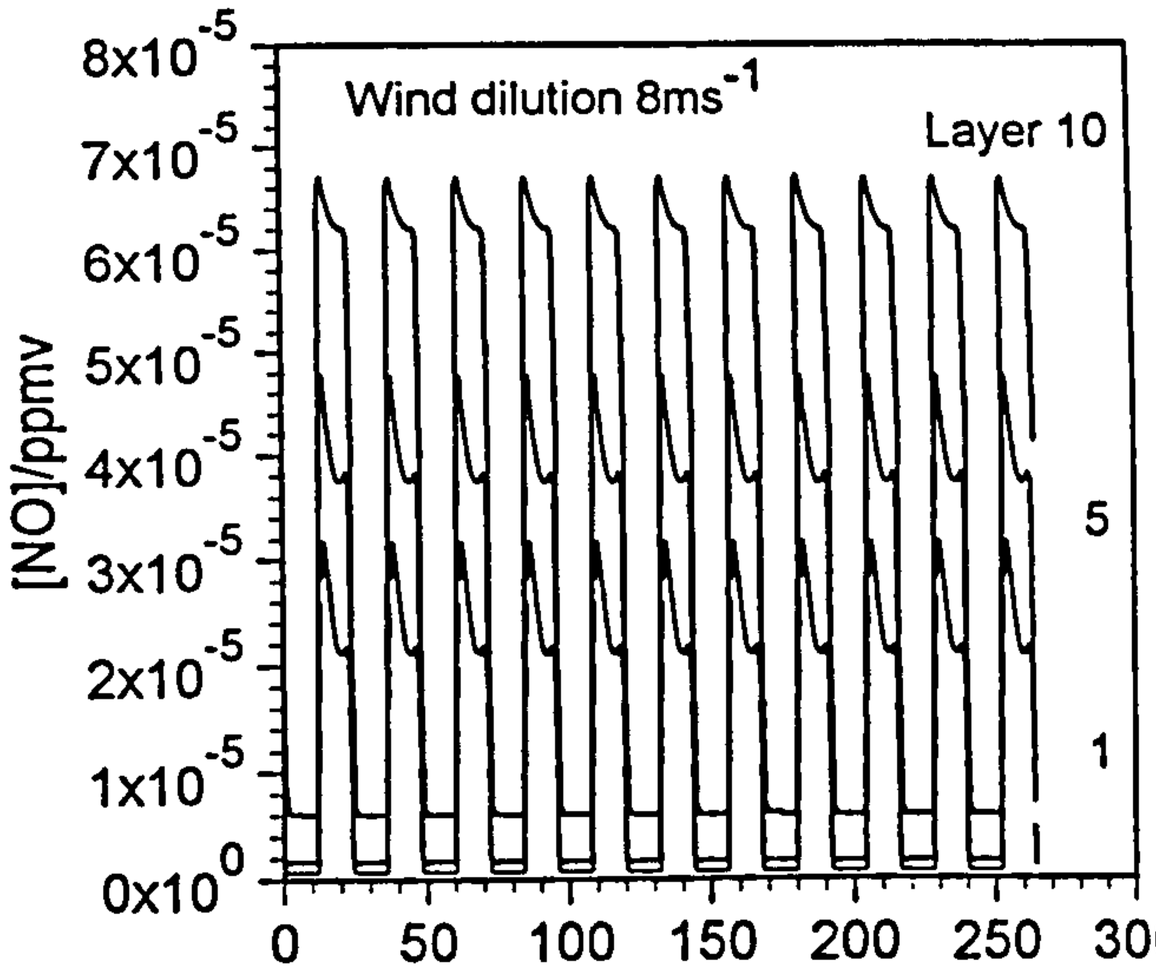

b)

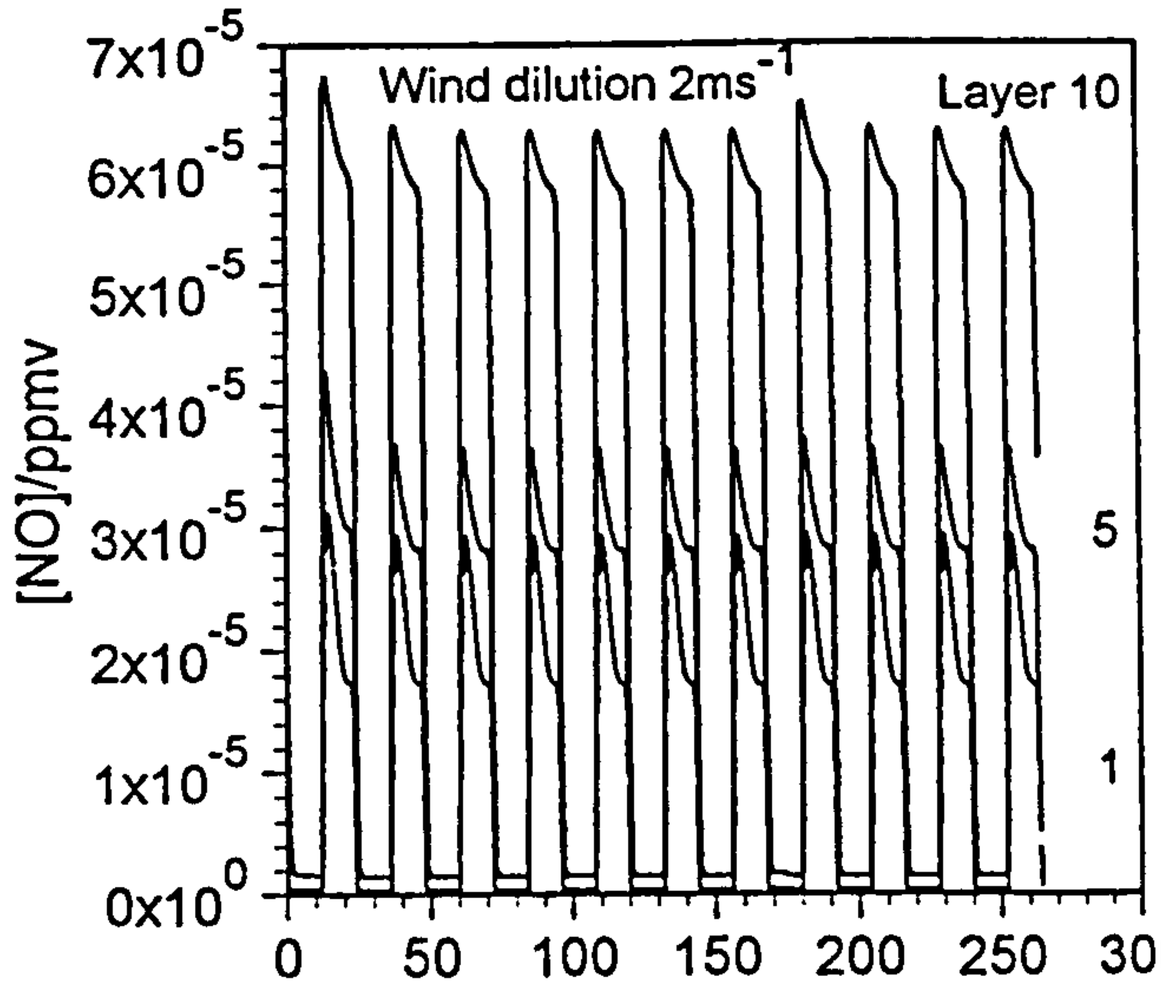

c)

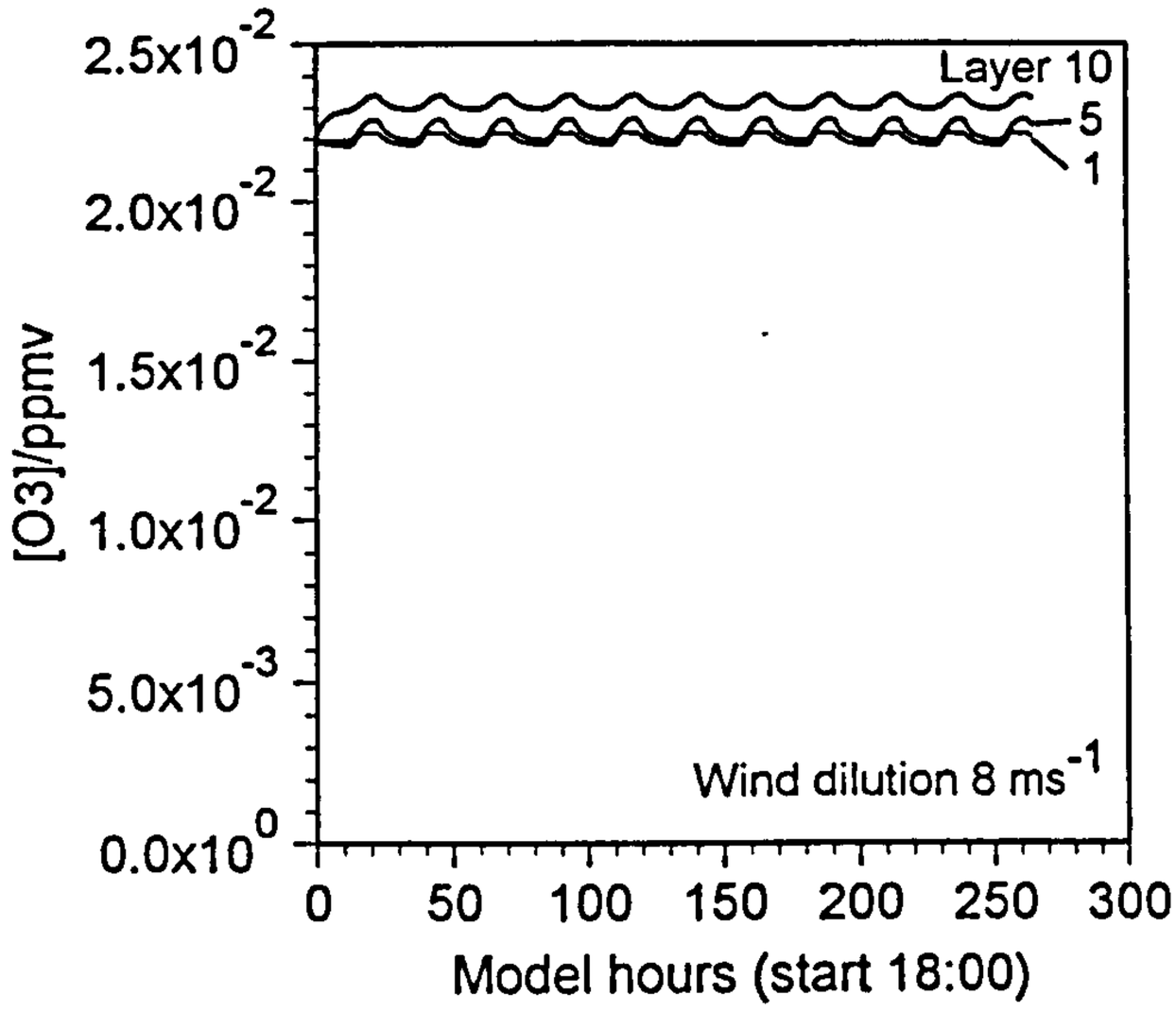

Figures 5.13 a) - c) Effect of including wind dilution at rates of between 2 and 8 ms^{-1} upon the profiles of NO and ozone for the lightning base case (CLL)

5.5.2.iii) Altering photolysis rates

Switching off the photolysis rates for the duration of the simulation led to a removal of the diurnality of NO and NO_2. The concentrations of NO drop to the levels of the minima in the base case as NO is still being destroyed by reactions and emitted at ground level and from the stratosphere but is not being produced. In the case of NO_2, the lack of photolysis means that NO_2 is only destroyed by non-photolytic reactions, and thus the concentration follows the diurnally-averaged levels of the base case. This is shown in Figures 5.14(a) and (b). In each case the input of NO_x led to a corresponding increase in the background, which tailed off immediately for NO, but remained for a few days in the case of NO_2. The extent of this increase was the same as the base case for NO, but varied by layer with NO_2.

The removal of the photolysis for the duration of the storm only led to very little difference in the NO profile compared to the base case (Figures 5.14 c) and d)). In the case of NO_2, the uppermost and lowest layers showed a smaller increase due to the input than the base case, but in the middle layers, where the concentration is lowest, the degree of enhancement during the input was greater by 10%. Compression of the lightning into the lowest layers led to increases in the NO_x input to those layers compared to the base case, which subsequently gave greater augmentation of the background. Figure 5.15 shows the effect of compressing the lightning into 5 layers, with layer 10 being the same as the blank, and layers 1 and 5 having a greater increase in concentration compared to the base case. However, the amount of increase observed was always less than that expected from simple calculation, and this would suggest that much of the NO_x which is input is immediately taken up by reactions with other species not involved in the NO_x store reactions. In all cases the values of the concentrations eventually levelled off to those of the base case and no lower.

Therefore it would appear that reducing the photolysis rates during a storm does not alter the overall effect of inputting NO_x, and that the total amount of NO_x input is the most important factor in determining the effect on the background concentration.

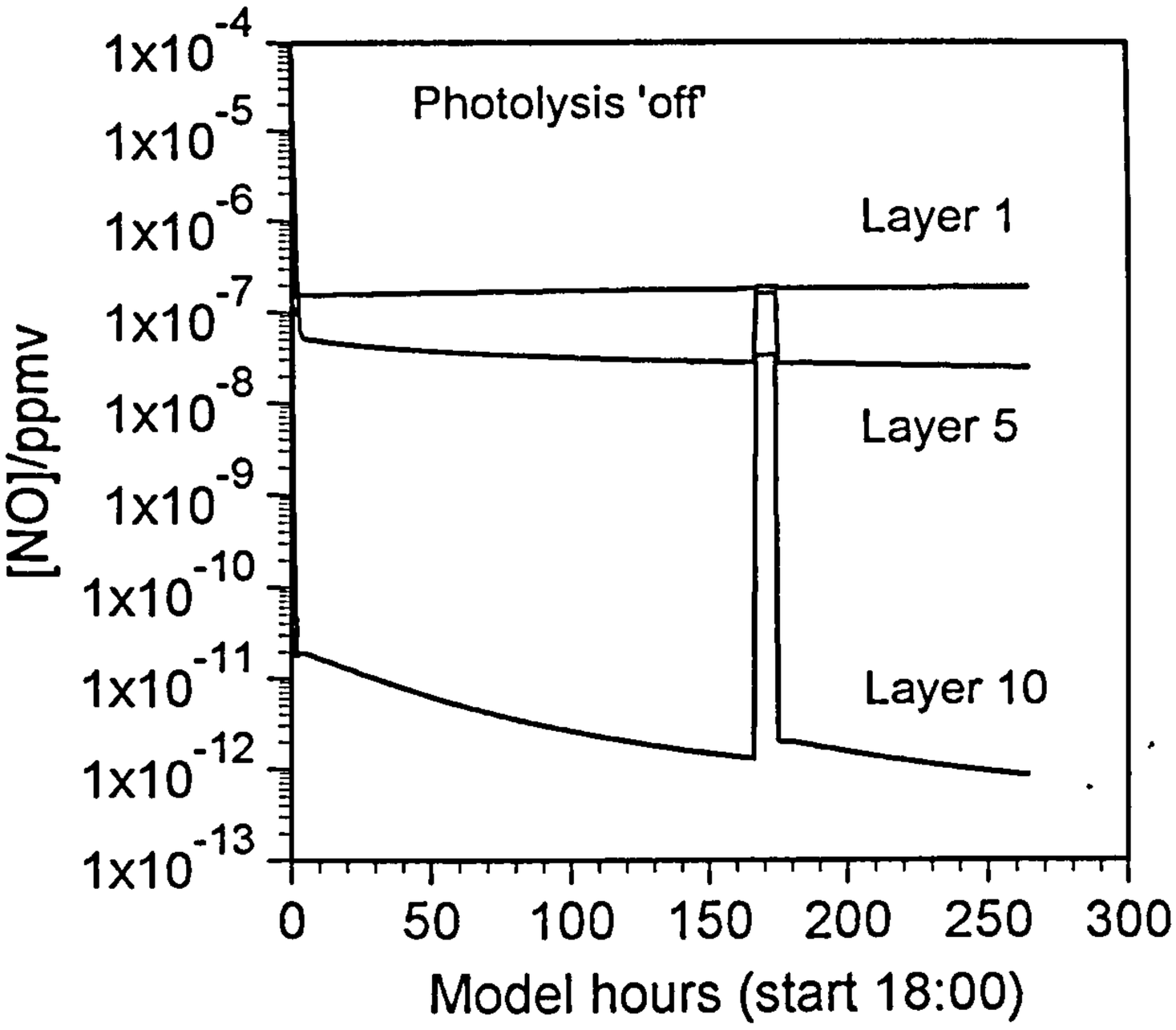

a)

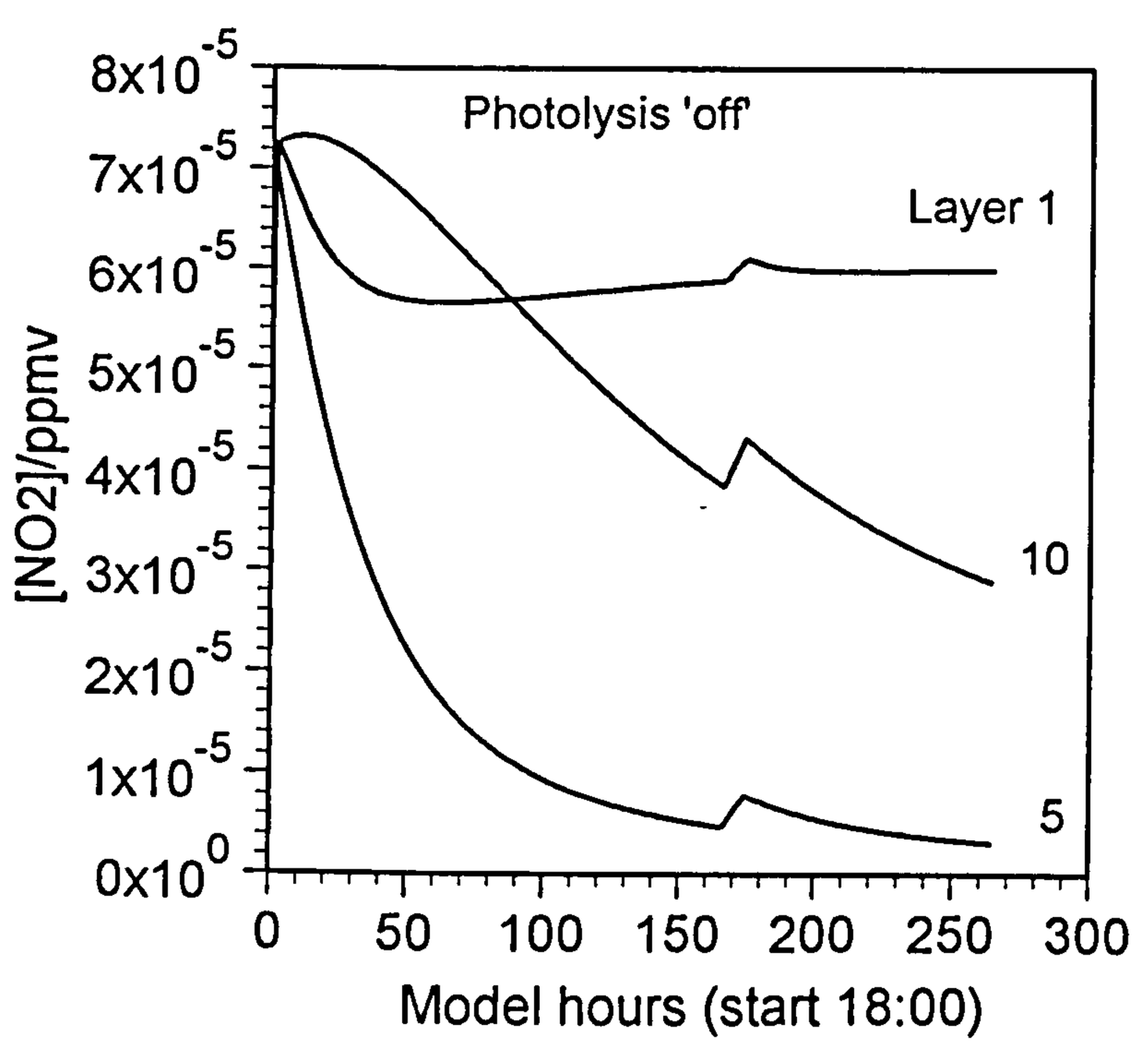

b)

Figures 5.14 a) and b) Effect of setting photolysis rates to zero during 11 day CLL simulation, with base case lightning input of NO_x; a) NO and b) NO_2.

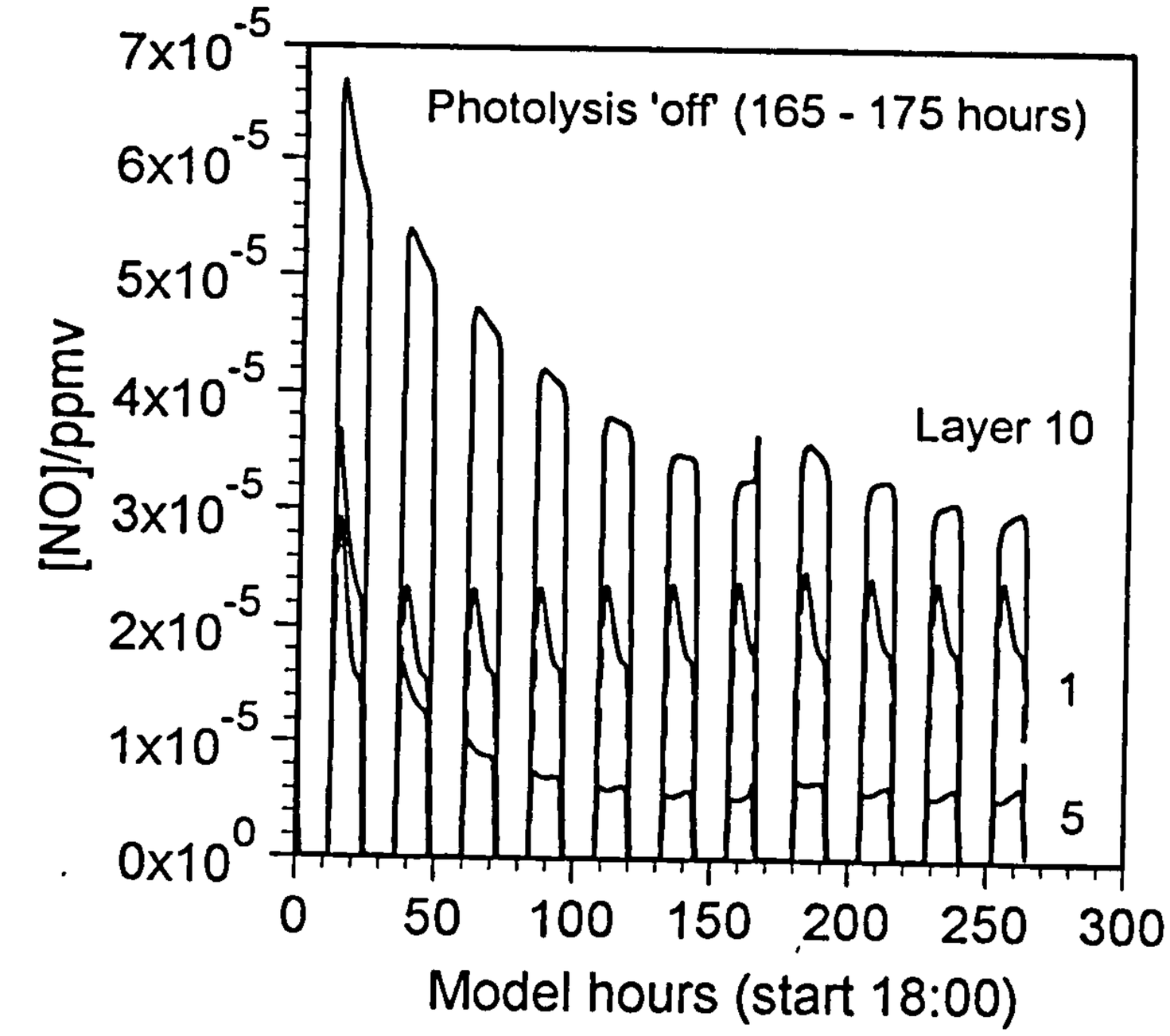

c)

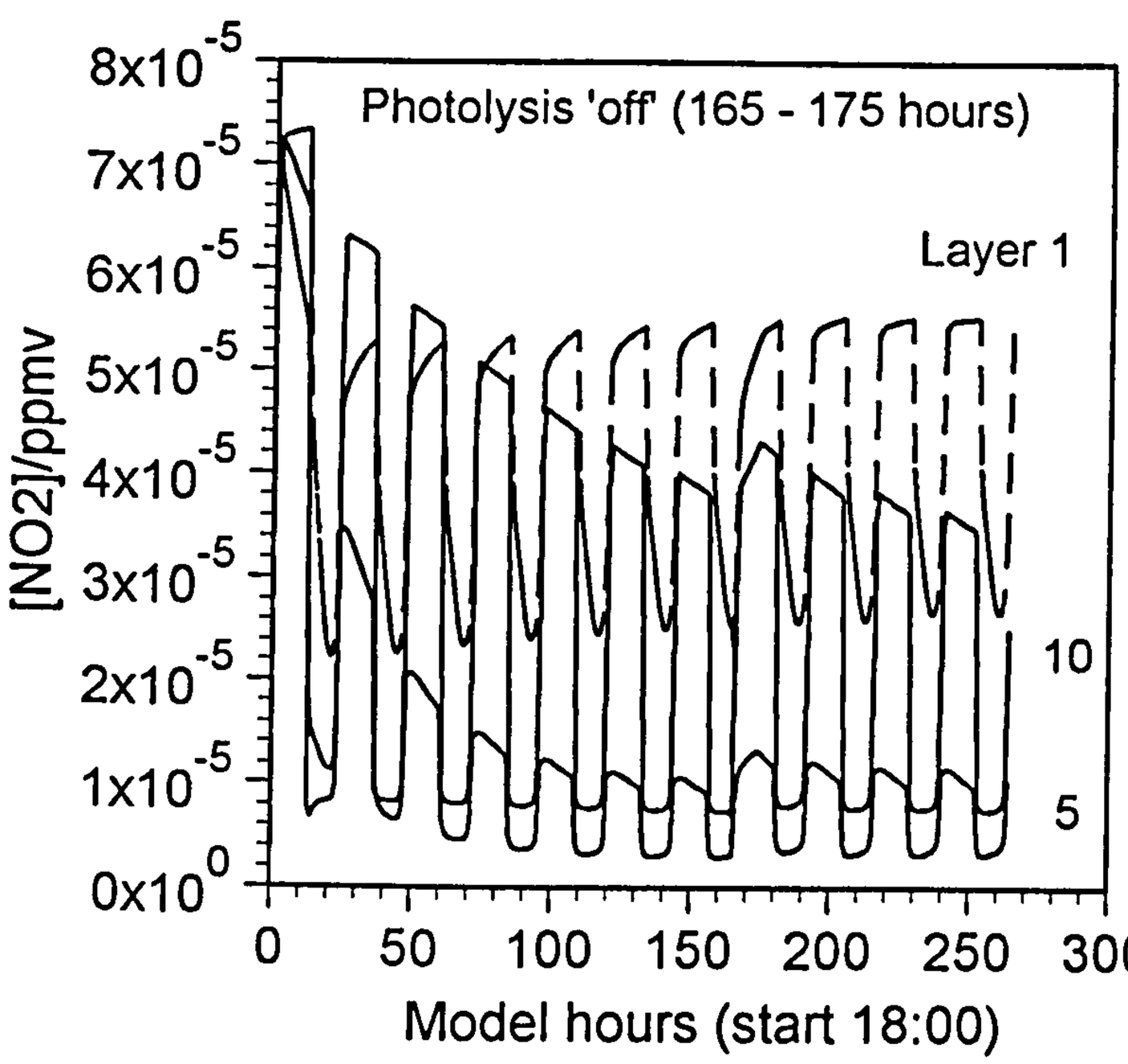

d)

Figure 5.14 c) and d) Effect of setting photolysis rates to zero during the 8 hour lightning input of NO_x; CLL base case conditions, 11 day simulation, c) NO and d) NO_2.

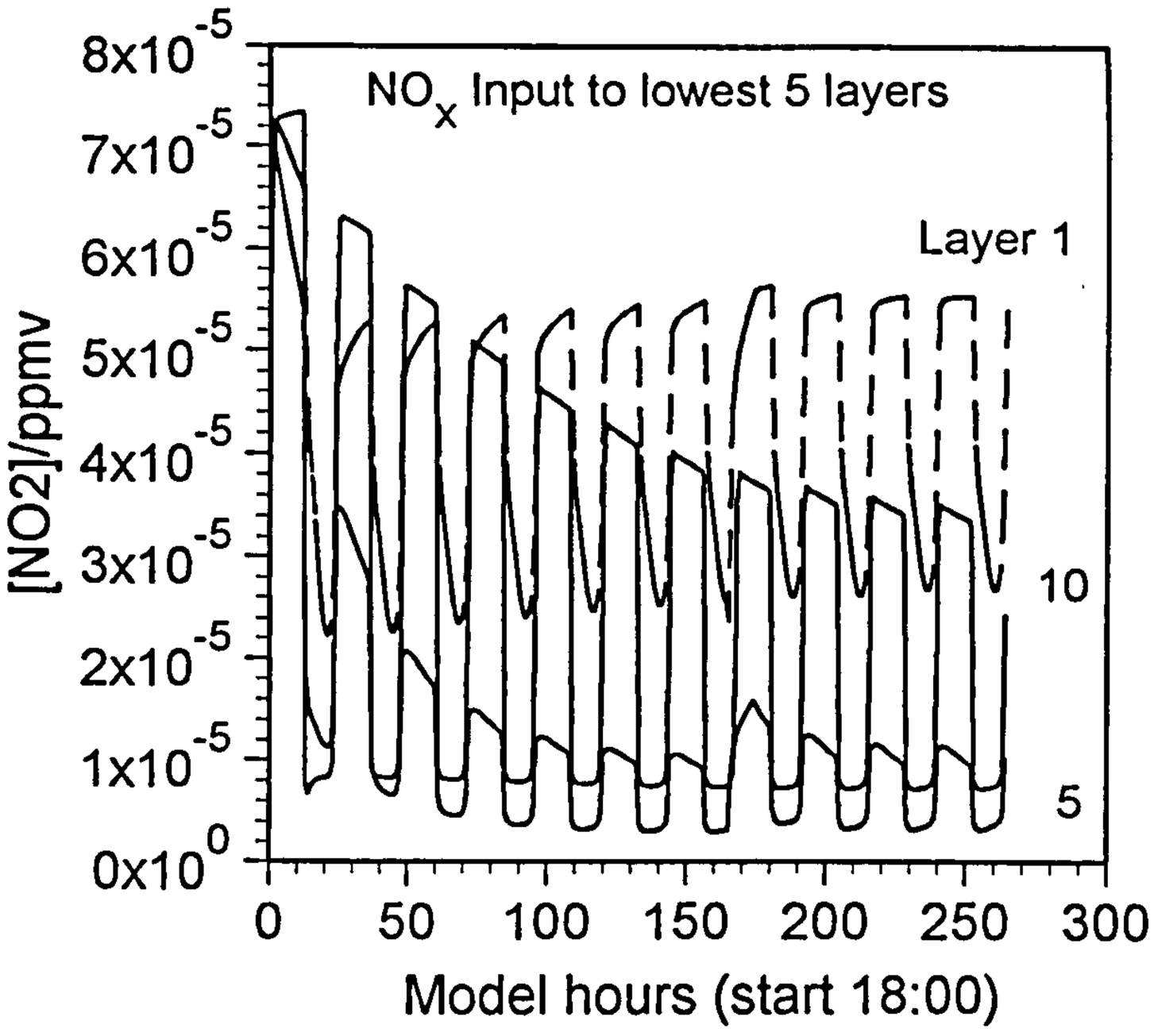

Figure 5.15 Effect of compressing lightning NO_x input into first 5 layers, with photolysis rates set to zero in these layers during 8 hour 'storm'; CLL base case, 11 day simulation.

5.6 Changing Model Input Parameters

5.6.1 Transfer Coefficients

The effect of changing the rates of vertical transport of species by doubling and halving both the eddy diffusion coefficient and the calculated transfer coefficients was investigated by looking at the concentration/time profiles of the tracer species and then NO_x, O_3 and OH. A plot of the tracer under CLL conditions (base case) is given in Figure 5.16, and shows that the tracer diffuses into all layers the concentration decreasing with layer. As there is no removal of the tracer the concentration builds up over time in all layers, but is greatest at the bottom due to the ground input. By the end of the 11 day simulations, the concentration in the upper layers is of the order 10^{-4} ppmv, compared to 10^{-2} ppmv in the bottom layers.

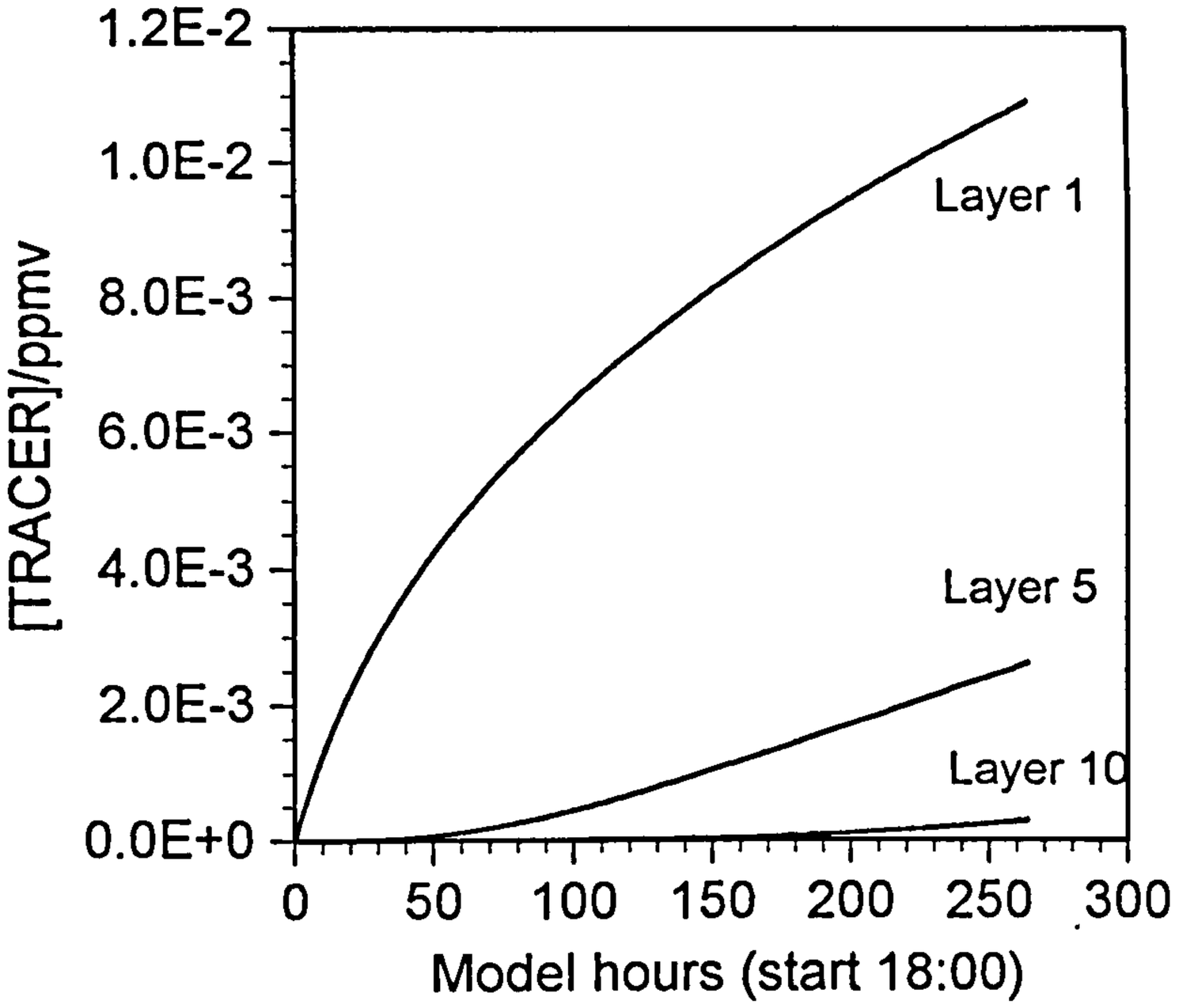

Figure 5.16 Concentration/time profile of tracer species for layers 1, 5 and 10; CLL scenario, 11 day simulation.

Increasing the eddy diffusion coefficient (K_z) by a factor of two leads to a greater amount of tracer being transported to the upper layers over an equivalent time period, and to a higher concentration in these layers at the end of the simulation. The opposite effect is observed when K_z is reduced by a factor of two, when the distribution of the tracer is greatest amongst the lower layers. Increasing and decreasing the transport coefficients by a factor of two has exactly the same result. Increasing the transport between the lowest four layers also distributes the tracer more equally between the layers. Figure 5.17 shows the distribution of the tracer for all layers at the end of the simulations. The results obtained here would be expected due to the unreactive nature of the tracer.

For more reactive species the effects of altering the transport may be expected to be less straightforward, as the transfer rate is dependent not only upon the eddy diffusion coefficient, but also on the concentration gradients between the layers and thus the reactivity of the species. For some of the species, such as NO_x, inputs are occurring at both the bottom and the top layers, therefore the concentrations in the middle layers are comparatively smaller. As explained in Section 5.2., the transfer

coefficients are calculated using three equations, one for the lowest layer, one for the uppermost layer and the other for the middle layers. Altering K_z may not change the transfer rates by a constant factor in each layer whereas directly changing the actual values of the transfer rates will and therefore different effects might be expected for each of the analyses.

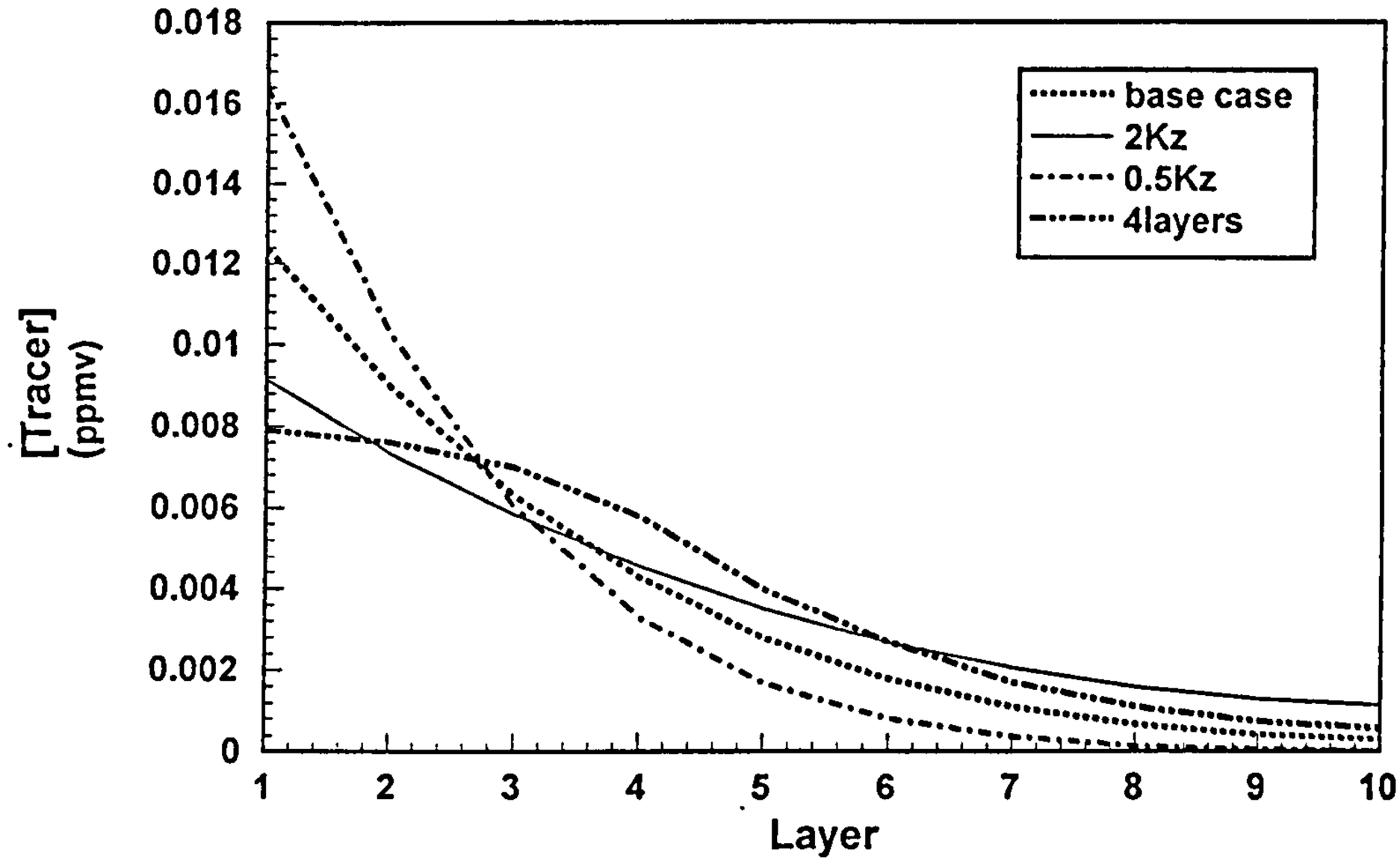

Figure 5.17 Distribution of tracer after 11 day CLL simulation over all layers at different vertical transfer rates. K_z = eddy diffusion coefficient; 4layers = increased transfer rates between bottom 4 layers.

This is examined by looking at the results for NO, NO_2, O_3, and OH. In each case the concentrations of layers 1, 5, and 10 were examined with time and the percentage changes relative to the base case of altering K_z and the transfer coefficients are given in Table 5.7. It is found that, in fact, the effects of changing K_z and the transfer coefficients are identical, but vary from species to species and by layer. The former indicates that K_z is the most important factor in determining the transfer rates, therefore must be calculated carefully.

Table 5.7 Effects of increasing and decreasing K_z and transfer coefficients by a factor of two

Species	Layer[a]	× 2[b]	÷ 2[c]	Species	Layer	× 2	÷ 2
NO	1- peak	+9%	-15%	NO_2	1- peak	+8%	-14%
	- min	-1%	-4%		- min	+9%	-9%
	5- peak	-10%	+18%		5- peak	-11%	+20%
	- min	-12%	+25%		- min	-9%	+26%
	10-peak	+12%	-16%		10-peak	+14%	-17%
	-min	-11%	+13%		-min	+27%	-15%
OH	1- peak	+1%	-1%	O_3	1	-2%	+3%
	- min	-1%	+3%				
	5- peak	-4%	+7%		5	-2%	+14%
	- min	-1%	+33%				
	10-peak	+6%	-3%		10	-2%	-13%
	-min	+11%	-7%				

[a] - peak and minimum concentrations taken after 7 days; NO - 148 and 158 model hours, NO_2 - 155 and 168 model hours, OH - 155 and 162 model hours, and O_3 at 168 model hours

[b] - δ[species] compared to CLL base case (no lightning) at times given in Note (a) after doubling K_z or transfer coefficients

[c] - δ[species] compared to CLL base case at times given in Note (a) after halving K_z or transfer coefficients

In all cases the effect of increasing the transfer rates is opposite to that caused by their decrease. This is to be expected. However, the effects upon each layer are quite different. In the case of NO and NO_2 the increase in transfer leads to approximately the same changes in concentration, with layers 1 and 10 decreasing, and layer 5 increasing relative to the base case. This is due to the faster transport of NO_x from

the upper and lower layers, where it is input, to the middle layers. Conversely, reducing the rate of transfer enhances the concentrations in the upper and lower layers and reduces that in layer 5.

The same is observed to a lesser degree for OH. As OH has no initial concentration and its concentration is determined by the reactions of other species, it would not be expected to be altered significantly in any of the layers. In the case of ozone, increasing the transfer rates leads to a decrease in the upper layers and an increase in the lower layers. This is explained by the fact that O_3 is only input from the stratosphere, and therefore will be more quickly transported downwards.

The overall effect of changing the rates of transfer by a factor of two is relatively small, averaging 10% changes in concentration in each layer. However, in any model of the atmosphere it is important to use input values which are as exact as possible in order to eliminate sources of error. For the purposes of this model it has been demonstrated that the value of the eddy diffusion coefficient is a major factor in the determination of the transfer coefficients, and thus should be determined with as much accuracy as possible for the region of interest.

5.6.2 Removing Stratospheric Incursion

The effects of stratospheric incursion of NO_x and ozone upon both the lightning event and the overall simulation were examined by removing the incursion rates individually from the scheme. This was intended to show the importance of stratospheric incursion upon the overall chemistry, especially in the upper layers. In the base case the input of NO is set at 4×10^2 molecules cm^{-3} s^{-1}, of NO_2 at double this, and of O_3, at 5×10^4 molecules cm^{-3} s^{-1}. All simulations were run with lightning input, although it was found to be unaffected by the changes in incursion rate, and is therefore not discussed further. The results of the study for NO, NO_2, OH, and O_3 are given in Figures 5.18(a) - (h).

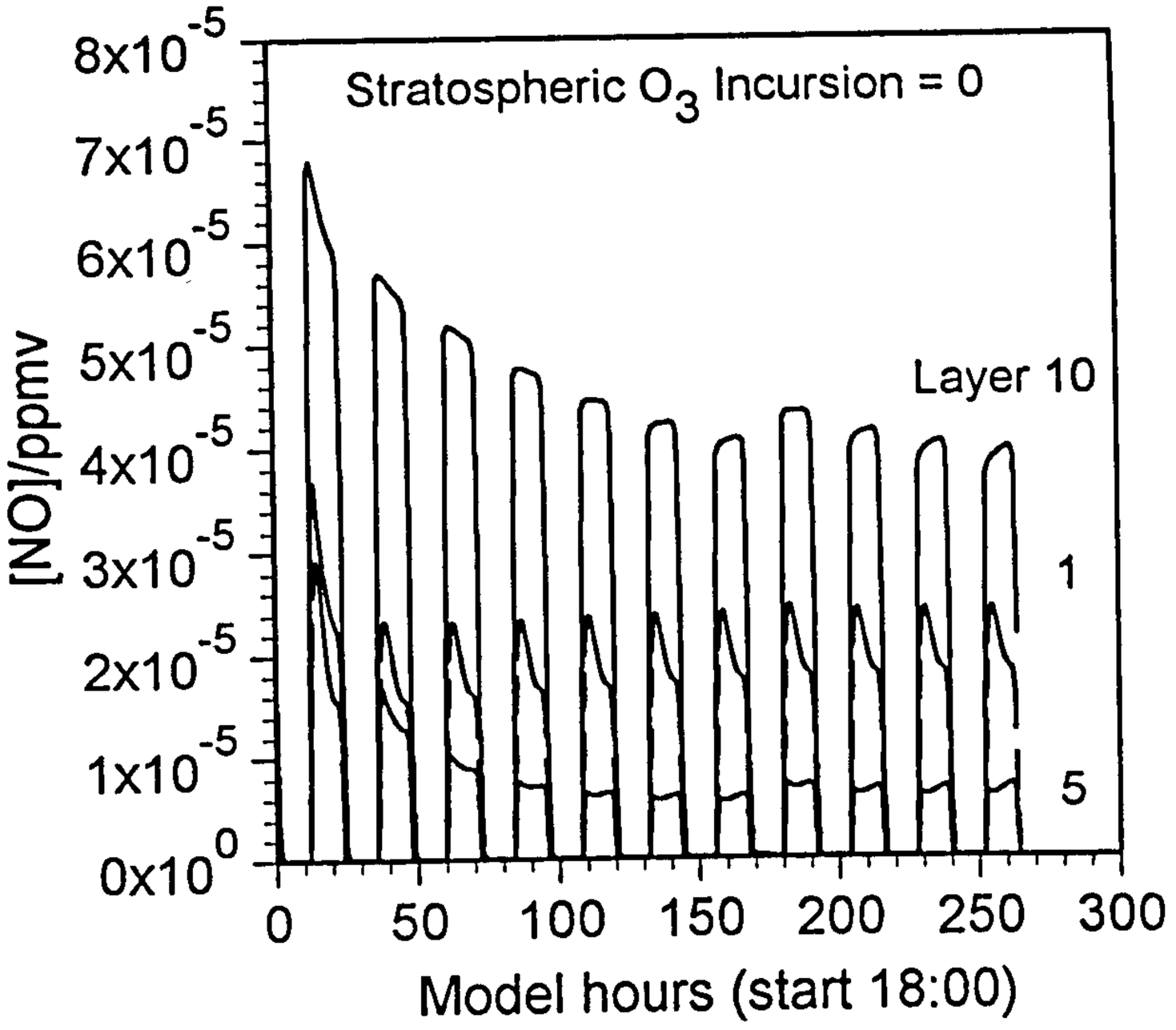

a)

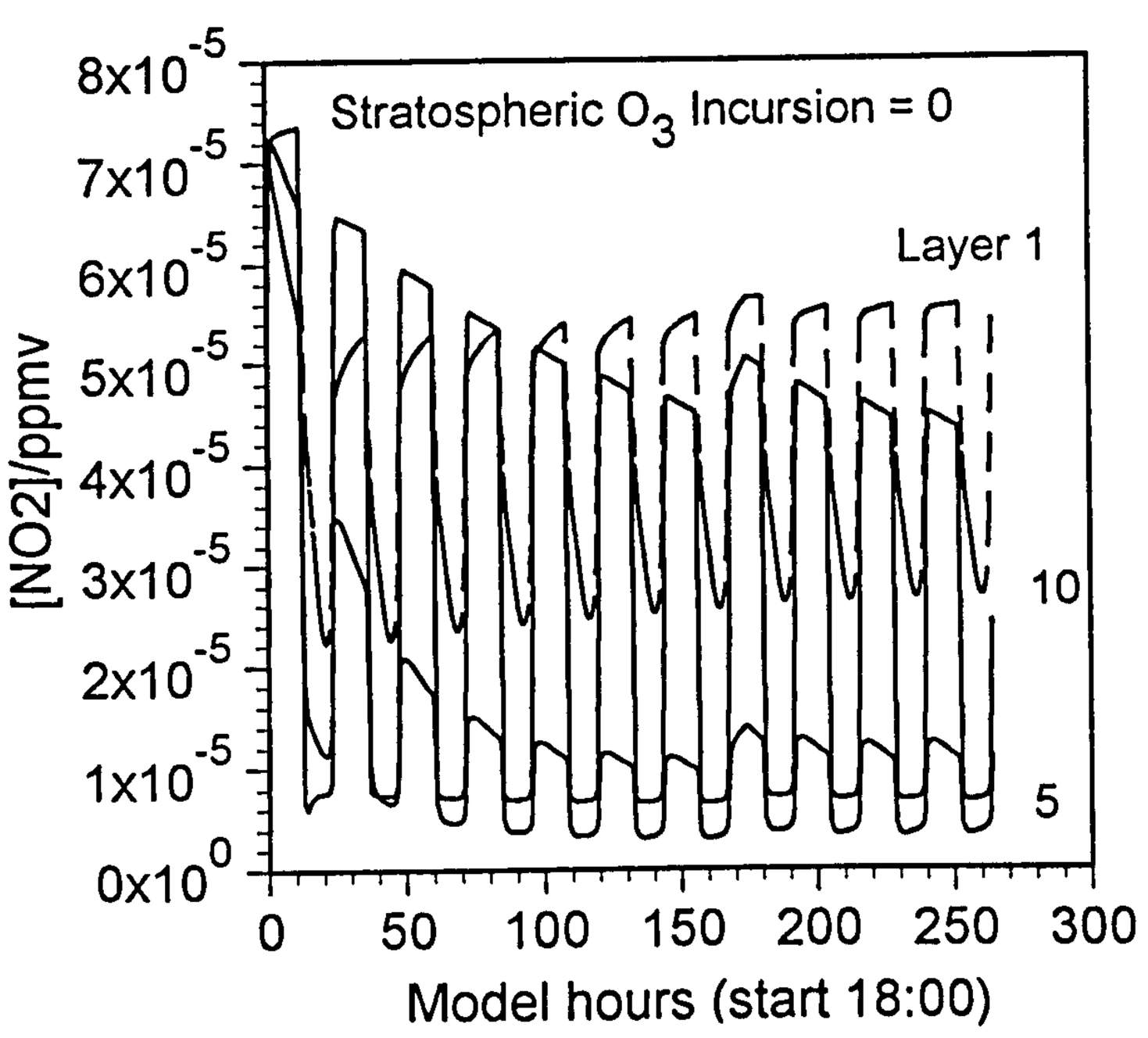

b)

Figure 5.18 a) and b) The effect upon a) NO and b) NO_2 of removing the stratospheric incursion of O_3. CLL conditions, lightning NO_x input included

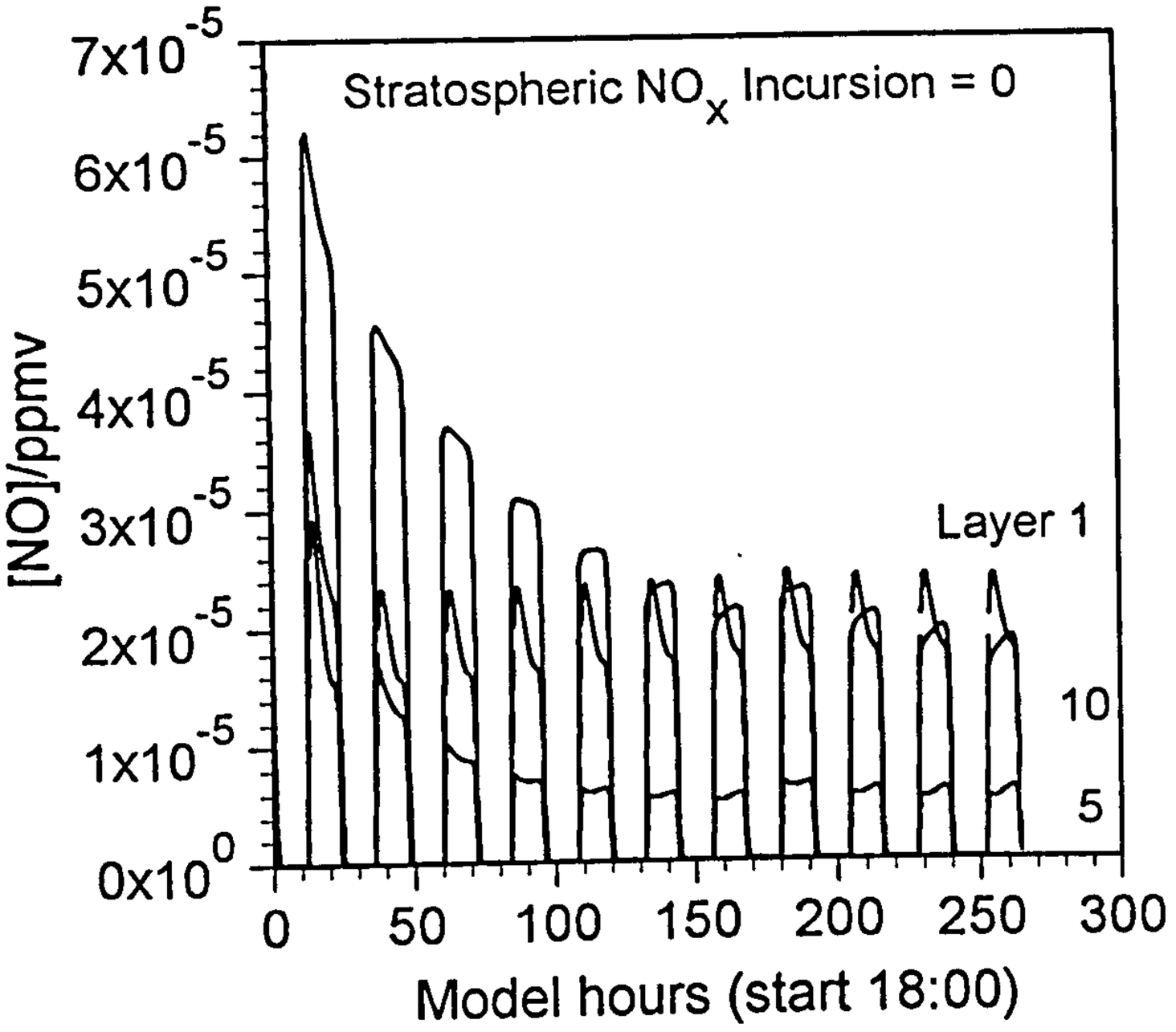

c)

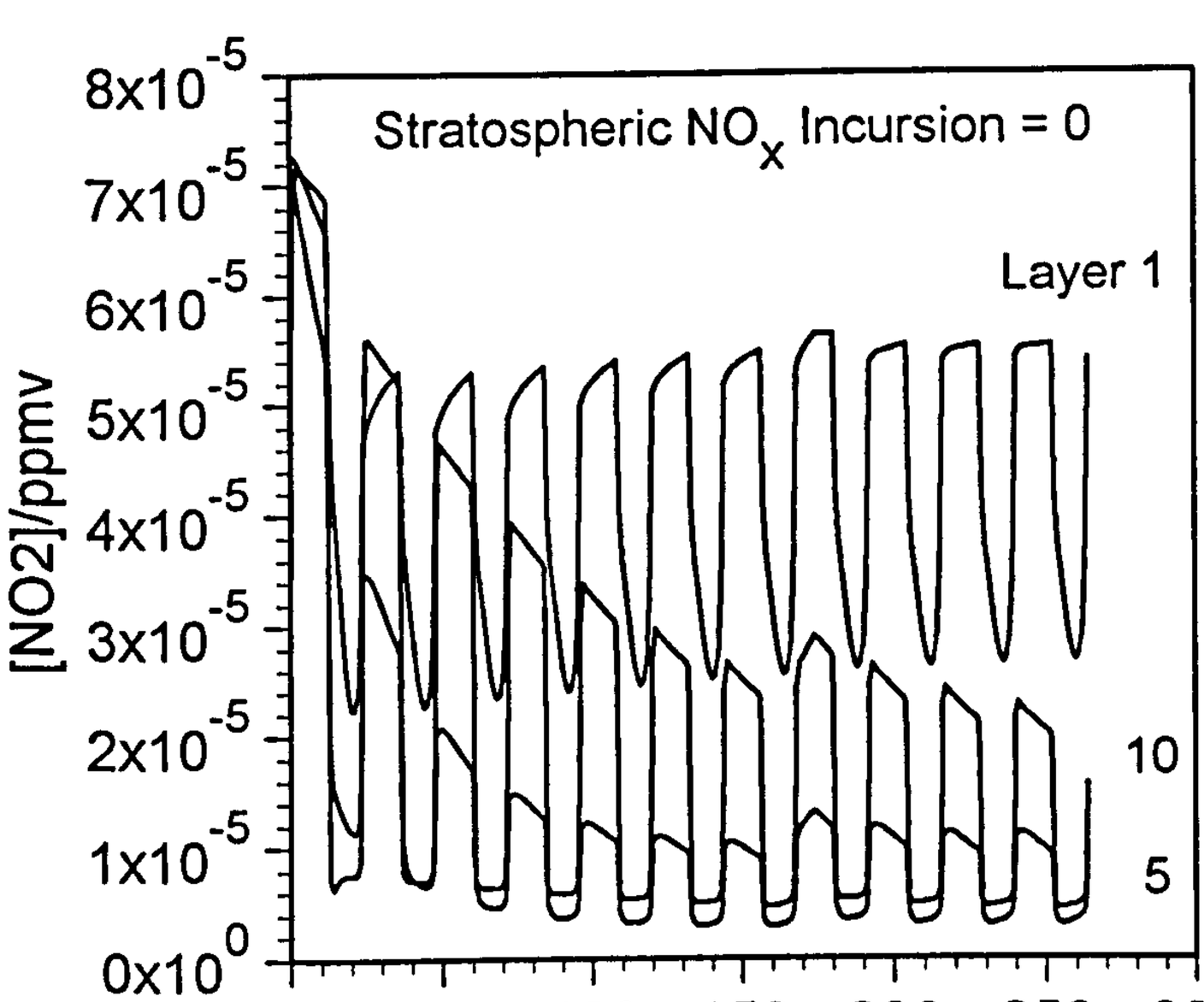

d)

Figure 5.18 c) and d) The effect upon c) NO and d) NO_2 of removing the stratospheric incursion of NO_x. CLL conditions, lightning NO_x input included.

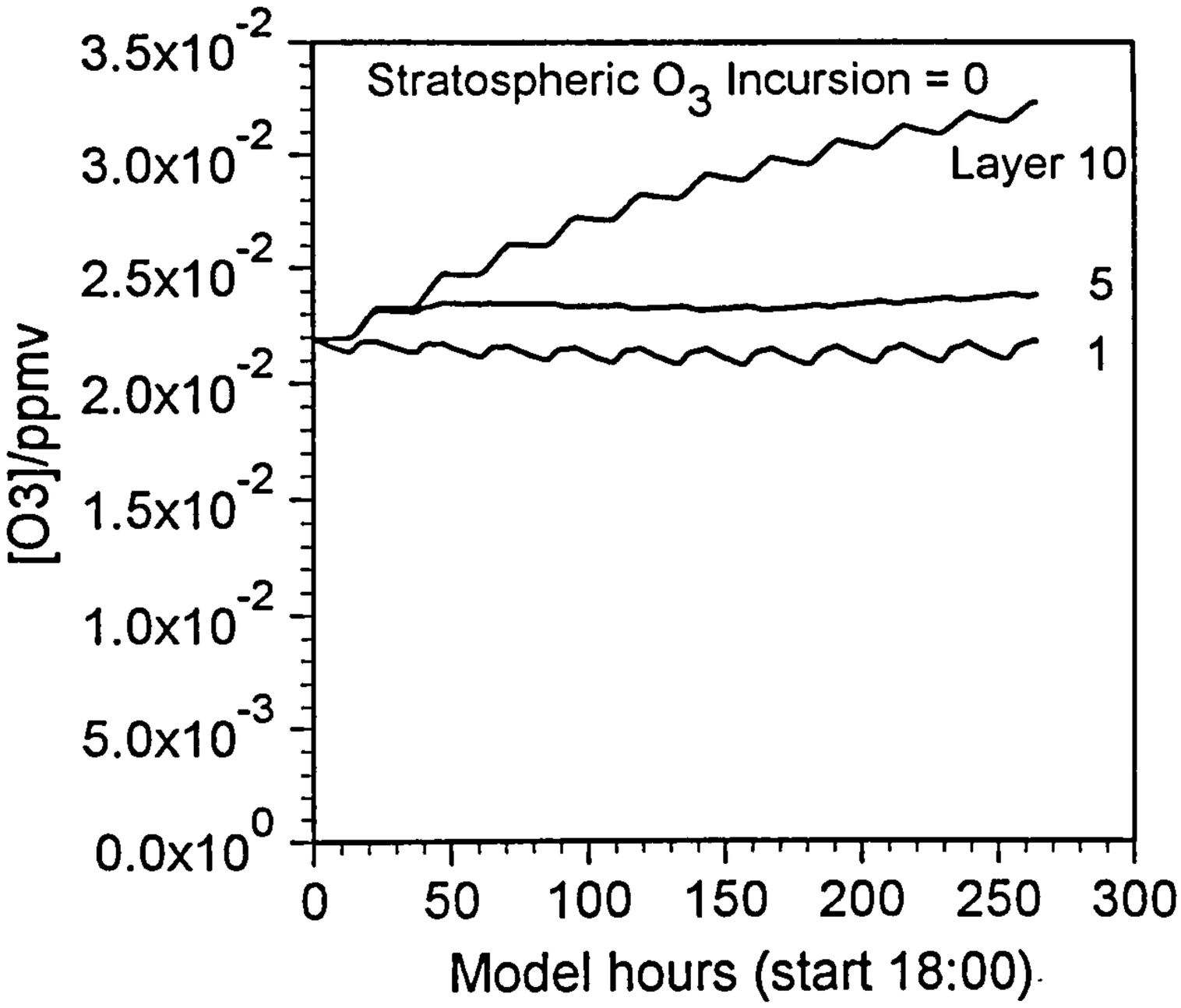

e)

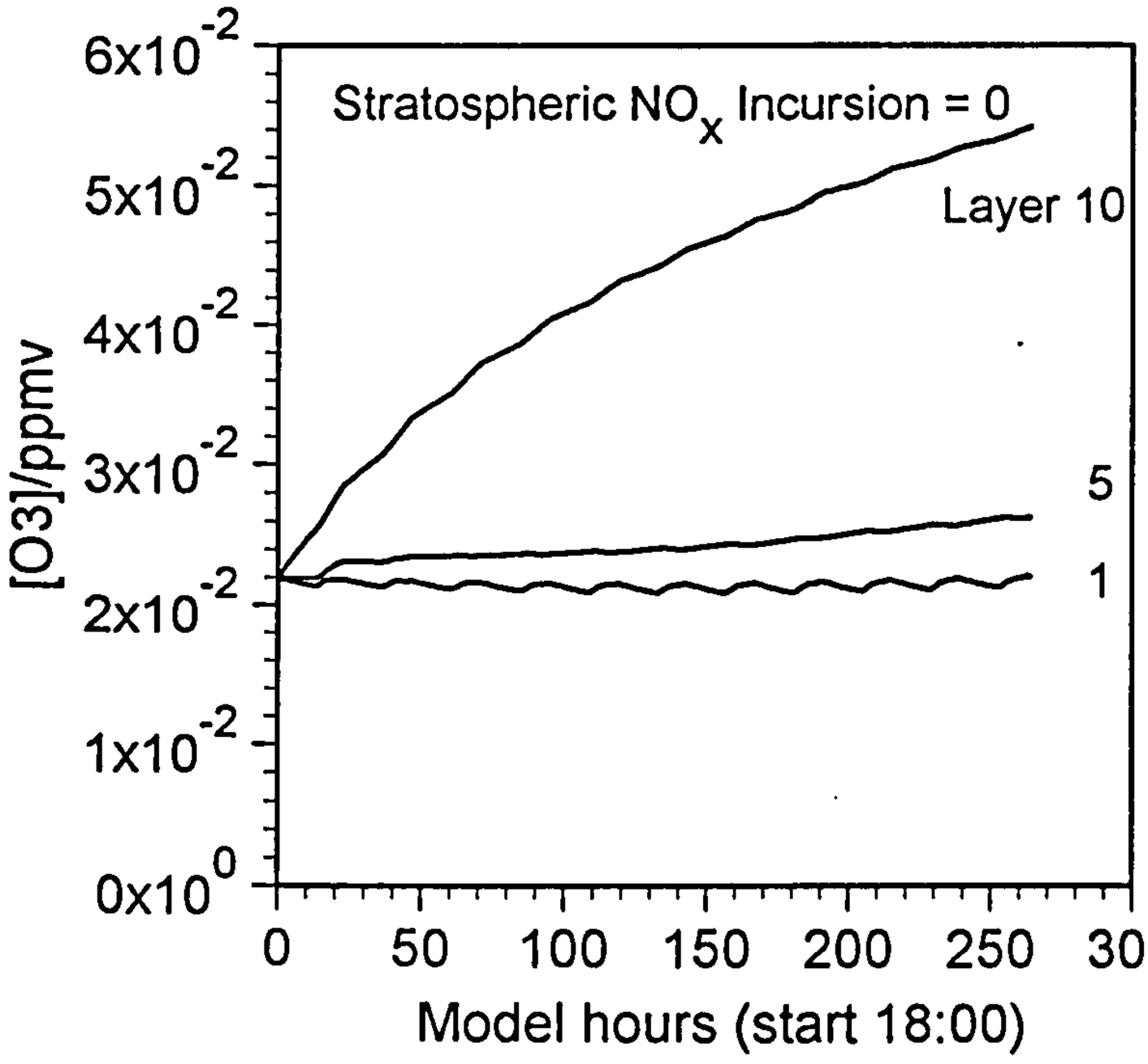

f)

Figure 5.18 e) and f) The effect upon ozone of removing e) stratospheric ozone and f) stratospheric NO_x incursion. CLL conditions, lightning NO_x input included.

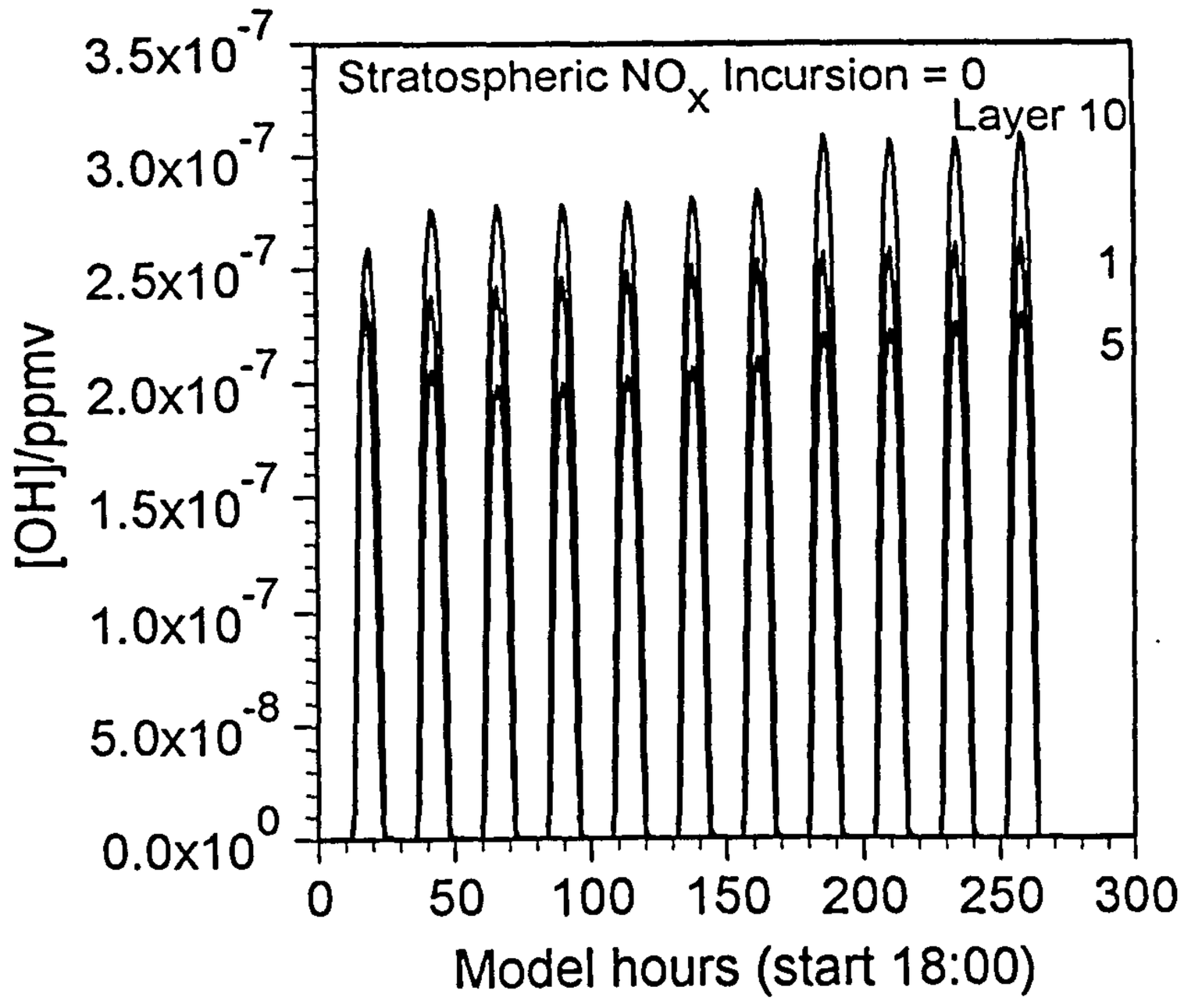

f)

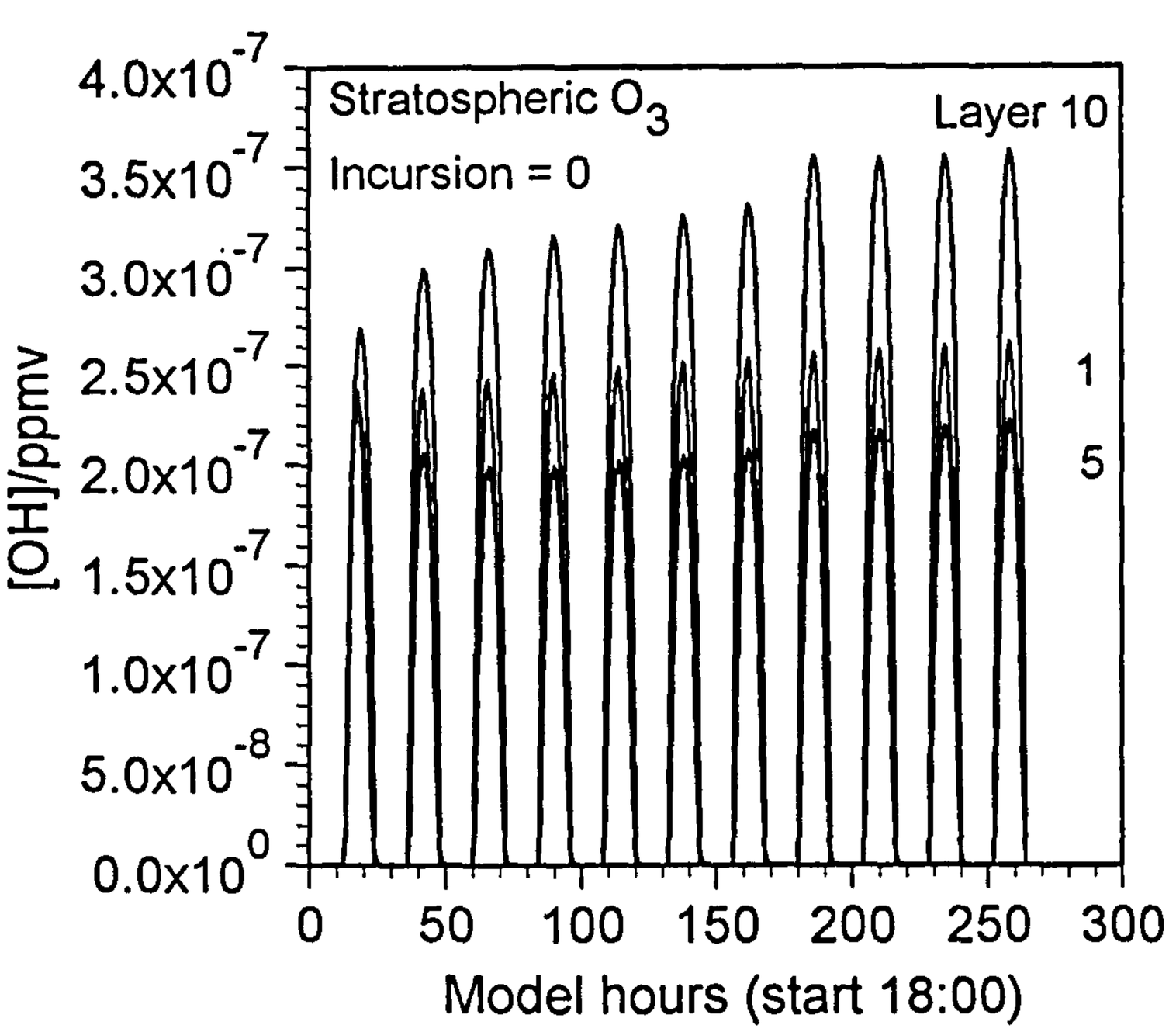

h)

Figure 5.18 g) and h) The effect upon OH of removing g) stratospheric NO_x and h) stratospheric O_3 incursion. CLL conditions, lightning NO_x input included.

5.6.2.i) Removal of O_3 incursion

Removal of O_3 incursion led to increases in the background concentrations of NO and NO_2 relative to the CLL base case. The concentrations of the lowest layers remained the same, and the increases observed were greater at higher altitudes, reaching up to 30% for NO and 20% for NO_2 relative to the base case. The minimum concentration values for NO_2 in the upper layers are 10% lower than the base case. The overall concentrations of OH in the upper layers only are smaller than in the base case, by 5% at peak values, and by up to 50% at the minima. The increase in $[NO_x]$ suggests that the presence of ozone leads to the removal of NO_x from the troposphere, and this is shown in reactions (1) and (4) (Appendix A). The reduction of [OH] in the upper layers is a result of the reduced photolysis of stratospherically incurred ozone as there is no change in [OH] in the lower layers.

5.6.2.ii) Removal of NO_x incursion

The effect of removing stratospheric incursion of NO_x is to reduce the concentrations of all three species, by up to 40% in the upper layers for NO and NO_2 and up to 20% for OH. The lowering of the NO and NO_2 concentrations as a result of removing NO_x incursion is obvious, but the fact that [OH] is reduced by a greater amount than when ozone incursion is removed indicates that the constant input of NO_x from the stratosphere leads to the production of OH in the upper layers. This corresponds to the findings of Section 5.4.1 for the lower troposphere, and is mainly due to the presence of VOCs in the base case at higher altitudes.

5.6.2.iii) The effect upon other species

The effect upon ozone was also investigated. In the base case the concentration of ozone increases in the upper layers over the course of the simulation, rising by a factor of 2.5 in layer 10 (22 ppbv to 56 ppbv). This is due to the incursion. However, removal of ozone incursion does not lead to constant concentration of ozone in all layers, with layer 10 rising from 22 ppbv to 32 ppbv at the end of the simulation.

Therefore the background of ozone must be affected by other species. If NO_x incursion is removed, the concentration of ozone over the course of the simulation rises by 4% less than in the base case. The incursion rate of NO_x is 10 times lower than that of ozone, and produces a 10 times lower decrease in the ozone, therefore implying that the presence of NO_x is as important as that of ozone in the determination of the background concentration. However, this is a direct result of the presence of VOCs, as discussed earlier, as in an NO_x-rich environment the production of O_3 is enhanced through the reaction of RO_2 with NO (reaction scheme 51), and removal of the NO_x will therefore lead to less ozone.

The other species analysed in this context were HNO_2, HNO_3, NO_3, and N_2O_5. The concentrations of all species in the upper layers were reduced by the removal of NO_x incursion; HNO_2 and NO_3 by up to 50% towards the end of the simulation, and HNO_3 and N_2O_5 by up to 10%. These differences are to be expected, HNO_3 having a greater background concentration, and therefore being less affected, and the other three having similar concentrations, but with N_2O_5 being a secondary product of the reaction of NO_2 and NO_3.

Therefore the incursion of NO_x and O_3 is quite significant in determining the background concentrations of the species considered, although in the case of OH and ozone, the reduction in concentrations relative to the base case as a result of lower NO_x is also related to the VOC concentration. This demonstrates the close interrelationship between the chemistry of organic and inorganic species, which was discussed in Section 5.4.2.

To examine this further, the background concentrations of the reactive VOC's, C_2H_6, C_2H_4, C_2H_2 and C_3H_8 were removed from the top 9 layers, and confined to layer 1. This had the effect of increasing the concentrations of NO and NO_2 by up to 25% in mid-layers, around 10% in the upper layers and around 2% in the lowest layers. Concentrations of OH are also enhanced, by up to 10% in the middle layers. As the reaction with OH is the most likely fate of the hydrocarbons, their removal will lead to an enhancement of [OH]. There will also be a dramatically reduced number of

RO_2 radicals available for reaction with NO, thus the concentration of the latter will also rise. This will lead to production of NO_2.

The increase of 10% observed in the OH concentration is quite significant when compared to the decreases of ~8% observed when increasing the methane background (Section 5.4.2). Although this applies to the mid-layers, where the concentrations are lower and therefore more susceptible to perturbations, the fact that OH is affected demonstrates the extent of reactivity of the higher hydrocarbons, and illustrates the importance of using accurate background concentrations within modelling studies.

Chapter Six

Conclusions and Future Work

6.1 Experimental Studies of Nitrogen Oxides

6.1.1. NO_x

This study found that NO was formed by the action of a small scale electrical discharge through air, and that the results agreed with similar studies by Harrison (1991). From this and the work of Stark *et al* (1995) it was suggested that NO was formed by a mechanism resulting from the thermal excitation of atoms and molecules in the heated channel of the discharge. The production of NO was dependent upon the pressure of the air in the reaction cell, which ranged from 300 - 1000 mbar, and upon the spark gap, which was set at distances of between 4 and 15 mm. However, on an experimental scale, this was believed to be due to losses of energy to the electrodes, which it was not possible to measure and which would not occur on an atmospheric scale in a lightning flash.

The results were used to predict a value for the NO formed per unit energy input to the spark, which could be used along with the estimated global energy dissipation by lightning to calculate a global production rate of NO by lightning. However, the experimental losses mentioned led to an underestimate of this NO J^{-1} value, and therefore it was necessary to assume the extent of energy loss in the system. If up to 90% of the energy was lost to the electrodes, this led to a suggested value of $9 \pm 2 \times 10^{16}$ NO J^{-1} by Stark *et al*, based upon the studies by Harrison, and upon other studies carried out at longer spark gaps.

However, the present work emphasises the many uncertainties which exist in the estimation of a global production rate of NO_x from lightning. Although the study of

NO_2 formation was not carried out in this work, previous studies are in disagreement as to whether NO_2 is formed in significant quantities by the discharge, and also as to the mechanism of its formation. If it is formed by the reaction of NO with O_3, does the NO react with ozone formed by the discharge, or with ozone already present in the air? And are the mechanisms which have been elucidated under experimental conditions similar to those which would occur on an atmospheric scale?

Clearly further studies are needed to describe fully the conditions occurring in a lightning flash, and to simulate these conditions more accurately in the laboratory. Studies using longer spark gaps in large reaction cells will allow the mixing process to be examined. It will be useful to investigate the effects of pressure and also temperature, in an almost loss-free system, to understand whether NO production is different at increasing altitudes.

6.1.2 N_2O

Similar studies were carried out to investigate the formation of N_2O from electrical discharges. The concentration of N_2O in a small reaction cell increased by up to a factor of three as a result of a spark, and it was dependent upon pressure and spark gap. However, the behaviour of N_2O was different to that of NO. At high spark gaps and pressures, the production of N_2O was comparatively much greater than that at lower values. Under these conditions it also appeared that N_2O was formed prior to the actual spark, by some pre-discharge mechanism, and then destroyed by the action of the spark.

It was suggested that N_2O was formed by the reaction of $N_2(^1\Sigma)$ (activated by collisions with pre-discharge electrons) with $O(^3P)$, also formed in the pre-discharge corona. It could then be destroyed to some extent by the photolysis occurring during the spark, and also by reaction with $O(^1D)$, formed by photolysis of ozone or of N_2O itself. Therefore the mechanism of formation was not thermal, and it was not possible to estimate a value of the amount of N_2O formed per unit energy in the same way as for NO.

The results obtained in this work would suggest that the formation of N_2O by lightning is not significant on a global scale. However, it is important to understand the processes occurring within a lightning flash, both chemical and physical, in order that accurate modelling studies can be performed. Therefore it would be useful to investigate the possibility of photolysis effects upon N_2O and other species, and also the mechanism of the corona discharge, which may be an important source of ozone.

Studies of N_2O at longer spark gaps, and in larger reaction vessels should be carried out in conjunction with those for NO_x, in order to gain a full understanding of the lightning phenomenon. This could be carried out using Tunable Diode Laser Spectroscopy, which will allow the analysis of NO, NO_2 and N_2O, and could be designed to be non-intrusive therefore reducing any errors due to scaling up and transfer of gases between reaction cell and detector. Study of the concentration changes of N_2O in the vicinity of the lightning flash, especially at higher altitudes, may also yield information about transport rates to the stratosphere in regions of high lightning activity.

6.2 Global Inventories

6.2.1 NO_x

An estimate of the global production rate of NO_x from lightning was made using the predicted values of NO J^{-1} (Stark *et al*, 1995), estimates of the energy of one flash, and the global flash frequency of lightning. A value of 16.9 ± 3.8 Tg (N) yr^{-1} for NO_x was calculated, based upon a flash energy of 5×10^9 J, and a global flash frequency of 100 s^{-1}, and assuming that 10% of NO_x was NO_2. This corresponds to around 20% of the total sources of NO_x currently identified.

However, there are a number of uncertainties associated with making such estimates. Firstly the experimental data, discussed above, needs to be obtained from experiments which are more representative of a lightning event. The lightning flash itself needs

to be more thoroughly characterised, both in terms of individual processes, such as energy dissipated, length of flash, altitude and type of flash (cloud-ground or intra-cloud), and in terms of frequency and distribution on a global scale. Monitoring of lightning by satellites will aid this.

Such studies will also allow regional distribution of NO_x to be more clearly examined. This work has investigated the global distribution of NO_x from lightning based upon satellite measurements of lightning carried out over a year. It appears that NO_x should be formed in greater abundance over the Northern Hemisphere, which agrees with atmospheric observations, and especially over the tropics. However, the flash frequencies suggested by the global distribution work are lower than those of other studies. It is also uncertain whether NO_x is formed by the first stroke of a flash, or by each stroke, and what the difference is in this respect between IC and CG flashes, whose distribution over the globe is dependent upon meteorological factors. Therefore there is much work to be done before a more accurate evaluation of lightning and its production of NO_x, both regionally and globally, can be obtained.

6.2.2 N_2O

The global significance of N_2O from lightning was predicted to be negligible, based upon the experimental results. However, the application of fertiliser to soils, which enhances the natural production of N_2O, is believed to be its major anthropogenic source, and is likely to continue increasing as the use of fertiliser increases. Therefore a study was carried out which related the use of fertiliser to population, and predicted the subsequent future emissions of N_2O up to the year 2025.

It was predicted that emissions would increase from 2.25 Tg (N) yr^{-1} in 1990 to 3.24 Tg (N) yr^{-1} in 2025. Up to 50% of this increase would be due to increases of fertiliser use in Asia. Despite the fact that tropical soils produce more N_2O, these regions are predicted to contribute only 14% to future increases in N_2O emissions, and then only if the rate of conversion of N_2O is double that of temperate soils. Therefore it is important to develop ways of improving fertiliser management

methods, whilst maintaining or even increasing yields, as the effects of N_2O emissions will be long term.

It is also essential to investigate the shortfall which exists in the global N_2O budget, which could be due to an overestimation of the sinks, or an underestimation of the sources. Further studies of soil emissions, both natural and anthropogenic, are needed, along with studies of other potential sources, such as oceans.

6.3 Modelling Studies

A 1D 10-layer photochemical computer model of the troposphere was employed to investigate the effects of long term and short term chemical and physical perturbations. The concentrations of species predicted by the model were in reasonable agreement with those obtained from atmospheric measurements. The studies were carried out on four chemically coherent regions, to investigate the effects of different chemical backgrounds.

6.3.1 Tropospheric Oxidants

Increasing the concentration of CH_4 by 30%, representing an increase of 1% yr^{-1} over a thirty year period, was found to decrease [OH] by up to 10%, with the greatest decrease occurring in the clean marine environment. The effect on ozone was to increase its concentration by up to 4%. The results agreed with those of Thompson *et al* (1990), who carried out a similar study using the same regions. The same methane increases with higher NO_x backgrounds lead to higher initial background concentrations of OH, but no change in the overall increase due to methane. However, there was a greater increase in ozone, due to the production of ozone from the oxidation of CH_4 in the presence of NO_x. A higher rate of increase of methane was found to produce a correspondingly higher decrease in OH and increase in ozone, and the effect of increasing the background concentration of CO was only found to have an effect on the upper layer OH.

Increases in NO_x ground emissions were found to lead to increasing OH levels in layer 1 up to a certain point, when the [OH] started to drop, due to reaction with NO_2. This was found to differ with each region, with the tropical region increasing OH levels at a lower NO_x emission rate, and the urban case requiring more NO_x to increase OH. This was ascribed to the photolysis rate in the tropics, which readily produces OH in NO_x-rich environments, and to the fact that in the urban region greater levels of CO could convert OH to HO_2, and therefore more NO_x was required to convert it back to OH. In the middle troposphere, OH levels also increased with rising NO_x emissions, but to a lesser extent. It is unlikely that enough OH would be formed for reaction with NO_2 to become important, but the work shows that in regions of high NO_x emissions the OH levels are affected up to the mid-troposphere.

The studies highlight the complex interactions which exist between the species and chemistry of the troposphere. Increases in CH_4 emissions may increase over the next decade due to the conversion of fuel from coal to natural gas, and therefore this may have consequences for the OH levels, and ability of the troposphere to remove pollutants. It is therefore necessary to ensure that leaks are minimised. Increases in NO_x emissions, whilst reduced in developed countries, may still be a problem in developing regions, where technology is not so good. Emissions of NO_x are especially important on a regional scale.

6.3.2 Lightning Studies

The input of NO_x over a period representing a lightning event at all altitudes led to the increase of the NO, NO_2 and OH concentrations for several days after the input. However, it is important to recognise the limitations of using the model for this purpose. The input of both NO and NO_2 directly is not strictly correct, as it is NO which is formed by the lightning, a proportion of which can react with ozone to form NO_2. Also the constant input of NO_x over an 8 hour period over a 10000 km^2 area is not truly representative, as in reality the storm is only a few kilometres wide, and can move, along with an air parcel, to cover such areas over a period of time. Therefore the use of a Lagrangian 1D model may also be informative, as it would

allow this air parcel to be modelled as it moves with the storm. It would also be of value to consider utilising a 2D model, which, by the use of a number of boxes in the horizontal plane, would allow the analysis of the chemistry of a region after the storm has passed through it. Although this would require more computational power, the chemistry could be simplified.

6.3.3 Physical Effects

Reducing the photolysis rates to zero during the storm event had very little effect upon the concentration/time profiles of the affected species, or upon the input of NO_x. When the photolysis rates were set to zero for the duration of the storm, the diurnality of the species was lost, but the input of NO_x and effect upon OH was retained. Therefore the photolysis rates have an insignificant effect upon the chemistry over such short time periods in this model.

Including wind dilution in the model gave artificially high concentrations of species, based upon their initial concentrations, and not upon the steady state obtained when all the radicals have been produced and the chemistry is properly initialised. This was due to the inadequate representation of wind dilution in the model, and needs to be developed in order that the conditions in the troposphere can be represented more accurately.

Investigation of the vertical transfer rates showed that it was important to use an accurate value of the eddy diffusion coefficient, but that the expressions used to calculate the transfer rates between each layer were equally dependent upon the concentrations of the species. The accuracy of this needs to be tested further.

Removing the stratospheric incursion of NO_x and ozone led to changes in the concentrations of all these species in the upper layers, again demonstrating the complex interactions between the species, and also the importance of stratospheric incursion as a source of these species. It is therefore important to ensure that the correct incursion rates are used, especially when studying the troposphere on a

regional basis.

The model has a number of limitations, but it is a useful tool for examining the chemistry in the troposphere. Future work would require enhancements to the model, such as improved representation of wind dilution, the removal of species from the top layer into the stratosphere. A separate scheme representing the boundary layer could also be incorporated, to investigate the effects of increasing emissions of pollutants and their transport to the free troposphere. It is important to remember that increasing the complexity of the model requires a greater amount of computational power, which may be undesirable. Therefore it is perhaps more important to get the features of the current model correct, thus reducing the uncertainties, than to add extra features which will only enhance the uncertainties in the results.

Appendix A

Reaction Scheme for 10 Layer Model

Many of the rate coefficients used in the model are dependent upon pressure, temperature or, for photolysis, upon the solar photon flux, all of which are variable with altitude, and can depend upon the inputs to the model. The expressions used by the model to account for this are complicated and are detailed in Fletcher (1989). Given below is a listing of the reactions included in the scheme, alongside the rate coefficients at 284.95K, assuming a third body (M) concentration of 2.43×10^{19} molecule cm^{-3}. All rate coefficients are quoted in cm^3 molecule^{-1} s^{-1} unless otherwise shown. An alteration has been made to the rate coefficient for the reaction of CH_4 + OH, with the value obtained by Vaghjiani and Ravishankara (1991) being used. All other rate coefficients are the same as in the original model.

No.	Reaction	Rate Coefficient [a]	Reference[#]
	<u>H/N/O Chemistry</u>		
1	$NO + O_3 \rightarrow NO_2 + O_2$	1.5×10^{-14}	A & L^T
2	$NO + NO + O_2 \rightarrow NO_2 + NO_2$	1.0×10^{-19} ∓	A & L^T
3	$NO_2 + h\upsilon + O_2 \rightarrow NO + O_3$	9.8×10^{-3} s^{-1}	PHOT
4	$NO_2 + O_3 \rightarrow NO_3 + O_2$	2.2×10^{-17}	A & L^T
5	$NO_3 + h\upsilon + O_2 \rightarrow NO_2 + O_3$	1.1×10^{-1} s^{-1}	PHOT
6	$NO_3 + h\upsilon \rightarrow NO + O_2$	4.3×10^{-2} s^{-1}	PHOT
7	$NO + NO_3 \rightarrow NO_2 + NO_2$	1.9×10^{-11}	A & L^T
8	$NO_2 + NO_3 \rightarrow NO + NO_2 + O_2$	3.3×10^{-16}	A & L^T
9	$NO_2 + NO_3 + M \rightarrow N_2O_5 + M$	1.2×10^{-12}	A & L^{PT}
10	$N_2O_5 + M \rightarrow NO_2 + NO_3 + M$	8.9×10^{-3} s^{-1}	M & T^{PT}
11	$N_2O_5 + H_2O \rightarrow HNO_3 + HNO_3$	1.3×10^{-20}	A & L
12	$O_3 + h\upsilon \rightarrow O(^1D) + O_2$	5.6×10^{-5}	PHOT
13	$O_3 + OH \rightarrow HO_2 + O_2$	5.9×10^{-14}	A & L^T
14	$HO_2 + HO_2 + M \rightarrow H_2O_2 + O_2 + M$	5.4×10^{-12}	A & L^{PT}
15	$OH + H_2O_2 \rightarrow HO_2 + H_2O$	1.6×10^{-12}	A & L^T

16	$O_3 + HO_2 \rightarrow OH + O_2 + O_2$	1.8×10^{-15}	A & L^T
17	$OH + HO_2 \rightarrow H_2O + O_2$	1.1×10^{-10}	B *et al*
18	$H_2O_2 + h\upsilon \rightarrow OH + OH$	1.1×10^{-5}	PHOT
19	$NO + OH + M \rightarrow HNO_2 + M$	7.3×10^{-12}	A & L^{PT}
20	$NO_2 + OH + M \rightarrow HNO_3 + M$	1.2×10^{-11}	A & L^{PT}
21	$NO + HO_2 \rightarrow OH + NO_2$	8.6×10^{-12}	A & L^T
22	$NO_2 + HO_2 + M \rightarrow HO_2NO_2 + M$	1.5×10^{-12}	A & L^{PT}
23	$HO_2NO_2 + M \rightarrow NO_2 + HO_2 + M$	1.7×10^{-2} s^{-1}	A & L^T
24	$HO_2NO_2 + h\upsilon \rightarrow NO_3 + OH$	9.8×10^{-5} s^{-1}	PHOT
25	$HNO_3 + h\upsilon \rightarrow NO_2 + OH$	8.4×10^{-7} s^{-1}	PHOT
26	$HNO_2 + h\upsilon \rightarrow NO + OH$	1.8×10^{-3} s^{-1}	PHOT
27	$HNO_3 + OH \rightarrow NO_3 + H_2O$	1.4×10^{-13}	A & L^T
28	$HNO_2 + OH \rightarrow NO_2 + H_2O$	6.6×10^{-12}	A & L
29	$NH_3 + OH \rightarrow NH_2 + H_2O$	1.4×10^{-13}	B *et al*^{T}
30	$NH_2 + NO \rightarrow H_2 + N_2O$	1.7×10^{-11}	B *et al*^{T}
31	$NH_2 + NO_2 \rightarrow H_2O + N_2O$	1.9×10^{-11}	B *et al*^{T}
32	$N_2O + h\upsilon \rightarrow NO + O(^1D)$	4.1×10^{-10} s^{-1}	PHOT
33	$OH + N_2O \rightarrow HO_2 + N_2$	3.8×10^{-17}	BZS
34	$O(^3P) + O_2 + M \rightarrow O_3 + M$	7.0×10^{8} s^{-1} ∓	A & L
35	$O(^1D) + H_2O \rightarrow OH + OH$	2.2×10^{-10}	A & L
36	$O(^1D) + N_2O \rightarrow NO + NO$	7.2×10^{-11}	B *et al*
37	$OH + H_2 + O_2 \rightarrow HO_2 + H_2O$	4.9×10^{-16}	B *et al*^{T}
	Hydrocarbon Chemistry		
38	$CO + OH + O_2 \rightarrow CO_2 + HO_2$	2.1×10^{-13}	B *et al*^{PT}
39	$CH_4 + OH + O_2 \rightarrow CH_3O_2 + H_2O$	6.3×10^{-15}	V & R^{PT}
40	$CH_3O_2 + NO + O_2$		
	$\rightarrow CH_3O + NO_2 + HCHO + HO_2$	7.9×10^{-12}	B *et al*^{T}
41	$CH_3O_2 + HO_2 \rightarrow CH_3OOH + O_2$	7.4×10^{-12}	B *et al*^{T}
42	$OH + CH_3OOH \rightarrow CH_3O_2 + H_2O$	5.0×10^{-12}	*
43	$OH + CH_3OOH \rightarrow OH + HCHO + H_2O$	5.0×10^{-12}	*
44	$C_2H_6 + OH + O_2 \rightarrow C_2H_5O_2 + H_2O$	2.3×10^{-13}	B *et al*^{T}
45	$C_2H_5O_2 + NO + O_2 \rightarrow HO_2 + CH_3CHO + NO_2$	7.9×10^{-12}	A & L^T
46	$C_2H_5O_2 + HO_2 \rightarrow C_2H_5OOH + O_2$	7.4×10^{-12}	*^{T}
47	$C_2H_5OOH + OH \rightarrow C_2H_5O_2 + H_2O$	5.0×10^{-12}	*

48	$C_2H_5OOH + OH \rightarrow OH + CH_3CHO + H_2O$	5.0×10^{-12}	*
49	$CH_3OOH + h\upsilon + O_2 \rightarrow OH + HO_2 + HCHO$	1.2×10^{-5} s^{-1}	PHOT
50	$C_2H_5OOH + h\upsilon + O_2 \rightarrow OH + HO_2 + CH_3CHO$	1.4×10^{-5} s^{-1}	PHOT
51	$C_3H_8 + OH + O_2 \rightarrow C_3H_7O_2 + H_2O$	9.7×10^{-13}	B *et al*[T]
52	$C_3H_7O_2 + NO + O_2 \rightarrow NO_2 + HO_2 + Me_2CO$	7.9×10^{-12}	A & L[T]
53	$C_3H_7O_2 + HO_2 \rightarrow PrOOH + O_2$	7.4×10^{-12}	*[T]
54	$PrOOH + OH \rightarrow C_3H_7O_2 + H_2O$	5.0×10^{-12}	*
55	$PrOOH + OH \rightarrow OH + Me_2CO + H_2O$	5.0×10^{-12}	*
56	$PrOOH + h\upsilon + O_2 \rightarrow OH + HO_2 + Me_2CO$	1.4×10^{-5} s^{-1}	PHOT
57	$HCHO + h\upsilon \rightarrow CO + H_2$	4.0×10^{-5} s^{-1}	PHOT
58	$HCHO + h\upsilon + 2O_2 \rightarrow HO_2 + HO_2 + CO$	3.2×10^{-5} s^{-1}	PHOT
59	$HCHO + OH + O_2 \rightarrow HO_2 + CO + H_2O$	1.0×10^{-11}	B *et al*
60	$HCHO + NO_3 + O_2 \rightarrow HNO_3 + HO_2 + CO$	6.3×10^{-16}	C1 *et al*
61	$CH_3CHO + h\upsilon + 2O_2 \rightarrow HO_2 + CO + CH_3O_2$	3.8×10^{-6} s^{-1}	PHOT
62	$CH_3CHO + OH + O_2 \rightarrow CH_3CO_3 + H_2O$	1.7×10^{-11}	B *et al*[T]
63	$CH_3CHO + NO_3 + O_2 \rightarrow HNO_3 + CH_3CO_3$	2.1×10^{-15}	C2 *et al*
64	$Me_2CO + h\upsilon + 2O_2 \rightarrow CH_3O_2 + CH_3CO_3$	1.8×10^{-6} s^{-1}	PHOT
65	$Me_2CO + OH + O_2 \rightarrow AcO_2 + H_2O$	2.3×10^{-13}	A & L[T]
66	$AcO_2 + NO + O_2 \rightarrow NO_2 + HO_2 + CH_3COCHO$	7.9×10^{-12}	A & L[T]
67	$CH_3COCHO + h\upsilon + 2O_2 \rightarrow HO_2 + CO + CH_3CO_3$	1.4×10^{-4} s^{-1}	PHOT
68	$CH_3COCHO + h\upsilon + 2O_2$ $\rightarrow HO_2 + CO + CO + CH_3O_2$	6.4×10^{-5} s^{-1}	PHOT
69	$AcO_2 + HO_2 \rightarrow OH + HO_2 + CH_3COCHO$	7.4×10^{-12}	*[T]
70	$CH_3COCHO + OH + O_2 \rightarrow CO + CH_3CO_3 + H_2O$	1.7×10^{-11}	A & L
71	$CH_3CO_3 + NO + O_2 \rightarrow CH_3O_2 + NO_2 + CO_2$	7.9×10^{-12}	A & L[T]
72	$CH_3CO_3 + NO_2 + M \rightarrow PAN + M$	4.7×10^{-12}	B & P
73	$PAN + M \rightarrow CH_3CO_3 + NO_2 + M$	4.5×10^{-5}	A & L[T]
74	$CH_3CO_3 + HO_2 \rightarrow CH_3CO_3H + O_2$	7.4×10^{-12}	*[T]
75	$CH_3CO_3H + h\upsilon \rightarrow CH_3O_2 + OH$	1.4×10^{-5} s^{-1}	PHOT
76	$CH_3CO_3H + OH \rightarrow CH_3CO_3 + OH$	5.0×10^{-12}	*
77	$CH_3O_2 + CH_3CO_3 + O_2$ $\rightarrow HO_2 + CH_3O_2 + HCHO + CO_2$	3.0×10^{-12}	*
78	$C_2H_5O_2 + CH_3CO_3 + O_2$ $\rightarrow HO_2 + CH_3O_2 + CH_3CHO + CO_2$	3.0×10^{-12}	*

79	$C_3H_7O_2 + CH_3CO_3 + O_2$		
	$\rightarrow HO_2 + CH_3O_2 + Me_2CO + CO_2$	3.0×10^{-12}	*
80	$CH_3CO_3 + AcO_2 + O_2$		
	$\rightarrow CH_3O_2 + HO_2 + MeCOCHO + CO_2$	3.0×10^{-12}	*
81	$CH_3CO_3 + CH_3CO_3 + O_2$		
	$\rightarrow CH_3O_2 + CH_3O_2 + 2CO_2$	3.0×10^{-12}	*
82	$C_2H_4 + OH + O_2 + M \rightarrow O_2EtOH + M$	8.6×10^{-12}	B *et al*[PT]
83	$O_2EtOH + NO + O_2$		
	$\rightarrow NO_2 + HO_2 + HCHO + HCHO$	7.9×10^{-12}	A & L[T]
84	$O_2EtOH + HO_2 \rightarrow OH + HO_2 + HCHO + HCHO$	7.4×10^{-12}	*[T]
85	$O_2EtOH + CH_3CO_3$		
	$\rightarrow CH_3O_2 + CO_2 + HO_2 + HCHO + HCHO$	3.0×10^{-12}	*
86	$C_2H_4 + O_3 \rightarrow HCHO$	1.2×10^{-18}	A & L[T]
87	$C_2H_4 + O_3 \rightarrow CO + CH_2OO$	4.7×10^{-19}	A & L[T]
88	$C_2H_4 + O_3 \rightarrow HO_2 + H_2$	1.4×10^{-19}	A & L[T]
89	$CH_3CHCH_2 + OH + O_2 + M \rightarrow PrO_2OH + M$	1.9×10^{-11}	B *et al*[PT]
90	$CH_3CHCH_2 + OH + O_2 + M \rightarrow PrOHO_2 + M$	1.0×10^{-11}	B *et al*[PT]
91	$PrO_2OH + NO + O_2$		
	$\rightarrow CH_3CHO + HO_2 + HCHO + NO_2$	7.9×10^{-12}	A & L[T]
92	$PrOHO_2 + NO + O_2$		
	$\rightarrow CH_3CHO + HO_2 + HCHO + NO_2$	7.9×10^{-12}	A & L[T]
93	$PrO_2OH + HO_2$		
	$\rightarrow OH + HO_2 + HCHO + CH_3CHO$	7.4×10^{-12}	*[T]
94	$PrOHO_2 + HO_2$		
	$\rightarrow OH + HO_2 + HCHO + CH_3CHO$	7.4×10^{-12}	*[T]
95	$CH_3CO_3 + PrO_2OH + O_2$		
	$\rightarrow CH_3O_2 + CH_3CHO + HO_2 + HCHO + CO_2$	3.0×10^{-12}	*
96	$CH_3CO_3 + PrOHO_2 + O_2$		
	$\rightarrow CH_3O_2 + CH_3CHO + HO_2 + HCHO + CO_2$	3.0×10^{-12}	*
97	$CH_3CHCH_2 + O_3 \rightarrow HCHO + CH_3CHO$	4.0×10^{-18}	A & L[T]
98	$CH_3CHCH_2 + O_3$		
	$\rightarrow HO_2 + CH_3O_2 + CH_2OO. + CH_3CHOO.$	1.6×10^{-18}	A & L[T]
99	$CH_3CHCH_2 + O_3 \rightarrow CO$	2.7×10^{-18}	A & L[T]
100	$CH_3CHCH_2 + O_3 \rightarrow OH$	7.7×10^{-19}	A & L[T]

101	$CH_2OO. + NO \rightarrow NO_2 + HCHO$	7.0×10^{-12}	A & L
102	$CH_2OO. + NO_2 \rightarrow NO_3 + HCHO$	7.0×10^{-13}	A & L
103	$CH_2OO. + H_2O \rightarrow HCOOH + H_2O$	4.0×10^{-18}	A & L
104	$CH_3CHOO + NO \rightarrow CH_3CHO + NO_2$	7.0×10^{-12}	A & L
105	$CH_3CHOO + NO_2 \rightarrow CH_3CHO + NO_3$	7.0×10^{-13}	A & L
106	$CH_3CHOO + H_2O \rightarrow CH_3COOH + H_2O$	4.0×10^{-18}	A & L
107	$C_2H_2 + OH + O_2 + M \rightarrow CHOCHO + OH + M$	6.1×10^{-13}	B *et al*[PT]
108	$CHOCHO + h\upsilon \rightarrow CO + HCHO$	1.1×10^{-5} s^{-1}	PHOT
109	$CHOCHO + h\upsilon \rightarrow CO + CO + H_2O$	7.2×10^{-5} s^{-1}	PHOT
110	$CHOCHO + OH + O_2 \rightarrow HO_2 + CO + CO + H_2O$	1.2×10^{-11}	A & L
	Chlorine Chemistry		
111	$CH_3Cl + OH + O_2 \rightarrow O_2CH_2Cl + H_2O$	3.7×10^{-14}	B *et al*[T]
112	$O_2CH_2Cl + NO + O_2 \rightarrow NO_2 + HO_2 + CO + HCl$	7.9×10^{-12}	A & L[T]
113	$O_2CH_2Cl + HO_2 \rightarrow OH + HO_2 + CO + HCl$	7.4×10^{-12}	*[T]
114	$O_2CH_2Cl + CH_3CO_3 + O_2$		
	$\rightarrow CH_3O_2 + HO_2 + CO + HCl + CO_2$	3.0×10^{-12}	*
115	$Cl + O_3 \rightarrow ClO + O_2$	1.1×10^{-11}	B *et al*[T]
116	$CH_4 + Cl + O_2 \rightarrow CH_3O_2 + HCl$	8.4×10^{-14}	B *et al*[T]
117	$C_2H_6 + Cl + O_2 \rightarrow CH_3CH_2O_2 + HCl$	5.6×10^{-11}	B *et al*[T]
118	$C_3H_8 + Cl + O_2 \rightarrow C_3H_7O_2 + HCl$	1.3×10^{-10}	A & A
119	$HCHO + Cl + O_2 \rightarrow HO_2 + CO + HCl$	7.3×10^{-11}	B *et al*[T]
120	$CH_3CHO + Cl + O_2 \rightarrow CH_3CO_3 + HCl$	7.3×10^{-11}	*[T]
121	$Me_2CO + Cl + O_2 \rightarrow AcO_2 + HCl$	5.6×10^{-11}	*[T]
122	$CH_3OOH + Cl \rightarrow OH + HCHO + HCl$	6.0×10^{-11}	*
123	$CH_3CH_2OOH + Cl \rightarrow OH + CH_3CHO + HCl$	4.0×10^{-11}	*
124	$PrOOH + Cl \rightarrow OH + Me_2CO + HCl$	2.0×10^{-11}	*
125	$ClO + NO_2 + M \rightarrow ClONO_2 + M$	2.4×10^{-12}	B *et al*[PT]
126	$ClONO_2 + h\upsilon \rightarrow NO_3 + Cl$	9.8×10^{-5} s^{-1}	PHOT
127	$ClO + HO_2 \rightarrow HOCl + O_2$	5.6×10^{-12}	B *et al*[T]
128	$ClO + NO \rightarrow NO_2 + Cl$	1.7×10^{-11}	B *et al*[T]
129	$ClONO_2 + OH \rightarrow NO_3 + HOCl$	3.8×10^{-13}	B *et al*[T]
130	$HOCl + h\upsilon \rightarrow OH + OH + Cl$	1.2×10^{-3} s^{-1}	PHOT
131	$HOCl + OH \rightarrow ClO + H_2O$	1.8×10^{-12}	B *et al*[T]
132	$HCl + OH \rightarrow Cl + H_2O$	6.3×10^{-13}	B *et al*[T]

133	$C_2H_4 + Cl + O_2 + M \rightarrow O_2CH_2CH_2Cl$	1.1×10^{-10}	$*^{PT}$
134	$CH_3CHCH_3 + Cl + M + O_2 \rightarrow O_2PrCl$	2.4×10^{-10}	$*^{T}$
135	$O_2EtCl + NO + O_2 \rightarrow NO_2 + HCHO + O_2CH_2Cl$	7.9×10^{-12}	A & L^{T}
136	$O_2EtCl + HO_2 \rightarrow OH + HCHO + O_2CH_2Cl$	7.4×10^{-12}	$*^{T}$
137	$O_2EtCl + CH_3CO_3 \rightarrow CH_3O_2 + HCHO + O_2CH_2Cl$	3.0×10^{-12}	*
138	$O_2PrCl + NO + O_2 \rightarrow NO_2 + CH_3CO_3 + O_2CH_2Cl$	7.9×10^{-12}	A & L^{T}
139	$O_2PrCl + HO_2 \rightarrow OH + CH_3CHO + O_2CH_2Cl$	7.4×10^{-12}	$*^{T}$
140	$O_2PrCl + CH_3CO_3 + O_2$ $\rightarrow CH_3O_2 + CH_3CHO + O_2CH_2Cl + CO_2$	3.0×10^{-12}	*

Notes

In some cases the stoichiometry is not written as correct for O, H or C. This is for simplicity in the hard copy of the model; when the model runs the stoichiometry is exact.

Me = CH_3; Et = CH_3CH_2; Pr = $CH_3CH_2CH_2$; Ac = $CH_3C(O)CH_2$;

PAN = peroxyacetylnitrate ($CH_3CO_3NO_2$); M = third body (N_2 or O_2)

\# **A & L**: Atkinson & Lloyd (1984)

M & T: Malko & Troe (1982)

B *et al*: Baulch et al (1984)

BZS: Biermann, Zetsch & Stuhl (1976)

C1 *et al*: Cantrell et al (1985)

C2 *et al*: Cantrell et al (1986)

B & P: Basco & Parmar (1987)

A & A: Atkinson & Aschmann (1985)

V & A: Vaghjiani & Ravishankara (1991)

PHOT: rate coefficients are dependent on solar photon flux. Listed value is maximum for latitude 60^0N on June 21st at 500 m altitude

* : recommended kinetic parameters for analagous species used

^{T} : temperature dependent rate coefficient

^{PT} : pressure & temperature dependent rate coefficient

∞ $\mp$: rate coefficient proportional to [M]

For a fuller description of the rate coefficient values and the temperature and pressure dependent expressions used the reader is referred to Fletcher (1989).

References

Adema, E. H., J. R. Ybema, P. Heeres & H. C. P. Wegh, The heterogeneous formation of N_2O in air containing NO_2, O_3 and NH_3, *J. Atmos. Chem.*, **11**, pp 255 - 269, 1990.

Anastasi, C., R. Hudson & V. J. Simpson, Effects of future fossil fuel use on CO_2 levels in the atmosphere, *Energy Policy*, pp 936-944, December 1990.

Anastasi, C., M. Dowding & V. J. Simpson, Future CH_4 emissions from rice production, *J. Geophys. Res.*, **97**, pp 7521-7525, 1992.

Anastasi, C. & V. J. Simpson, Future methane emissions from animals, *J. Geophys. Res.*, **98**, pp 7181 - 7186, 1993.

Arah, J., Modelling the exchange of nitrogen oxides between soils and the atmosphere, *Chemistry and Industry*, pp 530 - 532, 20 July 1992.

Atkinson, R. & A. C. Lloyd, Evaluation of kinetic and mechanistic data for modelling of photochemical smog, *J. Phys. Chem. Ref. Dat.*, **13**, pp 315 - 444, 1984.

Atkinson, R. & S. M. Aschmann, Kinetics of the gas phase reaction of Cl atoms with a series of organics at 296 ± 2 K and atmospheric pressure, *Int. J. Chem. Kinet.*, **17**, pp 33 - 41, 1985.

Badr, O. & S. D. Probert, Sources of atmospheric nitrous oxide, *Applied Energy*, **42**, pp 129 - 176, 1992.

Basco, N. & S. S. Parmar, The reaction of acetylperoxy with NO_2, *Int. J. Chem. Kinet.*, **19**, pp 115 - 128, 1987.

Baulch, D. L., R. A. Cox, R. F. Hampson, J. A. Kerr, J. Troe, & R. T. Watson, Evaluated kinetic and photochemical data for atmospheric chemistry: II. Codata task group on gas-phase chemical kinetics, *J. Chem. Phys. Ref. Data*, **13**, pp 1259 - 1380, 1984.

Bekki, S., K. S. Law & J. A. Pyle, Effect of ozone depletion on atmospheric CH_4 and CO concentrations, *Nature*, **371**, pp 595 - 597, 1994.

Berges, M. G. M., R. M. Hofmann, D. Scharffe, & P. J. Crutzen, Nitrous oxide emissions from motor vehicles in tunnels and their global extrapolation, *J. Geophys. Res.*, **98**, pp 18527 - 18531, 1993.

Biermann, H. W., C. Zetsch & F. Stuhl, Rate constant for the reaction of OH with N_2O at 298 K, *Ber. Bunsenges*, **80**, pp 909 - 911, 1976.

Blackmer, A. M., S. G. Robbins & J. M. Bremner, Diurnal variability in rate of emission of nitrous oxide from soils, *Soil Sci. Soc. Am. J.*, **46**, pp 937 - 942, 1982.

Bolle, J. J., W. Seiler & B. Bolin, Other greenhouse gases and aerosols, assessing their role for atmospheric radiative transfer, in *The Greenhouse Effect*, edited by B. Bolin et al., John Wiley, New York, 1986.

Borucki, W. J., & W. L Chameides, Lightning: Estimates of the rates of energy dissipation and nitrogen fixation, *Reviews of GeoPhysics and Space Physics*, **22**, pp 363 - 372, 1984.

Bouwman, A. F., Exchange of greenhouse gases between terrestrial ecosystems and the atmosphere, in *Soils and the Greenhouse Effect*, edited A. F. Bouwman, John Wiley, New York, 1990.

Cantrell, C. A., W. R. Stockwell, L. G. Anderson, K. L. Busarow, D. Perner, A. Schmeltekopf, J. G. Calvert, & H. S. Johnston, Kinetic study of the NO_3-CH_2O reaction and its possible role in nighttime tropospheric chemistry, *J. Phys Chem.*, **89**, pp 139 - 146, 1985.

Cantrell, C. A., J. A. Davidson, K. L. Busarow, J. G. Calvert, The CH_3CHO-NO_3 reaction and possible nighttime PAN generation, *J. GeoPhys. Res.*, **91**, pp 5437 - 5353, 1986.

Cates, R. L. & D. R. Keeney, N_2O production throughout the year from fertilised and manured fields, *J. Environ. Qual.*, **16**, pp 443 - 447, 1987.

Chameides, W. L., D. H. Stedman, R. R. Dickerson, D. W. Rusch & R. J. Cicerone, NO_x production in lightning, *J. Atm. Sciences*, **34**, pp 143 - 149, 1977.

Chameides, W. L., Effect of variable energy input on nitrogen fixation in instantaneous linear discharges, *Nature*, **277**, pp 123 - 124, 1979.

Cicerone. R. J., Analysis of sources and sinks of atmospheric nitrous oxide (N_2O), *J. Geophys. Res.*, **94**, pp 18265 - 18271, 1989.

Cofer, W. R., J. S. Levine, E. L. Winstead, & B. J. Stocks, New estimates of nitrous oxide emissions from biomass burning, *Nature*, **349**, pp 689 - 691, 1991.

Comfort, S. D., K. A. Kelling, D. R. Keeney, & J. C. Converse, Nitrous oxide production from injected liquid dairy manure, *Soil Sci. Soc. Am. J.*, **54**, pp 421 - 427, 1990.

Conrad, R., W. Seiler, & G. Bunse, Factors influencing the loss of fertiliser-nitrogen into the atmosphere as N_2O, *J. Geophys. Res.*, **88**, pp 6709 - 6718, 1983.

Crutzen, P. J. & P. H. Zimmermann, The changing photochemistry of the troposphere, *Tellus*, **43AB**, pp 136 - 151, 1991.

Dasch, J., Nitrous oxide emissions from vehicles, *J. Air Waste Manage. Assoc.*, **42**, pp 63 - 67, 1992.

Davis, D. D., J. D. Bradshaw, M. O. Rodgers, S. T. Sandholm & S. KeSheng, Free tropospheric and boundary layer measuerments of NO over the central and eastern North Pacific ocean, *J. GeoPhys Res.*, **92**, pp 2049 - 2070, 1987.

Dawson, G.A., Nitrogen fixation by lightning, *J. Atm Sciences*, **37**, pp 174 - 178, 1979.

Demerjian, K. L., K. L. Shere & J. T. Peterson, Theoretical estimates of actinic (spherically integrated) flux and photolytic rate constants of atmospheric species in the lower troposphere, *Adv. Environ. Sci. Technol.*, **10**, pp 369 - 459, 1980.

DeMore, W. & O. F. Raper, *J. Chem. Phys.*, **37**, pp 2048, 1962.

Derwent, R. G. et al., Oxides of nitrogen in the UK, 2nd report of UK photochemical oxidant review group, DoE, 1990.

Donohoe, K. G., F. H. Shair & O. R. Wulf, Production of O_3, NO & N_2O in a pulsed discharge at 1 atm., *Ind. Eng. Chem. Fundam.*, **16**, pp 208 - 215, 1977.

Dlugokencky, E. J., K. A. Masarie, P. M. Lang, P. P. Tans, L. P. Steele & E. G. Nisbet, A dramatic decrease in the growth rate of atmospheric methane in the Northern Hemisphere during 1992, *GeoPhys. Res. Lett.*, **22**, 45 - 48, 1994.

Dowdell, R. J., J. R. Burford & R. Crees, Losses of nitrous oxide dissolved in drainage water from agricultural land, *Nature*, **278**, pp 342 - 343, 1979.

Drapcho, D. L., D. Sisterson & R. Kumar, Nitrogen fixation by lightning activity in a thunderstorm, *Atm. Env.*, **17**, pp 729 - 734, 1983.

Duxbury, J. M., D. R. Bouldin, R. E. Terry, & R. L. Tate, Emissions of nitrous oxide from soils, *Nature*, **298**, pp 462 - 464, 1982.

Ehhalt, D. H., H. -P. Dorn & D. Poppe, The chemistry of the hydroxyl radical in the troposphere, *Proc. Royal Soc. Edinburgh*, **97B**, pp 17 - 34, 1990.

Eichner, M. J., N_2O emissions from fertilised soils: Summary of available data, *J. Environ. Qual.*, **19**, pp 272 - 280, 1990.

FAO, *Fertiliser Yearbook, Vol. 40*, Food and Agriculture Organisation of the United Nations, Rome, 1990.

Finlayson-Pitts, B. J. & J. N. Pitts Jnr., *Atmospheric Chemistry: Fundamentals and Experimental Techniques*, John Wiley & Sons, New York, 1986.

Firestone, M. K., M. S. Smith, R. B. Firestone & J. M. Tiedje, The influence of nitrate, nitrite and oxygen on the composition of the gaseous products of denitrification in soil, *Soil Sci. Soc. Am. J.*, **43**, pp 1140 - 1144, 1979.

Firestone, M. K. & E. A. Davidson, Microbiological basis of NO and N_2O production and consumption in soil, in *Exchange of Trace Gases between Terrestrial Ecosystems and the Atmosphere,* edited M. O. Andreae and D. S. Schimel, John Wiley and Sons, New York, 1989.

Fishman, J. & P. J. Crutzen, A numerical study of tropospheric chemistry using a one-dimensional model, *J. GeoPhys. Res.*, **82**, pp 5897 - 5906, 1977.

Fletcher, I. S., Modelling the chemistry of 'clean' air, 1. The gas phase oxidation of DMS in the marine boundary layer, National Power Report, 1989.

Fletcher, I.S., Modelling the chemistry of 'clean' air, 2. Major parameters affecting the composition of the marine troposphere, National Power Restricted Report, 1991.

Fowler, D. & J. H. Duyzer, Micrometeorological techniques for the measurement of trace gas exchange, in *Exchange of Trace Gases between Terrestrial Ecosystems and the Atmosphere,* edited M. O. Andreae and D. S. Schimel, John Wiley and Sons, New York, 1989.

Franzblau, E. & C. J. Popp, Nitrogen oxides produced from lightning, *J. GeoPhys. Res.*, **94**, pp 11089 - 11104, 1989.

Goldenbaum, G. C. & R. R. Dickerson, Nitric oxide production by lightning discharges, *J. GeoPhys. Res.*, **98**, pp 18333 - 18338, 1993.

Graedel, T. E. & P. J. Crutzen, Building Environmental Chemical Models, Chapter 15, pp 309-338, in *Atmosperic Change - an Earth System Perspective*, W.H. Freeman and Co., New York, 1993.

Griffing, G. W., Ozone and oxides of nitrogen production during thunderstorms, *J. GeoPhys. Res.*, **82**, pp 943 - 950, 1977.

Hameed, S. & J. Dignon, Changes in the geographical distribution of global emissions of NO_x and SO_x from fossil fuel combustion between 1966 and 1980, *Atm. Env.*, **22**, pp 441 - 449, 1988.

Harrison, J. T. H., Electrical discharge chemistry of nitrogen oxides, DPhil Thesis, Dept. of Chemistry, University of York, 1991.

Harteck, P. & S. Dondes, *J. Chem. Phys.*, **24**, pp 619, 1956.

Hill, R. D., R. G. Rinker & H. Dale Wilson, Atmospheric nitrogen fixation by lightning, *J. Atm. Sciences*, **37**, pp 179 - 192, 1980.

Hill, R. D., R. G. Rinker & A. Coucouvinos, Nitrous oxide production by lightning, *J. GeoPhys. Res.*, **89**, pp 1411 - 1421, 1984.

Holmes, C. R., E. W. Szymanski, S. J. Szymanski & C. B. Moore, Radar and acoustic study of lightning, *J. GeoPhys. Res.*, **85**, pp 7512 - 7532, 1980.

Houghton, J. T., B. A. Callendar & S. K. Varney (eds.), *Climate Change 1992, The Supplementary Report to the IPCC Scientific Assessment*, Cambridge University Press, New York, 1992.

Houghton, J. T. *et al* (eds), *Climate Change 1994*, IPCC Report, CUP, 1995.

Hutchinson, G. L. & A. R. Mosier, Improved soil cover for field measurement of nitrous oxide fluxes, *Soil Sci. Soc. Am. J.*, **45**, pp 311 - 316, 1981.

Keller, M., W. A. Kaplan, S. C. Wofsy, & J. M. Da Costa, Emissions of N_2O from tropical forest soils: response to fertilisation with NH_4^+, NO_3^-, and PO_4^{3-}, *J. Geophys. Res.*, **93**, pp 1600 - 1604, 1988.

Keller, M., & W. A. Reiners, Soil-atmosphere exchange of nitrous oxide, nitric oxide and methane under secondary succession of pasture to forest in the Atlantic lowlands of Costa Rica, *Global Biogeochemical Cycles*, **8**, pp 399 - 409, 1994.

Khalil, M. A. K. & R. A. Rasmussen, Causes of increasing atmospheric methane; depletion of hydroxyl radicals and the rise of emissions, *Atm. Env.*, **19**, pp 397 - 407, 1985.

Khalil, M. A. K. & R. A. Rasmussen, Nitrous oxide from coal-fired power plants: Experiments in the plumes, *J. Geophys. Res.*, **97**, pp 14645 - 14649, 1992a.

Khalil M. A. K. & R. A. Rasmussen, The global sources of nitrous oxide, *J. GeoPhys. Res.*, **97**, pp 14,651 - 14,660, 1992b.

Khalil, M. A. K. & R. A. Rasmussen, Decreasing trend of methane: unpredictability of future concentrations, *Chemosphere*, **26**, pp 803 - 814, 1993.

Khalil M. A. K., & R. A. Rasmussen, Global decrease in atmospheric carbon monoxide concentration, *Nature*, **370**, pp 639 - 641, 1994.

Kotaki, M. & C. Katoh, The global distribution of thunderstorm activity observed by the Ionosphere Sounding Satellite (ISS-b), *J. Atm. & Terr. Phys.*, **45**, pp 833 - 847, 1983.

Krehbiel, P. R., M. Brook, R. L. Lehrmitte & C. L. Lennon, Lightning charge structures in thunderstorms, in *Proceedings in Atmospheric Electricity*, ed. L. H. Runtham & J. Lantham, pp 408 - 411, Deepak, Hampton, Va., 1983.

Leuenberger, M. & U. Siegenthaler, Ice-age atmospheric concentration of nitrous oxide from an Antarctic ice core, *Nature*, **360**, pp 449-451, 1992.

Levine, J. S., R. E. Hughes, W. L. Chameides & W. E.. Howell, N_2O and CO production by electric discharges: atmospheric implications, *Geo. Res. Lett.*, **6**, pp 557 - 559, 1979.

Levine, J. S., R. S. Rogowski, G. L. Gregory, W. E. Howell & J. Fishman, Simultaneous measurements of NO_x, NO & O_3 production in a laboratory discharge: atmospheric implications, *GeoPhys. Res. Lett.*, **8**, pp 357 - 360, 1981.

Levine, J. S., & E. F. Shaw Jr., *In situ* measurements of enhanced levels of N_2O associated with thunderstorm lightning, *Nature*, **303**, pp 312 - 314, 1983.

Levine, J. S., T. R. Augustsson, I. C. Anderson, J. M. Hoell & D. A. Brewer, Tropospheric sources of NO_x: lightning and biology, *Atm. Env.*, **18**, pp 1797 - 1804, 1984.

Levine, J. S., C. P. Rinsland & G. M. Tennille, The photochemistry of methane and carbon monoxide in the troposphere in 1850 and 1985, *Nature*, **318**, pp 254 - 257, 1985.

Liaw, Y. P., D. L. Sisterson & N. L. Miller, Comparison of field, laboratory & theoretical estimates of global nitrogen fixation by lightning, *J. GeoPhys. Res.*, **95**, pp 22489 - 22494, 1990.

von Leibig, J., *Ann. Chem. Phys.*, **35**, pp 329, 1827.

Linak, W. P., J. A. McSorley, R. E. Hall, J. V. Ryan, R. K. Srivastava, J. O. L. Wendt, & J. B. Mereb, Nitrous oxide emissions from fossil fuel combustion, *J. Geophys. Res.*, **95**, pp 7533 - 7541, 1990.

Loftfield, N. S., R. Brumme & F. Beese, Automated monitoring of nitrous oxide and carbon dioxide flux from forest soils, *Soil Sci. Soc. Am. J.*, **56**, pp 1147-1150, 1992.

Lyon, R. K., J. C. Kramlich & J. A. Cole, Nitrous oxide: sources, sampling, and science policy, *Environ. Sci. Tech.*, **23**, No. 4, pp 392 - 393, 1989.

MacKerras, D. & M. Darveniza, Latitudinal variation of lightning occurrence characteristics, *J. GeoPhys. Res.*, **99**, pp 10813 - 10821, 1994.

Malko, M. W. & J. Troe, Analysis of the uni-molecular reaction $N_2O_5 + M \rightleftarrows NO_2 + NO_3 + M$, *Int. J. Chem. Kinet.*, **14**, pp 399 - 416, 1982.

Mazur, V., J. C. Gerlach & W. D. Rust, Lightning flash density versus altitude and storm structure from observations with UHF- and S-band radars, *GeoPhys. Res. Lett.*, **11**, pp 61 - 64, 1984.

McElroy, M. B. & S. C. Wofsy, Nitrous oxide sources and sinks, in *World Meteorological Organisation, Atmospheric Ozone 1985, Vol. 1*,, NASA, Washington, DC, 1985.

Molina, M. J., & F. S. Rowland, Stratospheric sink for chlorofluoromethanes: chlorine atom-catalysed destruction of ozone, *Nature*, **249**, pp 810, 1974.

Mosier, A. R., Chamber and isotope techniques, in *Exchange of Trace Gases between Terrestrial Ecosystems and the Atmosphere*, edited M. O. Andreae and D. S. Schimel, John Wiley and Sons, New York, 1989.

Mosier, A. R., Gas flux measurement techniques with special reference to techniques suitable for measurements over large ecologically uniform areas, in *Soils and the Greenhouse Effect*, edited by A. F. Bouwman, John Wiley, New York, 1990.

Mosier, A., D. Schimel, D. Valentine, K. Bronson, & W. Parton, Methane and nitrous oxide fluxes in native, fertilised and cultivated grasslands, *Nature*, **350**, pp 330 - 332, 1991.

Mosier, A. R., and D. S. Schimel, Influence of agricultural nitrogen on atmospheric methane and nitrous oxide, *Chemistry and Industry*, **23**, pp 874 - 877, 1991.

Novelli, P. C., K. A. Masarie, P. P. Tans & P. M. Lang, Recent changes in atmospheric carbon monoxide, *Science*, **263**, pp 1587 - 1590, 1994.

Noxon, J. F., Atmospheric nitrogen fixation by lightning, *GeoPhys. Res. Lett.*, **3**, pp 463 - 465, 1976.

Noxon, J. F., *J. GeoPhys. Res.*, **83**, pp 3051, 1978.

Peyrous, R. & R. M. Lapeyre, Gaseous products created by electrical discharges in the atmosphere & condensation nuclei resulting from gaseous phase reactions, *Atm. Env.*, **16**, pp 959 - 968, 1982.

Prasad, S.S., *Nature*, **289**, pp 386, 1981.

Prasad, S. S, Natural atmospheric sources and sinks of nitorus oxide: 1. An evaluation based upon 10 laboratory experiments, *J. GeoPhys. Res.*, **99**, pp 5285 - 5294, 1994.

Prentice, S. A. & D. MacKerras, The ratio of cloud-ground lightning flashes in thunderstorms, *J. Appl. Meteorol.*, **16**, pp 542 - 550, 1977.

Price, C. & D. Rind, What determines the CG lightning fraction in thunderstorms?, *GeoPhys. Res. Lett.*, **20**, pp 463 - 466, 1983.

Prinn, R., D. Cunnold, R. Rasmussen, P. Simmonds, F. Alyea, A. Crawford, P. Fraser, & R. Rosen, Atmospheric emissions and trends of nitrous oxide deduced from 10 years of ALE/GAGE data, *J. Geophys. Res.*, **95**, pp 18369 - 18385, 1990.

Prinn, R., D. Cunnold, P. Simmonds, F. Alyea, R. Boldi, P. Fraser, D. Gutzler, D. Hartley, R. Rosen, & R. Rasmussen, Global average concentration and trend for hydroxyl radicals deduced from ALE/GAGE trichloroethane (methyl chloroform) data for 1978 - 1990, *J. GeoPhys. Res.*, **97**, pp 2245 - 2461, 1992.

Rodhe, H., A comparison of the contribution of various gases to the greenhouse effect, *Science*, **248**, 1990.

Rasmussen, R. A. & M. A. K. Khalil, Atmospheric trace gases: Trends and distributions over the last decade, *Science*, **232**, pp 1623 - 1624, 1986.

Sanderson, M. G., Experimental and modelling studies of atmospheric chemistry, DPhil Thesis, University of York, 1991.

Schulz, G. G., *Phys. Rev.*, **135A**, pp 988, 1966.

Seiler, W. & R. Conrad, Contribution of tropical ecosystems to the global budgets of trace gases, especially CH_4, H_2, CO, and N_2O, in *The Geophysiology of Amazonia-Vegetation and Climate Interactions*, edited by R. E. Dickinson, John Wiley, New York, 1987.

Slemr, F., R. Conrad & W. Seiler, Nitrous oxide emissions from fertilised and unfertilised soils in a subtropical region (Andalusia, Spain), *Journal of Atmospheric Chemistry, 1,* pp 159 - 169, 1984.

Stark, M. S., C. Anastasi & J. T. H. Harrison, The formation of nitrogen oxides by electrical discharges and implications for atmospheric lightning, in press, 1995.

Stark. M., pers. comm.

Steele, L. P., E. J. Dlugokencky, P. M. Lang, P. P. Tans, R. C. Martin & K. A. Masarie, Slowing down of the global accumulation of atmospheric methane during the 1980s, *Nature*, **358**, pp 313 - 316, 1992.

Thiemens, M. H. & W. C. Trogler, Nylon production: An unknown source of atmospheric nitrous oxide, *Science*, **251**, pp 932 - 934, 1991.

Thompson, A. M. & R. J. Cicerone, Clouds and wet removal as causes of variability in the trace gas compositions of the marine troposphere, *J. GeoPhys. Res.*, **87**, pp 8811 - 8826, 1982.

Thompson, A. M. & R. J. Cicerone, Possible perturbations to atmospheric CO, CH_4 and OH, *J. Geophys. Res.*, **91**, pp 10853 - 10864, 1986.

Thompson, A. M., M. A. Huntley & R. W. Stewart, Perturbations to tropospheric oxidants 1985-2035; 1. Calculations of ozone and OH in chemically coherent regions, *J. Geophys. Res.*, **95**, pp 9829 - 9844, 1990.

Thompson, A. M., The oxidising capacity of the earth's atmosphere: probable past and future changes, *Science*, **256**, pp 1157 - 1163, 1992.

Tie, X. X. & E. J. Mroc, Potential changes of methane due to an assumed increased use of natural gas: a global 3-D study, *Chemosphere*, **26**, pp 769 - 776, 1993.

Trenberth, K. (ed), *Climate System Modelling*, CUP, New York, 1992.

Tuck, A. F., Production of nitrogen oxides from lightning discharges, *Quart. J. R. Met. Soc.*, **102**, pp 749 - 755, 1976.

Uman, M. A., All about lightning, 2nd ed., Dover, N. Y., 1986.

Uman, M. A., The lightning discharge, Academic, San Diego, Ca., 1987.

United Nations, *World Population Prospects, 1988, Population Studies No. 106*, Department of Economic and Social Affairs, New York, 1989.

United Nations, *Population and Vital Statistics Report (from 1 April 1992)*, Department of Economic and Social Development, Stat. Office, New York, 1992.

Vaghjiani, G. L. & A. R. Ravishankara, New measurement of the rate coefficient for the reaction of OH with methane, *Nature*, **350**, pp 406 - 408, 1991.

Wayne, R. P., *Chemistry of Atmospheres*, OUP, NY, 1991.

Weiss, R. F., The temporal and spatial distribution of tropospheric nitrous oxide, *J. Geophys. Res.*, **86**, pp 7185 - 7195, 1981.

Zel'dovich, Ya. B., & Yu. P. Raizer, *Physics of Shock Waves and High-Temperature Hydrodynamic Phenomena*, **Vol. 1**, pp 374 - 378, Academic Press, London, 1966.

Zipf, E. C., *Nature*, **287**, pp 523 - 524, 1980.

Zipf, E.C. & S.S. Prasad, *Nature*, **287**, pp 525 - 527, 1980.